Universitat d'Alacant
Universidad de Alicante

Design of N-doped carbon materials for ORR electrocatalysts through a combination between computational modelling and chemical synthesis

Javier Quílez Bermejo

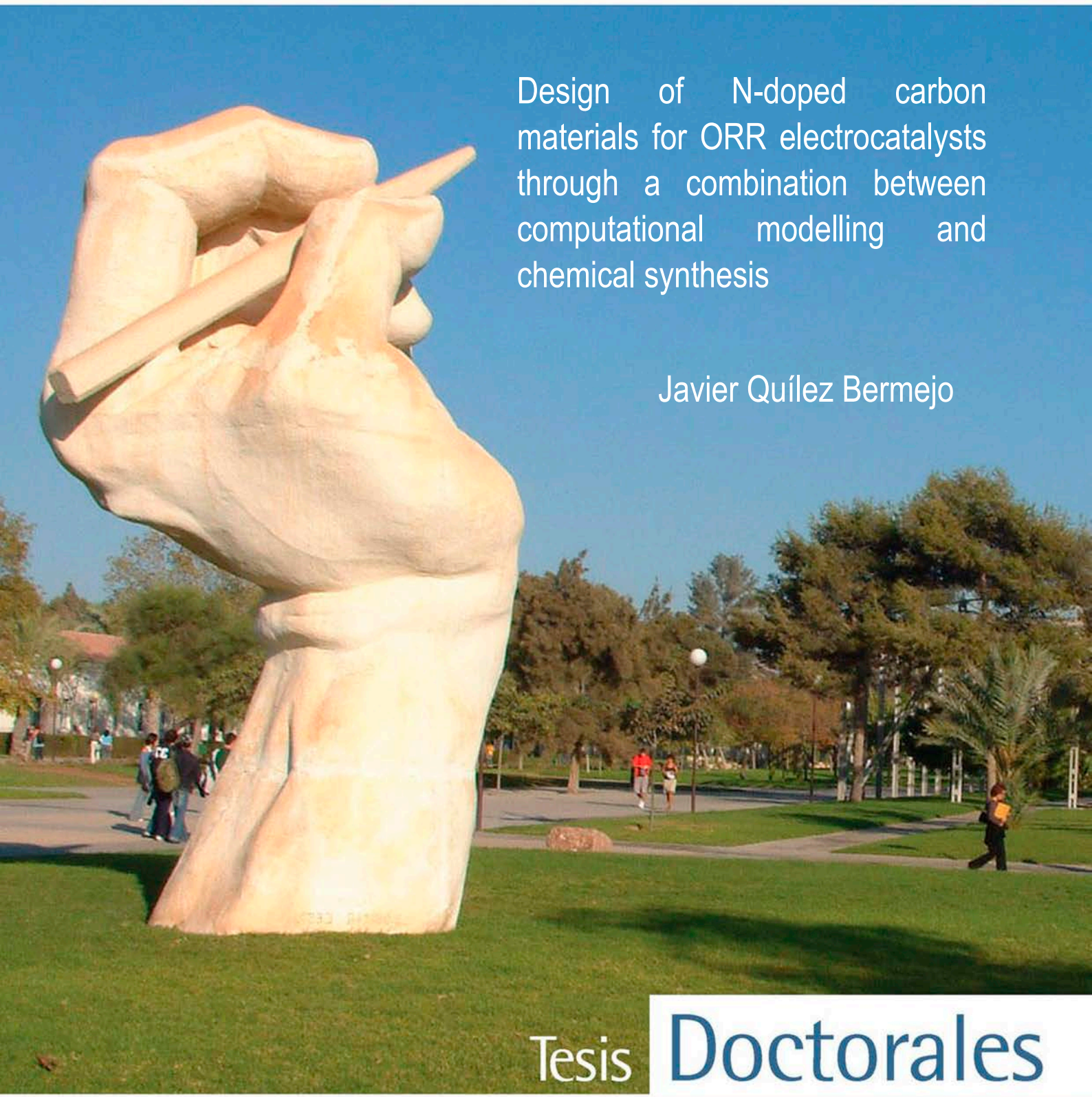

Tesis Doctorales
UNIVERSIDAD de ALICANTE

Unitat de Digitalització UA
Unidad de Digitalización UA

Universitat d'Alacant
Universidad de Alicante

Departamento de Química Inorgánica
Departamento de Química Física
Instituto Universitario de Materiales

Design of N-doped carbon materials for ORR electrocatalysts through the combination of computational modelling and chemical synthesis

Javier Quílez Bermejo

Tesis presentada para aspirar al grado de
DOCTOR por la Universidad de Alicante con
MENCIÓN DE DOCTOR INTERNACIONAL

DOCTORADO EN CIENCIA DE MATERIALES

Dirigida por:

Diego Cazorla Amorós
Catedrático de Química Inorgánica

Emilia Morallón Núñez
Catedrática de Química Física

AGRADECIMIENTOS

Es complicado mirar atrás y ver lo mucho que ha cambiado todo tras estos años de Tesis, es difícil saber cómo he llegado hasta aquí. Lo que tengo claro es que esto no es algo que haya hecho yo solo, son muchas las personas que han hecho esto posible y me han ayudado para que pueda llegar a defender mi Tesis Doctoral. Es a todas ellas a las que tengo mucho que agradecer. Me conozco lo suficiente para saber que estos agradecimientos no reflejarán en plenitud lo agradecido que estoy con todas las personas que han formado parte de esta etapa.

Mis primeras palabras no pueden ir dirigidas a otras personas que no sean mis directores de Tesis, Diego y Emilia. Desde un primer momento me dieron una oportunidad que, muy probablemente, no hubiese encontrado en ningún otro lugar. Solo encuentro palabras de agradecimiento por las innumerables conversaciones, consejos y todo tipo de ayuda que me han dado durante estos años. Ha sido un placer trabajar con vosotros.

A mis compañeros de laboratorio, muchos de los cuales se han convertido en verdaderos amigos.

A mis amigos de toda la vida, por las innumerables ocasiones en las que han tenido que lamentar mis ausencias durante este tiempo pero que, aun así, siempre han estado ahí.

A mi familia, especialmente, a mis abuelos. Es un auténtico placer saber que todos ellos van a poder leer este agradecimiento. Gracias por todo el cariño y apoyo.

A mis padres y hermanos, los que más han tenido que sufrir todas y cada una de mis charlas o proyectos. Estoy seguro de que ellos podrían defender esta tesis casi tanto como lo puedo hacer yo. Esta Tesis también es gran parte vuestra.

Y, por supuesto, a Ana. Es imposible agradecer lo suficiente la infinita paciencia, cariño y apoyo incondicional que me has brindado durante todo este tiempo. Por todos los viajes, por todos los consejos y por todo lo que nos queda por delante: gracias.

No abandones las ansias de hacer de tu vida algo extraordinario

- Walt Whitman

INDEX

CAPÍTULO 0

ESTRUCTURA Y CONTENIDO DE LA TESIS DOCTORAL

Introducción

La síntesis y propiedades de materiales carbonosos dopados con nitrógeno es bien conocida en la Ciencia de los Materiales de Carbón. Estos materiales han sido y son ampliamente utilizados en diferentes campos, tales como la catálisis o procesos de adsorción. En concreto, los materiales carbonosos dopados con nitrógeno han demostrado ser una alternativa muy prometedora como electrocatalizadores de la reacción de reducción de oxígeno. Las observaciones experimentales de estos materiales han resultado en múltiples publicaciones científicas que reportan su actividad catalítica, en la que, en algunos casos, logra alcanzar valores cercanos a los del catalizador comercial de platino. Teniendo en cuenta la diferente naturaleza de las funcionalidades de nitrógeno que se pueden encontrar en los materiales carbonosos y los factores adicionales como la estructura, porosidad, presencia de defectos, etc., que aumentan la complejidad del sistema de estudio, es sencillo entender que, prácticamente, todas las especies nitrogenadas han sido propuestas como sitios activos para la reacción de reducción de oxígeno. Esto pone de relieve la gran controversia existente en la comunidad científica. En este sentido, el objetivo principal de esta Tesis Doctoral consiste en profundizar sobre esta temática mediante la identificación de los grupos funcionales de nitrógeno que resultan en una mayor actividad catalítica para esta reacción. Con este fin, en el desarrollo de este trabajo de tesis, se ha empleado una combinación de trabajo experimental y modelado computacional.

Estructura

La presente Tesis Doctoral ha sido desarrollada en los grupos de Materiales Carbonosos y Medio Ambiente (MCMA) y de Electrocatálisis y Electroquímica de Polímeros (GEPE) que forman parte del Instituto Universitario de Materiales de la Universidad de Alicante (IUMA).

Esta Tesis Doctoral ha sido complementada con una estancia predoctoral en el Centre for Research in Ceramics and Composite Materials (CICECO) en Aveiro Institute of Materials en la Universidad de Aveiro, Portugal, bajo la supervisión del Dr Manuel Melle Franco.

Debido a que esta Tesis Doctoral opta a mención internacional, los capítulos correspondientes a los resultados obtenidos y las conclusiones generales se han redactado en inglés para cumplir con la normativa vigente.

Contenido

La presente Tesis Doctoral ha sido estructurada en un total de nueve capítulos que recogen una revisión bibliográfica, la explicación de las técnicas experimentales y los procedimientos de síntesis empleados, resultados experimentales y un último capítulo que recoge las conclusiones generales de esta Tesis Doctoral.

Capítulo I: Introducción General.

Este capítulo se centra en una revisión general de la importante contribución de los materiales carbonosos dopados con diferentes heteroátomos en la transición energética de los combustibles fósiles hacia las fuentes de energía renovables. En este contexto, uno de los factores limitantes de muchos de estos dispositivos, como pilas de combustible y baterías metal-aire, son los electrodos usados en el cátodo de estos dispositivos, en los que tiene lugar la reacción de reducción de oxígeno. El alto coste y la baja disponibilidad de los catalizadores comerciales hacen imprescindible la búsqueda de nuevos catalizadores menos costosos y más accesibles, manteniendo las prestaciones del catalizador comercial basado en platino. Una solución prometedora consiste en el uso de catalizadores basados en materiales carbonosos libre de metales como electrocatalizadores de la reacción de reducción de oxígeno (ORR), reduciendo así el coste del electrodo mientras se mantiene una alta actividad catalítica. Los defectos, porosidad, orden estructural, morfología y conductividad eléctrica son algunos parámetros que juegan un papel importante en la actividad catalítica de estos materiales. Aunque esos factores influyen en el rendimiento de los catalizadores, la introducción de heteroátomos es una de las rutas más prometedoras para conseguir catalizadores altamente eficientes. En este capítulo se revisa el papel de los diferentes grupos funcionales, junto con el efecto de otros parámetros estructurales, a partir de la bibliografía publicada.

La revisión bibliográfica desarrollada en este capítulo ha dado lugar a la siguiente publicación científica:

- J. Quílez-Bermejo, E. Morallón, D. Cazorla-Amorós, *Metal-free heteroatom-doped carbon-based catalysts for ORR. A critical assessment about the role of heteroatoms*, Carbon 165 (2020) 434-454.

Capítulo II: Técnicas experimentales

Este capítulo describe las técnicas experimentales que se han empleado durante el desarrollo de la presente Tesis Doctoral.

Chapter III: Effect of carbonization conditions of polyaniline on its catalytic activity towards ORR. Some insights about the nature of the active sites.

En este capítulo, se han obtenido materiales carbonosos dopados con nitrógeno a partir del tratamiento térmico de polianilina, obtenida químicamente y que será el precursor nitrogenado utilizado a lo largo de esta Tesis Doctoral. El tratamiento térmico de la polianilina se realizó utilizando diferentes temperaturas, 600 y 800ºC. Además, durante el tratamiento térmico se emplearon dos atmósferas diferentes: una atmosfera inerte (N_2) y otra que consiste en una mezcla de gases ligeramente oxidante (3000 ppm de O_2 en N_2). Los materiales preparados a 800ºC mostraron valores altos de capacidad específica, de hasta 170 y 255 $F \cdot g^{-1}$ en electrolitos básico y ácido, respectivamente. Se ha estudiado en medio básico y ácido la actividad electrocatalítica de todos los materiales en la reacción de reducción de oxígeno. Los materiales carbonosos obtenidos mediante tratamiento térmico a 600ºC no mostraron una buena actividad electrocatalítica debido a su baja conductividad eléctrica. Por otro lado, los materiales carbonosos obtenidos a 800ºC mostraron una actividad catalítica mejorada debido a su mayor conductividad y la presencia de grupos funcionales de nitrógeno y oxígeno en la superficie del material carbonoso. Merece destacar que el tratamiento térmico a 800ºC en atmósfera oxidante produce materiales carbonosos con una alta actividad en la ORR, que parece estar relacionada con una gran cantidad de especies nitrógeno y oxígeno en el borde de las láminas de grafeno. Estudios computacionales sugieren que la presencia de estas funcionalidades de nitrógeno y oxígeno en las proximidades de un átomo de carbono mejora el rendimiento catalítico. Dos

sitios N-C-O adyacentes parecen incrementar la selectividad de la ORR hacia la formación de moléculas de agua por un mecanismo de cuatro electrones.

Los resultados obtenidos en el presente capítulo de esta Tesis Doctoral han dado lugar a la siguiente publicación científica:

- J. Quílez-Bermejo, E. Morallón, D. Cazorla-Amorós, *Effect of the carbonization of polyaniline on its catalytic activity towards ORR. Some insights about the nature of the active sites*, Carbon 119 (2017) 62-71

Además, el trabajo realizado en este capítulo ha resultado en las siguientes contribuciones y premios:

- J. Quílez-Bermejo, C. Gonzalez-Gaitán, E. Morallón, D. Cazorla-Amorós, *Effect of carbonization conditions of polyaniline on its catalytic activity towards ORR. Some insights about the nature of the active sites*, HYCELTEC 2017, Oporto, Portugal. 19/06/2017-23/06/2017. Poster.
- J. Quílez-Bermejo, C. González-Gaitán, E. Morallón, D. Cazorla-Amorós, *Carbones dopados con nitrógeno obtenidos a partir de la carbonización de polianilina. Naturaleza de los sitios activos en la reacción de reducción de oxígeno,* XIV Reunión del Grupo Español del Carbón, Málaga, Spain, 22/10/2017-25/10/2017. Comunicación oral.
- J. Quílez-Bermejo, C. González-Gaitán, E. Morallón, D. Cazorla-Amorós, *Materiales carbonosos dopados con nitrógeno obtenidos a partir de la polianilina como electrodos en supercondensadores,* XIV Reunión del Grupo Español del Carbón, Málaga, Spain, 22/10/2017-25/10/2017. Poster.
- J. Quílez-Bermejo, E. Morallón, D. Cazorla-Amorós, *Effect of carbonization conditions of polyaniline on its catalytic activity towards ORR,* 1er WORKSHOP de la Red de Pilas de Combustible para un Futuro Energético Sostenible, Madrid, Spain, 10/05/2019. Comunicación oral.
- Premio mejor exposición oral otorgado en la XIV Reunión del Grupo Español del Carbón por la presentación *Carbones dopados con nitrógeno obtenidos a partir de la carbonización de polianilina.*

Naturaleza de los sitios activos en la reacción de reducción de oxígeno, Málaga, Spain, 22/10/2017-25/

Chapter IV: Oxygen-reduction catalysis of N-doped carbons prepared via heat treatment of polyaniline at over 1100ºC.

En este capítulo se han desarrollado catalizadores altamente eficientes para la reacción de reducción de oxígeno. Los catalizadores han sido preparados a partir del tratamiento térmico de polianilina a temperaturas superiores a 1100ºC. La caracterización detallada y cálculos computacionales sugieren que el motivo principal de esta tan alta actividad catalítica reside en la conversión a altas temperaturas de los grupos funcionales nitrogenados tipo piridina en especies nitrogenadas cuaternarias en posición zigzag.

Los resultados obtenidos en el presente capítulo de esta Tesis Doctoral han dado lugar a la siguiente publicación científica:

- J. Quílez-Bermejo, E. Morallón, D. Cazorla-Amorós, *Oxygen reduction catalysis of N-doped carbons prepared via heat treatment of polyaniline at over 1100ºC*, Chem. Comm. 54 (2018) 4441-4444

Además, los materiales carbonosos obtenidos, así como el procedimiento realizado en este capítulo dio lugar a la siguiente patente:

- Patente nacional P201830278 'Procedimiento de síntesis de materiales carbonosos para su aplicación como electrocatalizadores y material obtenido por medio de dicho proceso' Javier Quílez-Bermejo, Emilia Morallón y Diego Cazorla-Amorós.

El trabajo realizado en este capítulo también ha dado lugar a las siguientes contribuciones a congresos:

- J. Quílez-Bermejo, E. Morallón, D. Cazorla-Amorós, *Excellent ORR catalysts based on N-doped carbon materials prepared through heat treatment of PANI at high temperatures*, The World Conference on Carbon, Madrid, Spain, 01/07/2018-06/07/2018. Comunicación oral.

Chapter V: Towards understanding of the active sites for ORR in N-doped carbon materials through a fine-tuning of nitrogen functionalities: an experimental and computational approach.

El diseño de materiales carbonosos dopados con nitrógeno para la reacción de reducción de oxígeno es solo posible si primero se comprende en profundidad la naturaleza de los sitios activos. Existe una gran investigación que busca superar este desafío a través de enfoques teóricos o experimentales. Sin embargo, la combinación de ambos enfoques es necesaria para ahondar en el conocimiento sobre este tema. Este capítulo presenta una excelente concordancia entre los resultados experimentales y los modelos computacionales, lo que proporciona una evidencia de la naturaleza de los sitios más eficientes para esta reacción en materiales carbonosos dopados con nitrógeno. Los materiales carbonosos dopados con nitrógeno se han obtenido experimentalmente a través de un doble tratamiento térmico de la polianilina, primero en presencia de una atmósfera ligeramente oxidante y, posteriormente, en presencia de una atmósfera inerte a diferentes temperaturas (800-1200ºC). De acuerdo con la caracterización realizada, este método de síntesis permite la formación selectiva de especies de nitrógeno, sin conllevar cambios significativos en otros parámetros como el orden estructural o la porosidad. Las pruebas electrocatalíticas demuestran una alta actividad catalítica con valores, en cuanto a densidad de corriente límite y potencial de inicio de la reacción, similares a los obtenidos con los catalizadores comerciales basados en platino. La química computacional, a través de cálculos DFT, muestra que el nitrógeno cuaternario de tipo borde es el grupo funcional nitrogenado más efectivo para la catálisis de la ORR, en comparación con otros grupos como las piridinas, piridonas, pirroles o nitrógenos oxidados.

Los resultados obtenidos en el presente capítulo de esta Tesis Doctoral han dado lugar a la siguiente publicación científica:

- J. Quílez-Bermejo, M. Melle-Franco, E. San-Fabián, E. Morallón, D. Cazorla-Amorós, *Towards understanding the active sites for the ORR in N-doped carbon materials through fine-tuning of nitrogen functionalities: an experimental and computational approach*, J. Mat. Chem. A 7 (2019) 24239-24250.

El trabajo realizado en este capítulo también se ha presentado en los siguientes congresos:

- J. Quílez-Bermejo, E. San-Fabián, E. Morallón, D. Cazorla-Amorós, *Towards understanding of the catalytic active sites of N-doped carbon materials through experimental and DFT computational studies*, HYCELTEC 2019, Barcelona, Spain, 01/07/2019-03/07/2019. Comunicación oral.
- J. Quílez-Bermejo, E. San-Fabián, E. Morallón, D. Cazorla-Amorós, *A computational and experimental approach towards the knowledge of catalytic sites for oxygen reduction reaction in N-doped carbon materials*, The World Conference of Carbon, Lexington, Kentucky, United States of America, 14/07/2019-19/07/2019. Comunicación oral.
- J. Quílez-Bermejo, E. San-Fabián, E. Morallón, D. Cazorla-Amorós, *Towards understanding of the active sites for ORR in N-doped carbon materials*, 18th International Conference on Density-Functional Theory and its Applications, Alicante, Spain, 22/07/2019-26/07/2019. Poster.

Chapter VI: Silica and Titania-templated ordered mesoporous N-doped carbon thin films. Highly efficient catalysts towards oxygen reduction reaction.

Uno de los objetivos más desafiantes en los electrocatalizadores de la reacción de reducción de oxígeno basados en materiales carbonosos dopados con nitrógeno es el control sobre la estructura porosa y la obtención de películas delgadas nano-estructuradas que puedan incorporarse sobre el colector de corriente. Los métodos más comunes de obtención de materiales carbonosos dopados con nitrógeno son la carbonización de precursores como polímeros que contienen nitrógeno y el tratamiento térmico de una mezcla de materiales carbonosos y precursores nitrogenados. Sin embargo, de esta manera, el área superficial y la distribución de tamaños de poros no se controlan. Este capítulo se centra en la preparación de materiales carbonosos dopados con nitrógeno con estructura 2D definida. Para ello, se ha electropolimerizado la anilina dentro de la estructura porosa de dos plantillas diferentes con estructura bien definida (películas delgadas de Sílice y Titania mesoporosas). Así, se ha realizado la impregnación de la anilina en la estructura porosa y posteriormente se ha polimerizado mediante cronoamperometría a potencial constante. Las muestras

resultantes se trataron térmicamente a 900ºC con el objetivo de obtener materiales carbonosos con estructura 2D y dopados con nitrógeno dentro de la estructura de dichas plantillas. Todos los materiales han sido analizados mediante diferentes técnicas de caracterización. Merece destacar que los materiales carbonosos con estructura 2D dopados con nitrógeno resultaron ser electrocatalizadores altamente activos para la ORR gracias a formación de especies nitrogenadas del tipo nitrógeno cuaternario.

El trabajo realizado en este capítulo ha dado lugar a las siguientes contribuciones en congresos:

- J. Quílez-Bermejo, E. Morallón, D. Cazorla-Amorós, *Silica-templated ordered mesoporous N-doped carbon thin films. A highly efficient catalyst towards oxygen reduction reaction*, The World Conference of Carbon, Lexington, Kentucky, United States of America, 14/07/2019-19/07/2019. Comunicación oral.
- J. Quílez-Bermejo, E. Morallón, D. Cazorla-Amorós, *Titania-templated ordered N-doped mesoporous carbon thin films as highly efficient catalysts towards oxygen reduction reaction*, 8th International Conference on Carbon for Energy Storage and Environment Protection, Alicante, Spain, 20/10/2019-24/10/2019. Poster.

Chapter VII: On the origin of the effect of pH in ORR for non-doped and edge-type quaternary N-doped metal-free carbon-based catalysts.

Los catalizadores basados en materiales carbonosos han ganado mucha atención durante los últimos 15 años como una alternativa muy prometedora para sustituir los catalizadores comerciales actuales. Sin embargo, estos materiales solo han demostrado una alta actividad catalítica en electrolito alcalino. Desafortunadamente, las pilas de combustible de membrana de electrolito polimérico más optimizadas son aquellas que usan membranas de intercambio protónico. Esto significa que el cátodo está rodeado por un entorno protónico en el que los materiales carbonosos muestran una baja actividad electrocatalítica hacia la reducción de oxígeno. Por lo tanto, la búsqueda de catalizadores basados en materiales carbonosos altamente activos en medio ácido solo es posible si primero se entiende el origen de esta baja actividad en electrolito ácido. El presente capítulo aborda este tema tan importante a través

de un estudio combinado de química experimental y modelado computacional, proporcionando los principios fundamentales que pueden contribuir a comprender el origen del efecto del pH en la reducción del oxígeno en materiales carbonosos.

Los resultados obtenidos en el presente capítulo de esta Tesis Doctoral han dado lugar a la siguiente publicación científica:

- J. Quílez-Bermejo, K. Strutynski, M. Melle-Franco, E. Morallón, D. Cazorla-Amorós, *On the origin of the effect of pH in ORR for non-doped and edge-type quaternary N-doped metal-free carbon-based catalysts, Chemical Science,* En revisión.

Chapter VIII: Post-synthetic efficient functionalization of polyaniline with phosphorus-containing groups. Effect of phosphorus on electrochemical properties

Dada la importancia que tiene el material de partida en la preparación de materiales carbonosos dopados con diferentes heteroátomos, en este capítulo, se ha sintetizado un polímero basado en polianilina en el que se han incorporado grupos funcionales tipo fósforo. Así, la polianilina sintetizada químicamente ha sido post-modificada con grupos fósforo a partir de la reacción del polímero con tricloruro de fósforo (PCl_3) y clorodifenilfosfina (PPh_2Cl), en condiciones suaves. La reacción entre la polianilina y los precursores de fósforo ha demostrado ser muy selectiva, ya que solo los grupos imina participan en la funcionalización, alcanzando hasta un 5 % atómico de fósforo tras la reacción. Todos los polímeros resultantes han sido caracterizados por diferentes técnicas y los resultados fueron avalados por cálculos teóricos. Los resultados experimentales y de DFT han demostrado que la reacción ocurre a través de los grupos imina de la polianilina y los átomos de fósforo de los compuestos de partida, generando enlaces N-P. Las propiedades electroquímicas de los materiales han sido evaluadas, así como la actividad catalítica de los polímeros hacia la ORR. Se ha demostrado que un número elevado de grupos fenilo en el precursor, afecta negativamente a la actividad catalítica del catalizador, ya que impide el acceso de las moléculas de oxígeno a los sitios activos. Sin embargo, una cantidad menor de estos grupos o el uso de otros precursores, como el PCl_3,

evita este impedimento y da como resultado una actividad catalítica mejorada con respecto al polímero original.

Los resultados obtenidos en el presente capítulo de esta Tesis Doctoral han dado lugar a la siguiente publicación científica:

- J. Quílez-Bermejo, A. Ghisolfi, D. Grau-Marín, E. San-Fabián, E. Morallón, D. Cazorla-Amorós, *Post-synthetic efficient functionalization of polyaniline with phosphorus-containing groups. Effect of phosphorus on electrochemical properties*, Eur. Pol. J. 119 (2019) 272-280.

El trabajo realizado en este capítulo también ha resultado en las siguientes contribuciones:

- J. Quílez-Bermejo, A. Ghisolfi, E. San-Fabián, E. Morallón, D. Cazorla-Amorós, *Phosphorus and nitrogen co-doped carbon materials through carbonization of phosphorus-modified polyaniline and its catalytic activity towards oxygen reduction reaction*, HYCELTEC 2019, Barcelona, Spain, 01/07/2019-03/07/2019. Comunicación oral.

Capítulo IX: General Conclusions

Este capítulo recoge las conclusiones generales de esta Tesis Doctoral.

CAPÍTULO I

INTRODUCCIÓN GENERAL

1.1 Introducción

La quema de combustibles fósiles engloba gran parte de la demanda energética mundial y, debido a esto, es también la principal causa del calentamiento global y cambio climático que actualmente experimentamos [1–4]. El Acuerdo de París [5], bajo la Convención Marco de las Naciones Unidas sobre el Cambio Climático, establece como objetivo principal el mantener el aumento de la temperatura media mundial por debajo de 1.5 ºC. En este contexto, el descenso de la utilización de combustibles fósiles como fuente de energía y el uso masivo de energías renovables es un aspecto obligatorio. Para ello, deben implementarse nuevas fuentes de energía que sean más eficientes y menos dañinas para el medioambiente.

Una de estas opciones consiste en la tecnología "power to gas", en la cual el excedente de las energías renovables se convierte en combustible gaseoso que, posteriormente, puede ser usado bajo demanda o que, también, puede ser empleado en el sector del transporte [6,7]. Una de las alternativas más prometedoras es la síntesis de hidrógeno gas (H_2) a partir de la electrólisis del agua que podría usarse en el transporte o en la red eléctrica, siendo un ejemplo de la economía del hidrógeno. El H_2 se emplearía como combustible en las pilas de combustible debido a su alta eficiencia en la generación de energía y a la baja producción de contaminantes [8,9].

Las pilas de combustible son dispositivos electroquímicos que convierten energía química en energía eléctrica. De entre todas las pilas de combustible, las pilas de combustible de membrana de electrolito polimérico (PEMFC, por sus siglas en inglés) son una de las alternativas más interesantes hacia el reemplazo de los motores de combustión interna de los vehículos actuales debido a su alta eficiencia energética en el uso de combustibles verdes (H_2), la no generación de contaminantes y la no necesidad de recargar el combustible y el oxidante [10–13].

La Figura 1.1 esquematiza el funcionamiento de una PEMFC, mostrando la reacción de oxidación del hidrógeno (HOR, por sus siglas en inglés) en el ánodo y la reacción de reducción del oxígeno (ORR, por sus siglas en inglés) en el cátodo, siendo necesario en ambos electrodos el uso de un catalizador. La ORR

es de especial interés para la comunidad científica pues ésta presenta grandes limitaciones en términos de sobrepotencial, baja densidad de corriente límite y alto coste de los electrodos.

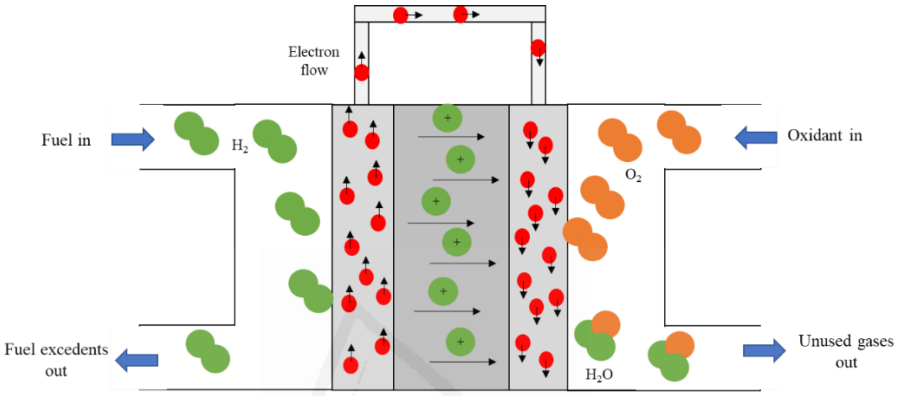

Figura 1.1: Ilustración esquematizada de una pila de combustible de membrana de electrolito polimérico (PEMFC) trabajando en condiciones ácidas.

La reacción de reducción de oxígeno no es sólo importante en las PEMFC, existen también dispositivos o aplicaciones donde esta reacción también juega un papel relevante como las baterías metal-aire, la producción de peróxido de hidrógeno, etc. Las baterías metal-aire son dispositivos electroquímicos que generan energía eléctrica a partir de reacciones redox entre un metal y el oxígeno [14,15]. A diferencia de otros tipos de baterías, las baterías metal-aire poseen mayor densidad energética gracias a que el oxígeno no se almacena, pudiendo utilizarse el aire. A pesar de que el uso de oxígeno es considerado como la principal ventaja de estos dispositivos, el electrodo que se encarga de su reducción es considerado como el componente más complejo y, en muchos casos, el más caro de las baterías metal-aire [14,15]. Por otro lado, la producción de peróxido de hidrógeno (H_2O_2) es una temática muy atractiva de cara a diferentes aplicaciones industriales [16,17]. El H_2O_2 es considerado una sustancia química muy versátil y multifuncional, pues posee propiedades muy interesantes como consecuencia de ser un buen agente oxidante. Además, la producción mundial de este compuesto excede los 4 millones de toneladas por año y la industria implicada mueve, aproximadamente, 4000 millones de dólares anuales [16,17]. El principal problema se encuentra en su procedimiento

industrial de síntesis, basado en el proceso antraquinona, el cual consiste en múltiples y costosas etapas que elevan el coste final de este producto. Es por esto por lo que uno de los objetivos más desafiantes en la comunidad científica se centra en la síntesis de H_2O_2 a través de la reducción electroquímica del oxígeno molecular, proceso mucho más seguro, limpio desde un punto de vista medioambiental y que, también, permite trabajar a presión y temperatura ambiente.

El mecanismo por el cual transcurre la reducción de oxígeno es ampliamente conocido y depende del electrolito (ácido o alcalino) y la selectividad del catalizador utilizado. La ORR puede transcurrir a través de (i) una ruta de 4 electrones, dando así lugar a la producción de H_2O y OH^- (en electrolito ácido y alcalino, respectivamente) y siendo la reacción más deseada puesto que implica mayor producción de energía, y (ii) una ruta de 2 electrones, la cual conduce a la producción de H_2O_2 o HO_2^- (en electrolito ácido y alcalino, respectivamente). No obstante, estas especies H_2O_2 o HO_2^- pueden ser de nuevo reducidas a H_2O y OH^-, dando así lugar a la ruta de 2+2 electrones.

Medio ácido	Medio alcalino
$O_2 + 4H^+ + 4e^- \rightarrow 2H_2O$	$O_2 + 2H_2O + 4e^- \rightarrow 4OH^-$
$O_2 + 2H^+ + 2e^- \rightarrow H_2O_2$	$O_2 + H_2O + 2e^- \rightarrow HO_2^- + OH^-$
$H_2O_2 + 2H^+ + 2e^- \rightarrow 2H_2O$	$HO_2^- + H_2O + 2e^- \rightarrow 3OH^-$

El catalizador más activo y selectivo hacía la formación de agua se basa en nanopartículas de platino soportadas sobre materiales carbonosos [18,19]. Esto se considera un problema ya que este metal es poco abundante en la naturaleza y extremadamente costoso. Además, este cátodo también presenta inconvenientes como baja estabilidad, disolución del catalizador y alta desactivación por presencia de monóxido de carbono. Todo esto hace imposible la comercialización a gran escala de estos catalizadores basados en platino [18,19].

Además, cabe destacar que mientras la carga de platino en el ánodo es de tan solo 0.05 mg·cm^{-2}, el contenido en platino en el cátodo es superior al 0.4 mg cm^{-2} [20]. Esto se traduce en que aproximadamente el 90 % del platino de una

PEMFC se concentra en el cátodo, donde la reacción de reducción de oxígeno tiene lugar. En consecuencia, la búsqueda de nuevos catalizadores para la ORR se convierte en un tema de gran interés en el ámbito científico y tecnológico, tal y como demuestra el gran aumento de publicaciones en esta temática en los últimos 15 años [21]. Tales estudios pueden clasificarse de acuerdo a la naturaleza del catalizador; (i) catalizadores basados en metales no preciosos y (ii) catalizadores libres de metales.

En lo referente al primer grupo, pese a que la presencia de un metal precioso, como el platino, se ha reducido debido al uso de catalizadores basados en metales no preciosos, éstos pueden lixiviar y aglomerar, produciendo pérdidas en la eficiencia con el tiempo [22]. Sin embargo, se han producido grandes avances en el desarrollo de nuevos catalizadores basados en metales más económicos, como el hierro, el cobalto, etc., [22–29]. No obstante, este tipo de catalizadores no se estudiará durante el desarrollo de esta Tesis Doctoral.

La segunda, y probablemente, alternativa más innovadora consiste en el uso de catalizadores basados en materiales carbonosos dopados con heteroátomos libres de metal. Debido a la ausencia de metales en su composición, el desarrollo de este tipo de catalizadores puede traducirse en una significativa disminución del coste de estos electrodos que podría facilitar la comercialización de las PEMFC a gran escala. La fuerte actividad investigadora en materiales carbonosos como electrocatalizadores para la ORR empezó hace cerca de 12 años, cuando Gong y col. reportaron la síntesis de nanotubos de carbono dopados con nitrógeno con excelente actividad catalítica, comparable con el catalizador comercial basado en platino [30]. Desde entonces, se están realizando grandes esfuerzos en mejorar el rendimiento de los catalizadores basados en materiales carbonosos. Sin embargo, muchos de estos trabajos son contradictorios y han generado una gran controversia en la identificación de los sitios activos, así como de los mecanismos de reacción por los cuales transcurre la ORR en estos catalizadores. Esto en gran parte se debe a la complejidad de los materiales carbonosos, en los cuales la química superficial, la porosidad y su estructura son tres factores fundamentales que, en general, determinan su comportamiento. En muchas ocasiones, la interpretación de los resultados se centra en tan solo uno de estos factores, omitiendo los otros que pueden tener una contribución relevante. Además, las impurezas metálicas pueden ser también responsables de estos resultados contradictorios, pues pequeñas trazas metálicas pueden mejorar significativamente la actividad catalítica de los

materiales carbonosos [31]. Consecuentemente, es necesaria una alta pureza de los materiales carbonosos si se quiere obtener información específica de estos catalizadores de materiales carbonosos libres de metal.

En este sentido, este capítulo de la Tesis Doctoral proporciona un resumen exhaustivo de los estudios más relevantes en la catálisis de la ORR por materiales carbonosos sin dopar y dopados con heteroátomos. Este capítulo se centra principalmente en los materiales carbonosos dopados con heteroátomos, los cuales constituyen una pequeña parte de la amplia y compleja temática de los defectos en materiales carbonosos. En los últimos años se han publicado numerosos trabajos de revisión interesantes que se centran en catalizadores basados en materiales carbonosos libres de metales y que presentan importante información desde un punto de vista experimental y también teórico [32–37]. Sin embargo, en este capítulo de Tesis Doctoral se ha tratado de profundizar en el origen de los sitios activos, así como en la contribución de cada grupo funcional del heteroátomo, considerando los fundamentos de la Ciencia de los Materiales de Carbón. Por lo tanto, en este capítulo se presenta información relevante del efecto de la química superficial sin, a su vez, omitir el papel de la porosidad y la estructura de los materiales carbonosos en su actividad catalítica en la ORR. Además, toda esta información se aborda a través de un enfoque experimental y de Química Computacional que sienta las bases de los siguientes capítulos de la presente Tesis Doctoral.

Llegado a este punto, es importante aclarar que cuando se habla de estructura y química superficial, se incluye también los defectos, ya que son los responsables de muchas de las propiedades de los materiales carbonosos. La relevancia de éstos es bien conocida y es objeto de un análisis profundo en las disciplinas de Física y Química del Estado Sólido. Por lo tanto, es importante recalcar que el dopado con heteroátomos, las vacantes o los átomos de carbono insaturados (diferentes tipos de defectos puntuales) así como otros defectos estructurales (es decir, defectos topológicos como el defecto de Stone-Wales, pentágonos, heptágonos, etc.) se encuentran con mucha frecuencia en estos materiales. El control sobre la naturaleza y la cantidad de defectos determinará las propiedades del material carbonoso, incluidas la actividad catalítica y la actividad electrocatalítica. Esto hace de la ingeniería de defectos un área fascinante de investigación que puede ser un área esencial en el futuro. Algunos ejemplos interesantes sobre este tema se pueden encontrar en las siguientes referencias [38–43].

1.2 Descripción general del mecanismo de la reacción de reducción de oxígeno en materiales carbonosos

Previamente, se ha comentado que la ORR es un proceso en el que el oxígeno se reduce a través de rutas que engloban procesos de dos o cuatro electrones. Sin embargo, esto es solo una simplificación de un proceso mucho más complejo. La ORR involucra múltiples etapas elementales, como la adsorción de O_2, transferencia de electrones y protones y la desorción de los productos finales que hacen de esta reacción una temática muy compleja. La Figura 1.2 resume los posibles mecanismos de la ORR que es posible vislumbrar tras el análisis de las diferentes publicaciones que se citan en la presente Tesis Doctoral. Esto, no obstante, no manifiesta que todas las rutas propuestas hayan sido previamente demostradas como mecanismos viables, sino que se plasman aquellos mecanismos que el análisis bibliográfico realizado en este capítulo permite entrever. Asimismo, la Tabla 1.1 clasifica los mecanismos propuestos de acuerdo al modo de quimisorción del oxígeno molecular y al número de electrones transferidos durante la reacción.

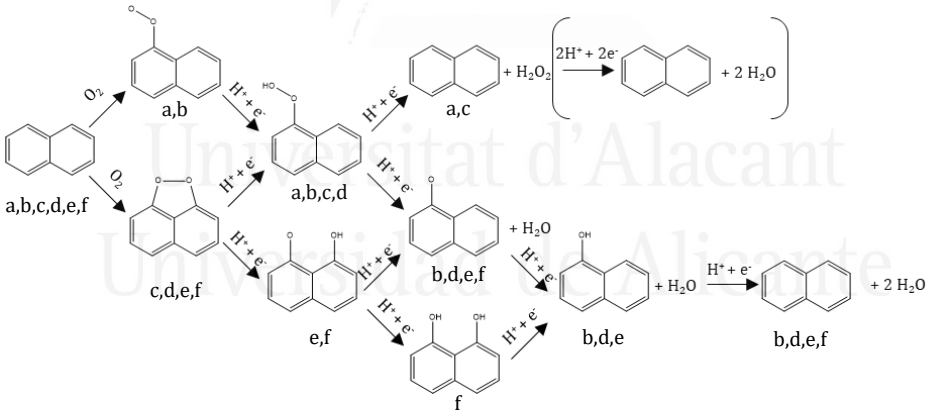

Figura 1.2: Resumen de los mecanismos para la catálisis de la ORR en catalizados basados en materiales carbonosos.

La primera etapa de la ORR consiste en la adsorción de la molécula de dioxígeno en la superficie del catalizador carbonoso. Esto puede ocurrir a través de un enlace terminal o un enlace tipo puente, lo que se traduce en que la molécula de dioxígeno se adsorbe a través de uno o dos átomos de carbono,

respectivamente. El mecanismo disociativo conlleva la ruptura del enlace oxígeno-oxígeno, mientras que el mecanismo asociativo mantiene dicho enlace unido.

Tabla 1.1: Representación de los diferentes modos de adsorción del oxígeno, número de electrones involucrados y diferente mecanismo propuesta en la Figura 1.2.

Ruta	Modo de adsorción	Nº de electrones	Mecanismo
a	Terminal	2	Asociativo
b	Terminal	4	Disociativo
c	Tipo puente	2	Asociativo
d	Tipo puente	4	Asociativo
e	Tipo puente	4	Disociativo
f	Tipo puente	4	Disociativo

Si el oxígeno se adsorbe a través de un único sitio activo (o enlace tipo terminal), el primer aporte del par electrón-protón conlleva la formación de un intermedio tipo C-O-O-H. Posteriormente, el siguiente par electrón-protón puede provocar la ruptura del enlace C-O, generando la formación de peróxido de hidrógeno (ruta *a*) o, por otro lado, la ruptura del enlace O-O (ruta *b*), el cual resulta en la formación de una molécula de agua y el intermedio de reacción C-O en la superficie del material carbonoso. A esta ruta *b* le siguen las posteriores etapas de reducción de este oxígeno terminal hasta la formación de una segunda molécula de agua.

Por otro lado, si la quimisorción tiene lugar a través de dos sitios activos (o enlace tipo puente), se proponen cuatro mecanismos diferentes. En primer lugar, la ruptura de un enlace C-O en el primer aporte de un par electrón-protón, lo que daría lugar a la formación del intermedio C-O-O-H (rutas *c* y *d*). Llegado a este punto, las posibilidades son las mismas que las indicadas en las rutas *a* y *b*, en las que la única diferencia se obtendría en el modo de quimisorción inicial. La segunda posibilidad conlleva la ruptura del enlace O-O tras el aporte de este primer electrón-protón (rutas *e* y *f*), donde ambas configuraciones conllevan un

mecanismo de 4 electrones en los que el producto final son dos moléculas de agua.

1.2 Catalizadores basados en materiales carbonosos libres de metal

Las propiedades y aplicaciones de los materiales carbonosos están principalmente determinadas por su estructura, porosidad y química superficial. Estos tres factores pueden dar lugar a múltiples posibilidades y hacen de la Ciencia de los Materiales de Carbón una temática muy rica y, a su vez, compleja. En el caso específico de la ORR, el principal factor que causa las mayores diferencias en la actividad catalítica de los materiales carbonosos radica en la introducción de heteroátomos diferentes al oxígeno. De entre los heteroátomos, es de destacar el efecto singular de los grupos funcionales nitrogenados. Sin embargo, los efectos de la porosidad y la estructura no pueden ser omitidos puesto que tienen gran contribución en el comportamiento general del material: la microporosidad puede actuar como nanoreactores y, debido a que esta reacción implica un proceso de transferencia de electrones, la conductividad eléctrica del material carbonoso (determinada por la estructura del mismo) es esencial para que esta reacción se produzca. Otro tipo de defectos, como los átomos de carbono insaturados, vacantes o defectos estructurales también juegan un papel relevante como sitios activos en esta reacción.

De acuerdo con estas consideraciones, en esta introducción de Tesis Doctoral se ha realizado una revisión del efecto de la porosidad, la estructura y la presencia de defectos en los materiales carbonosos, en definitiva, aquellos efectos no vinculados al dopado y también se comentará brevemente el efecto de los grupos oxigenados (que se encuentran de manera intrínseca en todo material carbonoso). Posteriormente, se resumirán los trabajos realizados sobre catalizadores de la ORR basados en materiales carbonosos dopados con heteroátomos de N, P, B y S, haciendo especial hincapié en el nitrógeno, el cual ha demostrado ser el dopante más prometedor para esta reacción.

1.3.1 Materiales carbonosos sin dopar

El efecto de la porosidad es, en muchas ocasiones, obviado en la discusión de la actividad catalítica en catalizadores basados en materiales carbonosos. Sin embargo, algunos estudios han demostrado el importante papel que este factor juega en la catálisis de la ORR. Appleby y col. destacaron este aspecto durante

el estudio cinético de la ORR con una serie de materiales carbonosos en electrolito alcalino; demostraron que la actividad catalítica en la ORR está estrechamente relacionada con el área superficial BET de los negros de carbón estudiados [44]. Sin embargo, esta misma tendencia no fue observada cuando el análisis cinético se realizó sobre carbones activados, cuya porosidad es mucho más compleja [44]. En este sentido, Gabe y col. [45] estudiaron, mediante modelado matemático y resultados experimentales, la influencia de la microporosidad en la ORR. Los autores encontraron que la alta actividad está ciertamente correlacionada con la microporosidad y la forma de las curvas de ORR depende de la distribución de tamaños de microporo, estando favorecida la formación de H_2O_2 en los microporos más estrechos (tamaño menor a 0.7 nm) [45]. Liu y col. [46] estudiaron el efecto de la microporosidad y la mesoporosidad en catalizadores basados en materiales carbonosos. Estos autores concluyeron que la microporosidad es la responsable de la actividad catalítica, mientras que los mesoporos son también necesarios para facilitar la accesibilidad a los sitios activos dentro de los microporos [46]. El papel crucial que los mesoporos juegan para lograr una adecuada transferencia del oxígeno a los microporos fue estudiado por Bandosz y col. [47]. Además, los autores también concluyeron que la fuerte adsorción de la molécula de dioxígeno tiene lugar en los ultamicroporos de naturaleza hidrofóbica [47] y recientemente se ha propuesto que los ultramicroporos pueden ser los sitios activos para esta reacción [48].

En lo que concierne a la estructura de los materiales carbonosos, su efecto ha sido ampliamente demostrado en la catálisis de la reacción de reducción de oxígeno. Este hecho se ve reflejado en la mayor actividad catalítica que muestran los nanotubos de carbono (CNT, por sus siglas en inglés) en comparación con electrodos basados en grafito/grafeno [49,50]. El menor número de láminas de grafeno y la curvatura de los CNTs, especialmente aquellos que tienen menor diámetro, puede ser responsable de este efecto. Además, esta curvatura no solo modifica la actividad catalítica, sino que la selectividad de la reacción también se ve afectada, siendo los CNT los que dan lugar a mecanismos en los que el número de electrones es próximo a 4 [50]. El origen del efecto de la curvatura procede, principalmente, del cambio de hibridación de los átomos de carbono que afecta a la estructura electrónica [51]. La estructura conjugada de una lámina de grafeno impide el cambio de hibridación de sp^2 a sp^3 y, consecuentemente, la quimisorción del oxígeno que

estaría principalmente restringida en los bordes de las láminas [51]. Sin embargo, el uso de CNTs hace posible el control sobre el grado de hibridación sp^3 [51]. Un ejemplo interesante se encuentra en el estudio computacional realizado sobre grafeno y CNT dopados con silicio, en los que la energía de adsorción del oxígeno y la energía libre de la etapa determinante de la velocidad de la ORR son menores cuando la quimisorción de oxígeno tiene lugar dentro de los nanotubos (con curvatura negativa) [52]. Además, cálculos computacionales, basados en la Teoría de Funcional de Densidad (DFT, por sus siglas en inglés) revelaron la importancia de la longitud de los CNTs en la energía de adsorción del oxígeno; a mayor longitud de los CNTs, menor la energía de quimisorción de moléculas de oxígeno en el plano basal de los CNTs [53].

De acuerdo con los trabajos previos, la química de los bordes también tiene influencia en la actividad catalítica en la ORR. Deng y col. [54] estudiaron la actividad electrocatalítica en la ORR, de láminas de grafeno sintetizadas con diferentes tamaños, teniendo en cuenta que cuanto menor es el tamaño de la lámina de grafeno, mayor es la cantidad de átomos de carbono en el borde. Cabe señalar que el material de láminas de grafeno con menor tamaño fue el que mostró mayor actividad catalítica hacia la ORR, lo que demuestra el papel crucial que la química de los bordes de las láminas tiene en electrocatálisis [54]. Cálculos teóricos que profundizaron en este asunto indicaron que la actividad catalítica de estos materiales procedía de los sitios bordes tipo zig-zag [54]. Chen y col. [55] estudiaron este hecho con el dopado de azufre en óxido de grafeno reducido mediante un tratamiento hidrotermal. El dopado con S induce la formación de abundantes sitios borde y de defectos en materiales basados en grafeno dando lugar a una alta actividad catalítica. Los autores proponen que la densidad de spin asimétrica, así como el mayor número de defectos en el plano basal son responsables de la alta actividad catalítica en la ORR [55]. De hecho, otros autores han propuesto que la reactividad hacia la transferencia de electrones de los bordes es, al menos, dos veces mayor que la de los planos basales de la lámina de grafeno [56]. Esta alta reactividad no solo se ha observado en la reducción de oxígeno, sino que también se ha demostrado que juega un papel importante en otras reacciones como la oxidación electroquímica de ácido ascórbico y del dinucleótido de nicotinamida y adenina (NADH), entre otros [57].

La ingeniería de defectos estructurales está ganando cada vez más atención debido a la aparición de interesantes artículos que relacionan la presencia de éstos con un aumento en la actividad catalítica de los materiales carbonosos. En la gran mayoría de los catalizadores basados en materiales carbonosos, los defectos estructurales (como anillos de cinco o siete átomos de carbono, vacantes, defectos en los bordes y defectos unidimensionales) se encuentran presentes intrínsecamente. Jia y col. [58] reportaron una estrategia de síntesis para la generación de defectos específicos; el grafito pirolítico altamente orientado (HOPG, por sus siglas en inglés) se trató con plasma de argón para formar ranuras uniformes en la superficie. La muestra obtenida (Ar-HOPG) se lavó y posteriormente se trató a 700ºC en presencia de amoniaco. A la muestra resultante de grafito pirolítico dopado con nitrógeno (N-HOPG) se le realizó un tratamiento térmico hasta 1150ºC bajo atmosfera de nitrógeno. De esta forma se obtuvo un HOPG con un elevado número de defectos topológicos y vacantes (D-HOPG). La Espectroscopía Fotoelectrónica de Rayos-X (XPS, de sus siglas en inglés) y la espectroscopía Raman indicaron la eliminación completa de los átomos de nitrógeno en D-HOPG y un aumento en los defectos debido al tratamiento térmico. Mediante absorción de Rayos-X cerca del borde (XANES, de sus siglas en inglés), aniquilación de positrones, microscopías electrónicas de barrido y de transmisión de campo oscuro y elevado ángulo y cálculos con teoría del funcional de la densidad (DFT, de sus siglas en inglés), los autores confirman que el aumento en el número de defectos estructurales se produce por la reconstrucción de los átomos del borde de la red de carbono del N-HOPG, específicamente, a través de la conversión de grupos funcionales nitrogenados del tipo piridina en anillos de cinco átomos de carbono [58]. Merece destacar, que el material D-HOPG presenta la actividad catalítica más alta para la ORR, con un potencial de inicio de la reacción de 0.81 V vs RHE en electrolito ácido, mientras que N-HOPG muestra un potencial de inicio de reacción de 0.76 V vs RHE. Medidas de la función de trabajo sugieren que los pentágonos tienen la mayor capacidad de donar electrones y, por tanto, la mayor habilidad para la transferencia de carga con el oxígeno. Esto se confirmó por la mayor actividad catalítica de los materiales carbonosos que contienen defectos en comparación con los que contienen grupos piridina. Otros trabajos experimentales y computacionales corroboran la alta eficiencia de los defectos que consisten en anillos de cinco átomos de carbono [43,59,60].

Además de la formación de pentágonos o heptágonos, la formación de sitios carbeno tipo zigzag y sitios carbino tipo "armchair" en los bordes de las láminas de grafeno son posibles mecanismos de la desactivación de nuevos sitios reactivos [61]. Radovic y col. propusieron que en presencia de aire, parte de los bordes zigzag y "armchair" forman estructuras tipo carbenos, carbinos o radicales libres [62] y éstos no deberían descartarse como posibles centros activos de la ORR. La principal consecuencia de la presencia de este tipo de defectos es la respuesta ferromagnética de algunos materiales carbonosos, la cual puede ser interpretada considerando la presencia de estructuras tipo carbeno en los bordes zigzag de las láminas de los materiales carbonosos [62]. Además, la presencia de carbenos conduce a un modo de quimisorción del dioxígeno diferente a los previamente comentados para materiales carbonosos. Esto se debe a que, debido a la falta de átomos de hidrógeno terminal, la molécula de oxígeno puede adsorberse a través de dos enlaces C-O en un único átomo de carbono y en una configuración C-O-O, siendo la primera de estas opciones la configuración más estable (Figura 1.3A) [63,64]. Esto no solo revela un nuevo modo de quimisorción, sino que también explica otros fenómenos como la ORR [65], la oxidación de materiales carbonosos con la generación de CO_2 [64] e, incluso, la creación de grupos funcionales oxigenados en el plano basal de los materiales carbonosos [63]. Este enfoque está de acuerdo con estudios experimentales en los cuales se demostró una estrecha correlación entre la actividad catalítica en la ORR y la reactividad hacia la gasificación con oxígeno en materiales carbonosos sin dopar [50].

Por lo tanto, la presencia de defectos estructurales, en sus múltiples posibilidades, es necesaria para explicar la actividad catalítica de los catalizadores basados en materiales carbonosos. No obstante, la contribución de los defectos solo puede ser positiva si la conductividad eléctrica de los catalizadores es suficientemente alta para proporcionar los electrones a los sitios activos [66]. En el momento en el que la introducción de defectos genera una conductividad eléctrica inferior a 70 $S \cdot m^{-1}$, el efecto positivo de tales defectos es eclipsado por la alta resistencia a la transferencia electrónica de los catalizadores [66].

Los grupos funcionales oxigenados se encuentran de forma intrínseca en los materiales carbonosos y se forman con mucha facilidad cuando el material carbonoso se pone en contacto con la atmósfera. Los grupos funcionales oxigenados pueden ser creados o modificados en la superficie del material

carbonoso mediante metodologías bien establecidas que permiten, incluso, modificar la naturaleza química de estos grupos funcionales. Todo esto se traduce en la imposibilidad de sintetizar materiales carbonosos puros. No obstante, la influencia de este tipo de grupos hacía la ORR no parece ser importante o, al menos, no parece que puedan ser considerados como los principales responsables de la actividad de los mejores catalizadores basados en materiales carbonosos libres de metales publicados para esta reacción. En la década de los 90, varios estudios profundizaron en el efecto de los grupos oxigenados en carbón vítreo. La oxidación de electrodos como el carbón vítreo da lugar a un ligero aumento de la actividad catalítica; sin embargo, la actividad es muy diferente de la que se obtiene con el catalizador comercial de platino. Los autores atribuyen este comportamiento catalítico de los electrodos carbonosos a la presencia de radicales ariloxi, que serían los responsables del aumento del paramagnetismo, que acompaña la oxidación química y electroquímica de estos materiales [67–69]. Estos centros paramagnéticos pueden reducir a los intermedios HO_2^- a OH^-, dando lugar de esta forma a un incremento del número de electrones involucrados durante la ORR [67–69]. Sin embargo, este incremento también se asoció a un aumento del área superficial de los materiales carbonosos que también cambia con el pretratamiento [69] y podría también explicar el mayor número de electrones en la ORR. Sin embargo, un estudio más reciente destaca el papel positivo que ejercen los grupos epoxi y éter en la selectividad de la ORR hacía la formación de H_2O_2 [70]. Otro trabajo reciente ha demostrado que los grupos funcionales oxigenados no producen un aumento importante de la actividad catalítica en la ORR, y que esta aumenta significativamente si se incorpora otro heteroátomo como el nitrógeno al material carbonoso [71]. No obstante, es importante destacar que, pese a que los grupos funcionales oxigenados muestran una baja actividad catalítica, éstos pueden generar un efecto sinérgico importante con otros grupos funcionales, es decir, en la presencia de otro heteroátomo; este aspecto se discutirá en la siguiente sección.

1.3.2 Materiales carbonosos dopados con heteroátomos

El dopar un material carbonoso con átomos más electronegativos como el nitrógeno crea un densidad de carga positiva en el átomo de carbono adyacente que facilita la adsorción del oxígeno molecular y la transferencia de carga, lo que puede resultar en una mejora en la actividad catalítica [30]. Por el otro lado, la estrategia opuesta consiste en dopar un material carbonoso con un

heteroátomo que presente una electronegatividad menor, como el boro o el fósforo, de esta forma, es el heteroátomo el que presentará una densidad de carga positiva y actuará como sitio activo en la adsorción y reducción de las moléculas de oxígeno [72].

En las siguientes secciones se presentarán los resultados más interesantes en lo que concierne a la actividad catalítica de los materiales carbonosos dopados con nitrógeno, azufre, fósforo y boro, así como la estrecha relación que existe entre la eficiencia en la ORR y la naturaleza de los sitios activos. Se prestará una atención especial al heteroátomo de nitrógeno, pues es el que ha presentado mejores prestaciones en la catálisis de la ORR y, además, es el objeto principal de esta Tesis Doctoral.

1.3.2.1 Materiales carbonosos dopados con nitrógeno

La introducción de átomos de nitrógeno en la matriz carbonosa es el tipo de dopado más estudiado en la bibliografía para la reacción estudiada en esta Tesis Doctoral. No obstante, a pesar de las prometedoras prestaciones de algunos de estos materiales carbonosos dopados con nitrógeno, solo unos pocos estudios han logrado sintetizar catalizadores con altas prestaciones hacia la ORR y, gran parte de estos, los han estudiado en electrolito alcalino. Por contra, la mayoría de los materiales carbonosos dopados con nitrógeno muestran una actividad catalítica mucho menor que los catalizadores basados en platino, pese a que la caracterización realizada indica que presentan grupos funcionales nitrogenados similares a aquellos de los mejores catalizadores de materiales carbonosos dopados con nitrógeno. Estos resultados han generado una enorme controversia sobre la naturaleza de los sitios activos originados por la presencia de este heteroátomo en la estructura carbonosa. Este amplio debate sobre la naturaleza de los sitios más activos reside, principalmente, en la dificultad de aislar una única especie nitrogenada en un material carbonoso. El aislamiento de una especie de nitrógeno incorporada en la estructura del material carbonoso no es tarea sencilla. Incluso aunque esto se lograra, la ausencia de control sobre otras propiedades importantes (tales como orden estructural, morfología, defectos y porosidad, entre otras) que pueden tener también una gran influencia en el comportamiento de estos catalizadores libres de metales (sección 1.3.1), hace muy complicado profundizar en esta temática.

Como se comentó anteriormente, los materiales carbonosos dopados con nitrógeno surgieron en 2009 como una alternativa prometedora como cátodo

para las pilas de combustible, cuando Gong y col. [30] mostraron la alta actividad catalítica de CNT dopados con nitrógeno alineados verticalmente (VA-NCNT). Su actividad era comparable con los valores obtenidos por el catalizador comercial de platino (Figura 1.3B). El mecanismo de reacción determinado fue de 2+2 electrones, donde el oxígeno molecular es primero reducido a HO_2^- y, después, reducido de nuevo a OH^-. Junto con los nanotubos de carbono, los electrodos de grafeno y de materiales basados en grafeno han sido los materiales carbonosos más estudiados para el dopado con nitrógeno, puesto que su estructura bien definida, proporciona un excelente modelo para entender el efecto de las funcionalidades de nitrógeno en la catálisis de la ORR. Qu y col. [73] demostraron la gran actividad catalítica de grafeno dopado con nitrógeno, obtenido mediante depósito químico en fase vapor (CVD por sus siglas en inglés) (Figura 1.3C). Pese a que el potencial de inicio de reacción es menor que el del catalizador comercial basado en platino, la densidad de corriente es tres veces mayor. Además, las importantes diferencias en ambos parámetros al comparar con el grafeno sin dopar revelan la importancia de los heteroátomos de nitrógeno. Sheng y col. [74] reportaron una ruta de síntesis de grafeno dopado con nitrógeno a través de un tratamiento térmico de óxido de grafeno a diferentes temperaturas (700-1000ºC) usando melamina como precursor nitrogenado. A 700ºC el contenido atómico de nitrógeno fue del 10.1 %. A mayores temperaturas, el contenido en nitrógeno y, a su vez, el de oxígeno disminuye. La actividad catalítica del material preparado a 700ºC fue atribuida a la incorporación de átomos de nitrógeno en las láminas de grafeno, ya que modifican la estructura electrónica de los átomos de carbono adyacentes [74]. Además de la metodología CVD [73,75–77], otros estudios han mostrado la mejora en la actividad catalítica de materiales basados en grafeno tras el dopado con nitrógeno mediante descarga de arco [78], tratamientos térmicos con NH_3 [79] o urea [80], entre otros.

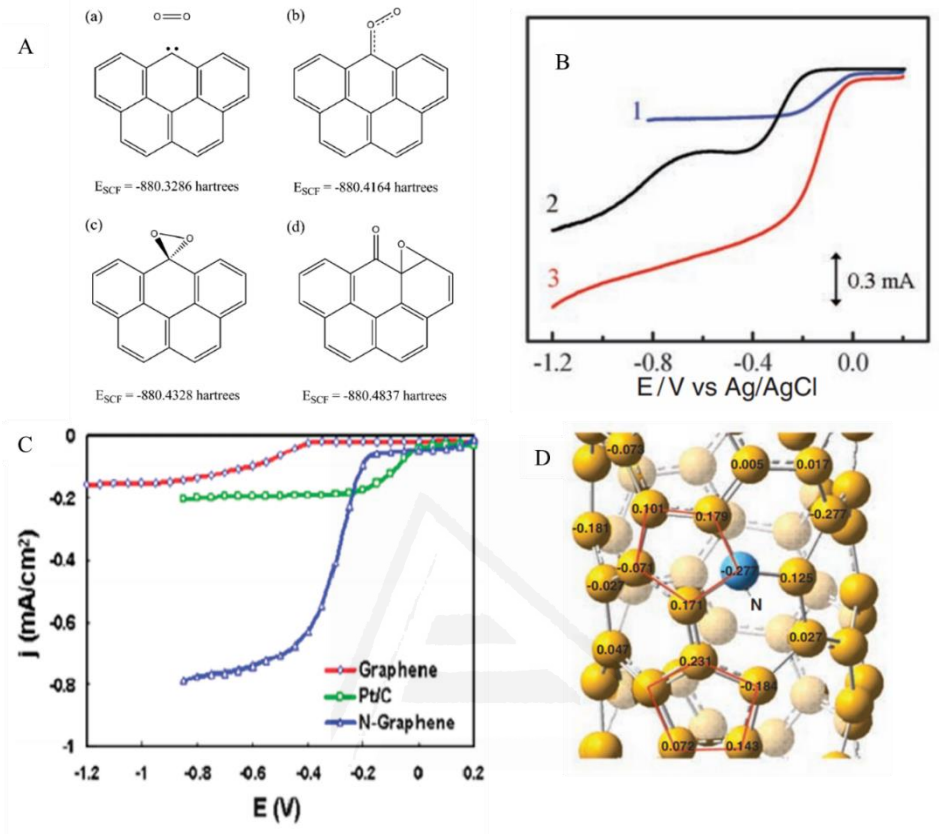

Figura 1.3: (A) Configuración y energías de los modelos de grafeno (C19H10) que ilustran los mecanismos de quimisorción del oxígeno en sitios borde con especies carbenos [Adaptado de Ref. 63, Copyright 2009, American Chemical Society]. **(B)** Curvas LSV de la reacción de reducción de oxígeno en atmósfera saturada en aire de una disolución 0.1 M de KOH para el catalizador comercial de platino (curva 1), CNT sin dopar (curva 2) y CNT dopado con nitrógeno (curva 3) [Adaptado de Ref. 30 con permiso de AAAS]. **(C)** Curvas LSV para la ORR en atmósfera saturada en aire en una disolución 0.1 M de KOH para el grafeno sin dopar (curva roja), el grafeno dopado con nitrógeno (curva azul) y el catalizador comercial basado en platino (curva verde) [Adaptado de Ref. 73, Copyright 2010, American Chemical Society]. **(D)** Distribución de la densidad de carga de los CNT dopados con nitrógeno de la Figura 1.3B [Adaptado de Ref. 30 con permiso de AAAS].

A pesar de que los electrocatalizadores de CNT y grafeno dopado con nitrógeno son la demostración más sencilla del efecto positivo de los átomos de nitrógeno en la mejora de la actividad catalítica hacia la ORR, las rutas más

extendidas de síntesis de materiales carbonosos dopados con nitrógeno se basan en la carbonización de precursores con alto contenido en nitrógeno, como polímeros o líquidos iónicos y la reacción directa entre un material carbonoso y un precursor nitrogenado, como la urea o el amoniaco [81–85]. Todas estas metodologías de síntesis no permiten un control preciso de propiedades como morfología, orden estructural, porosidad, conductividad eléctrica, etc., que hacen muy difícil reconocer el papel de las especies nitrogenadas en la actividad catalítica de la reducción de oxígeno. Por esta razón, algunos estudios han intentado reducir estas limitaciones empleando plantillas de SiO_2 [83,86–89] o TiO_2 [90,91]. El precursor nitrogenado es depositado, química o electroquímicamente, en el interior de la estructura porosa de la plantilla. Una vez este precursor es introducido, se realiza un tratamiento térmico que da lugar a la formación de materiales carbonosos ricos en nitrógeno con estructura ordenada.

En cualquier caso, se han sintetizado materiales carbonosos dopados con nitrógeno con excelente actividad catalítica mediante el uso de métodos convencionales y sin el uso de plantillas. Por ejemplo, Wang y col. [92] sintetizaron catalizadores altamente eficientes mediante tratamiento térmico a 1000ºC de la familia de nucleobases más conocida (adenina, guanina, citosina, timina y uracilo) mezcladas con 1-etil-3metilimidazolio dicianoamida. Las muestras obtenidas muestran comportamientos similares a los del catalizador comercial basado en platino con un alto potencial de inicio de la reacción [92]. Por otro lado, Men y col. [93] sintetizaron materiales compuestos de porosidad jerárquica grafeno/carbón dopados con nitrógeno (NPGC) a partir del tratamiento térmico a 950ºC de glucosa. El material NPGC mostró un potencial de inicio de reacción elevado (0.91 V vs RHE) con un número de electrones cercano a cuatro, lo que se traduce en una reducción directa del oxígeno a agua.

A pesar de que la mayoría de las investigaciones sobre este tema se centran en la síntesis de materiales carbonosos dopados con nitrógeno en metodologías de prueba y error, podemos encontrar cada vez más estudios que intentan profundizar en la naturaleza de los sitios activos en los materiales carbonosos dopados con nitrógeno y las razones por las cuales este heteroátomo provoca tal mejora. Obviamente, este conocimiento es esencial para definir las bases del futuro diseño de catalizadores avanzados y de la ingeniería a nanoescala de estos catalizadores libres de metal para la reacción de reducción de oxígeno.

No solo los resultados experimentales son importantes a la hora de ahondar en este tema, sino que también los estudios computacionales pueden jugar un papel muy relevante a la hora de adquirir una visión más precisa y completa de esta compleja temática. Por ejemplo, Gong y col. reportaron que la mayor afinidad electrónica del átomo de nitrógeno puede producir una densidad de carga positiva en el átomo de carbono adyacente, lo que facilitaría la quimisorción del oxígeno (Figura 1.3D) [30]. La alta actividad de CNTs dopados con nitrógeno fue respaldada por Hu y col. [94]. Estos autores proponen que la introducción de nitrógeno conlleva la reducción de la banda de energía prohibida ("band gap") entre el orbital molecular ocupado de más alta energía (HOMO, por sus siglas en ingles) y el orbital molecular no ocupado de menor energía (LUMO, por sus siglas en inglés), gracias al incremento del nivel de energía del HOMO [94], facilitando así la transferencia electrónica al oxígeno adsorbido. Además, mediante cálculos DFT, se ha podido demostrar que la densidad de carga positiva del átomo de carbono adyacente a un átomo de nitrógeno facilita la quimisorción y, por tanto, la reducción del oxígeno [30,94,95]. Todos estos trabajos permiten concluir que los sitios activos para la catálisis de la ORR no son los átomos de nitrógeno por sí mismos, sino que son los átomos de carbono adyacentes al heteroátomo, donde la molécula de oxígeno es atraída, quimisorbida y, entonces, reducida.

No obstante, la identificación de las especies nitrogenadas que crean los sitios catalíticos más activos está aún bajo intenso debate en la investigación actual. Esto se ve reflejado en el hecho de que casi todas las especies nitrogenadas han sido propuestas como responsables de la excelente actividad catalítica de los materiales carbonosos dopados con nitrógeno. Algunos autores atribuyen directamente la alta actividad catalítica de estos catalizadores al contenido en nitrógeno, que se considera la clave para entender la catálisis de la ORR [96–98]. Sin embargo, estudios más recientes no están de acuerdo con esta propuesta, pues en algunos trabajos se ha observado que una mayor cantidad de nitrógeno no siempre se traduce en mayores eficiencias en la ORR, sino que la actividad catalítica parece estar más relacionada con grupos funcionales específicos [99–101]. Así, es necesario el análisis y discusión exhaustivos acerca de la naturaleza de los sitios activos para entender mejor la ORR en materiales carbonosos dopados con nitrógeno. Por lo tanto, en las siguientes secciones se realizará una discusión de los resultados más relevantes, hasta la

fecha, que discuten el papel que tienen las diferentes funcionalidades de nitrógeno en la actividad catalítica.

1.3.2.1.1 Grupos nitrogenados tipo piridina

De entre todos los grupos funcionales nitrogenados, los nitrógenos piridínicos son las especies que más se han propuesto como posibles responsables de la alta actividad catalítica de los materiales carbonosos dopados con nitrógeno. Por ejemplo, Rao y col. [102] prepararon CNTs dopados con nitrógeno y alineados verticalmente empleando diferentes precursores poliméricos. La mejora en la actividad catalítica de estos materiales en comparación a su homólogo no dopado se atribuye al aumento en el porcentaje atómico de las especies de nitrógeno piridínico ya que, a mayor porcentaje atómico de éste, mayor resultó ser la actividad catalítica en la ORR.

Esta tendencia es ampliamente observada en la bibliografía. Otro ejemplo puede ser encontrado en el trabajo de Miao y col. [103], en el cual prepararon óxido de grafeno reducido dopado con nitrógeno a través del método hidrotermal, seguido de un tratamiento térmico. La temperatura del tratamiento térmico permitió controlar el contenido de las especies nitrogenadas. El contenido en nitrógeno piridínico aumentó conforme lo hacía la temperatura (de 600 a 800ºC), así como la actividad catalítica de los materiales resultantes, lo que sugiere que las especies nitrogenadas piridínicas son los centros activos de estos materiales carbonosos dopados con nitrógeno. Por otro lado, Ensafi y col. [104] estudiaron la alta actividad catalítica de óxido de grafeno reducido y, posteriormente, funcionalizado con piridinas (Py-EGO), en comparación con un material carbonoso dopado con nitrógeno preparado mediante método hidrotermal en presencia de amoniaco (NrGO). El material Py-EGO presentó mayor contenido en grupos piridínicos y mayor actividad catalítica que el NrGO. Chang y col. [105] contrastaron el papel de las especies piridínicas en la ORR a través del test de la actividad catalítica de nanoláminas de grafeno dopadas con un alto contenido en grupos piridínicos y su comparación con las muestras sin dopar. Las muestras con alto contenido en grupos piridínicos mostraron mayor actividad catalítica que aquellas que no fueron dopadas, lo que evidencia el papel crucial de los grupos piridínicos. Por otro lado, Lv y col. [106] reportaron la formación selectiva de grupos piridina en "graphdiyne" (2-grafino) sustituido con hidrógeno (HsGDY) y que estas especies dan lugar a un actividad catalítica elevada en la ORR.

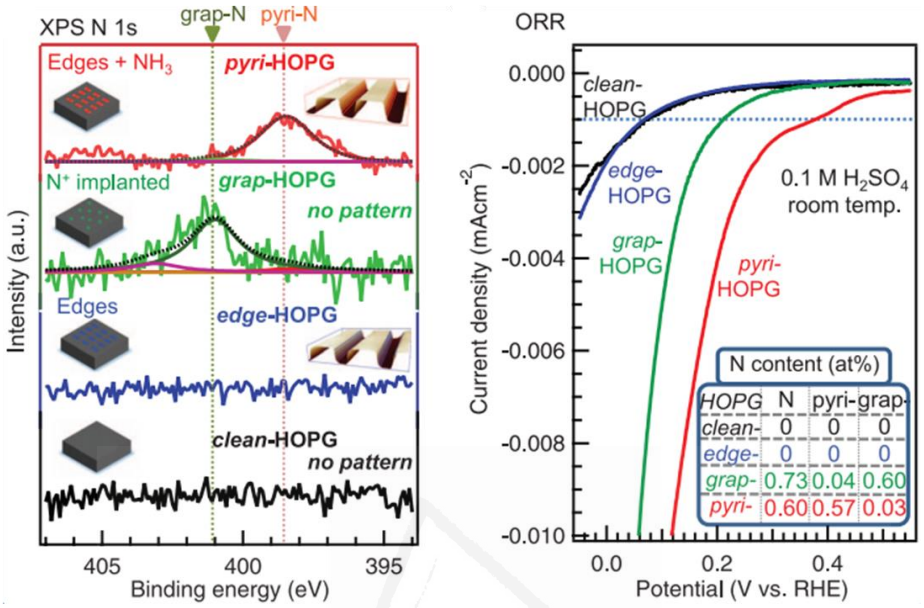

Figura 1.4: Espectros N1s (izq) y resultados ORR (dcha) de los materiales HOPG inicial (clean-HOPG), HOPG con defectos (edge-HOPG), HOPG con especies de nitrógeno cuaternario (grap-HOPG) y HOPG con especies de nitrógeno piridínicos (pyri-HOPG) [Adaptado de Ref. 107].

Sin embargo, uno de los trabajos más interesantes hasta la fecha es el realizado por Guo y col. [107], en el cual los autores caracterizaron los sitios activos de la ORR en materiales carbonosos dopados con nitrógeno obtenidos a partir del dopado bien controlado de HOPG (clean-HOPG) (Figura 1.4). Con este propósito, las muestras de clean-HOPG fueron bombardeadas con un haz de iones de Ar^+ a través de una delgada lámina metálica para crear un material con alta concentración de sitios borde (edge-HOPG). Este edge-HOPG fue expuesto a un tratamiento térmico a 973K en una atmósfera de NH_3, creando la muestra pyri-HOPG que tan solo contenía especies nitrogenadas tipo piridina según el análisis XPS. Del mismo modo, clean-HOPG fue tratado a 1073K bajo ultra alto vacío (UHV) durante 15 min y, después, esta muestra fue dopada con nitrógeno mediante el bombardeo con haces de iones de nitrógeno a 600K. La muestra obtenida, denominada grap-HOPG tan solo presentó especies de nitrógeno cuaternario. Todos estos materiales fueron evaluados en la ORR en electrolito ácido. pyri-HOPG fue la muestra que mostró una mayor actividad catalítica, aunque también se observó una mejora significativa para la muestra

grap-HOPG. Merece señalar que los análisis mediante XPS tras la reacción, post-ORR, demostraron la transformación de las especies piridina en especies nitrógeno tipo piridona. Los autores emplearon las diferencias en el análisis XPS antes y después del test catalítico para proponer al átomo de carbono adyacente al átomo de nitrógeno piridínico como sitio activo y no las especies piridinas por sí solas.

En el mismo contexto, tres materiales de varias capas de grafeno dopados con nitrógeno fueron obtenidos a partir de óxidos de grafeno y diferentes tratamientos de dopado y fuentes de nitrógeno [108]. Los análisis XPS posteriores al test catalítico mostraron un incremento en la cantidad de especies OH en los átomos de carbono adyacentes al heteroátomo y, consecuentemente, se atribuyó a la generación de especies piridona durante la catálisis de la ORR (Figura 1.5A). Esto fue relacionado con la formación de etapas intermedias de la reacción en materiales carbonosos con especies nitrogenadas tipo piridinas, donde el dioxígeno reaccionaría a través del átomo de carbono vecino a través de una configuración terminal C-O-O, creando, así, especies N-C-O durante la ORR [108].

Sin embargo, estas interesantes observaciones sugieren una pregunta importante: ¿son estas especies piridínicas las responsables de la creación de los sitios activos de la ORR o lo son los grupos tipo piridona formados en los estados iniciales de la reacción? La siguiente sección evalúa las especies N-C-O como sitios activos en la ORR, pero antes de tratar esta temática, es importante entender los mecanismos de la ORR propuestos mediante química computacional para especies tipo piridina.

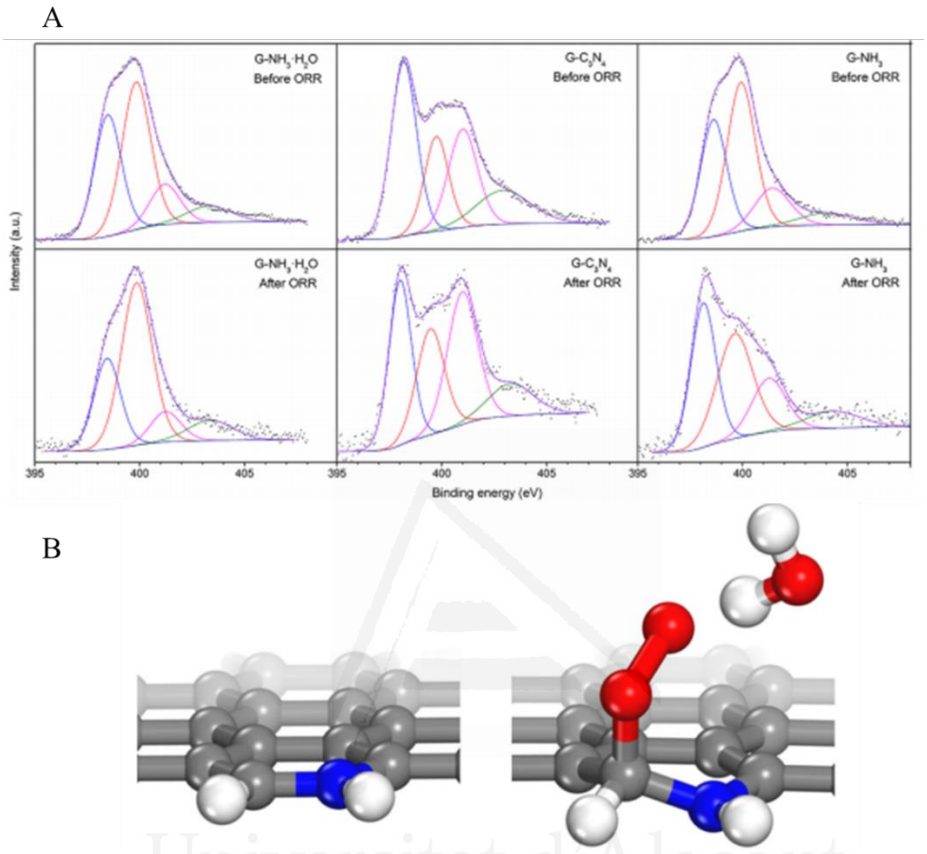

Figura 1.5: (A) Espectros XPS de tres materiales carbonosos antes y después del análisis en la ORR [Adaptado de Ref. 108]. **(B)** Ilustración de la geometría de un grupo funcional piridínico en posición "armchair" antes y después de la quimisorción de oxígeno [Adaptado de Ref. 118].

El modo de enlace tipo terminal es el más ampliamente aceptado en la ORR para especies tipo piridina. Esto significa que el oxígeno molecular se adsorbe mediante una configuración C-O-O. Sin embargo, si el mecanismo es asociativo o disociativo aún está en controversia para este sitio activo. Mientras que algunos autores demostraron un mecanismo cercano a 4 (o 2+2) electrones para materiales carbonosos con alto contenido en grupos piridínicos [98,109,110], otros reportaron una alta selectividad hacia la formación de peróxido de hidrógeno [111–115]. En electrolito ácido, la formación de H_2O_2 por las especies piridina fue demostrado por Sun y col. [113]. La pirólisis del material

carbonoso CMK-3 junto con polietilimina (PEI, por sus siglas en inglés) condujo a la formación de un material carbonoso rico en nitrógeno con la gran mayoría de los grupos funcionales en forma de piridinas, que alcanzó una selectividad hacía la formación de peróxido de hidrógeno superior al 95%. Por otro lado, el mecanismo de cuatro (o 2+2) electrones parece predominar en medio alcalino [98,109,110]. Por tanto, el electrolito usado juega un papel importante en la selectividad de los materiales carbonosos ricos en grupos piridina. Se propuso un mecanismo detallado para las rutas de 2 y 2+2 electrones en materiales carbonosos que contienen especies piridina de tipo "armchair", en las que el electrolito puede determinar la ruta que se sigue durante la reacción (Figura 1.6) [107]. Aquí es importante no obviar factores como la porosidad o el área superficial que también pueden jugar un papel clave (ver sección 1.3.1).

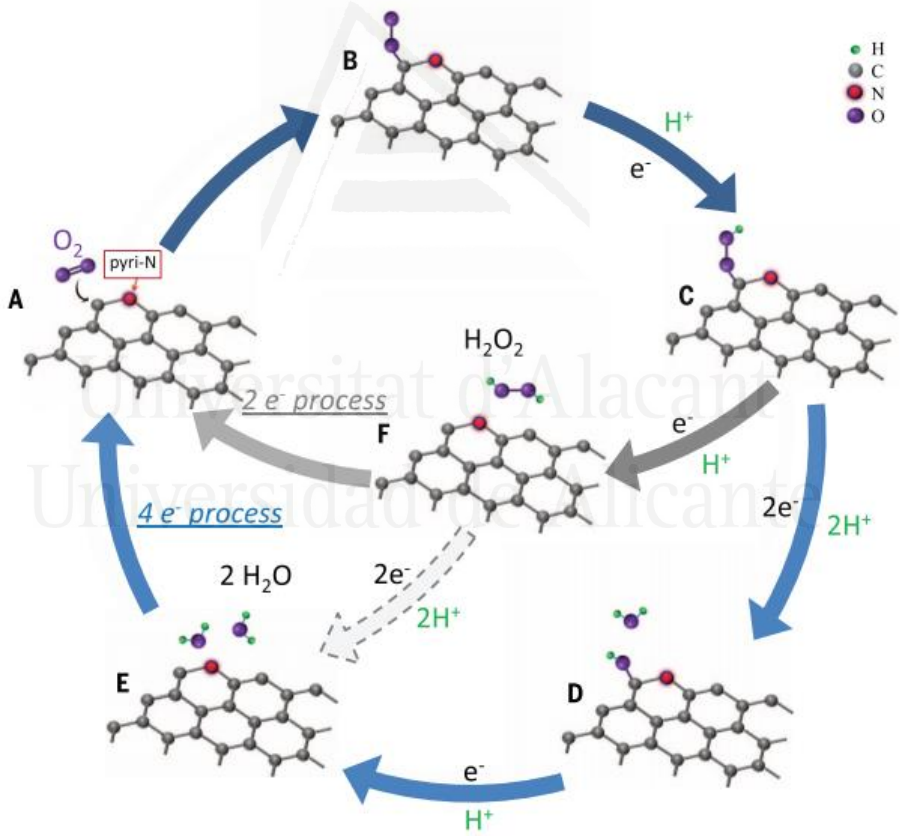

Figura 1.6: Mecanismo de la ORR en especies de nitrógeno piridínico en posición armchair [Adaptado de Ref. 107].

Las especies nitrogenadas tipo piridina no son solo las especies de nitrógeno más evaluadas en la ORR desde un punto de vista experimental, sino que también lo son desde el enfoque de química computacional. Cálculos DFT mostraron que el nitrógeno tipo piridina en posición "armchair" mejora la adsorción del oxígeno molecular en el átomo de carbono adyacente al heteroátomo gracias a la, ya comentada, densidad de carga positiva generada y la alta densidad de spin en el átomo de carbono debido a la mayor electronegatividad del átomo de nitrógeno y, por tanto, su efecto de electrón-atrayente [75]. No obstante, la evaluación del nitrógeno piridínico en posición zigzag mostró una pobre actividad catalítica [116], siendo ésta menor que la del material carbonoso sin dopar. Una explicación más detallada de este trabajo se presenta en el Capítulo V de la presente Tesis Doctoral. El átomo de carbono adyacente a un nitrógeno tipo piridina en posición zigzag requiere de una mayor energía para modificar su hibridación. Siguiendo con esta tendencia, Huang y col. [117] reportaron que los grupos tipo piridina en estas posiciones zigzag no aportaban ningún beneficio en la catálisis de la reducción de oxígeno. Con el objetivo de profundizar en este aspecto, Ferre-Vilaplana y col. [118] evaluaron y compararon la quimisorción del oxígeno en grupos piridina con diferente estructura y posición en la lámina de grafeno (posición zigzag y "armchair") (Figura 1.5B). Es interesante señalar que la quimisorción del oxígeno molecular en el átomo de carbono adyacente al de un átomo de nitrógeno piridínico en posición "armchair" es más favorable en comparación con la quimisorción en el átomo de carbono adyacente de un nitrógeno piridínico en posición zigzag. Los resultados obtenidos confirmaron la formación de grupos tipo N-C-O-O a través de la adsorción de la molécula de O_2 en el átomo de carbono adyacente a especies piridina en posición "armchair" (Figura 1.5B).

Todos estos estudios revelan el papel fundamental que juega la posición de las funcionalidades y, consecuentemente, la estructura local del material carbonoso en la ORR. Esto también ayuda a entender la gran variedad de resultados que se pueden encontrar en la bibliografía, pues la concentración de sitios zigzag o "armchair" de los grupos piridina en materiales carbonosos dependerá en gran medida de los métodos de preparación y de los precursores utilizados. Además, esta discusión da pie al estudio del catalizador después de su uso o, idealmente, bajo condiciones in situ ("operando").

1.3.2.1.2. Grupos nitrogenados tipo piridona

La evaluación de especies N-C-O como sitios activos en materiales carbonosos dopados con nitrógeno está estrechamente relacionada con la presencia de átomos de nitrógeno en forma de piridina ya que, como hemos comentado anteriormente, el átomo de carbono adyacente al nitrógeno piridina parece reaccionar con el dioxígeno creando especies N-C-O como intermedios de la reacción, pero que también se detectan tras la reacción. Por tanto, se plantea la cuestión de si el sitio activo lo constituyen las especies tipo piridina o las piridonas que se forman. En esta sección, se presentan varios ejemplos de trabajos que proponen que la actividad catalítica proviene de estas especies N-C-O.

Uno de estos trabajos fue desarrollado durante la presente Tesis Doctoral y se tratará de forma más extendida en el Capítulo III. A modo de resumen, la polianilina fue tratada térmicamente bajo dos condiciones: en atmósfera inerte y en presencia de una atmósfera ligeramente oxidante hasta 800ºC. La caracterización de los materiales resaltó el hecho de que la utilización de una atmósfera oxidante resultaba en un incremento de los sitios tipo N-C-O, lo que también originó una mejora de la actividad catalítica de los materiales en comparación con su equivalente en atmósfera inerte. Esto sugirió que tales especies N-C-O pueden no ser solo intermedios de reacción, sino también sitios activos en los que la ORR se ve favorecida.

La alta actividad catalítica de especies N-C-O se apoya, también, en otros interesantes trabajos. Por ejemplo, Li y col. [119] sintetizaron nanotelas de carbón dopadas con nitrógeno y oxígeno mediante la pirólisis de nanotelas de polipirrol y posterior activación con KOH. El efecto sinérgico entre los átomos de oxígeno (procedentes de la activación con KOH) y los grupos nitrogenados (del precursor) condujeron a la creación de grupos tipo piridona en la matriz carbonosa. Los materiales co-dopados exhibieron una alta actividad catalítica que no ocurre cuando el material se sintetiza sin la incorporación del oxígeno. Silva y col. [120] reportaron la síntesis de materiales carbonosos co-dopados con oxígeno y nitrógeno vía pirólisis de composites PANI/SBA-15. De nuevo, la alta actividad catalítica de los materiales fue atribuida a un efecto sinérgico del oxígeno (procedente de la sílice) y de las especies nitrogenadas (del precursor polimérico).

A pesar de la baja popularidad de las especies piridona como sitios activos hacia la ORR, el descubrimiento del intermedio N-C-O en la reducción de oxígeno ha producido un importante incremento del número de publicaciones relacionadas con el co-dopado con átomos de O y N en materiales carbonosos para la electrocatálisis de la ORR [71,121–123].

La estructura de las especies piridona responsables de la actividad catalítica está estrechamente relacionada con la discusión incluida en la sección anterior. Solo los grupos piridona en posición "armchair" serían responsables de una alta actividad catalítica. Así, los sitios borde tipo "armchair" serían preferibles para crear una alta concentración de sitios activos.

Cálculos computacionales mediante DFT estudiaron la actividad catalítica de estas especies piridona en la reacción de reducción de oxígeno, obteniéndose resultados que indican que estas especies presentan un mejor comportamiento catalítico que los materiales carbonosos sin dopar. Los resultados obtenidos se muestran en más detalle en los capítulos III y V de la presente Tesis Doctoral. A modo introductorio se puede mencionar que los átomos de nitrógeno y de oxígeno retiran carga del átomo de carbono con el que están enlazados, generando en este último una fuerte densidad de carga positiva, en la cual el oxígeno puede verse atraído, quimisorbido y posteriormente reducido.

1.3.2.1.3. Grupos nitrogenados tipo pirrol

Los átomos de nitrógeno pirrólicos son aquellos que se encuentran en un anillo heterocíclico de cinco miembros y que están enlazados a dos átomos de carbono. Estas especies nitrogenadas son poco abundantes en materiales carbonosos debido a su baja estabilidad térmica, lo que hace que tras tratamientos térmicos o carbonizaciones la concentración de estos grupos funcionales sea baja [124]. Este hecho queda reflejado en el estudio de Lin y col. [125], que tras la carbonización de polipirrol a 1000ºC, el cual inicialmente posee el 100% de sus nitrógenos en forma de pirroles, los grupos pirrólicos desaparecen completamente. A pesar de esto, varios trabajos asocian la actividad catalítica de los materiales carbonosos con la cantidad de átomos de nitrógeno en forma de pirroles.

Por ejemplo, Li y col. [126] proponen la transformación de especies piridínicas en grupos funcionales tipo pirrol a altas temperaturas. El incremento observado en la actividad catalítica fue considerado como indicativo de la alta actividad de los grupos pirrólicos. Por otro lado, Unni y col. [127] observaron

una relación entre el contenido en grupos pirrol y la actividad catalítica de grafeno dopado con nitrógeno. Los autores propusieron que el alto contenido en grupos tipo pirrol junto con el incremento en el área específica eran responsables de la alta actividad catalítica del material carbonoso obtenido a partir del tratamiento térmico a diferentes temperaturas (800-1000ºC) de óxido de grafeno con monómero pirrol adsorbido. Li y col. [128] estudiaron la síntesis de materiales carbonosos con alto contenido en nitrógeno soportados sobre una plantilla SBA-15. La actividad catalítica más alta fue alcanzada en el material carbonoso que poseía la mayor cantidad de especies piridina y pirrol. En el mismo sentido, Feng y col. [129] reportaron la síntesis de materiales carbonosos dopados con grupos piridina y pirrol empleando la misma plantilla SBA-15. Los materiales obtenidos presentaron actividades catalíticas similares a las del catalizador comercial de platino.

En base a resultados de XPS de alta resolución y resultados experimentales de la actividad catalítica de negros de carbón dopados con nitrógeno, Liu y col. [130] propusieron el siguiente orden en la actividad catalítica de los diferentes grupos funcionales nitrogenados: nitrógeno tipo piridina > nitrógeno pirrólico > nitrógenos cuaternarios o grafíticos > grupos nitrogenados oxidados > material carbonoso sin dopar, destacando la alta actividad catalítica de los grupos nitrogenados en forma de pirrol así como la actividad catalítica de los grupos piridina [130].

En lo que concierne a los mecanismos de reacción propuestos para estas especies, diferentes autores sugirieron que los materiales carbonosos dopados con especies nitrogenadas tipo pirrol, inducen la reducción de oxígeno a través de una ruta de 4 electrones mediante una quimisorción tipo puente en las proximidades del átomo de nitrógeno [131]. Posteriormente, las etapas de reducción conducirían a una ruptura del enlace O-O, dando lugar a la formación de dos intermedios C-O-H, los cuales dan lugar a la formación final de dos moléculas de agua [131].

Sin embargo, cabe señalar que estas afirmaciones se basan en la difícil interpretación de los espectros XPS, pues resulta imposible diferenciar las especies nitrogenadas tipo pirrol de las especies N-C-O o piridona, ya que aparecen a la misma energía de ligadura. De hecho, no es difícil encontrar en la literatura trabajos que solo asignan el pico de XPS de 400.5 eV a los grupos nitrogenados tipo pirrol, obviando de esta manera la posible presencia de grupos

piridona. Por tanto, teniendo en cuenta la baja estabilidad de los grupos pirrólicos a altas temperaturas, la dificultad de una identificación sencilla (que puede confundirse con grupos piridona) y que los grupos piridona pueden generar alta actividad catalítica (ver sección 1.3.2.1.2), puede entenderse que la mayor parte de la comunidad científica considere a los grupos tipo pirrol como especies no activas para la ORR [99,116,132–135].

1.3.2.1.4. Grupo nitrógenos cuaternarios.

Junto con los grupos piridina, los nitrógenos cuaternarios o también conocidos como grafíticos son una de las funcionalidades de nitrógeno que más han sido propuestas como sitios activos en la ORR. No obstante, la mayoría de estos trabajos no distinguen entre nitrógenos cuaternarios de tipo borde o de tipo basal y, simplemente, atribuyen, de manera general, la alta actividad de algunos materiales carbonosos dopados con nitrógeno a estas especies. Sin embargo, estas presentan grandes diferencias estructurales y, en consecuencia, una gran diferencia en actividad catalítica hacía la ORR. Este aspecto fue estudiado en profundidad con cálculos DFT mediante la evaluación de las energías libres de Gibbs de las diferentes etapas en la reacción de reducción de la molécula de oxígeno, en láminas de grafeno con diferente localización del átomo de nitrógeno cuaternario [136]. No solo la posición del nitrógeno cuaternario parece tener un efecto en la actividad catalítica, sino también en la selectividad [136].

A pesar de no ser muchos, existen algunos trabajos que mencionan explícitamente a los nitrógenos cuaternarios basales como responsables de la actividad catalítica de ciertos materiales carbonosos. Por ejemplo, Gong y col. [30] explicaron la catálisis altamente eficiente hacia la ORR de CNTs dopados con nitrógeno por la presencia de átomos de nitrógeno cuaternarios basales. Estos átomos de nitrógeno pueden aportar electrones al sistema π de la lámina de grafeno, lo que resulta en un incremento del carácter nucleofílico de los átomos de carbono vecinos [30]. Consecuentemente, aumenta la adsorción del oxígeno y la ORR mejora.

Sin embargo, estudios computacionales y experimentales contradicen este argumento previo. Flyagina y col. [137] evaluaron mediante cálculos DFT, la variación de energía en la adsorción de oxígeno en un nitrógeno cuaternario situado en el plano basal de una lámina de grafeno. Conforme la distancia entre el oxígeno molecular y la matriz carbonosa disminuía de 2.8 a 1.6 Å, la energía

aumentaba gradualmente. Este hecho es indicativo del gran coste energético necesario para que la quimisorción del oxígeno tenga lugar en el átomo de carbono adyacente a esta especie nitrogenada. Esta conclusión fue apoyada por Ikeda y col. [116], quienes demostraron que la quimisorción del O_2 en la vecindad de los nitrógenos cuaternarios de tipo basal es menos favorable que en un material carbonoso sin dopar desde un punto de vista termodinámico.

Se puede concluir que la quimisorción de la molécula de oxígeno en los sitios generados por los átomos de nitrógeno cuaternarios basales, no es favorable debido a la dificultad en el cambio de hibridación de los átomos de carbono en la lámina de grafeno. Tal y como ocurría con los grupos piridina en posición zigzag, el átomo adyacente al nitrógeno cuaternario se encuentra en una situación de hibridación sp^2 en el centro de la matriz carbonosa. Al no encontrarse en un borde, el cambio de hibridación conlleva un coste energético mayor y, de este modo, la quimisorción del oxígeno se encuentra impedida termodinámicamente.

Los nitrógenos cuaternarios de tipo borde, junto con los grupos piridina, son las funcionalidades más propuestas en la bibliografía como sitios activos hacia la ORR en materiales carbonosos dopados con nitrógeno. El nitrógeno cuaternario en posición basal se localiza en el interior de la lámina de grafeno lo que promueve una variación de la densidad de carga en su interior. Sin embargo, como se ha explicado anteriormente, esta configuración no permite la quimisorción del oxígeno molecular en los átomos de carbono vecinos [116,136,138]. No obstante, la introducción de esta especie nitrogenada cercana a los bordes de la lámina facilita la retirada de electrones en los átomos de carbono del borde, siendo éste un factor crítico para entender la actividad catalítica de estas especies.

La alta actividad catalítica producida por los nitrógenos cuaternarios de tipo borde fue propuesta por Sharifi y col. [139] en un estudio en el que analizaban la temperatura del tratamiento térmico para generar CNTs dopados con nitrógeno. Estos autores propusieron que el tratamiento a altas temperaturas generaba una transformación de los grupos piridina y pirrol en nitrógenos cuaternarios de tipo borde debido a reacciones de condensación (N-Qvalley a partir de grupos pirrol y N-Qvalley y NQ-centre a partir de grupos piridina, Figura 1.7A) [139]. Los grupos en los bordes (N-Qvalley) son los responsables de la alta actividad catalítica observada con el aumento de la temperatura de

tratamiento (Figura 1.7A). Estas reacciones de transformación de grupos nitrogenados son conocidas desde que Pels y col. las propusiesen en 1995 [140].

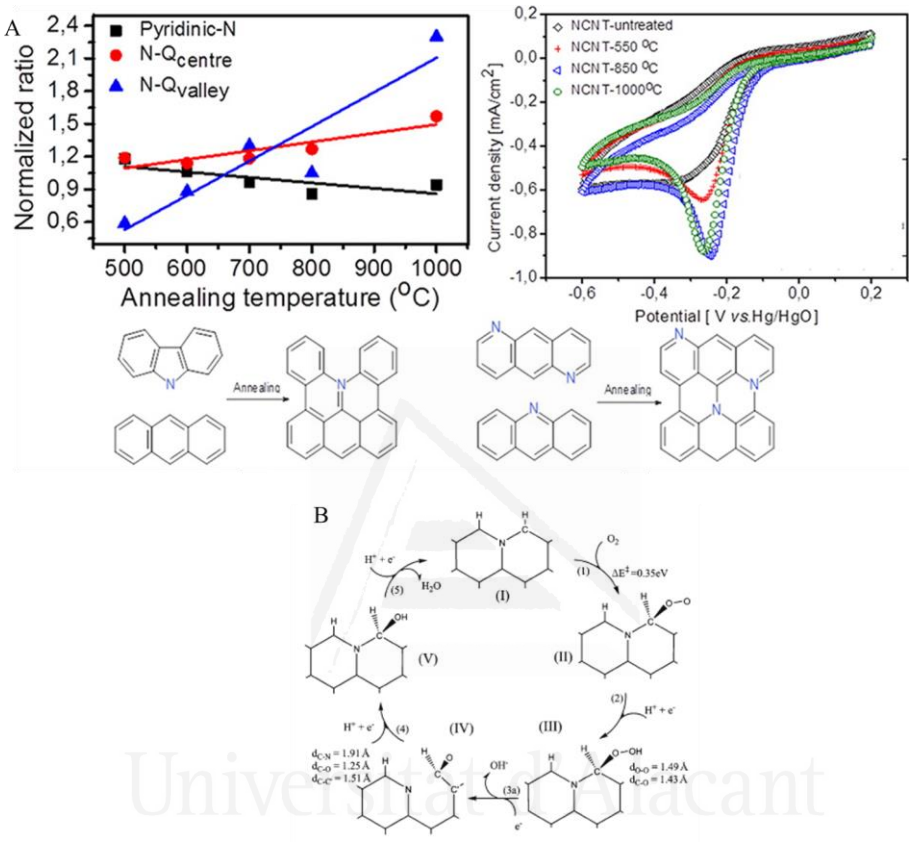

Figura 1.7: (A) Relación normalizada de los grupos funcionales de nitrógeno vs. temperatura del tratamiento térmico. Voltagramas de CNT dopados con nitrógeno (NCNT) a diferentes temperaturas junto con la propuesta del mecanismo de la reacción de condensación en la que nitrógenos en forma de piridinas y pirroles se transforman en nitrógenos cuaternarios en posición zigzag [Adaptado de Ref. 139)]. **(B)** Ciclo catalítico de la ORR para nitrógenos cuaternarios en posición zigzag que involucran la ruptura del anillo [Adaptado de Ref. 138].

Este mismo efecto se ha observado al tratar térmicamente un polímero rico en nitrógeno, como la polianilina, a temperaturas superiores a 1100ºC. Este estudio se presentará con más detalle durante el desarrollo del Capítulo IV de esta Tesis Doctoral. Igualmente, a modo resumen, se puede destacar que el tratamiento térmico a altas temperaturas de la polianilina condujo a la

transformación de grupos piridina y piridona en nitrógenos cuaternarios. Las temperaturas del tratamiento térmico más altas (superiores a 1100ºC) resultaron en un material carbonoso con un alto porcentaje del nitrógeno en forma de nitrógeno cuaternario. Junto con esta transformación, la actividad catalítica de los materiales mejoró hasta valores similares a los del catalizador comercial de platino.

El mecanismo de la ORR para estas especies de nitrógeno cuaternario sigue aún bajo debate. Fundamentalmente, son dos los mecanismos que han sido planteados para este grupo funcional nitrogenado, en el que intervienen uno o dos átomos de carbono, que dan lugar a diferentes caminos de reducción del oxígeno. Kim y col. [138] reportaron la quimisorción a través de un único átomo de carbono, el cual resulta en la reducción del oxígeno molecular a través de un mecanismo de cuatro electrones, donde se produce una ruptura del enlace N-C y, consecuentemente, se produce la apertura del anillo de seis átomos (Figura 1.7B). Este modo de quimisorción puede verse más favorecido con la presencia de defectos adyacentes a los nitrógenos cuaternarios en el borde como, por ejemplo, carbenos [64].

No obstante, el mecanismo de quimisorción que parece estar más aceptado en la bibliografía consiste en la adsorción a través de dos átomos de carbono, con un enlace tipo puente C-O-O-C en el que cada átomo de oxígeno se enlaza con un átomo de carbono diferente [51,116,136,141]. Esto es posible en esta especie ya que dos de los tres átomos de carbono vecinos al heteroátomo se encuentran en una posición borde. Una vez el oxígeno es adsorbido con esta configuración, la introducción del primer par electrón-protón, es decir, en la primera etapa de reducción, el enlace O-O se rompe dando lugar a la formación de un enlace de hidrógeno entre ambos átomos de oxígeno. Este mecanismo disociativo finalmente conduce a la formación de dos moléculas de agua y, por lo tanto, transcurre a través de una reacción con cuatro electrones, pero sin la apertura del anillo. Se presentará una explicación más profunda en los Capítulos IV y V de la presente Tesis Doctoral.

1.3.2.2. Materiales carbonosos dopados con fósforo

El átomo de fósforo posee la misma configuración electrónica de los electrones de valencia que el átomo de nitrógeno; sin embargo, su electronegatividad es menor que la de los átomos de nitrógeno y carbono. Además, el fósforo puede utilizar sus orbitales 3d para formar enlaces. El dopado con fósforo en materiales carbonosos ha sido ampliamente estudiado por sus interesantes propiedades para inhibir la gasificación del carbón [142,143]. Esto hace del dopado con fósforo una metodología muy atractiva para la protección de los materiales carbonosos frente a la oxidación [144,145] y para su uso como material ignífugo [146]. Los grupos funcionales de fósforo conllevan modificaciones efectivas en las propiedades eléctricas y la reactividad química de los materiales carbonosos, dando lugar a numerosas aplicaciones, especialmente en catálisis [146,147], debido a sus propiedades ácidas.

En el campo de la catálisis de la ORR, las investigaciones acerca del dopado con fósforo en materiales carbonosos no abundan en comparación con el nitrógeno. Esto se debe, principalmente, a que la mejora de la actividad catalítica obtenida por estos materiales no es tan significativa. A pesar de esto, es posible encontrar algunos trabajos sobre el dopado con fósforo de materiales carbonosos para su uso como electrocatalizadores en la ORR [147].

En 2011, Liu y col. [148] estudiaron la síntesis de materiales de grafito dopados con fósforo, así como su evaluación en la catálisis de la reducción de oxígeno. El grafito dopado con fósforo se preparó a través de la pirólisis de tolueno y trifenilfosfina (TPP, por sus siglas en inglés) a 1000ºC. Con propósitos comparativos, se realizó el mismo procedimiento en ausencia de TPP. La introducción de átomos de fósforo en la estructura carbonosa se confirmó por XPS y la evaluación de la actividad catalítica evidenció el efecto beneficioso de los átomos de fósforo. En este mismo contexto, Guo y col. [149] compararon CNTs dopados con fósforo (P-CNT) y CNTs sin dopar. Al introducir fósforo en los nanotubos de carbono se observó una mejora en la actividad catalítica, tanto en el potencial de inicio de la reacción como en la densidad de corriente límite (Figura 1.8A). Sin embargo, estos trabajos no entran en detalle a la hora de explicar el origen de esta mejora en la actividad catalítica. Por el contrario, Yang y col, [150] atribuyeron la mayor actividad catalítica de carbones mesoporosos dopados con P a los átomos de fósforo enlazados covalentemente en la red carbonosa.

El efecto positivo del dopado con P, también ha sido relacionado con el aumento de la concentración de defectos que, generalmente, conlleva el proceso de dopado del material [151]. Estos defectos pueden incrementar la deslocalización electrónica, gracias a las buenas propiedades electrón-dador del átomo de fósforo, favoreciendo la ORR [152].

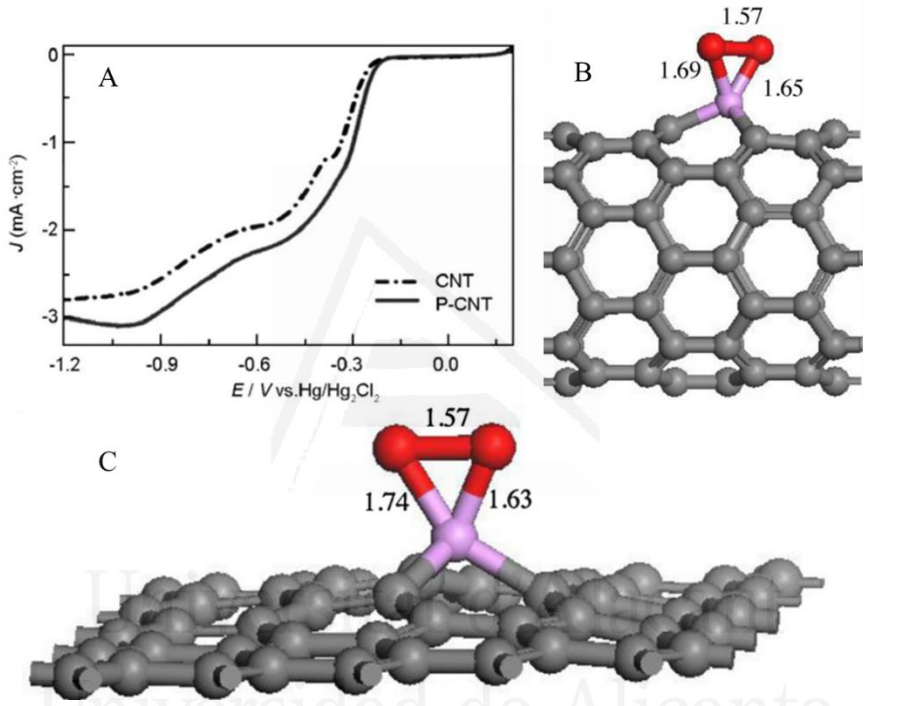

Figura 1.8: (A) Curvas LSV de CNT sin dopar (CNT) y CNT dopados con fósforo (P-CNT) a una velocidad de barrido de 5 $mV \cdot s^{-1}$ y una velocidad de rotación de 1600 rpm en una disolución de KOH 0,1 M saturada en oxígeno [Adaptado de Ref. 149]. **(B)** Estructura optimizada de la adsorción de oxígeno en un CNT dopado con fósforo [Adaptado de Ref. 153]. **(C)** Estructura optimizada de la adsorción de oxígeno en grafeno dopado con fósforo [Adaptado de Ref. 153].

Para obtener información más detallada acerca de la naturaleza de los sitios activos y comprender si los átomos de fósforo juegan un papel directo en la catálisis de la ORR, los diferentes grupos funcionales de fósforo se evaluaron mediante simulaciones DFT [153]. La adsorción del oxígeno molecular en grafeno y en nanotubos de carbono se ve favorecida por la presencia del fósforo.

Las moléculas de oxígeno se enlazan en una configuración tipo puente en la que ambos átomos de oxígeno se unen con el átomo de fósforo, generando así dos enlaces P-O (Figura 1.8B y 1.8C) [153]. Tras la quimisorción de la molécula de oxígeno, la reducción pueden darse a través de la disociación de la molécula de oxígeno o bien la hidrogenación para formar especies OOH, siendo esta segunda posibilidad la más favorable [154]. Sin embargo, es importante destacar que estos estudios teóricos no tienen en cuenta que el P puede inducir la formación de defectos que pueden ser esenciales para entender la actividad catalítica, como sugieren otros autores [151,152].

Si bien el dopado con fósforo no parece producir una mejora importante en la actividad catalítica en la ORR, el co-dopado con otro heteroátomo (especialmente nitrógeno) está ganando mucha atención en los últimos años. Esto se debe a que el cambio en las propiedades electrónicas locales de los materiales carbonosos codopados puede aumentar la actividad catalítica hacía la reacción de evolución de oxígeno (OER), lo que es útil para el diseño de catalizadores bifuncionales en pilas de combustible reversibles [155,156].

En este sentido, Zhang y col. [157] desarrollaron un enfoque alternativo para preparar materiales carbonosos mesoporosos, con estructura tridimensional, con grupos funcionales de nitrógeno y fósforo a partir de la pirólisis de polianilina dopada con fósforo, obtenida a partir de la polimerización química de la polianilina en presencia de ácido fítico. El material obtenido no solo muestra una excelente actividad catalítica hacia la ORR, sino que también lo hace en la OER [157]. Los autores, en base a cálculos DFT, asocian esta actividad a un efecto sinérgico entre ambos grupos funcionales en la matriz carbonosa [157]. Este efecto sinérgico positivo también fue propuesto por Borghei y col. [158]. Los autores reportaron materiales electroactivos obtenidos a partir de carbones activados conteniendo nitrógeno y fósforo. Estos materiales se obtuvieron mediante activación con ácido fosfórico a 550ºC para, posteriormente, someter a dicho material a un nuevo tratamiento en presencia de urea como fuente de nitrógeno [158]. A pesar del bajo contenido en nitrógeno, la actividad de la ORR aumentó significativamente después del tratamiento con urea [158]. Además del efecto sinérgico, la actividad catalítica observada en los catalizadores basados en materiales carbonosos se atribuyó también a la presencia de mesoporos y la gran proporción de nitrógeno grafítico y piridina [158] . Este efecto beneficioso no solo se ha observado en materiales carbonosos, sino también en polianilina dopada con P. La modificación con

grupos de fósforo de la polianilina es objeto de estudio en esta Tesis Doctoral y se presentará en el Capítulo IX más detalladamente.

No obstante, no todos los trabajos relacionados con el codopado de nitrógeno y fósforo atribuyen la mejora en la actividad catalítica a la presencia de ambos heteroátomos. Es posible que, también, el efecto beneficioso se deba a un aumento en el orden estructural que produce la presencia de fósforo durante la preparación de los materiales. Este hecho se ha observado en la preparación de fibras de carbón a partir de poliacrilonitrilo en presencia de pequeñas cantidades de ácido fosfórico [159]; dicho aumento en el orden estructural debería resultar en una mejora en la conductividad eléctrica, parámetro clave en la ORR (ver Sección 1.3.1).

En lo que concierne a los sitios activos en estos materiales, Li y col. [160] proponen, a través de simulaciones DFT, que los átomos de nitrógeno cuaternarios junto con los grupos de fósforo son los responsables de la mejora de la actividad catalítica. Además, se demostró que la ruta de codopado más favorable empieza con la introducción de átomos de fósforo y, posteriormente, con la introducción de las funcionalidades de nitrógeno [161]. Esto se explica considerando que la presencia de fósforo produce cambios estructurales locales que promueven la formación de grupos de nitrógeno cuaternario, donde los átomos de P actuarían como agente de autosacrificio al sustituirse por los átomos de nitrógeno [161].

1.3.2.3. Materiales carbonosos dopados con boro

Los materiales carbonosos dopados con boro pueden ser otra alternativa prometedora como catalizadores libres de metal. Del mismo modo que el fósforo, el átomo de boro posee una electronegatividad menor que el nitrógeno y el carbono. Este heteroátomo ha sido ampliamente estudiado en reacciones de inhibición de la reacción C-O_2 [162,163]. Algunos trabajos interesantes destacan el uso de catalizadores basados en materiales carbonosos dopados con boro con actividades catalíticas hacía la ORR cercanas a las obtenidas por los catalizadores comerciales basados en platino [164,165]. Comúnmente, la alta actividad de estos catalizadores se asocia con el carácter electrón-deficiente de los átomos de boro. Cálculos DFT demostraron que la mayor electronegatividad del átomo de carbono adyacente induce una densidad de carga positiva en el átomo de boro y esta densidad de carga positiva favorece la quimisorción del oxígeno. En contra del átomo del nitrógeno, donde el oxígeno se adsorbe en el

átomo de carbono adyacente, en los carbones dopados con boro, la adsorción de la molécula de oxígeno se produce directamente en el átomo de boro [72], de forma similar a como ocurre con el átomo de P. No obstante, esto solo ocurre en especies del tipo borinina, mientras que en los átomos de B sustitucionales en posición orto- con respecto a los sitios borde saturados con H, la quimisorción de la molécula de oxígeno se ve favorecida en los dos átomos de carbono vecinos [64]. Al igual que en el caso del fósforo, la introducción de boro en los materiales también puede inducir la formación de defectos que actúen como sitios activos hacia la ORR [151].

En cualquier caso, no es posible encontrar una gran cantidad de estudios sobre materiales carbonosos dopados con boro para la ORR que sugieran que se puedan diseñar catalizadores prometedores con tan solo este heteroátomo. Sin embargo, sí es posible encontrar numerosos estudios en los que se trabaja con materiales carbonosos dopados con boro y otro heteroátomo, generalmente nitrógeno.

Por ejemplo, Zao y col. [166] estudiaron dos rutas de síntesis diferentes para la preparación de CNTs dopados con B y N a través de la metodología del depósito químico en fase vapor. La primera de estas rutas consta de un dopado secuencial de boro y nitrógeno mediante el uso de trifenilborano en el CVD y, después, el tratamiento térmico del material en presencia de amoniaco con el fin de introducir especies de nitrógeno en la estructura carbonosa; de esta forma, las especies de N y de B se encuentran separadas entre ellas. Por otro lado, la segunda de las rutas se basa en el dopado simultaneo con boro y nitrógeno durante el CVD, el cual, conduce a la formación de especies N-B-C [166]. Los resultados experimentales y teóricos sugieren que las especies N-B-C no generan un aumento de la actividad catalítica en la ORR; sin embargo, las funcionalidades por separado sí que la mejoran (Figura 1.9A) [166].

No obstante, sí que han sido publicados trabajos en los que se ha propuesto el efecto sinérgico entre el B y el N como el principal responsable de la mejora en la actividad catalítica de la ORR. Así, Zheng y col. [167] sintetizaron y testaron grafeno dopado con boro y nitrógeno que presentó una mayor actividad catalítica hacia la ORR que los materiales carbonosos dopados con solo uno de los heteroátomos. En concreto, se propuso al átomo de boro en posición meta con respecto a los átomos de nitrógeno en grupos piridina como los centros activos para la ORR [167]. Cabe mencionar que Gong y col. [168] estudiaron

materiales carbonosos codopados con estos dos heteroátomos, los cuales presentaron una excelente actividad catalítica para la ORR, incluso mayor que los catalizadores comerciales de platino. Además, con el fin de obtener una mayor comprensión de estos fenómenos, los autores evaluaron mediante cálculos DFT cinco posibles configuraciones B-N en las que los heteroátomos de boro y nitrógeno podían encontrarse en un material carbonoso: (i) un par BN en el plano basal de las láminas de grafeno, (ii) un BN ubicado en los bordes, (iii) tres pares de BN en el borde, (iv) una larga línea de pares BN en los bordes de una lámina de nanografeno y (v) localizados en la interfase entre la especie BN y los dominios de grafeno (Figura 1. 9B). La quimisorción del oxígeno en la posición (i) se determinó como desfavorable termodinámicamente, mientras que la adsorción en las especies BN localizadas en el borde de las láminas de grafeno se veía fuertemente favorecida, lo cual indica la posible mejora de la actividad catalítica de los materiales [168]. Este estudio comparativo revela que la ruta del codopado con boro y nitrógeno puede jugar un papel clave en la mejora del rendimiento de catalizadores basados en materiales carbonosos, al menos en comparación con aquellos que solo son dopados con un único heteroátomo [168].

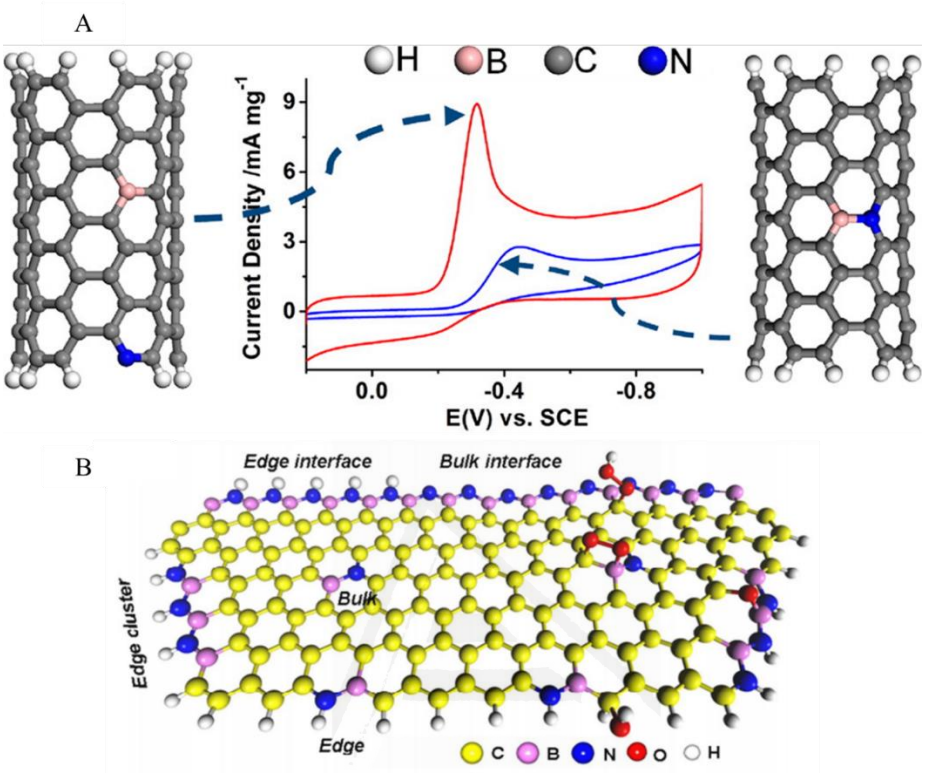

Figura 1.9: (A) Ilustración de configuraciones de especies N-B y su actividad catalítica en la ORR [Adaptado de Ref. 166]. **(B)** Representación esquemática de los modelos estructurales y sus intermedios de reacción en la ORR [Adaptado de Ref. 168].

En la búsqueda por conocer las razones de la alta actividad catalítica de estos materiales, Ozaki y col. realizaron varios estudios centrados en esta materia. En 2006, los autores demostraron que el dopado simultáneo con boro y nitrógeno en el material carbonoso es una forma efectiva de mejorar la actividad catalítica [169]. Además, encontraron que existe una estrecha relación entre la concentración de especies B-N-C superficiales y de nitrógeno en los bordes, con la actividad catalítica de los materiales en la ORR [170]. En 2010, profundizaron en el papel que ambos heteroátomos jugaban en la catálisis de la ORR mediante simulaciones DFT [171]. En ellas confirmaron la efectividad del codopado en materiales carbonosos al emplear boro y nitrógeno como heteroátomos. Se evaluó la adsorción del oxígeno, así como los siguientes pasos de reducción del oxígeno molecular sobre los grupos funcionales B-N- [171]. Cabe señalar que la fuerte interacción interatómica atractiva entre ambos heteroátomos ayuda al

nitrógeno a ocupar sitios específicos, en los que éste es más adecuado para catalizar la ORR [171]. No solo esto, las especies B-N son también responsables de la reducción de la energía libre de la adsorción de moléculas de oxígeno, lo que es indicativo de la mejora en la actividad catalítica. Más recientemente, también estudiaron el mecanismo por el cual la ORR transcurre en estos catalizadores [172]. Los autores propusieron una vía de 2+2 electrones, donde el oxígeno se reduce primero a peróxido de hidrógeno y éste, por la acción de las especies BN, se reduce para dar moléculas de agua [172].

1.3.2.4. Materiales carbonosos dopados con azufre

Es posible encontrar diferentes tipos de grupos funcionales de azufre en la superficie de un material carbonoso. Se pueden clasificar atendiendo al número de átomos de carbono unidos a los átomos de azufre: sulfuros o sulfóxidos (dos átomos de carbono) y tioles o tioquinonas (un átomo de carbono), también pueden encontrarse disulfuros. Las funcionalidades más comunes en materiales carbonosos son los tioles y los sulfóxidos [173].

El dopado con azufre en materiales carbonosos ha sido de interés general en la comunidad científica gracias a sus interesantes propiedades. Los materiales carbonosos dopados con azufre juegan un papel importante en la adsorción de gases [174], condensadores electroquímicos [175], baterías recargables [176], fotoactividad [177] e, incluso, aplicaciones electrónicas [178].

A pesar de que no son muchos los trabajos relacionados con el dopado del azufre, la introducción de este heteroátomo se ha propuesto, también, como una estrategia prometedora para la mejora de la catálisis en la ORR de materiales carbonosos. Uno de los ejemplos de estos estudios es el realizado por Yang y col. [179], quienes sugieren que el dopado con azufre aumenta la cantidad de sitios de tipo borde en los materiales carbonosos, además de aumentar el desorden estructural de las láminas de grafeno. Debido a todo esto, los autores atribuyen la mejora en la actividad catalítica a los cambios de densidad de spin originados por la introducción de dichos heteroátomos. Otro autores consideran que la presencia de azufre es, al igual que el fósforo y el boro, responsable indirecto de la mejora en la actividad catalítica [151]. Junto con la introducción de estos heteroátomos se genera, además, una importante cantidad de defectos en el material carbonoso [151]. Son estos últimos los que actúan como sitios activos según los autores.

Por otro lado, Wang y col. [180], estudiaron la síntesis de materiales carbonosos con estructura mesoporosa (OMC, por sus siglas en inglés) utilizando sacarosa como fuente de carbono. Con el fin de dopar las muestras con azufre, se siguió el mismo procedimiento, pero añadiendo disulfuro de bencilo como precursor del azufre (OMC-S). Del análisis mediante XPS, se detectaron dos estados de oxidación de los átomos de azufre correspondientes a grupos sulfuro y átomos de azufre oxidados [180]. La proporción de ambas especies varía según la cantidad de disulfuro de bencilo empleado en la síntesis, a mayor cantidad empleada, mayor la contribución de los grupos sulfuro. Interesantemente, todos los materiales muestran un potencial de inicio de la reacción de reducción de oxígeno muy parecido; sin embargo, la densidad de corriente limite aumenta con la cantidad de especies de sulfuro [180]. En el mismo sentido, Park y col. [181] estudiaron la síntesis de grafeno dopado con azufre a través del tratamiento térmico de grafeno en presencia de CS_2. El posterior análisis XPS reveló la formación selectiva de grupos tipo tiofeno. Una vez más, a mayor concentración de azufre en el material carbonoso, mayor resultó ser la densidad de corriente límite, sin observar cambios en el potencial de inicio de reacción. Estas observaciones están de acuerdo con el efecto del azufre en aumentar la concentración de defectos similares en actividad catalítica a los del material original, pero que no genera sitios más activos.

Seredych y col. [182] analizaron óxido de grafito reducido dopado con azufre (RGOS, por sus siglas en inglés). Para introducir átomos de azufre en RGO, el material se calentó hasta 800ºC en presencia de sulfuro de hidrógeno (1000 ppm de H_2S en atmósfera de nitrógeno), dando como resultado el dopado del RGO con azufre. Los autores atribuyeron la buena actividad catalítica del material RGOS a la presencia de ambos átomos, azufre y oxígeno, y que cuando ambos átomos se encuentran en concentraciones atómicas similares es cuando se alcanza el mejor efecto sinérgico en la ORR. No obstante, otros factores como la porosidad y la hidrofobicidad inducida por el azufre no pueden descartarse como responsables de la mejora en la actividad catalítica. Por lo tanto, en este artículo concluyen que no es solamente el azufre quien mejora las prestaciones hacia la ORR de los materiales carbonosos, sino que es la presencia del azufre junto con el oxígeno, quienes a través de un efecto sinérgico mejoran la actividad catalítica [182]. Estas conclusiones están en concordancia con otro trabajo que estudió el codopado de azufre y nitrógeno [183]. El efecto sinérgico

del azufre y el nitrógeno en estos materiales era lo que parecía mejorar la catálisis hacia la reducción de oxígeno.

Con el objetivo de demostrar el efecto positivo de los átomos de azufre hacia la ORR, Poh y col. [184] reportaron el dopado de azufre en grafeno durante la exfoliación térmica de óxido de grafito. Para ello, emplearon tres precursores de azufre diferentes (H_2S, CS_2 y SO_2). Las propiedades físicas y químicas de los materiales destacaron que todos los materiales de grafeno sin dopar mostraban un mayor número de defectos que su homólogo dopado con este heteroátomo, lo cual contradice la mayor parte de la bibliografía científica sobre esta materia. Interesantemente, el estado de oxidación del átomo de azufre fue similar para todos los materiales y fue asociado con la presencia de grupos de azufre oxidados (en forma de $-SO_3H$) para todos los precursores de azufre y para todos los métodos utilizados. La formación de sitios activos con mayor actividad catalítica hacia la ORR debido a la presencia de estos grupos de azufre fue confirmada ya que todos los materiales carbonosos dopados con azufre mostraron un potencial de inicio de reacción mayor que sus equivalentes sin dopar.

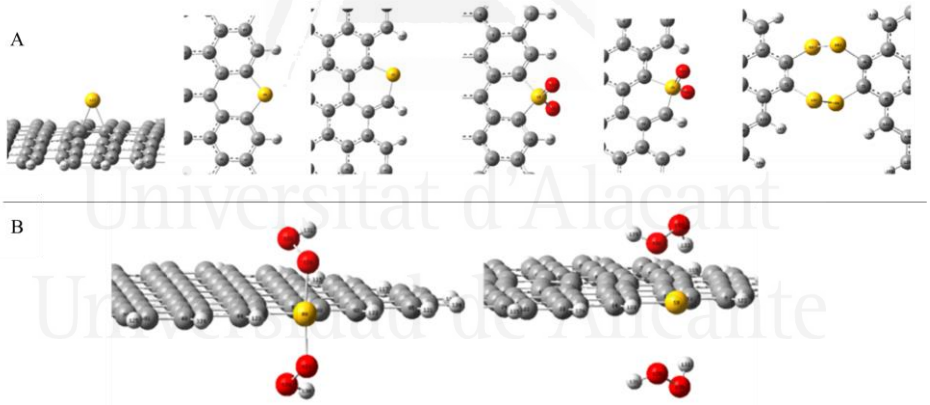

Figura 1.10: (A) Ilustración de posibles configuraciones de grafeno dopado con azufre [Adaptado de Ref.185]. **(B)** Mecanismo de 2 electrones en el modelo de grafeno dopado con especies de azufre [Adaptado de Ref. 185].

Con respecto a la química computacional, Zhang y col. [185] realizaron simulaciones DFT con el fin de entender el mecanismo de reacción y la naturaleza de los sitios activos en los materiales de grafeno dopado con azufre. Para ello, evaluaron cuatro estructuras de dopado con azufre: átomo de S adsorbido en la lámina de grafeno, introducción de un átomo de azufre en sitios

de tipo borde, especies -SO_2 en los bordes y anillos de azufre que conectan dos láminas de grafeno (Figura 1.10A). Las energías de formación de estas configuraciones resaltan que la quimisorción de azufre superficial es la más estable; además, los átomos de azufre en los sitios de tipo borde en posición zigzag tienen una energía de formación menor que la sustitución de azufre en las posiciones "armchair". Por otro lado, los resultados también indicaron que los defectos Stone-Walker facilitan el dopado de estos materiales con azufre. Con respecto a los sitios activos hacia la ORR en estos materiales, los autores concluyen que las densidades de carga y de spin determinan la actividad catalítica, y proponen que los átomos de azufre sustitucionales o los átomos de carbono en los bordes de la lámina en posición zigzag, o cercanos a las especies -SO_2 pueden ser sitios activos en la ORR [185].

En lo que respecta al mecanismo de reacción, el mecanismo que involucra 2 electrones parece ser la ruta más probable en el caso de los átomos de azufre sustitucionales (Figura 1.10B), mientras que la ruta de cuatro electrones tiene lugar en átomos de carbono con densidad de carga positiva o alta densidad de spin (Figura 1.10C). Las especies -SO_2 son las que producen el mayor aumento en la densidad de carga positiva y la densidad de spin en los átomos de carbono vecinos, en los que es más favorable el mecanismo de 4 electrones. Los autores concluyen que los defectos Stone-Wales facilitan el dopado con azufre en materiales de grafeno, y mejoran la actividad catalítica de estos materiales dopados con azufre [185].

En resumen, el dopado con azufre puede mejorar la actividad catalítica de los materiales carbonosos, ya sea a través de un aumento en la cantidad de defectos, que actuarían de sitios activos, o mediante la activación de átomos de carbono cercanos al heteroátomo, debido al aumento en la densidad de carga o de spin, inducido por las especies de azufre. En este caso, el azufre oxidado es la funcionalidad que produce una mayor activación y la preferida para diseñar materiales más activos.

1.4 Resumen breve, investigación futura y perspectivas

Los catalizadores basados en materiales carbonosos libres de metal han recibido gran atención durante los últimos años gracias a sus prometedoras prestaciones en la electrocatálisis de la reducción de oxígeno. Las propiedades intrínsecas de los materiales carbonosos sin dopar, tales como porosidad y

defectos han demostrado jugar un papel fundamental. De hecho, los defectos parecen ser uno de los desafíos más prometedores, ya que un gran número de estudios han demostrado su importancia en muchas aplicaciones, incluida la electrocatálisis de la ORR, lo que hace necesario un intenso esfuerzo investigador en la ingeniería de defectos. Entre los diferentes defectos, el que parece ser uno de los más relevantes en la mejora de la actividad catalítica en la ORR es la presencia de heteroátomos en la estructura carbonosa y, de entre todos ellos, el que destaca por haber mostrado un mejor comportamiento en esta reacción es el átomo de nitrógeno.

La síntesis y propiedades de los materiales carbonosos que contienen nitrógeno es bien conocida en la Ciencia de los Materiales de Carbón y han sido utilizados y estudiados para múltiples aplicaciones, como catálisis o procesos de adsorción. La evaluación de los materiales carbonosos dopados con nitrógeno como electrocatalizadores de la ORR ha mostrado que estos catalizadores presentan actividades catalíticas prometedoras y esta observación experimental ha desembocado en la publicación de un gran número de trabajos científicos con actividades que, en algunos casos, son próximas a los catalizadores basados en platino. Considerando la diferente naturaleza de las funcionalidades de nitrógeno que pueden encontrarse en los materiales carbonosos junto con factores adicionales como porosidad, orden estructural, defectos, etc., que aumentan la complejidad del sistema en estudio, puede llegar a entenderse que todas las especies nitrogenadas hayan sido propuestas como sitios activos para la ORR. Sin embargo, el importante trabajo realizado sobre este tema durante los últimos quince años ha ayudado a adquirir información importante sobre la naturaleza de los sitios activos. En las secciones anteriores, se ha tratado de discutir sobre el efecto de los diferentes grupos funcionales nitrogenados en la actividad catalítica de los materiales carbonosos en la ORR. Interesantemente, a partir de la combinación de estudios experimentales con una detallada caracterización y trabajos computacionales, se han podido obtener conclusiones muy importantes que ya son aceptadas por la comunidad científica. Por lo tanto, dos son las especies nitrogenadas que se aceptan principalmente como responsables de la formación de los sitios activos de mayor actividad en estos catalizadores: grupos piridina y nitrógeno cuaternario.

Aunque esto puede considerarse como una conclusión general, es muy importante tener en cuenta que la estructura de estos grupos funcionales

determina la actividad catalítica, pues las especies de nitrógeno cuaternario ubicadas en el interior de la lámina de grafeno apenas contribuyen a una mejora de la actividad catalítica; sin embargo, si el mismo heteroátomo se encuentra cerca del borde de la lámina, el efecto es totalmente distinto. La alta electronegatividad del átomo de nitrógeno promueve la retirada de electrones de los dos átomos de carbono vecinos, lo que resulta en una densidad de carga positiva y, por lo tanto, en la quimisorción favorable de la molécula de oxígeno. La posición de las especies piridina también es decisiva, ya que las especies en posición zigzag no producen actividad catalítica en sus átomos de carbono vecinos. Ambos átomos de carbono no están ubicados en posición borde, lo que dificultará el cambio de su hibridación y, por tanto, la quimisorción de la molécula de oxígeno. Sin embargo, si los grupos piridina se ubican en la posición "armchair", un átomo de carbono adyacente se localiza en el borde, y el oxígeno molecular puede adsorberse fácilmente.

El análisis de las muestras después de estudiar la actividad en la ORR ha demostrado que la naturaleza de las funcionalidades de nitrógeno cambia y se generan especies piridona o de tipo N-C-O. Esto significa que los grupos piridina en posición "armchair" pueden producir grupos piridona y, en consecuencia, la actividad catalítica observada podría deberse, también, a las especies piridona en lugar de los grupos piridina. Aunque ambas especies están estrechamente relacionadas, el mecanismo de reacción podría ser diferente dependiendo de la especie que realmente participa en las condiciones de reacción. Esto significa que se debe prestar una mayor atención al estado del material en las condiciones de reacción, haciendo que la caracterización de los materiales en estas condiciones sea muy necesaria, siendo estas mediciones uno de los temas más importantes a abordar en futuras investigaciones.

Finalmente, las excelentes propiedades catalíticas de los materiales carbonosos dopados con nitrógeno se han medido habitualmente en electrolito alcalino, siendo mucho peores en condiciones ácidas. La tecnología para las pilas de combustible de membrana de electrolito polimérico está bien desarrollada en condiciones ácidas en las que las membranas presentan un buen comportamiento. Esto significa que es necesario comprender las razones por las cuales la actividad catalítica depende tan fuertemente del electrolito, con el fin de diseñar, en lo posible, un material que pueda funcionar adecuadamente en condiciones ácidas. Este es el segundo aspecto que requiere de una fuerte investigación en un futuro cercano.

Otro factor importante que debe plantearse es la aplicación práctica de estos catalizadores basados en materiales carbonosos, ya que, a menudo, estos materiales son probados en electrodos rotatorios de disco-anillo (RRDE, por sus siglas en inglés), pero no en dispositivos cercanos a la aplicación final. El RRDE es una herramienta muy útil para evaluar la actividad catalítica de los materiales; sin embargo, pueden surgir diferentes problemas una vez que el catalizador se introduce en la pila de combustible, que pueden resultar en la inaplicabilidad del material. Por lo tanto, el uso y estudio de estos catalizadores en estaciones de Pilas de Combustible es uno de los próximos desafíos científicos.

Los materiales carbonosos dopados con fósforo, boro y azufre también han demostrado tener una alta eficiencia hacia la ORR, aunque dicha mejora parece ser menor que la obtenida por el heteroátomo de nitrógeno. De particular interés es el origen de esta actividad, la cual todavía no está clara. Existen, principalmente, dos hipótesis para explicar los resultados observados; la creación de defectos, inducidos por el dopado con heteroátomos y el cambio en las propiedades electrónicas de los átomos de carbono vecinos al heteroátomo. Todavía es necesaria una investigación más profunda para comprender el efecto de estos heteroátomos. Sin embargo, parece que la presencia de dichas especies puede mejorar el rendimiento de las funcionalidades de nitrógeno. Por lo tanto, el dopado conjunto o codopado podría ser una metodología muy atractiva para mejorar la actividad catalítica no solo de los catalizadores para ORR, sino también de los catalizadores bifuncionales que pueden ser eficientes para ORR y OER.

Es interesante destacar que la introducción de heteroátomos con mayor electronegatividad que el carbono parece ser una metodología atractiva para mejorar la actividad de los catalizadores basados en materiales carbonosos, especialmente si el heteroátomo introducido es el nitrógeno. Pero, por otro lado, la introducción de heteroátomos de menor electronegatividad también se ha propuesto como una ruta rentable para incrementar la actividad hacia la ORR de estos materiales. Sin embargo, el heteroátomo más alentador, el nitrógeno, es aquel que presenta un tamaño de átomo y una configuración electrónica similar a la del átomo de carbono. Esto significa que la introducción de especies nitrogenadas crea especies estables en la matriz carbonosa, lo que es una propiedad necesaria para producir sitios activos estables. A su vez, el nitrógeno también es capaz de crear especies estables con otros heteroátomos, como el fósforo o el boro. Por lo tanto, la combinación del nitrógeno con otro

heteroátomo puede ser una opción atractiva para el diseño de catalizadores avanzados basados en materiales carbonosos con altas eficiencias.

Además del codopado de dos funcionalidades, otra alterativa interesante es la combinación de heteroátomos y defectos adicionales, en los cuales el efecto positivo de ambos enfoques pueden trabajar juntos hacia una mejora de la actividad catalítica de estos materiales carbonosos sin metales.

Además, debe prestarse especial atención a las impurezas metálicas, que también pueden mejorar significativamente la velocidad de la ORR de los materiales carbonosos, aunque sea con una concentración muy baja [31] y que puede ser una fuente de error importante cuando se muestran resultados de catalizadores basados en materiales carbonosos libres de metales. Sin embargo, esto puede ser también una oportunidad, puesto que la introducción controlada de cantidades muy pequeñas de metales no preciosos puede ser, también, una dirección para mejorar aún más los catalizadores basados en materiales carbonosos.

La reacción de reducción de oxígeno es tan solo el punto de partida en lo que concierne a los catalizadores basados en materiales carbonosos libres de metales, puesto que también hay muchas otras aplicaciones en las que estos catalizadores pueden tener un alto rendimiento. El conocimiento sobre reacciones como la reacción de evolución de hidrógeno (HER), la reacción de evolución de oxígeno (OER), la reacción de reducción de peróxido de hidrógeno (H_2O_2RR) o, incluso, la reacción de reducción de dióxido de carbono (CO_2RR), entre otras, aún están en desarrollo. La comprensión en la catálisis de estas reacciones mediante la ingeniería de defectos en materiales carbonosos puede ser una contribución muy importante hacia la transición energética de los combustibles fósiles a fuentes de energía libres de carbono.

1.5 Referencias

[1] IPCC; 2018: Global Warming of 1.5ºC. An IPCC Special Report on the impacts of global warming of 1.5ºC above pre-industrial levels and related global greenhouse gas emission pathways, in the context of strengthening the global response to the threat of climate change, sustainable development, and efferots to eradicate poverty [V. Masson-Delmotte, P. Zhai, H. -O. Pörtner, D. Roberts, J. Skea, P.R. Shukla, A. Pirani, W. Moufouma-Okia, C. Péan, R. Pidcock, S. Connors, J. B. R. Matthews, Y. Chen, X. Zhou, M.I. Gomis, E. Lonnoy, T. Maycock, M. Tignor and T. Waterfield (eds.). In press.

[2] M. Kampa, E. Castanas, Human health effect of air polution, Environ. Pollut. 151 (2008) 362–367.

[3] J.N. Galloway, A.R. Townsend, J.W. Erisman, M. Bekunda, Z. Cai, J.R. Freney, L.A. Martinelli, S.P. Seitzinger, M.A. Sutton, Transformation of the nitrogen cycle: Recent trends, questions, and potential solutions, Science 320 (2008) 889–892.

[4] S.C. Doney, V.J. Fabry, R.A. Feely, J.A. Kleypas, Ocean Acidification: The Other CO2 Problem, Ann. Rev. Mar. Sci. 1 (2009) 169–192.

[5] United Nations Framework Convention on Climate Change. (2015). Paris Agreement (Annex to decision 1/CP.21, document FCCC/CP/201510/Add.1 Paris: United Nations. Retrieved from http://unfccc.int/resource/docs/2015/cop21/eng/10a01.pdf.

[6] A. Mazza, E. Bompard, G. Chicco, Applications of power to gas technologies in emerging electrical systems, Renew. Sustain. Energy Rev. 92 (2018) 794–806.

[7] W. Liu, F. Wen, Y. Xue, Power-to-gas technology in energy systems: current status and prospects of potential operation strategies, J. Mod. Power Syst. Clean Energy 5 (2017) 439–450.

[8] B.C.H. Steele, A. Heinzel, Materials for fuel-cell technologies, Nature 414 (2001) 345–352.

[9] M. Winter, R.J. Brodd, What are batteries, fuel cells, and supercapacitors?, Chem. Rev. 104 (2004) 4245–4270.

[10] R. Borup, J. Meyers, B. Pivovar, Y.S. Kim, R. Mukundan, N. Garland, D. Myers, M. Wilson, F. Garzon, D. Wood, P. Zelenay, K. More, K. Stroh, T. Zawodzinski, X.J. Boncella, J.E. Mcgrath, O.M. Inaba, K. Miyatake, M. Hori, K. Ota, Z. Ogumi, S. Miyata, A. Nishikata, Z. Siroma, Y. Uchimoto, K. Yasuda, K. Kimijima, N. Iwashita, Scientific Aspects of Polymer Electrolyte Fuel Cell Durability and Degradation, Chem. Rev. 107 (2007) 3904–3951.

[11] M. Shao, Q. Chang, J.P. Dodelet, R. Chenitz, Recent Advances in Electrocatalysts for Oxygen Reduction Reaction, Chem. Rev. 116 (2016) 3594–3657.

[12] Q. Li, R. He, J.O. Jensen, N.J. Bjerrum, Approaches and Recent Development of Polymer Electrolyte Membranes for Fuel Cells Operating above 100 °C, Chem. Mater. 15 (2003) 4896–4915.

[13] Y. Wang, K.S. Chen, J. Mishler, S.C. Cho, X.C. Adroher, A review of polymer electrolyte membrane fuel cells: Technology, applications, and needs on fundamental research, Appl. Energy. 88 (2011) 981–1007.

[14] Z.L. Wang, D. Xu, J.J. Xu, X.B. Zhang, Oxygen electrocatalysts in metal-air

batteries: from aqueous to nonaqueous electrolytes, Chem. Soc. Rev. 43 (2014) 7746–7786.

[15] F. Cheng, J. Chen, Metal-air batteries: From oxygen reduction electrochemistry to cathode catalysts, Chem. Soc. Rev. 41 (2012) 2172–2192.

[16] M. Melchionna, P. Fornasiero, M. Prato, The Rise of Hydrogen Peroxide as the Main Product by Metal-Free Catalysis in Oxygen Reductions, Adv. Mater. 31 (2019) 1802920.

[17] W. Zhou, X. Meng, J. Gao, A.N. Alshawabkeh, Hydrogen peroxide generation from O2 electroreduction for environmental remediation: A state-of-the-art review, Chemosphere. 225 (2019) 588–607.

[18] J. Stacy, Y.N. Regmi, B. Leonard, M. Fan, The recent progress and future of oxygen reduction reaction catalysis: A review, Renew. Sustain. Energy Rev. 69 (2017) 401–414.

[19] A. Morozan, B. Jousselme, S. Palacin, Low-platinum and platinum-free catalysts for the oxygen reduction reaction at fuel cell cathodes, Energy Environ. Sci. 4 (2011) 1238.

[20] H.A. Gasteiger, J.E. Panels, S.G. Yan, Dependence of PEM fuel cell performance on catalyst loading, J. Power Sources 127 (2004) 162–171.

[21] Source Scopus, keywords: "oxygen reduction reaction" and "ORR", (Date: 13/01/2020).

[22] F. Jaouen, E. Proietti, M. Lefèvre, R. Chenitz, J.-P. Dodelet, G. Wu, H.T. Chung, C.M. Johnston, P. Zelenay, Recent advances in non-precious metal catalysis for oxygen-reduction reaction in polymer electrolyte fuelcells, Energy Environ. Sci. 4 (2011) 114–130.

[23] J. Tang, D. Chen, Q. Yao, J. Xie, J. Yang, Recent advances in noble metal-based nanocomposites for electrochemical reactions, Mater. Today Energy. 6 (2017) 115–127.

[24] C. Zhu, H. Li, S. Fu, D. Du, Y. Lin, Highly efficient nonprecious metal catalysts towards oxygen reduction reaction based on three-dimensional porous carbon nanostructures, Chem. Soc. Rev. 45 (2016) 517–531.

[25] X. Wang, Z. Li, Y. Qu, T. Yuan, W. Wang, Y. Wu, Y. Li, Review of Metal Catalysts for Oxygen Reduction Reaction: From Nanoscale Engineering to Atomic Design, Chem 5 (2019) 1486–1511.

[26] H. Zhong, C.A. Campos-Roldán, Y. Zhao, S. Zhang, Y. Feng, N. Alonso-Vante, Recent advances of cobalt-based electrocatalysts for oxygen electrode reactions and hydrogen evolution reaction, Catalysts 8 (2018) 559.

[27] Y. Yang, H. Zhang, Z. Liang, Y. Yin, B. Mei, F. Song, F. Sun, S. Gu, Z. Jiang,

Y. Wu, Z. Zhu, Role of local coordination in bimetallic sites for oxygen reduction: A theoretical analysis, J. Energy Chem. 44 (2020) 131–137.

[28] T. Li, H. Deng, J. Liu, C. Jin, Y. Song, F. Wang, First-row transition metals and nitrogen co-doped carbon nanotubes: The exact origin of the enhanced activity for oxygen reduction reaction, Carbon 143 (2019) 859–868.

[29] Z. Lu, G. Xu, C. He, T. Wang, L. Yang, Z. Yang, D. Ma, Novel catalytic activity for oxygen reduction reaction on MnN4 embedded graphene: A dispersion-corrected density functional theory study, Carbon 84 (2014) 500–508.

[30] K. Gong, F. Du, Z. Xia, M. Durstock, L. Dai, Nitrogen-Doped Carbon Nanotube Arrays with High Electrocatalytic Activity for Oxygen Reduction, Science 323 (2009) 760–764.

[31] S.M. Tan, M. Pumera, Two-Dimensional Materials on the Rocks: Positive and Negative Role of Dopants and Impurities in Electrochemistry, ACS Nano. 13 (2019) 2681–2728.

[32] R. Ma, G. Lin, Y. Zhou, Q. Liu, T. Zhang, G. Shan, M. Yang, J. Wang, A review of oxygen reduction mechanisms for metal-free carbon-based electrocatalysts, Npj Comput. Mater. 5 (2019) 78.

[33] L. Yang, J. Shui, L. Du, Y. Shao, J. Liu, L. Dai, Z. Hu, Carbon-Based Metal-Free ORR Electrocatalysts for Fuel Cells: Past, Present, and Future, Adv. Mater. 31 (2019) 1804799.

[34] L. Zhang, C. Lin, D. Zhang, L. Gong, Y. Zhu, Z. Zhao, Q. Xu, H. Li, Z. Xia, Guiding Principles for Designing Highly Efficient Metal-Free Carbon Catalysts, Adv. Mater. 31 (2019) 1805252.

[35] H. Singh, S. Zhuang, B. Ingis, B.B. Nunna, E.S. Lee, Carbon-based catalysts for oxygen reduction reaction: A review on degradation mechanisms, Carbon 151 (2019) 160–174.

[36] C. Tang, M. Titirici, Q. Zhang, A review of nanocarbons in energy electrocatalysis: Multifunctional substrates and highly active sites, J. Energy Chem. 26 (2017) 1077–1093.

[37] A. Sinthika, U. V. Waghmare, R. Thapa, Structural and Electronic Descriptors of Catalytic Activity of Graphene-Based Materials: First-Principle Theoretical Analysis, Small 14 (2017) 1703609.

[38] J. Ortiz-Medina, Z. Wang, R. Cruz-Silva, A. Morelos-Gomez, F. Wang, X. Yao, M. Terrones, M. Endo, Defect Engineering and Surface Functionalization of Nanocarbons for Metal-Free Catalysis, Adv. Mater. 31 (2019) 1805717.

[39] X. Yan, Y. Jia, X. Yao, Defects on carbons for electrocatalytic oxygen reduction, Chem. Soc. Rev. 47 (2018) 7628–7658.

[40] Y. Jia, J. Chen, X. Yao, Defect electrocatalytic mechanism: concept, topological structure and perspective, Mater. Chem. Front. 2 (2018) 1250–1268.

[41] Y. Jia, K. Jiang, H. Wang, X. Yao, The Role of Defects Sites in Nanomaterials for Electrocatalytic Energy Conversion, Chem 5 (2019) 1371–1397.

[42] D. Liu, L.I. Tao, D. Yan, Y. Zou, S. Wang, Recent Advances on Non-precious Metal Porous Carbon-based Electrocatalysts for Oxygen reduction reaction, ChemSusChem 5 (2018) 1775-1785.

[43] H. Zhao, C. Sun, Z. Jin, D. Wang, X. Yan, Z. Chen, G. Zhu, X. Yao, Carbon for the oxygen reduction reaction: a defect mechanism, J. Mater. Chem. A 3 (2015) 11736–11739.

[44] A.J. Appleby, J. Marie, Kinetics of oxygen reduction on carbon materials in alkaline solution, Electrochim. Acta. 24 (1979) 195–202.

[45] A. Gabe, R. Ruiz-Rosas, C. González-Gaitán, E. Morallón, D. Cazorla-Amorós, Modeling of oxygen reduction reaction in porous carbon materials in alkaline medium. Effect of microporosity, J. Power Sources. 412 (2019) 451–464.

[46] Y. Liu, K. Li, B. Ge, L. Pu, Z. Liu, Influence of Micropore and Mesoporous in Activated Carbon Air-cathode Catalysts on Oxygen Reduction Reaction in Microbial Fuel Cells, Electrochim. Acta. 214 (2016) 110–118.

[47] M. Seredych, A. Szczurek, V. Fierro, A. Celzard, T.J. Bandosz, Electrochemical Reduction of Oxygen on Hydrophobic Ultramicroporous PolyHIPE Carbon, ACS Catal. 6 (2016) 5618–5628.

[48] D. Barrera, M. Florent, M. Kulko, T.J. Bandosz, Ultramicropore-influenced mechanism of oxygen electroreduction on metal-free carbon catalysts, J. Mater. Chem. A 7 (2019) 27110–27123.

[49] A.B. Silva-Tapia, X. García-Carmona, L.R. Radovic, Similarities and differences in O2 chemisorption on graphene nanoribbon vs. carbon nanotube, Carbon 50 (2012) 1152–1162.

[50] A. Gabe, R. Ruiz-Rosas, E. Morallón, D. Cazorla-Amorós, Understanding of oxygen reduction reaction by examining carbon-oxygen gasification reaction and carbon active sites on metal and heteroatoms free carbon materials of different porosities and structures, Carbon 148 (2019) 430–440.

[51] G.L. Chai, Z. Hou, D.J. Shu, T. Ikeda, K. Terakura, Active sites and mechanisms for oxygen reduction reaction on nitrogen-doped carbon alloy catalysts: Stone-wales defect and curvature effect, J. Am. Chem. Soc. 136 (2014) 13629–13640.

[52] P. Zhang, X. Hou, J. Mi, Y. He, L. Lin, Q. Jiang, M. Dong, From two-dimension to one-dimension: The curvature effect of silicon-doped graphene and carbon nanotubes for oxygen reduction reaction, Phys. Chem. Chem. Phys. 16 (2014) 17479–17486.

[53] X. Hu, C. Liu, Y. Wu, Z. Zhang, Density functional theory study on nitrogen-doped carbon nanotubes with and without oxygen adsorption: The influence of length and diameter, New J. Chem. 35 (2011) 2601–2606.

[54] D. Deng, L. Yu, X. Pan, S. Wang, X. Chen, P. Hu, L. Sun, X. Bao, Size effect of graphene on electrocatalytic activation of oxygen, Chem. Commun. 47 (2011) 10016–10018.

[55] R. Sharma, J.H. Baik, C.J. Perera, M.S. Strano, Anomalously large reactivity of single graphene layers and edges toward electron transfer chemistries, Nano Lett. 10 (2010) 398–405..

[56] Y. Chen, J. Li, T. Mei, X. Hu, D. Liu, J. Wang, M. Hao, J. Li, J. Wang, X. Wang, Low-temperature and one-pot synthesis of sulfurized graphene nanosheets via in situ doping and their superior electrocatalytic activity for oxygen reduction reaction, J. Mater. Chem. A. 2 (2014) 20714–20722.

[57] W. Yuan, Y. Zhou, Y. Li, C. Li, H. Peng, J. Zhang, Z. Liu, L. Dai, G. Shi, The edge- and basal-plane-specific electrochemistry of a single-layer graphene sheet, Sci. Rep. 3 (2013) 2248.

[58] Y. Jia, L. Zhang, L. Zhuang, H. Liu, X. Yan, X. Wang, J. Liu, J. Wang, Y. Zheng, Z. Xiao, E. Taran, J. Chen, D. Yang, Z. Zhu, S. Wang, L. Dai, X. Yao, Identification of active sites for acidic oxygen reduction on carbon catalysts with and without nitrogen doping, Nat. Catal. 2 (2019) 688-695.

[59] J. Zhu, Y. Huang, W. Mei, C. Zhao, C. Zhang, J. Zhang, I.S. Amiinu, S. Mu, Effects of Intrinsic Pentagon Defects on Electrochemical Reactivity of Carbon Nanomaterials, Angew. Chemie - Int. Ed. 58 (2019) 3859–3864.

[60] Y. Jiang, L. Yang, T. Sun, J. Zhao, Z. Lyu, O. Zhuo, X. Wang, Q. Wu, J. Ma, Z. Hu, Significant Contribution of Intrinsic Carbon Defects to Oxygen Reduction Activity, ACS Catal. 5 (2015) 6707–6712.

[61] L.R. Radovic, A.F. Silva-Villalobos, A.B. Silva-Tapia, F. Vallejos-Burgos, On the mechanism of nascent site deactivation in graphene, Carbon 49 (2011) 3471–3487.

[62] L.R. Radovic, B. Bockrath, On the chemical nature of graphene edges: Origin of stability and potential for magnetism in carbon materials, J. Am. Chem. Soc. 127 (2005) 5917–5927.

[63] L.R. Radovic, Active sites in graphene and the mechanism of CO2 formation in carbon oxidation, J. Am. Chem. Soc. 131 (2009) 17166–17175.

[64] L.R. Radovic, A.J.A. Salgado-Casanova, C. V Mora-Vilches, On the active sites for the oxygen reduction reaction catalyzed by graphene-based materials, Carbon 156 (2020) 389–398.

[65] L.R. Radovic, A.B. Silva-Tapia, F. Vallejos-Burgos, Oxygen migration on the

graphene surface. 1. Origin of epoxide groups, Carbon 49 (2011) 4218–4225.

[66] Q. Yang, Z. Xiao, D. Kong, T. Zhang, X. Duan, S. Zhou, Y. Niu, Y. Shen, H. Sun, W. Shaobin, Z. Linjie, New insight to the role of edges and heteroatoms in nanocarbons for oxygen reduction reaction, Nano Energy. 66 (2019) 104096.

[67] C. Paliteiro, A. Hamnett, J.B. Goodenough, The electroreduction of oxygen on pyrolytic graphite, J. Electroanal. Chem. 233 (1987) 147–159.

[68] R.J. Taylor, A.A. Humffray, Electrochemical studies on glassy carbon electrodes. II. Oxygen reduction in solutions of high pH (pH>10), J. Electroanal. Chem. 64 (1975) 63–84.

[69] J. Xu, W. Huang, R.L. McCreery, Isotope and surface preparation effects on alkaline dioxygen reduction at carbon electrodes, J. Electroanal. Chem. 410 (1996) 235–242.

[70] H.W. Kim, M.B. Ross, N. Kornienko, L. Zhang, J. Guo, P. Yang, B.D. McCloskey, Efficient hydrogen peroxide generation using reduced graphene oxide-based oxygen reduction electrocatalysts, Nat. Catal. 1 (2018) 282–290.

[71] M.J. Mostazo-López, D. Salinas-Torres, R. Ruiz-Rosas, E. Morallón, D. Cazorla-Amorós, Nitrogen-doped superporous activated carbons as electrocatalysts for the oxygen reduction reaction, Materials 12 (2019) 1346.

[72] L. Yang, S. Jiang, Y. Zhao, L. Zhu, S. Chen, X. Wang, Q. Wu, J. Ma, Y. Ma, Z. Hu, Boron-doped carbon nanotubes as metal-free electrocatalysts for the oxygen reduction reaction, Angew. Chemie - Int. Ed. 50 (2011) 7132–7135.

[73] L. Qu, Y. Liu, J.-B. Baek, L. Dai, Nitrogen-Doped Graphene as Efficient Metal-Free Electrocatalysts for Oxygen Reduction in Fuel Cells, ACS Nano. 4 (2010) 1321–1326.

[74] Z.H. Sheng, L. Shao, J.J. Chen, W.J. Bao, F. Bin Wang, X.H. Xia, Catalyst-free synthesis of nitrogen-doped graphene via thermal annealing graphite oxide with melamine and its excellent electrocatalysis, ACS Nano. 5 (2011) 4350–4358.

[75] J. Wu, L. Ma, R.M. Yadav, Y. Yang, X. Zhang, R. Vajtai, J. Lou, P.M. Ajayan, Nitrogen-doped graphene with pyridinic dominance as a highly active and stable electrocatalyst for oxygen reduction, ACS Appl. Mater. Interfaces. 7 (2015) 14763–14769.

[76] J.Y. Liu, Z. Wang, J.Y. Chen, X. Wang, Nitrogen-doped carbon nanotubes and graphene nanohybrid for oxygen reduction reaction in acidic, alkaline and neutral solutions, J. Nano Res. 30 (2015) 50–58.

[77] M.S. Yazici, M.A. Azder, O. Salihoglu, CVD grown graphene as catalyst for acid electrolytes, Int. J. Hydrogen Energy. 43 (2018) 10710–10716.

[78] W. Xiaohui, L. Lu, T. Pei, L. Meixian, S. Zujin, Influence of nitrogen precursors

on the structure, composition, and oxygen reduction reaction performance of dual heteroatom doped carbon nanohorns, RSC Adv. 6 (2016) 63730–63735.

[79] Y. Zhan, X. Yu, L. Cao, B. Zhang, X. Wu, F. Xie, W. Zhang, J. Chen, W. Xie, W. Mai, H. Meng, The influence of nitrogen source and doping sequence on the electrocatalytic activity for oxygen reduction reaction of nitrogen doped carbon materials, Int. J. Hydrogen Energy. 41 (2016) 13493–13503.

[80] B. Zheng, J. Wang, F. B. Wang, X.H. Xia, Synthesis of nitrogen doped graphene with high electrocatalytic activity toward oxygen reduction reaction, Electrochem. Commun. 28 (2013) 24–26..

[81] Z. Jiang, J. Yu, T. Huang, M. Sun, Recent Advance on Polyaniline or Polypyrrole-Derived Electrocatalysts for Oxygen Reduction Reaction, Polymers. 10 (2018) 1397.

[82] Y. Deng, Y. Xie, K. Zou, X. Ji, Review on recent advances in nitrogen-doped carbons: Preparations and applications in supercapacitors, J. Mater. Chem. A. 4 (2016) 1144–1173.

[83] M. Liu, L. Liu, Y. Zhang, Y. Yu, A. Chen, Synthesis of n-doped mesoporous carbon by silica assistance as electrode for supercapacitor, J. Mater. Sci. Mater. Electron. 30 (2019) 3214–3221.

[84] M. Inagaki, M. Toyoda, Y. Soneda, T. Morishita, Nitrogen-doped carbon materials, Carbon 132 (2018) 104–140.

[85] K. Gao, B. Wang, L. Tao, B. V. Cunning, Z. Zhang, S. Wang, R.S. Ruoff, L. Qu, Efficient Metal-Free Electrocatalysts from N-Doped Carbon Nanomaterials: Mono-Doping and Co-Doping, Adv. Mater. 31 (2019) 1805121.

[86] Y. Xia, Z. Yang, R. Mokaya, Mesostructured hollow spheres of graphitic N-doped carbon nanocast from spherical mesoporous silica, J. Phys. Chem. B. 108 (2004) 19293–19298.

[87] M. Chen, H. Xuan, X. Zheng, J. Liu, X. Dong, F. Xi, N-doped mesoporous carbon by a hard-template strategy associated with chemical activation and its enhanced supercapacitance performance, Electrochim. Acta. 238 (2017) 269–277.

[88] J. Du, L. Liu, Y. Yu, Y. Zhang, H. Lv, A. Chen, N-doped ordered mesoporous carbon spheres derived by confined pyrolysis for high supercapacitor performance, J. Mater. Sci. Technol. 35 (2019) 2178–2186.

[89] X. Sheng, N. Daems, B. Geboes, M. Kurttepeli, S. Bals, T. Breugelmans, A. Hubin, I.F.J. Vankelecom, P.P. Pescarmona, N-doped ordered mesoporous carbons prepared by a two-step nanocasting strategy as highly active and selective electrocatalysts for the reduction of O2 to H2O2, Appl. Catal. B Environ. 176–177 (2015) 212–224.

[90] G.S. Shao, L. Liu, T.Y. Ma, Z.Y. Yuan, Exotemplating synthesis of nitrogen-doped carbon materials with hierarchically porous structure and their application for lysozyme adsorption, Chem. Eng. J. 174 (2011) 452–460.

[91] Y. Li, M. Li, P. Xu, S. Tang, C. Liu, Efficient photocatalytic degradation of acid orange 7 over N-doped ordered mesoporous titania on carbon fibers under visible-light irradiation based on three synergistic effects, Appl. Catal. A Gen. 524 (2016) 163–172.

[92] W. Yang, T.P. Fellinger, M. Antonietti, Efficient metal-free oxygen reduction in alkaline medium on high-surface-area mesoporous nitrogen-doped carbons made from ionic liquids and nucleobases, J. Am. Chem. Soc. 133 (2011) 206–209.

[93] B. Men, Y. Sun, M. Li, C. Hu, M. Zhang, L. Wang, Y. Tang, Y. Chen, P. Wan, J. Pan, Hierarchical Metal-Free Nitrogen-Doped Porous Graphene/Carbon Composites as an Efficient Oxygen Reduction Reaction Catalyst, ACS Appl. Mater. Interfaces. 8 (2016) 1415–1423.

[94] X. Hu, Y. Wu, H. Li, Z. Zhang, Adsorption and activation of O2 on nitrogen-doped carbon nanotubes, J. Phys. Chem. C. 114 (2010) 9603–9607.

[95] T. Wang, Z.X. Chen, Y.G. Chen, L.J. Yang, X.D. Yang, J.Y. Ye, H.P. Xia, Z.Y. Zhou, S.G. Sun, Identifying the Active Site of N-Doped Graphene for Oxygen Reduction by Selective Chemical Modification, ACS Energy Lett. 3 (2018) 986–991

[96] D. Higgins, Z. Chen, Z. Chen, Nitrogen doped carbon nanotubes synthesized from aliphatic diamines for oxygen reduction reaction, Electrochim. Acta. 56 (2011) 1570–1575.

[97] Z. Chen, D. Higgins, Z. Chen, Nitrogen doped carbon nanotubes and their impact on the oxygen reduction reaction in fuel cells, Carbon 48 (2010) 3057–3065.

[98] Z. Chen, D. Higgins, H. Tao, R.S. Hsu, Z. Chen, Highly active nitrogen-doped carbon nanotubes for oxygen reduction reaction in fuel cell applications, J. Phys. Chem. C. 113 (2009) 21008–21013.

[99] L. Lai, J.R. Potts, D. Zhan, L. Wang, C.K. Poh, C. Tang, H. Gong, Z. Shen, J. Lin, R.S. Ruoff, Exploration of the active center structure of nitrogen-doped graphene-based catalysts for oxygen reduction reaction, Energy Environ. Sci. 5 (2012) 7936-7942.

[100] D. Geng, H. Liu, Y. Chen, R. Li, X. Sun, S. Ye, S. Knights, Non-noble metal oxygen reduction electrocatalysts based on carbon nanotubes with controlled nitrogen contents, J. Power Sources. 196 (2011) 1795–1801.

[101] A. Zhao, J. Masa, M. Muhler, W. Schuhmann, W. Xia, N-doped carbon synthesized from N-containing polymers as metal-free catalysts for the oxygen

reduction under alkaline conditions, Electrochim. Acta. 98 (2013) 139–145.

[102] C.V. Rao, C.R. Cabrera, Y. Ishikawa, In search of the active site in nitrogen-doped carbon nanotube electrodes for the oxygen reduction reaction, J. Phys. Chem. Lett. 1 (2010) 2622–2627.

[103] H. Miao, S. Li, Z. Wang, S. Sun, M. Kuang, Z. Liu, J. Yuan, Enhancing the pyridinic N content of Nitrogen-doped graphene and improving its catalytic activity for oxygen reduction reaction, Int. J. Hydrogen Energy. 42 (2017) 28298–28308.

[104] A.A. Ensafi, M. Jafari-Asl, B. Rezaei, Pyridine-functionalized graphene oxide, an efficient metal free electrocatalyst for oxygen reduction reaction, Electrochim. Acta. 194 (2016) 95–103.

[105] D.W. Chang, H.J. Choi, J.B. Baek, Wet-chemical nitrogen-doping of graphene nanoplatelets as electrocatalysts for the oxygen reduction reaction, J. Mater. Chem. A. 3 (2015) 7659–7665.

[106] Q. Lv, W. Si, J. He, L. Sun, C. Zhang, N. Wang, Z. Yang, X. Li, X. Wang, W. Deng, Y. Long, C. Huang, Y. Li, Selectively nitrogen-doped carbon materials as superior metal-free catalysts for oxygen reduction, Nat. Commun. 9 (2018) 3376.

[107] D. Guo, R. Shibuya, C. Akiba, S. Saji, T. Kondo, J. Nakamura, Active sites of nitrogen-doped carbon materials for oxygen reduction reaction clarified using model catalysts, Science 351 (2016) 361–365.

[108] T. Xing, Y. Zheng, L.H. Li, B.C.C. Cowie, D. Gunzelmann, S.Z. Qiao, S. Huang, Y. Chen, Observation of active sites for oxygen reduction reaction on nitrogen-doped multilayer graphene, ACS Nano. 8 (2014) 6856–6862.

[109] H. Zhong, S. Zhang, J. Jiang, D. Li, P. Tang, N. Alonso-Vante, Y. Feng, Improved Electrocatalytic Performance of Tailored Metal-Free Nitrogen-Doped Ordered Mesoporous Carbons for the Oxygen Reduction Reaction, ChemElectroChem 5 (2018) 1899–1904.

[110] S. Li, R. Xu, H. Wang, D.J.L. Brett, S. Ji, B.G. Pollet, R. Wang, Ultra-high surface area and mesoporous N-doped carbon derived from sheep bones with high electrocatalytic performance toward the oxygen reduction reaction, J. Solid State Electrochem. 21 (2017) 2947–2954.

[111] K.H. Wu, D.W. Wang, D.S. Su, I.R. Gentle, A Discussion on the Activity Origin in Metal-Free Nitrogen-Doped Carbons for Oxygen Reduction Reaction and their Mechanisms, ChemSusChem. 8 (2015) 2772–2788.

[112] B. Zheng, X.L. Cai, Y. Zhou, X.H. Xia, Pure Pyridinic Nitrogen-Doped Single-Layer Graphene Catalyzes Two-Electron Transfer Process of Oxygen Reduction Reaction, ChemElectroChem. 3 (2016) 2036–2042.

[113] Y. Sun, S. Li, Z.P. Jovanov, D. Bernsmeier, H. Wang, B. Paul, X. Wang, S. Kühl, P. Strasser, Structure, Activity, and Faradaic Efficiency of Nitrogen-Doped Porous Carbon Catalysts for Direct Electrochemical Hydrogen Peroxide Production, ChemSusChem. 11 (2018) 3388–3395.

[114] Z. Luo, S. Lim, Z. Tian, J. Shang, L. Lai, B. MacDonald, C. Fu, Z. Shen, T. Yu, J. Lin, Pyridinic N doped graphene: Synthesis, electronic structure, and electrocatalytic property, J. Mater. Chem. 21 (2011) 8038–8044.

[115] A.C. Ramírez-Pérez, J. Quílez-Bermejo, J.M. Sieben, E. Morallón, D. Cazorla-Amorós, Effect of Nitrogen-Functional Groups on the ORR Activity of Activated Carbon Fiber-Polypyrrole-Based Electrodes, Electrocatalysis 9 (2018) 697–705.

[116] T. Ikeda, M. Boero, S.F. Huang, K. Terakura, M. Oshima, J. Ozaki, Carbon alloy catalysts: Active sites for oxygen reduction reaction, J. Phys. Chem. C. 112 (2008) 14706–14709.

[117] S.F. Huang, K. Terakura, T. Ozaki, T. Ikeda, M. Boero, M. Oshima, J.I. Ozaki, S. Miyata, First-principles calculation of the electronic properties of graphene clusters doped with nitrogen and boron: Analysis of catalytic activity for the oxygen reduction reaction, Phys. Rev. B - Condens. Matter Mater. Phys. 80 (2009) 235410.

[118] A. Ferre-Vilaplana, E. Herrero, Understanding the chemisorption-based activation mechanism of the oxygen reduction reaction on nitrogen-doped graphitic materials, Electrochim. Acta. 204 (2016) 245–254.

[119] L. Li, A. Manthiram, O- and N-doped carbon nanowebs as metal-free catalysts for hybrid Li-air batteries, Adv. Energy Mater. 4 (2014) 1301795.

[120] R. Silva, D. Voiry, M. Chhowalla, T. Asefa, Efficient metal-free electrocatalysts for oxygen reduction: Polyaniline-derived N- and O-doped mesoporous carbons, J. Am. Chem. Soc. 135 (2013) 7823–7826.

[121] J. Sun, S. Wang, Y. Wang, H. Li, H. Zhou, B. Chen, X. Zhang, H. Chen, K. Qu, J. Zhao, One Simple Strategy towards Nitrogen and Oxygen Codoped Carbon Nanotube for Efficient Electrocatalytic Oxygen Reduction and Evolution, Catalysts 9 (2019) 159.

[122] J. Yan, D. Zhu, Y. Lv, W. Xiong, M. Liu, L. Gan, Water-in-salt electrolyte ion-matched N/O codoped porous carbons for high-performance supercapacitors, Chinese Chem. Lett. 31 (2019) 579-582.

[123] J. Zeng, Y. Mu, X. Ji, Z. Lin, Y. Lin, Y. Ma, Z. Zhang, S. Wang, Z. Ren, J. Yu, N,O-codoped 3D graphene fibers with densely arranged sharp edges as highly efficient electrocatalyst for oxygen reduction reaction, J. Mater. Sci. 54 (2019) 14495–14503.

[124] D. Deng, X. Pan, L. Yu, Y. Cui, Y. Jiang, J. Qi, W.X. Li, Q. Fu, X. Ma, Q. Xue,

G. Sun, X. Bao, Toward N-doped graphene via solvothermal synthesis, Chem. Mater. 23 (2011) 1188–1193.

[125] Z. Lin, G.H. Waller, Y. Liu, M. Liu, C.P. Wong, 3D Nitrogen-doped graphene prepared by pyrolysis of graphene oxide with polypyrrole for electrocatalysis of oxygen reduction reaction, Nano Energy. 2 (2013) 241–248.

[126] M. Li, H. Zhang, T. Xiao, S. Wang, B. Zhang, D. Chen, M. Su, J. Tang, Low-cost biochar derived from corncob as oxygen reduction catalyst in air cathode microbial fuel cells, Electrochim. Acta. 283 (2018) 780–788.

[127] S.M. Unni, S. Devulapally, N. Karjule, S. Kurungot, Graphene enriched with pyrrolic coordination of the doped nitrogen as an efficient metal-free electrocatalyst for oxygen reduction, J. Mater. Chem. 22 (2012) 23506–23513.

[128] M. Li, Z. Liu, F. Wang, J. Xuan, The influence of the type of N dopping on the performance of bifunctional N-doped ordered mesoporous carbon electrocatalysts in oxygen reduction and evolution reaction, J. Energy Chem. 26 (2017) 422–427.

[129] L. Feng, X. Chen, Y. Cao, Y. Chen, F. Wang, Y. Chen, Y. Liu, Pyridinic and pyrrolic nitrogen-rich ordered mesoporous carbon for efficient oxygen reduction in microbial fuel cells, RSC Adv. 7 (2017) 14669–14677.

[130] J. Liu, P. Song, W. Xu, Structure-activity relationship of doped-nitrogen (N)-based metal-free active sites on carbon for oxygen reduction reaction, Carbon 115 (2017) 763–772.

[131] L. Zhang, Z. Xia, Mechanisms of oxygen reduction reaction on nitrogen-doped graphene for fuel cells, J. Phys. Chem. C. 115 (2011) 11170–11176.

[132] H. Deng, Q. Li, J. Liu, F. Wang, Active sites for oxygen reduction reaction on nitrogen-doped carbon nanotubes derived from polyaniline, Carbon 112 (2017) 219–229.

[133] Z. Lin, G. Waller, Y. Liu, M. Liu, C.P. Wong, Facile synthesis of nitrogen-doped graphene via pyrolysis of graphene oxide and urea, and its electrocatalytic activity toward the oxygen-reduction reaction, Adv. Energy Mater. 2 (2012) 884–888.

[134] S. Ratso, I. Kruusenberg, U. Joost, R. Saar, K. Tammeveski, Enhanced oxygen reduction reaction activity of nitrogen-doped graphene/multi-walled carbon nanotube catalysts in alkaline media, Int. J. Hydrogen Energy. 41 (2016) 22510–22519.

[135] Y. Liao, Y. Gao, S. Zhu, J. Zheng, Z. Chen, C. Yin, X. Lou, D. Zhang, Facile Fabrication of N-Doped Graphene as Efficient Electrocatalyst for Oxygen Reduction Reaction, ACS Appl. Mater. Interfaces. 7 (2015) 19619–19625.

[136] X. Bao, X. Nie, D. Von Deak, E.J. Biddinger, W. Luo, A. Asthagiri, U.S. Ozkan,

C.M. Hadad, A first-principles study of the role of quaternary-N doping on the oxygen reduction reaction activity and selectivity of graphene edge sites, Top. Catal. 56 (2013) 1623–1633.

[137] I.S. Flyagina, K.J. Hughes, D.C. Mielczarek, D.B. Ingham, M. Pourkashanian, Identifying the Catalytic Active Sites in Heteroatom-Doped Graphene for the Oxygen Reduction Reaction, Fuel Cells. 16 (2016) 568–576.

[138] H. Kim, K. Lee, S.I. Woo, Y. Jung, On the mechanism of enhanced oxygen reduction reaction in nitrogen-doped graphene nanoribbons, Phys. Chem. Chem. Phys. 13 (2011) 17505-17510.

[139] T. Sharifi, G. Hu, X. Jia, T. Wågberg, Formation of active sites for oxygen reduction reactions by transformation of nitrogen functionalities in nitrogen-doped carbon nanotubes, ACS Nano 6 (2012) 8904–8912.

[140] J.R. Pels, F. Kapteijn, J.A. Moulijn, Q. Zhu, K.M. Thomas, Evolution of nitrogen functionalities in carbonaceous materials during pyrolysis, Carbon 33 (1995) 1641–1653.

[141] X. Hou, Q. Hu, P. Zhang, J. Mi, Oxygen reduction reaction on nitrogen-doped graphene nanoribbons: A density functional theory study, Chem. Phys. Lett. 663 (2016) 123–127.

[142] D.W. Mckee, The catalyzed gasification of carbon, in: P.L. Walker (Ed.), Chem. Phys. Carbon, New York, 1981: p. Vol. 16.

[143] D.W. Mckee, C.L. Spiro, E.J. Lamby, The inhibition of graphite oxidation by phosphorus additives, Carbon 22 (1984) 285–290.

[144] X. Wu, L.R. Radovic, Inhibition of catalytic oxidation of carbon/carbon composites by phosphorus, Carbon 44 (2006) 141–151.

[145] J.M. Rosas, R. Ruiz-Rosas, J. Rodríguez-Mirasol, T. Cordero, Kinetic study of the oxidation resistance of phosphorus-containing activated carbons, Carbon 50 (2012) 1523–1537.

[146] T.J. Bandosz, Surface chemistry of carbon materials, in: P. Serp, J.L. Figueiredo (Eds.), Carbon Mater. Catal., John Wiley, New York, 2008: pp. 45–92.

[147] A.M. Puziy, O.I. Poddubnaya, B. Gawdzik, J.M.D. Tascón, Phosphorus-containing carbons: Preparation, properties and utilization, Carbon 157 (2020) 796–846.

[148] Z.W. Liu, F. Peng, H.J. Wang, H. Yu, W.X. Zheng, J. Yang, Phosphorus-doped graphite layers with high electrocatalytic activity for the O2 reduction in an alkaline medium, Angew. Chemie - Int. Ed. 50 (2011) 3257–3261.

[149] M.Q. Guo, J.Q. Huang, X.Y. Kong, H.J. Peng, H. Shui, F.Y. Qian, L. Zhu, W.C. Zhu, Q. Zhang, Hydrothermal synthesis of porous phosphorus-doped carbon

nanotubes and their use in the oxygen reduction reaction and lithium-sulfur batteries, New Carbon Mater. 31 (2016) 352–362.

[150] D.S. Yang, D. Bhattacharjya, M.Y. Song, J.S. Yu, Highly efficient metal-free phosphorus-doped platelet ordered mesoporous carbon for electrocatalytic oxygen reduction, Carbon 67 (2014) 736–743.

[151] K. Preuss, A.M. Siwoniku, C.I. Bucur, M.M. Titirici, The Influence of Heteroatom Dopants Nitrogen, Boron, Sulfur, and Phosphorus on Carbon Electrocatalysts for the Oxygen Reduction Reaction, Chempluschem. 84 (2019) 457–464.

[152] D.S. Yang, D. Bhattacharjya, S. Inamdar, J. Park, J.S. Yu, Phosphorus-doped ordered mesoporous carbons with different lengths as efficient metal-free electrocatalysts for oxygen reduction reaction in alkaline media, J. Am. Chem. Soc. 134 (2012) 16127–16130.

[153] H.M. Wang, H.X. Wang, Y. Chen, Y.J. Liu, J.X. Zhao, Q.H. Cai, X.Z. Wang, Phosphorus-doped graphene and (8, 0) carbon nanotube: Structural, electronic, magnetic properties, and chemical reactivity, Appl. Surf. Sci. 273 (2013) 302–309.

[154] X. Zhang, Z. Lu, Z. Fu, Y. Tang, D. Ma, Z. Yang, The mechanisms of oxygen reduction reaction on phosphorus doped graphene: A first-principles study, J. Power Sources. 276 (2015) 222–229.

[155] T. Sadhasivam, K. Dhanabalan, S.H. Roh, T.H. Kim, K.W. Park, S. Jung, M.D. Kurkuri, H.Y. Jung, A comprehensive review on unitized regenerative fuel cells: Crucial challenges and developments, Int. J. Hydrogen Energy. 42 (2017) 4415–4433.

[156] B. Paul, J. Andrews, PEM unitised reversible/regenerative hydrogen fuel cell systems: State of the art and technical challenges, Renew. Sustain. Energy Rev. 79 (2017) 585–599.

[157] J. Zhang, Z. Zhao, Z. Xia, L. Dai, A metal-free bifunctional electrocatalyst for oxygen reduction and oxygen evolution reactions, Nat. Nanotechnol. 10 (2015) 444–452.

[158] M. Borghei, N. Laocharoen, E. Kibena-Põldsepp, L.S. Johansson, J. Campbell, E. Kauppinen, K. Tammeveski, O.J. Rojas, Porous N,P-doped carbon from coconut shells with high electrocatalytic activity for oxygen reduction: Alternative to Pt-C for alkaline fuel cells, Appl. Catal. B Environ. 204 (2017) 394–402.

[159] Z. Zhou, K. Liu, C. Lai, L. Zhang, J. Li, H. Hou, D.H. Reneker, H. Fong, Graphitic carbon nanofibers developed from bundles of aligned electrospun polyacrylonitrile nanofibers containing phosphoric acid, Polymer 51 (2010) 2360–2367.

[160] Z. Li, W. Zhao, C. Yin, L. Wei, W. Wu, Z. Hu, M. Wu, Synergistic Effects between Doped Nitrogen and Phosphorus in Metal-Free Cathode for Zinc-Air Battery from Covalent Organic Frameworks Coated CNT, ACS Appl. Mater. Interfaces 9 (2017) 44519–44528.

[161] G. Zhao, L. Shi, J. Xu, X. Yan, T.S. Zhao, Role of phosphorus in nitrogen, phosphorus dual-doped ordered mesoporous carbon electrocatalyst for oxygen reduction reaction in alkaline media, Int. J. Hydrogen Energy. 43 (2018) 1470–1478.

[162] D.W. McKee, C.L. Spiro, E.J. Lamby, The effects of boron additives on the oxidation behavior of carbons, Carbon 22 (1984) 507–511.

[163] D.J. Allardice, P. Walker, The effect of substitutional boron on the kinetics of the carbon-oxygen reaction, Carbon 8 (1970) 375–385.

[164] A.R. Jang, Y.W. Lee, S.S. Lee, J. Hong, S.H. Beak, S. Pak, J. Lee, H.S. Shin, D. Ahn, W.K. Hong, S. Cha, J.I. Sohn, I.K. Park, Electrochemical and electrocatalytic reaction characteristics of boron-incorporated graphene: Via a simple spin-on dopant process, J. Mater. Chem. A. 6 (2018) 7351–7356.

[165] X. Bo, L. Guo, Ordered mesoporous boron-doped carbons as metal-free electrocatalysts for the oxygen reduction reaction in alkaline solution, Phys. Chem. Chem. Phys. 15 (2013) 2459–2465.

[166] Y. Zhao, L. Yang, S. Chen, X. Wang, Y. Ma, Q. Wu, Y. Jiang, W. Qian, Z. Hu, Can boron and nitrogen co-doping improve oxygen reduction reaction activity of carbon nanotubes?, J. Am. Chem. Soc. 135 (2013) 1201–1204.

[167] Y. Zheng, Y. Jiao, L. Ge, M. Jaroniec, S.Z. Qiao, Two-Step Boron and Nitrogen Doping in Graphene for Enhanced Synergistic Catalysis, Angew. Chem. Int. Ed. 52 (2013) 3110–3116.

[168] Y. Gong, H. Fei, X. Zou, W. Zhou, S. Yang, G. Ye, Z. Liu, Z. Peng, J. Lou, R. Vajtai, B.I. Yakobson, J.M. Tour, P.M. Ajayan, Boron- and nitrogen-substituted graphene nanoribbons as efficient catalysts for oxygen reduction reaction, Chem. Mater. 27 (2015) 1181–1186.

[169] J.I. Ozaki, T. Anahara, N. Kimura, A. Oya, Simultaneous doping of boron and nitrogen into a carbon to enhance its oxygen reduction activity in proton exchange membrane fuel cells, Carbon 44 (2006) 3358–3361.

[170] J.I. Ozaki, N. Kimura, T. Anahara, A. Oya, Preparation and oxygen reduction activity of BN-doped carbons, Carbon 45 (2007) 1847–1853.

[171] T. Ikeda, M. Boero, S.F. Huang, K. Terakura, M. Oshima, J.I. Ozaki, S. Miyata, Enhanced catalytic activity of carbon alloy catalysts codoped with boron and nitrogen for oxygen reduction reaction, J. Phys. Chem. C. 114 (2010) 8933–8937.

[172] T. Ishii, T. Maie, N. Kimura, Y. Kobori, Y. Imashiro, J.I. Ozaki, Enhanced catalytic activity of nanoshell carbon co-doped with boron and nitrogen in the oxygen reduction reaction, Int. J. Hydrogen Energy. 42 (2017) 15489–15496.

[173] C. González-Gaitán, R. Ruiz-Rosas, E. Morallón, D. Cazorla-Amorós, Electrochemical Methods to Functionalize Carbon Materials, in: Chemical Functionalization of Carbon Nanomaterials, 2015: pp. 256-287.

[174] Y. Xia, Y. Zhu, Y. Tang, Preparation of sulfur-doped microporous carbons for the storage of hydrogen and carbon dioxide, Carbon 50 (2012) 5543–5553.

[175] M. Seredych, K. Singh, T.J. Bandosz, Insight into the capacitive performance of sulfur-doped nanoporous carbons modified by addition of graphene phase, Electroanalysis. 26 (2014) 109–120.

[176] Y. Li, J. Wang, X. Li, D. Geng, M.N. Banis, Y. Tang, D. Wang, R. Li, T.K. Sham, X. Sun, Discharge product morphology and increased charge performance of lithium-oxygen batteries with graphene nanosheet electrodes: The effect of sulphur doping, J. Mater. Chem. 22 (2012) 20170–20174.

[177] T.J. Bandosz, J. Matos, M. Seredych, M.S.Z. Islam, R. Alfano, Photoactivity of S-doped nanoporous activated carbons: A new perspective for harvesting solar energy on carbon-based semiconductors, Appl. Catal. A Gen. 445–446 (2012) 159–165.

[178] H. Gao, Z. Liu, L. Song, W. Guo, W. Gao, L. Ci, A. Rao, W. Quan, R. Vajtai, P.M. Ajayan, Synthesis of S-doped graphene by liquid precursor, Nanotechnology. 23 (2012) 275605.

[179] Z. Yang, Z. Yao, G. Li, G. Fang, H. Nie, Z. Liu, X. Zhou, X. Chen, S. Huang, Sulfur-Doped Graphene as an Efficient Metal-free Cathode Catalyst for Oxygen Reduction, ACS Nano. 6 (2012) 205–211.

[180] H. Wang, X. Bo, Y. Zhang, L. Guo, Sulfur-doped ordered mesoporous carbon with high electrocatalytic activity for oxygen reduction, Electrochim. Acta. 108 (2013) 404–411.

[181] J.E. Park, Y.J. Jang, Y.J. Kim, M.S. Song, S. Yoon, D.H. Kim, S.J. Kim, Sulfur-doped graphene as a potential alternative metal-free electrocatalyst and Pt-catalyst supporting material for oxygen reduction reaction, Phys. Chem. Chem. Phys. 16 (2014) 103–109.

[182] M. Seredych, T.J. Bandosz, Confined space reduced graphite oxide doped with sulfur as metal-free oxygen reduction catalyst, Carbon 66 (2014) 227–233.

[183] J. Liang, Y. Jiao, M. Jaroniec, S.Z. Qiao, Sulfur and nitrogen dual-doped mesoporous graphene electrocatalyst for oxygen reduction with synergistically enhanced performance, Angew. Chemie - Int. Ed. 51 (2012) 11496–11500.

[184] H.L. Poh, P. Simek, Z. Sofer, M. Pumera, Sulfur-Doped Graphene via Thermal

Exfoliation of Graphite Oxide in H2S, SO2, or CS2 Gas, ACS Nano. 7 (2013) 5262–5272.

[185] L. Zhang, J. Niu, M. Li, Z. Xia, Catalytic mechanisms of sulfur-doped graphene as efficient oxygen reduction reaction catalysts for fuel cells, J. Phys. Chem. C. 118 (2014) 3545–3553

.

CAPÍTULO II

TÉCNICAS EXPERIMENTALES

2.1 Introducción

Este capítulo presenta los fundamentos teóricos de las técnicas de caracterización empleadas durante la presente Tesis Doctoral. No obstante, las condiciones experimentales, materiales y reactivos utilizados serán explicados con detalle en el apartado *Experimental* de cada capítulo, puesto que muchos de ellos son diferentes para cada capítulo.

2.2 Caracterización Fisicoquímica

2.2.1 Espectroscopía Fotoelectrónica de Rayos-X (XPS)

La espectroscopia fotoeléctrica de rayos X (XPS) [1] se trata de una técnica de análisis que consiste en determinar la energía cinética de los electrones emitidos por la muestra cuando ésta es irradiada con un haz monocromático de rayos X, con una energía superior a 1 keV, que arranca electrones de las capas internas de los átomos de la muestra. Esta emisión de fotoelectrones nos proporciona información sobre la energía de cada nivel y, por tanto, sobre la naturaleza de cada átomo emisor (Figura 2.1). El número de fotoelectrones emitidos da información acerca de la cantidad de átomos que hay y su concentración. Además, la energía cinética con la que salen los electrones proporciona información sobre el estado químico en el que se encuentran los átomos de la muestra.

Se trata de una técnica superficial en la que los fotoelectrones que consiguen salir de las muestras se encuentran en torno a 1-3 nm de profundidad. La cámara del XPS se encuentra en condiciones de ultra alto vacío para evitar interferencias de la radiación con el aire o moléculas gaseosas y, por tanto, se aplica principalmente a muestras sólidas.

Figura 2.1: Representación esquemática del proceso de extracción de un electrón de un átomo como consecuencia de la irradiación de un haz de rayos-X.

Durante los últimos 20 años, este tipo de espectroscopía ha surgido como una herramienta clave en el análisis de superficies, principalmente debido a dos

características principales: la posibilidad de análisis cuantitativo y la información de la naturaleza química y el estado de oxidación de los elementos detectados. Otra ventaja importante es que es una técnica no destructiva.

El equipo empleado para el presente trabajo es un espectrómetro *VG-Microtech Mutilab 3000* ubicado en los Servicios Técnicos de Investigación de la Universidad de Alicante, equipado con un analizador de electrones semiesférico con 9 channeltrons (con energía de paso de 2-200eV) y una fuente de radiación de rayos X con ánodos de Mg (Kα 1253.6 eV). Las deconvoluciones de los espectros XPS fueron realizadas mediante ajuste por mínimos cuadrados utilizando curvas gaussianas-lorentzianas, mientras que se usó el método Shirley para la determinación de fondo.

2.2.2 Análisis Elemental (AE)

Esta técnica se ha empleado para la determinación cuantitativa de carbono, nitrógeno, hidrógeno y azufre de algunas de las muestras sintetizadas.

La técnica de análisis elemental [2] se basa en la oxidación completa e instantánea de la muestra mediante una combustión con oxígeno puro a una temperatura de 950 a 1100ºC. La presión, temperatura y volumen son parámetros que se controlan a lo largo de todo el proceso.

Los productos de combustión CO_2, H_2O, N_2O y SO_2 se transportan mediante un gas portador (He) a través de un tubo de reducción y después son selectivamente separados en columnas específicas para ser luego desorbidos térmicamente. Para finalizar, los gases pasan de forma separada por un detector de conductividad térmica que proporciona una señal proporcional a la concentración de cada uno de los componentes individuales de la mezcla.

El equipo empleado es el *EA 1108-Elemental Analyser* de la marca *Carlo Erba Instruments* se encuentra en los Servicios Técnicos de Investigación de la Universidad de Alicante.

2.2.3 Isotermas de adsorción

La adsorción física de gases es la técnica más utilizada para la caracterización de las propiedades texturales de sólidos porosos. Esto se realiza a través de la determinación de las isotermas de adsorción, las cuales consisten en introducir una cantidad conocida de adsorbato (sólido) en contacto con un adsorbente (gas) en un recipiente de volumen conocido a una temperatura y

presión controlada. Conforme el gas se adsorbe en la superficie del adsorbente, la presión disminuirá hasta alcanzar un equilibrio. Si este procedimiento se repite varias veces a la misma temperatura y a diferentes presiones, se obtendrá una isoterma de adsorción, donde el volumen adsorbido se representa frente a la presión relativa. A partir de este gráfico, es posible obtener información sobre la porosidad del material, incluyendo parámetros tales como área superficial específica, distribución del tamaño de poro y volumen de poro, entre otros.

En la presente Tesis Doctoral, la textura porosa de los materiales ha sido estudiada por isotermas de adsorción de N_2 a -196ºC y de CO_2 a 0ºC en un sistema automático de adsorción (Autosorb-6, Quantachrome). Previo a las medidas, las muestras se desgasificaron durante 4h a 250ºC.

La interpretación de las isotermas de adsorción requiere de la aplicación de varias teorías. Las más empleadas son la teoría de Brunauer, Emmet y Teller (BET) y el modelo de Dubinin-Radushkevich.

2.2.3.1 Teoría BET

La teoría Brunauer-Emmett-Teller (BET) está basada en un modelo de adsorción en multicapas [3]. La siguiente ecuación es la que se deduce en esta teoría:

$$\frac{\frac{P}{P_0}}{n(1-\frac{P}{P_0})} = \frac{1}{n_m C} + \frac{C-1}{n_m}\frac{P}{P_0}$$

donde P y P_0 son la presión y la presión de saturación, respectivamente; n y n_m son los moles adsorbidos por gramo de adsorbente a una determinada presión, P, y en la monocapa superficial, respectivamente; y C es un parámetro relacionado con el calor de adsorción.

Representando $(P/P_0)/(n_m(1-P/P_0))$ frente a P/P_0 se obtiene una recta, de cuya pendiente y ordenada en el origen se pueden obtener los parámetros n_m y C. A partir del valor n_m es posible determinar la superficie específica del material al multiplicarlo por el área media de la molécula adsorbida (N_2 en este caso) y el número de Avogadro. La ecuación BET debe aplicarse en un intervalo de presiones relativas comprendido entre 0,05 y 0,3, aproximadamente. Esto se debe a que a presiones relativas inferiores no se cumple la suposición de superficie energéticamente homogénea y a presiones relativas superiores se

debe tener en cuenta el efecto de las interacciones entre las moléculas de adsorbato.

2.2.3.2 Teoría de Dubinin-Radushkevich

La segunda de las teorías más utilizadas para el análisis de isotermas de adsorción consiste en la teoría de Dubinin-Radushkevich [4]. Esta teoría permite determinar el volumen de microporos de un material a partir de las isotermas de adsorción. La ecuación utilizada para dicho análisis supone la condensación del adsorbato en los microporos en capas de potenciales iguales y consiste en:

$$\frac{V}{V_0} = exp\left(-\frac{1}{(E_0\beta)^2}\cdot\left(RT\cdot Ln\frac{P}{P_0}\right)^2\right)$$

donde V es el volumen adsorbido a una presión, P, V_0 es el volumen de microporos del sólido, E_0 es la energía característica dependiente de la estructura porosa, β es el coeficiente de afinidad característico del adsorbato y P_0 es la presión de saturación del adsorbato a la temperatura de trabajo.

Representando LnV frente a $(Ln(P_0/P))^2$ se puede obtener el valor de V_0 a partir de la ordenada en el origen. Aplicando esta ecuación a isotermas de N_2 y CO_2 se puede determinar el volumen de microporos total y el volumen de microporos más estrechos, respectivamente.

2.2.4 Desorción a temperatura programada (DTP)

La técnica conocida como desorción a temperatura programa (DTP) [5–7] tiene gran importancia en el estudio de materiales carbonosos, debido a que permite caracterizar su química superficial con gran precisión. La técnica consiste en someter a la muestra a un programa de temperaturas controlado en atmósfera inerte. Los gases procedentes de la descomposición de los grupos superficiales se analizan en un espectrómetro de masas, el cual se encuentra acoplado a la salida de la termobalanza.

Los gases desorbidos por la muestra son, generalmente, CO, CO_2 y H_2O procedentes de la descomposición de grupos funcionales oxigenados de la superficie del material. Estos grupos funcionales oxigenados desorben a diferentes temperaturas, lo que está relacionado con la distinta energía de descomposición, y formando diferentes gases. Los grupos carboxílicos, lactonas y anhídridos descomponen como CO_2 a distintas temperaturas según la estabilidad de los mismos, aunque suelen ser a temperaturas bajas. En cambio,

grupos oxigenados como los carbonilos, fenoles, éteres o quinonas son más estables y, en consecuencia, descomponen a mayores temperaturas como CO.

La cantidad total de oxígeno superficial en las muestras es determinada a partir de las cantidades de CO y CO_2 desorbidas al someter las muestras hasta una temperatura de 950ºC, usando la ecuación $CO + 2\ CO_2$.

En el presente trabajo se ha utilizado un equipo DSC-TGA (TA Instruments, SDT Q600 Simultaneous) acoplado a un espectrómetro de masas (Thermostar, Balzers, BSC 200). En los experimentos realizados, se utilizaron 10 mg de muestra y el análisis ha sido realizado usando un flujo de He como gas de arrastre (100 $mL \cdot min^{-1}$) desde temperatura ambiente hasta 950ºC pasando por un secado intermedio a 120ºC durante dos horas. La velocidad de calentamiento empleada fue de 20ºC/min y el equipo se purgó previamente durante 2 h en He.

2.2.5 Microscopía electrónica de transmisión (TEM)

La microscopía electrónica de transmisión (TEM, por sus siglas en inglés) [8] se basa en la emisión de un haz de electrones (>100 keV) dirigido hacia el objeto que se desea observar. Una parte de los electrones son absorbidos o retrodispersados por el objeto mientras que la otra parte lo atraviesan. Estos últimos se enfocan sobre un detector, generalmente una pantalla fluorescente o capa fotográfica. Un hecho indispensable para el buen funcionamiento de la técnica consiste en la preparación de la muestra, siendo necesario el depósito en finas capas sobre un soporte, de grosor inferior a unos 100 nm, permitiendo de esta forma el paso de los electrones y obteniendo así una buena calidad de imagen. Los microscopios electrónicos de transmisión pueden llegar a aumentar un objetivo hasta un millón de veces.

Los electrones que atraviesan la muestra pueden sufrir varios procesos como la dispersión al interaccionar con ésta. Los electrones responsables de la imagen de la muestra son los electrones no dispersados, los electrones dispersados elásticamente forman imágenes de difracción y los dispersados de forma inelástica son los responsables del ruido de fondo, observable en cualquier imagen TEM.

El microscopio electrónico de transmisión se compone de diferentes partes:

- Cañón de electrones: formado por un filamento de wolframio o hexaboruro de lantano conectado a una fuente capaz de emitir electrones muy energéticos. El tipo de cañón más frecuentemente utilizado es el cañón termoiónico.
- Sistema de lentes: consiste en lentes magnéticas cuyo objetivo es dirigir y enfocar el haz de electrones hacia la muestra.
- Sistema de vacío: el vacío habitual ronda los 10^{-5} Pa y es necesario para evitar que el haz de electrones interactúe con las partículas del aire.
- Sistema de detección: con él es posible detectar los electrones que pasan a través de la muestra y que, finalmente, vemos sobre la pantalla. Tras detectar estas señales, es común su digitalización y escaneo de las imágenes resultantes.
- Sistema de registro.

La microscopia electrónica de transmisión permite obtener información morfológica y estructural de los materiales.

En el presente trabajo se ha utilizado el microscopio electrónico de transmisión modelo JEOL JEM-2010 (200kV) procedente de los Servicios Técnicos de la Universidad de Alicante, con una resolución espacial de 0,24 nm.

2.2.6 Espectroscopía Raman

Al incidir la luz sobre una molécula, el campo eléctrico oscilante de la radiación incidente provoca una oscilación de la densidad electrónica de las moléculas. Este efecto viene representado por la aparición de un momento dipolar eléctrico oscilante inducido que actúa, a su vez, como fuente de radiación, originando las dispersiones Rayleigh y Raman [9].

Existen distintas fuentes de radiación, además del dipolo eléctrico oscilante, como el dipolo magnético oscilante y los cuadrupolos eléctricos. Pero estos últimos presentan contribuciones mucho más pequeñas, por lo que se consideran despreciables frente al dipolo eléctrico oscilante.

La mayor parte de la luz es elásticamente dispersada, dando lugar a la dispersión Rayleigh, sin cambio en la energía de los fotones, pero algunos fotones intercambian energía con la muestra y son dispersados inelásticamente, con la consecuente variación de la longitud de onda. Este es el llamado efecto Raman.

El efecto Raman proporciona gran cantidad de información cualitativa de la muestra a partir de los cambios característicos en la energía de los fotones dispersados. El equipo empleado fue un espectrómetro Jasco NRS-5100. Para ello se utilizó un láser He-Ne de 3,9mW a 633nm. Los espectros se adquirieron durante 120s de medida. El detector era un dispositivo de carga acoplada con una célula Peltier (1024 x 255 pixeles). La calibración del espectrómetro se realizó con sílice (521 2 ± cm^{-1}). Este equipo se encuentra disponible en los Servicios Técnicos de Investigación de la Universidad de Alicante.

2.2.7 Análisis termogravimétrico (TGA)

El análisis termogravimétrico (TGA, por sus siglas en inglés) [10] consiste en la medida de la variación de la masa al aplicarle un programa de temperaturas en atmósfera controlada.

El perfil de la gravimetría da información poco específica sobre el material, no obstante, informa con precisión sobre su estabilidad frente al tratamiento térmico en unas condiciones determinadas. Es útil para la determinación de la humedad en el material y el agua de hidratación. Además, es posible apreciar diferencias en el tratamiento térmico entre atmósferas diferentes.

En el presente trabajo, los experimentos de termogravimetría se realizaron empleando un equipo DSC-TGA (TA Instruments, SDT Q600 Simultaneous).

2.3 Caracterización electroquímica

Existen múltiples técnicas electroquímicas para la caracterización de materiales. En la presente Tesis Doctoral, se emplearon tres técnicas de caracterización electroquímica; voltametría cíclica (CV), cronoamperometría (CA) y espectroscopía de impedancia electroquímica (EIS). Todos estos estudios se realizaron en una celda electroquímica de tres electrodos. La celda se llena con un electrolito (ácido o alcalino) a fin de garantizar una conductividad suficiente. Dicha celda consta de un electrodo de referencia (RE), un electrodo de trabajo (WE), que corresponde al material a caracterizar y, finalmente, un contraelectrodo (CE).

2.3.1 Voltametría cíclica

La técnica de voltametría o voltamperometría cíclica [11] es una de las técnica de caracterización electroquímica más común.

La representación de la corriente que circula entre el electrodo de trabajo y el contraelectrodo frente al potencial aplicado cuando se varía el potencial del electrodo de trabajo según la ecuación $E = E_0 \pm v \cdot t$, frente a un electrodo de referencia, da lugar a un voltagrama cíclico. El perfil potencial-tiempo de un ciclo es de tipo triangular, como se puede observar en la Figura 2.2a. Si al potencial inicial (E_o) no se produce ningún proceso redox, no se registra corriente farádica. Cuando se aumenta el potencial del electrodo de trabajo hacia valores más positivos, y si existe un compuesto en la disolución que puede oxidarse, la corriente empieza a aumentar como consecuencia de la reacción de oxidación ($A \rightarrow A^+ + e^-$) hasta que la especie A se agota en la superficie del electrodo. A partir de ese momento se produce una disminución de la corriente obteniéndose un pico de oxidación. A un valor determinado de potencial (E_2), se invierte la dirección del barrido y se produce el proceso opuesto, es decir, en las proximidades del electrodo tenemos la especie A^+ oxidada y comienza a reducirse ($A^+ + e^- \rightarrow A$) conforme se disminuye el potencial, originando una corriente de reducción y un pico de reducción. Este proceso, por tanto, es reversible obteniéndose lo que denominamos voltagrama cíclico (Figura 2.2b).

Si el potencial varía desde un potencial inicial a un potencial final, la técnica se denomina voltametría de barrido lineal (LSV, por sus siglas en inglés), y será la técnica utilizada en los ensayos de actividad catalítica frente a la reacción de reducción de oxígeno.

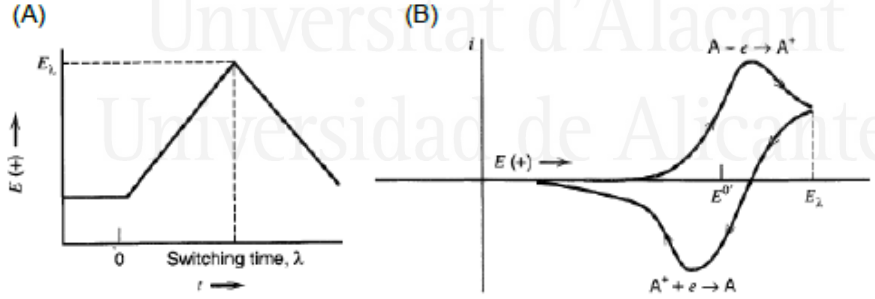

Figura 2.2: (A) Diagrama potencial-tiempo de un ciclo y (B) voltagrama típico de una especie redox en disolución, A, que reacciona reversiblemente.

El dispositivo experimental utilizado en los estudios de voltametría se compone de una célula electroquímica como la que se muestra en la Figura 2.3, la cual se compone de diferentes partes:

- Cuerpo de la célula: éste puede adoptar diferentes formas, pero todas ellas tienen en común las bocas de entrada para el electrodo de trabajo, para el pasador de gases y para el Luggin.
- Pasador de gases: dispositivo empleado para realizar la desoxigenación de la disolución en la atmósfera de nitrógeno y para después saturar la atmósfera en oxígeno (en los experimentos de ORR).
- Luggin: capilar donde se sitúa el electrodo de referencia permitiendo poner en contacto eléctrico este electrodo con la disolución de trabajo, pero evita la mezcla de las disoluciones.
- Un potenciostato que permite el uso de un sistema de tres electrodos: un electrodo de trabajo (WE), un contraelectrodo (CE) y un electrodo de referencia (RE), conectado a un ordenador que registra el voltagrama.

En este trabajo se ha utilizado un potenciostato Autolab PGSTAT302 que integra el generador de señales y el potenciostato en un solo equipo y se registra el voltagrama usando el software NOVA 2.0.2.

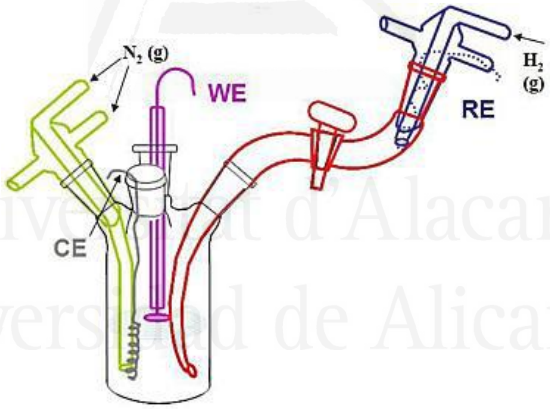

Figura 2.3: Celda electroquímica con todos sus componentes: (I) electrodo de referencia en su correspondiente Luggin como RE, (II) electrodo de trabajo como WE y (III) contraelectrodo de platino como CE.

2.3.2 Cronoamperometría (CA)

La técnica de cronoamperometría es ampliamente utilizada para el análisis cuantitativo de procesos capacitivos y procesos redox [12]. La Figura 2.4 muestra de forma esquematizada un experimento cronoamperométrico de corriente vs tiempo cuando se aplica un programa de potencial vs tiempo

mostrado también la Figura 2.4. Esta técnica, generalmente, implica saltos de potencial del electrodo de trabajo, desde un potencial inicial E_i a un potencial final, E_1. Tras esto, la respuesta de la corriente con el tiempo refleja el cambio en la velocidad de reacción (corriente) que ocurre en la superficie del electrodo de trabajo.

En la presente Tesis Doctoral, esta técnica ha sido empleada con el fin de realizar análisis de estabilidad de los materiales, así como en la síntesis electroquímica de polianilina.

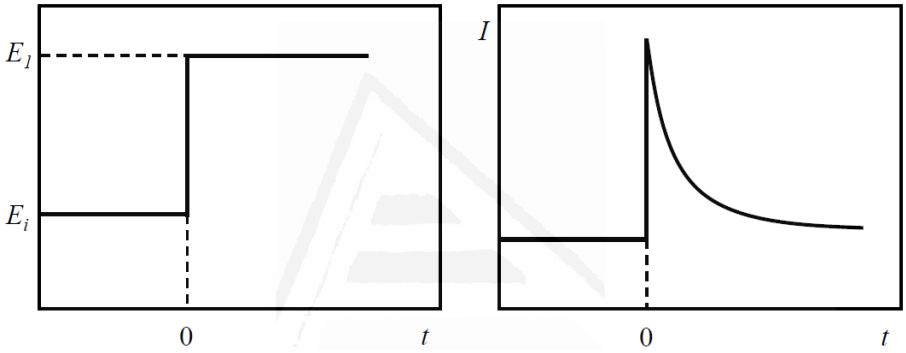

Figura 2.4: Experimento cronoamperométrico, en el que se muestra el perfil potencial vs tiempo (a la izquierda) y el resultado de este tratamiento en función de un gráfico corriente vs tiempo.

2.3.3 Espectroscopía de impedancia electroquímica (EIS)

La espectroscopía de impedancia electroquímica es una técnica muy útil para la caracterización de electrodos en diferentes aplicaciones; corrosión, baterías, pilas de combustible y sensores [13]. Es muy empleada con el fin de obtener información acerca de parámetros de reacción, velocidades de corrosión, porosidad de la superficie del electrodo, transporte de masas, conductividad eléctrica, etc. Esta técnica se basa en la perturbación del potencial del electrodo utilizando una señal oscilatoria de pequeña magnitud. En un sistema lineal, la respuesta a un potencial sinusoidal será una sinusoide a la misma frecuencia, pero desplazada en fase con un ángulo θ.

Los valores obtenidos se representan, generalmente, a partir del diagrama de Nyquist, el cual representa la parte imaginaria de la impedancia con respecto a la parte real.

2.3.4 Electrodo rotatorio de disco-anillo (RRDE)

El electrodo rotatorio de disco (RDE, por sus siglas en inglés) [14] es una técnica electroquímica de convección forzada, y utilizada para limitar el espesor de la capa de difusión. El RDE consta de un disco (por ejemplo, de Pt, Ni, Cu, carbón vítreo, grafito, etc) fijado a un aislante. El electrodo se hace girar alrededor de su eje vertical (Figura 2.5) a velocidades entre 400 y 10.000 rpm. La teoría hidrodinámica en el RDE supone que el electrodo es uniformemente accesible y proporciona un control preciso y reproducible de la convección y difusión del reactivo al electrodo.

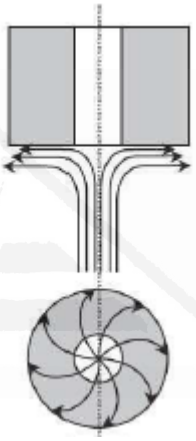

Figura 2.5: Líneas de corriente para el flujo en un electrodo rotatorio de disco.

Es posible obtener el perfil de concentración de reactivo al RDE y, a través de un tratamiento teórico, y definir la capa de difusión de espesor de δ_0, donde la difusión es el único modo de transporte de masa. En la Figura 2.6 se observa el perfil de concentraciones en el estado estacionario de un RDE mostrando el seno de la disolución bien agitada donde domina la convección y la capa de difusión en las proximidades de la superficie donde domina el fenómeno de difusión.

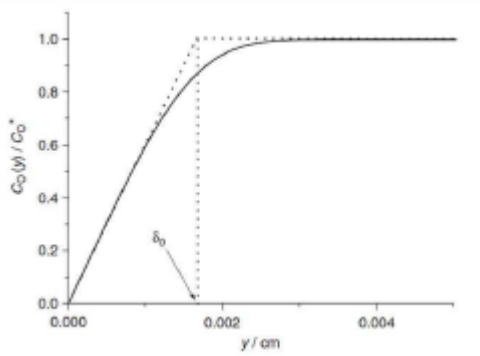

Figura 2.6: Perfil de concentraciones en estado estacionario en un RDE

Las curvas de densidad de corriente frente al potencial obtenidas en el electrodo de disco en una voltametría de barrido lineal muestran tres zonas bien definidas, las cuales son: zonas de corriente controladas por transferencia de carga, control mixto y corrientes limitadas por difusión (Figura 2.7).

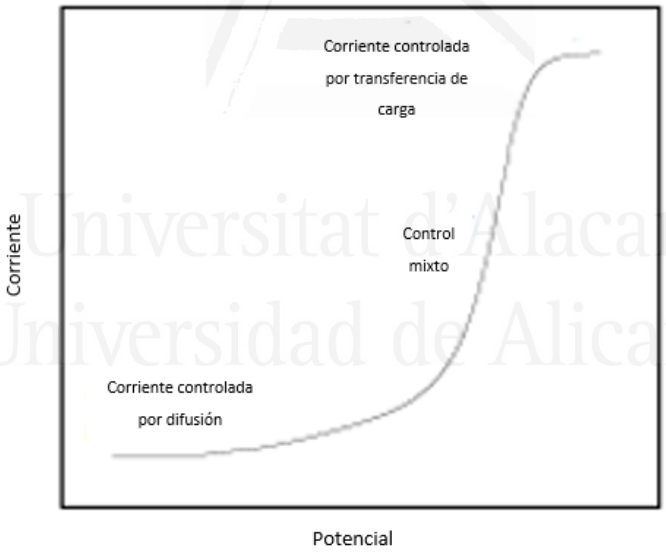

Figura 2.7: Voltagrama de barrido lineal obtenido para una reacción de reducción obtenida en un electrodo de disco rotatorio.

Uno de los refinamientos más importantes del RDE es el electrodo rotatorio de anillo/disco (RRDE, por sus siglas en inglés) [15], donde el disco central está

rodeado por un anillo aislante, y luego por un segundo electrodo de trabajo anular. El propósito de esta configuración es llevar a cabo experimentos de generación en estado estacionario. Típicamente el disco actúa como generador mientras que el anillo lo hace como colector. La geometría de este tipo de electrodos permite la determinación en el anillo de los productos generados en la reacción ocurrida en el disco.

En la presente Tesis Doctoral, el estudio de la actividad electrocatalítica de los materiales hacia la ORR fue llevado a cabo en un potenciostato Autolab PGSTAT302. Como electrodo de trabajo se empleó un electrodo rotatorio de disco-anillo (RRDE, Pine Research Instruments, EEUU) equipado con un disco de carbón vítreo (5,61mm de diámetro) y un anillo de platino, como contraelectrodo una barra de grafito y como electrodo de referencia un electrodo reversible de hidrógeno (RHE) sumergido en el electrolito de trabajo.

2.4 Cálculos computacionales

La Química Computacional [16] es una rama de la Química que hace uso de modelos matemáticos para simular interacciones entre los átomos y así resolver problemas de índole química. La Química Computacional introduce la mayor complejidad posible en sus cálculos e intenta predecir los valores de propiedades observadas experimentalmente. Es decir, procura obtener resultados con valor predictivo.

Esta área de la Química cumple dos funciones: (i) permite explicar comportamientos observados experimentalmente y (ii) proporciona instrumentos predictivos, lo que permite generar nuevo conocimiento en situaciones en las que estudios experimentales no podrían demostrarlo.

La química computacional abarca un gran abanico de métodos matemáticos que pueden clasificarse en dos categorías: mecánica cuántica y mecánica molecular. Dentro de la mecánica cuántica destacan, actualmente, los métodos semiempíricos, ab initio y de la teoría del funcional de la densidad (DFT, de sus siglas en inglés). Los métodos ab initio resuelven de manera aproximada la ecuación de Shrödinger para obtener la energía y la función de onda electrónica del sistema de interés. Los métodos semiempíricos emplean parámetros cuyos valores se ajustan para concordar los cálculos ab initio con los datos experimentales; el método DFT no intenta calcular la función de onda molecular

como los dos métodos anteriores, sino que calcula la densidad de probabilidad electrónica molecular y la energía electrónica molecular a partir de ella. La ventaja que presentan el método DFT es su gran eficiencia y mayor velocidad que los métodos ab initio [17].

Dentro del método DFT destacan diversos funcionales. La diferencia entre todos ellos radica en las aproximaciones que se realizan en torno a las energías de correlación e intercambio. El funcional más comúnmente utilizado dentro de los cálculos DFT es B3LYP. Este funcional resulta adecuado para la mayoría de los sistemas y destaca en programas de optimización molecular.

Los conjuntos de funciones base o "Basis Sets" son los que definen la forma y el tamaño del orbital. Los orbitales moleculares se expresan como una combinación lineal de funciones denominadas funciones base. Estas funciones están habitualmente centradas en los núcleos por lo que se les conoce también por orbitales atómicos.

En la presente Tesis Doctoral, se ha empleado el funcional híbrido B3LYP, con excepciones en los que los requerimientos de los cálculos eran mayores, en los que se ha empleado el funcional de Minnesota M06-2X a fin de incrementar la precisión del cálculo y añadir factores procedentes de interacciones tales como los puentes de hidrógeno. Además, se ha empleado el conjunto de bases 6-31g(d) y 6-31g(d,p). Todos estos cálculos han sido realizados a través del software Gaussian 09. Generalmente, a fin de representar de la mejor forma posible el ambiente en el que se desarrollan las reacciones simuladas, se ha añadido un modelo de polarización continua, empleando la constante dieléctrica del agua. De esta forma, la presencia del electrolito también queda reflejada en los resultados computacionales. Cuando se previeron efectos mayores del electrolito, se ha introducido moléculas explicitas de disolvente, en las que las interacciones electrolito-electrodo quedan analizadas con mayor precisión.

2.5 Referencias

[1] S. Tougaard, Surface Nanostructure Determination by X-ray Photoemission Spectroscopy Peak Shape Analysis, J. Vac. Sci. Technol. A Vacuum, Surfaces, Film. 14 (1996) 1415–1423.

[2] V.P. Fadeeva, V.D. Tikhova, O.N. Nikulicheva, Elemental analysis of organic compounds with the use of automated CHNS analyzers, J. Anal. Chem. 63 (2008) 1094–1106.

[3] S. Brunauer, P.H. Emmett, E. Teller, Adsorption of Gases in Multimolecular Layers, J. Am. Chem. Soc. 60 (1938) 309–319.

[4] C. Nguyen, D.D. Do, The Dubinin-Radushkevich equation and the underlying microscopic adsorption description, Carbon 39 (2001) 1327–1336.

[5] T.J. Bandosz, Surface chemistry of carbon materials, in: P. Serp, J.L. Figueiredo (Eds.), Carbon Mater. Catal., John Wiley, New York, 2008: pp. 45–92.

[6] J.. Figueiredo, M.F.. Pereira, M.M.. Freitas, J.J.. Órfão, Modification of the surface chemistry of activated carbons, Carbon 37 (1999) 1379–1389.

[7] Y. Otake, R.G. Jenkins, Characterization of oxygen-containing surface complexes created on a microporous carbon by air and nitric acid treatment, Carbon 31 (1993) 109–121.

[8] D. Williams, D. Carter, C. Barry, Transmission Electrons Microscopy: A Textbook for Materials, 2009.

[9] P. Larkin, Infrated and Raman Spectroscopy: Principles and Spectral Interpretation, 2nd ed.; Elsevier: Stanford, 2018.

[10] M.E. Brown, Introduction to Thermal Analysis: Techniques and Applications. ed: Springer, 2001.

[11] A.J. Bard, L.R. Faulkner, Electrochemical Methods: Fundamentals an Applications. Electrochemistry. ed: 2nd., 2000.

[12] J. Wang, Analytical electrochemistry, ed: 3rd, John Wiley & Sons, Inc, 2001.

[13] K. Krause, Encyclopedia of Electrochemistry, Wiley-VCH Verlag GmbH & Co, Weinheim, Germany, 2007.

[14] K. Tokuda, H. Matsuda, Theory of a.c. voltammetry at a rotating disk electrode: Part I. A reversible electrode process, Science 1–2 (1977) 157–171.

[15] Z. Jia, G. Yin, J. Zhang, Rotating Ring-Disk Electrode Method, in: Rotating Electrode Methods Oxyg. Reduct. Electrocatal., 2014: pp. 199–229.

[16] K.I. Ramachandran, G. Deepa, K. Namboori, Computational Chemistry and Molecular Modeling: Principles and Applications, 2008.

[17] E.J. Baerends, P. Sautet, R.A. Van Santen, Basics Aspects of Density Functional Theory, in: Comput. Methods Catal. Mater. Sci. An Introd. Sci. Eng., 2009: pp. 23–32.

CHAPTER III

EFFECT OF CARBONIZATION CONDITIONS OF POLYANILINE ON ITS CATALYTIC ACTIVITY TOWARDS ORR. SOME INSIGHTS ABOUT THE NATURE OF THE ACTIVE SITES

3.1 Introduction

The oxygen reduction reaction (ORR) occurring in the cathode of the fuel cells is a key factor in the development and commercialization of these devices [1]. This reaction is the limiting factor of the fuel cells due to its slow kinetics and high overpotential, which makes necessary the use of high efficient catalysts for its practical use [2]. The most commonly used electrocatalysts are based on platinum as active phase supported on different carbon materials [3–7]. So far, these catalysts show the best activities; however, their high cost, low availability of the metal in nature, the vulnerability to poisoning and electrochemical deactivation, affect their efficiency and useful life [8,9]. Therefore, it is necessary to develop new catalysts for the ORR with higher efficiencies for their use in fuel cells.

Nowadays, significant scientific efforts focus on the development of new non-noble metal catalysts. There are two different approaches in order to replace Pt and other noble metals. One is the use of non-noble metals – usually transition metals as Co, Ni, Fe –, which have a higher availability and lower costs [10]. The second and more innovative alternative is the development of metal-free catalysts based on carbon materials doped with different heteroatoms [11,12]. In this sense, nitrogen-doped carbon materials are one of the most promising materials due to their high activity and stability at the working conditions [13]. The effect of nitrogen is still under study; some authors suggest that the presence of nitrogen changes the geometry and the electron-donor character of the material, which affects the acidity/basicity of the carbon material [14,15]. It causes a redistribution of the electronic density in the vicinity of the heteroatoms and the nitrogen atoms induce a positive charge in the carbon atom located in the vicinities, which promotes the chemisorption of oxygen and weakens the oxygen-oxygen bond [16–19].

Nitrogen-doped carbon materials can be synthesized by several methods [13,19–22]: (i) thermal decomposition of a nitrogen-containing precursor or polymer in the presence of the carbon material, (ii) reaction of a carbon material with a nitrogen-containing reagent, (e.g. ammonia, urea, NO), (iii) carbonization or chemical vapor deposition, followed or not by a chemical or physical activation of a nitrogen-containing precursor and (iv) hydrothermal carbonization of nitrogen-containing biomass precursors. The first of these

methods comprises the use of different polymers with a high nitrogen content. Polypyrrole (PPy) and polyaniline (PANI) are good alternatives for this use and several studies have shown that their carbonization leads to materials with a high nitrogen content and other properties, which are promising for electrocatalysis and energy storage applications [21,23].

Heat treatment at different temperatures of PPy and PANI has been analyzed in inert or reducing atmosphere generating a carbon material with a good ORR activity [24]. However, to the best of our knowledge the use of an oxidant-containing atmosphere has not yet been studied. In this sense, this work presents the preparation of nitrogen-doped carbon materials synthesized by heat treatment of PANI at different temperatures using inert or a slightly oxidant atmosphere during the treatment. The electrochemical behavior and the physicochemical properties of the prepared materials were determined and their electrocatalytic activity towards ORR in alkaline and acid media has been assessed. The use of the slightly oxidizing atmosphere produces materials with the highest ORR activity, which is a consequence of the changes in surface chemistry induced by this treatment. A detailed analysis of the surface chemistry of the prepared materials allows to propose some insights about the nature of the active sites for this reaction.

3.2 Experimental

3.2.1 Materials and reagents

Aniline was purchased from Sigma Aldrich and was distilled by refluxing under reduced pressure prior its use in order to remove the impurities (e.g. aniline dimers formed by oxidation during the storage). Ammonium persulfate ($(NH_4)_2(S_2O_8)$), ammonium hydroxide (NH_4OH), potassium hydroxide (KOH), polytetrafluoroethylene (60% PTFE) and Pt/Vulcan (20% loading) were purchased from Sigma-Aldrich. Hydrochloric acid (37 % HCl) and perchloric acid (60%, $HClO_4$) were purchased from VWR-Chemicals Prolabo. All the solutions were prepared using ultrapure water (18 MOhms Millipore ® Milli-Q® water). The gases N_2 (99.999%), O_2 (99.995%) and H_2 (99.999%) were provided by Air Liquide and were used without any further purification or treatment.

3.2.2 PANI preparation

PANI was prepared by chemical polymerization from a solution of 1 M HCl containing 0.67 M of aniline and ammonium persulfate in a stoichiometric ratio [21]. The mixture was kept under stirring (500 rpm) for 2 h at 0 ºC. In order to remove the Cl^- counter ion, after the 2 h of the polymerization process, the obtained PANI was treated with 1 M NH_4OH for 24 h, resulting in de-doped PANI (PANId). The synthesized PANI and PANId were washed several times with distilled water and dried at 120 ºC overnight.

3.2.3 Heat treatment

The samples (150 mg of PANI or PANId) were heat-treated in a tubular furnace at 600 and 800 ºC for 1 h using a heating rate of 5ºC·min^{-1}. Two different atmospheres were used for the treatment: an inert (N_2) and slight oxidant atmospheres (3000 ppm O_2 in N_2). The furnace was purged for 1 h before the heat treatment in the correspond ding atmosphere, the flow rate was maintained at 100 ml min^{-1} during the treatment. The samples are referred to as PANI_X_Y and PANId_X_Y for the as-synthesized PANI and de-doped PANI, respectively, being X the atmosphere and Y the carbonization temperature used during the heat treatment.

3.2.4 Physicochemical characterization

The textural properties of the materials have been evaluated by N_2 adsorption isotherms at -196 °C and CO_2 adsorption at 0ºC in an automatic adsorption system (Autosorb-6, Quantachrome). Before the measurements, the samples were degassed at 250 °C for 4 h. Apparent surface areas have been determined by BET method (S_{BET}) and total micropore volume (pores of size < 2 nm) has been assessed by applying Dubinin-Radushkevich (DR) equation to the N_2 adsorption isotherms. The narrow micropore volume (pores of size < 0.7 nm) was calculated from CO_2 adsorption isotherms at 0 ºC using DR equation [25].

The samples were characterized by Transmission Electron Microscopy (TEM) coupled to EDX with a JEOL JEM-2010 microscope operating at 200 kV with a spatial resolution of 0.24 nm. Raman spectra were collected on a Jasco NRS-5100 spectrometer. A He–Ne excitation laser was used at 633 nm at 3.9 mW. The spectra were acquired for 120 s. The detector was a Peltier cooled charge-coupled device (CCD) (1024 × 255 pixels). Calibration of the spectrometer was performed with a Si slice (521 ± 2 cm^{-1}).

The surface composition and oxidation states of the elements of the prepared materials were studied using XPS in a VG-Microtech Mutilab 3000 spectrometer with an Al Kα radiation source (1253.6 eV). The deconvolution of the N1s XPS spectra was done by least-squares fitting using Gaussian-Lorentzian curves, while a Shirley line was used for the background determination. Elemental analysis of the materials was performed in an Elemental CHNS Microanalyzer with Micro TruSpec detection system from LECO.

In order to check the role of the oxygen during the heat treatment, PANId sample was subjected to thermogravimetric analysis in different conditions using a thermobalance (SDT 2960 instrument, TA). Heat treatment of PANId was performed in air at 250 ºC until the weight was stable (1 h 15 min), then the atmosphere was changed to N_2 and heated up at 800 ºC for 30 min (heating rate of 5 ºC·min^{-1}). Heat treatment in N_2 was also performed in a different sample for comparison purposes.

Temperature programmed desorption (TPD) experiments were performed in a DSC-TGA equipment (TA Instruments, SDT 2960 Simultaneous) coupled to a mass spectrometer (Thermostar, Balzers, GSD 300 T3) which was used to follow the m/z lines related to the decomposition of surface functional groups from the surface of the carbon materials. The thermobalance was purged for 2 hours under a helium flow rate of 100 ml min^{-1} and then heated up to 950°C (heating rate 20°C min^{-1}).

3.2.5 Electrochemical measurements

The electrochemical characterization of the materials was performed in a Biologic VSP potentiostat using a standard three-electrode cell configuration, with a platinum wire as counter electrode and Ag/AgCl electrode as the reference electrode. However, all potentials will be referred to as the reversible hydrogen electrode (RHE).

The electrochemical behaviour was studied by cyclic voltammetry (CV) in 0.1 M KOH and 0.1 M $HClO_4$ between 0.0 and 0.8 V (vs. RHE). The working electrode was prepared by mixing the carbon material with acetylene black as a conductive promoter and PTFE as a binder in a proportion 90:5:5, respectively. A disk moulded of the dry paste containing ~ 15 mg and 1 cm^2 was placed in a stainless-steel mesh and pressed for 5 min at 2 tons to guarantee a homogeneous thickness.

The study of the electrocatalytic activity towards ORR was performed in an Autolab PGSTAT302 (Metrohm, Netherlands) potentiostat. A rotating ring-disk electrode (RRDE, Pine Research Instruments, USA) equipped with a glassy carbon disk (5.61 mm diameter) and an attached platinum ring was used as the working electrode, a platinum wire as the counter electrode and a reversible hydrogen electrode (RHE) immersed in the working electrolyte as the reference electrode. The amount of catalyst on the disk electrode was optimized in order to reach the highest limiting current intensity, being 120 µg the optimum value. Therefore, the glassy carbon disk was modified with the samples using 120 µl of a 1 mg ml^{-1} dispersion of each carbon material (20% isopropanol, 0.02% Nafion®), obtaining a catalyst loading of 0.48 mg cm^{-2}.

The electrocatalytic activity towards ORR was studied by linear sweep voltammetry (LSV) in O_2 saturated 0.1 M KOH and 0.1 M $HClO_4$ between 0.0 and 1.0 V (vs. RHE) at different rotation rates, from 400 to 2025 rpm and at a scan rate of 5 mV s^{-1}. The potential of the ring was held constant at 1.5 V (vs. RHE) during all measurements. The onset potential was measured at a current density of -0.3 mA cm^{-2} for all samples. The electron transfer number was calculated from the hydrogen peroxide oxidation in the Pt ring as follows:

$$n = \frac{4\, I_d}{I_d + I_r/N} \qquad \text{Eq. 1}$$

Where I_r and I_d are the intensity measured at the ring and the disk, respectively, and N is the collection efficiency of the ring, which was experimentally determined to be 0.37.

In order to study the stability of the catalysts, chronoamperometric experiments were performed. The disk was held at a potential of 0.57 V (vs. RHE) using a rotation rate of 1600 rpm. The tests lasted for 15 hours, and the current in the disk was tracked during the experiment.

3.2.6 Computational calculations

Initial representative structures of the proposed active sites were drawn in Avogadro Version 2.0.8.0 [26], which was also used for the geometrical optimization. The determination of the electronic density was performed with Gaussian 09 software, using density functional theory (DFT) with the B3LYP/6-31G(d) level of approximation [27].

3.3 Results & Discussion

3.3.1 Materials preparation

The carbonization yields obtained after the heat treatment performed to the PANI and PANId are presented in Table 3.1. The values for the materials prepared from PANId are slightly higher independently of the temperature and atmosphere used during the heat treatment. These differences can be attributed to the loss of the Cl^- counter ion in the PANI-based samples. Additionally, the use of an inert atmosphere also renders to a lower yield (around 10 wt.% lower), indicating that the presence of oxygen promotes the crosslinking reactions between the polymer chains, which favor the condensation reactions during the carbonization. These crosslinking reactions are well-known in stabilization processes of different carbon materials (for example those used for carbon fiber preparation) that occur at low temperatures due to oxygen chemisorption [28]. It is important to note that, for the sample mass/gas flow ratio employed in this study and the low O_2 concentration used, most of the O_2 is used in the stabilization reactions occurring in the pristine polymer (in agreement with the observed higher yields) and in the oxidation of the decomposition molecules formed during the carbonization, which have a higher reactivity than the remaining carbon material.

To check the relevance of the crosslinking reactions occurring at low temperatures, the carbonization of PANId sample was studied by TG, with or without any stabilization treatment in O_2. The results in Figure 3.1 show that the heat treatment in N_2 up to 800ºC produces a yield of around 46 wt% (blue line in Figure 3.1), whereas a previous heat treatment in air at 250ºC results in a final yield around 66 wt% (red line in Figure 3.1), being these values in agreement with the final yields obtained in the tubular furnace (Table 3.1).

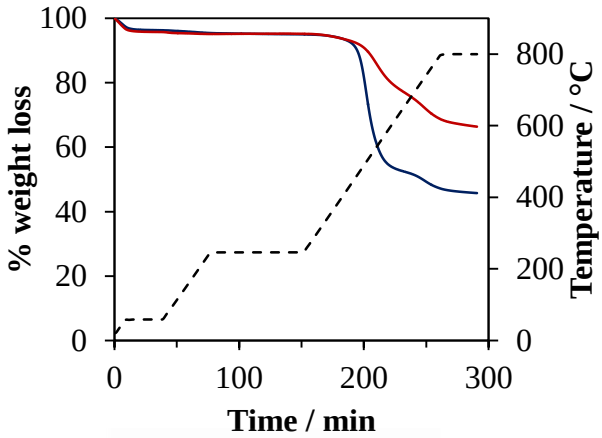

Figure 3.1: TG profiles of PANId treated in air at 250ºC and then heated up at 800ºC in N_2-atmosphere (red line) and PANId treated at in N_2-atmosphere at 800ºC (blue line). The dashed line shows the temperature profile during the treatment.

Table 3.1: Carbonization yields and porous texture characterization results for all materials

Sample	Yield / wt.%	S_{BET} / $m^2\ g^{-1}$	V_{DR} (N_2) / $cm^3\ g^{-1}$	V_{DR} (CO_2) / $cm^3\ g^{-1}$
PANI_N2_600	57	384	0.16	0.16
PANId_N2_600	68	340	0.14	0.14
PANI_O2_600	60	403	0.17	0.16
PANId_O2_600	76	394	0.16	0.13
PANI_N2_800	47	530	0.20	0.24
PANId_N2_800	58	526	0.20	0.24
PANI_O2_800	58	628	0.24	0.26
PANId_O2_800	71	584	0.22	0.24

3.3.2 Physicochemical characterization

Figure 3.2 shows the N_2 adsorption isotherms for all materials and Table 3.1 summarizes the porous texture data. All materials present type I isotherms,

characteristic of microporous materials. The BET surface areas calculated for all materials show that a heat treatment at 800 ºC renders a higher surface area independently of the atmosphere used. The treatment in an oxidant atmosphere only leads to materials with a somewhat higher surface area when the PANI sample is heated at 800ºC, that can be related with the more complex carbonization process that includes the evolution of Cl^- anions probably as HCl molecules. The micropore volumes calculated from N_2 and CO_2 are similar for each sample, indicating that they all have similar pore size distribution consisting of a homogeneous narrow microporosity of size around 0.7 nm [25].

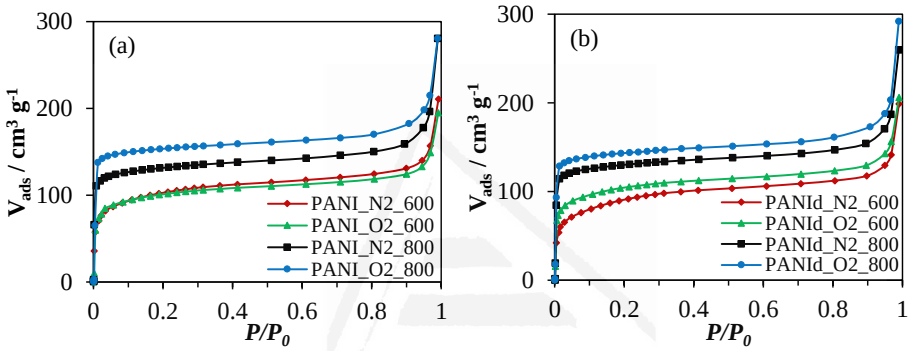

Figure 3.2: N_2 adsorption isotherms at -196 °C of the materials prepared at (a) 600 ºC and (b) 800 ºC.

The morphology of the prepared materials was characterized by transmission electron microscopy (TEM). The images (Figure 3.3) show a similar laminar morphology for all samples and only small differences are observed for the sample treated in O_2-containing atmosphere at 800ºC. It seems that the sample PANId_O2_800 presents a higher roughness at the borders, suggesting a different chemical structure in this region, which is related to the use of slightly oxidant atmosphere during the treatment.

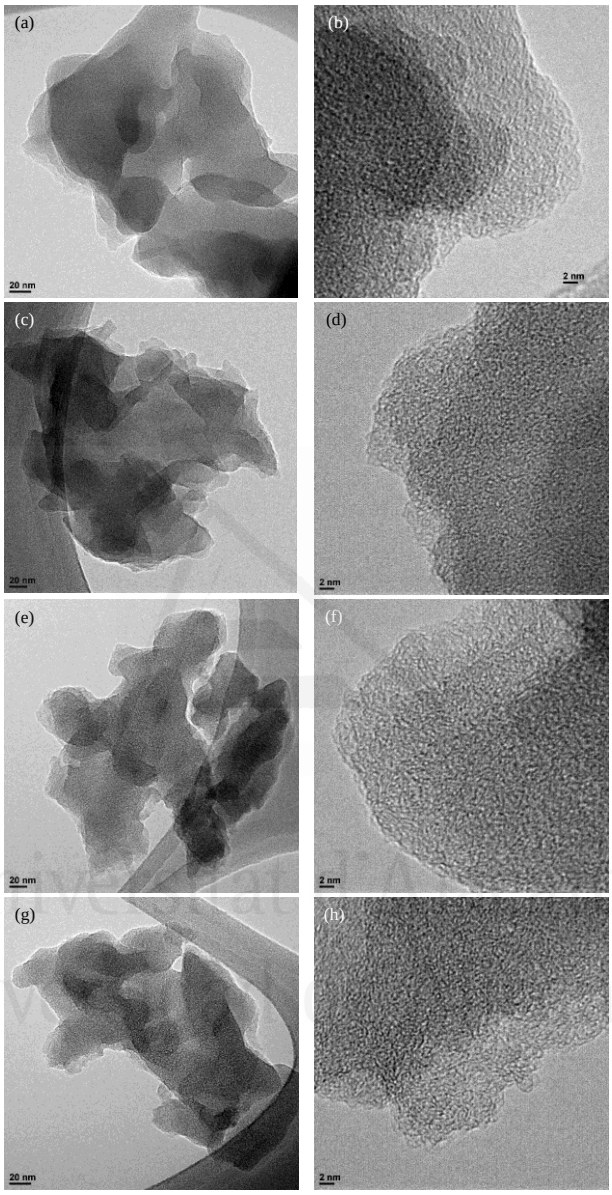

Figure 3.3: TEM images of (a) and (b) PANId_N2_600, (c) and (d) PANId_O2_600, (e) and (f) PANId_N2_800 and (g) and (h) PANId_O2_800.

Raman spectroscopy was used for structural characterization of the materials. Raman spectra (Figure 3.4) reveal the D and G bands, characteristic of graphene-based carbons [29]. The G band corresponds to an ideal graphitic

lattice vibration mode and the D band is related to the presence of defects [29]. All the spectra were normalized versus the D band for comparison purposes. The ratio between the D and G bands intensity are usually used as an indicator of the graphitic structure of the materials. The spectra and the values of the I_D/I_G are similar for all samples.

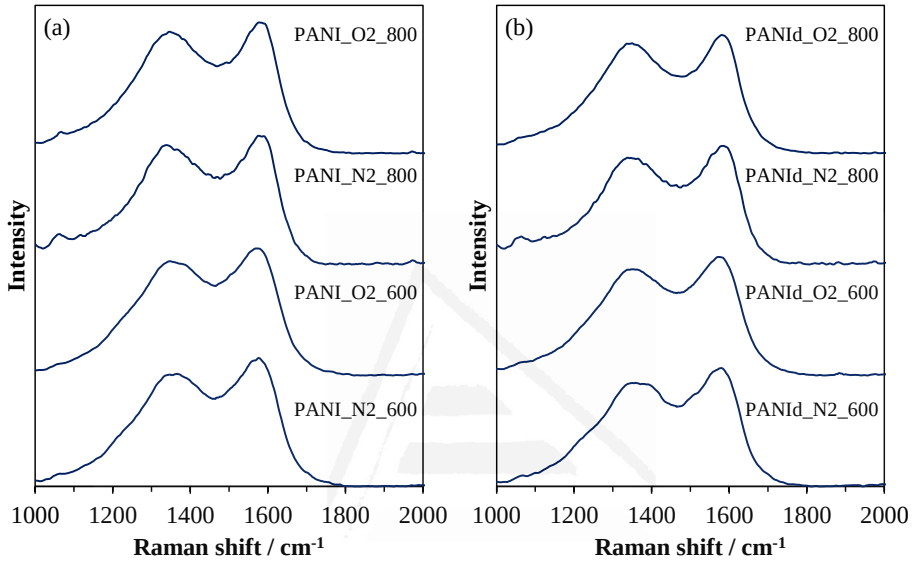

Figure 3.4: Raman spectra of all materials.

Table 3.2 presents the bulk elemental composition of all materials obtained by elemental analysis using a CHNS Microanalyzer. PANI and PANId present differences in their elemental composition. The main difference is the lower amount of carbon in PANI sample and a high oxygen content calculated by difference, which includes the O and Cl content in this sample. The carbon content of the materials treated in a N_2 atmosphere is always higher than the samples treated in the O_2-containing atmosphere at the corresponding temperature. Furthermore, the nitrogen content for the samples treated at 600 °C are similar between them independently of the atmosphere used during the heat treatment. On the other hand, when the heat treatment is performed in an O_2-containing atmosphere at 800 °C, the nitrogen content slightly increases. In general, all materials have a high nitrogen content, from 6.6 to 12.7 wt%.

Table 3.2: Elemental composition of the materials obtained by elemental analysis

SAMPLE	C / wt %	N / wt %	H / wt %	O / wt % *
PANI	57.8	12.4	4.9	24.9**
PANId	74.5	15.2	4.6	5.7
PANI_N2_600	76.2	12.1	2.7	9.0
PANId_N2_600	76.6	12.4	2.8	8.2
PANI_O2_600	73.7	12.0	1.9	12.4
PANId_O2_600	75.6	12.7	2.2	9.5
PANI_N2_800	80.2	6.6	1.4	11.8
PANId_N2_800	80.3	7.0	1.4	11.3
PANI_O2_800	76.1	7.4	1.4	15.1
PANId_O2_800	76.9	7.6	1.3	14.2

*Oxygen content was calculated by difference

**This value includes the O and Cl content

The chemical nature of the N functionalities has been studied by XPS. N1s spectra for all materials show differences in the type of nitrogen species present in the samples depending on the temperature used in the heat treatment (Figure 3.5). After a heat treatment at 600 ºC, two different contributions can be distinguished, at around 398.5 and 400.3 eV, associated to the presence of pyridine and pyrrole and/or pyridone groups, respectively [30–32]. On the other hand, when the heat treatment is performed at 800 ºC, a new peak appears above 401 eV, assigned to quaternary nitrogen [31], which is in agreement with previous results [32] and with the PANI carbonization mechanism reported in the literature [33,34]. Starting at 400 ºC, the breaking of bonds and cross-linking reactions occur [34] and up to 600 ºC the reconstruction of the backbone of the polymer takes place [33]. The initial amino groups of the aniline form pyridine and pyrrole species. The heat treatment up to 800 ºC results in condensation reactions where quaternary nitrogen species are formed, and the amount of pyrrole groups decreases. It seems that the differences among both atmospheres in XPS peak position are minor except for a small shift of B.E. to higher values in some cases when O_2 is used in the carbonization atmosphere, what can be related to the higher oxygen content of these samples.

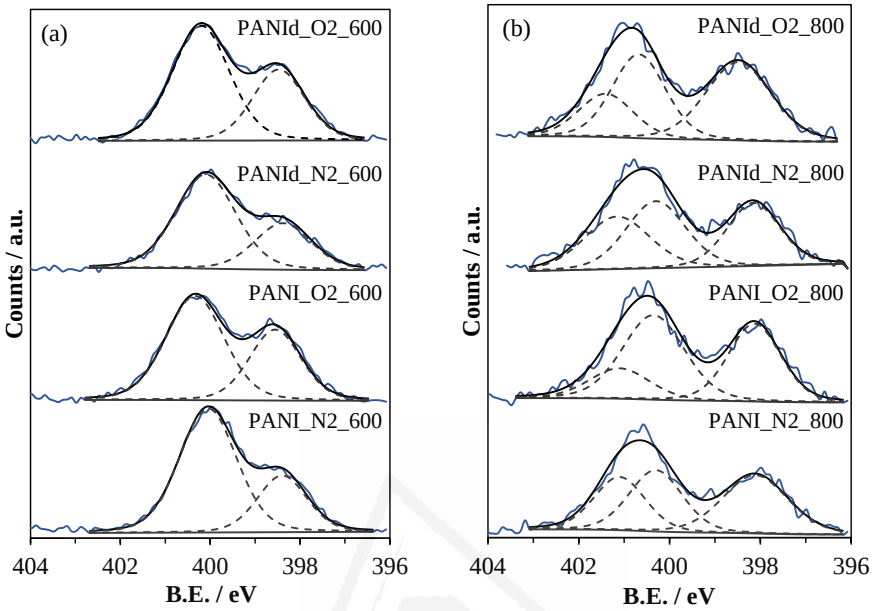

Figure 3.5: N1s spectra of the materials prepared at (a) 600 ºC and (b) 800 ºC.

Table 3.3 Percentage of each nitrogen group for all materials obtained from XPS analysis.

Sample	% Pyridine	% Pyrrole/Pyridone	% Quaternary nitrogen
PANI_N2_600	32	68	--
PANId_N2_600	34	66	--
PANI_O2_600	39	61	--
PANId_O2_600	36	64	--
PANI_N2_800	39	33	28
PANId_N2_800	31	37	32
PANI_O2_800	37	47	17
PANId_O2_800	43	37	20

However, if we observe the percentage of each N-species obtained from the XPS deconvolution (Table 3.3), some interesting aspects should be emphasized. Firstly, there are no significant differences between the samples prepared at 600 ºC. However, the heat treatment at 800 ºC produces differences depending on the atmosphere used during the heat treatment. The use of a slightly oxidant atmosphere produces a higher contribution of pyridine and pyrrole/pyridone-like nitrogen species and a lower amount of quaternary nitrogen. This means that the use of an O_2-containing atmosphere produces a higher concentration of N-species at edge sites and less at basal planes, what is an interesting observation.

The surface chemistry related to oxygen functional groups was studied by temperature-programmed desorption (TPD). The decomposition of surface oxygen functionalities using TPD is a well-known process that has been extensively used for characterizing the surface functionalities of carbon materials [35–40]. CO evolution is related to the decomposition of neutral and basic groups such as carbonyl, quinones, phenols and ethers groups, which evolve as CO at different temperatures. Likewise, CO_2 desorption is primarily related to the decomposition of acid groups, such as carboxylic, anhydride and lactone groups [35–40]. For these materials, CO_2 desorption (not included) does not show significant differences among both treatments. However, the CO profile reveals important changes. Figure 3.6 shows the CO-TPD profiles for PANId_N2_800 and PANId_O2_800. In both samples, the CO profile has a peak at around 750 ºC related to the presence of phenolic groups [35]. However, this peak has a higher intensity for the PANId_O2_800 sample, which points out that the O_2-containing atmosphere promotes the formation of this kind of species.

This means that the samples heat-treated in the O_2-containing atmosphere at 800ºC contain a larger concentration of pyridine, pyridone/pyrrole N functionalities and a higher amount of phenol-like oxygen groups, being all of them at edge sites.

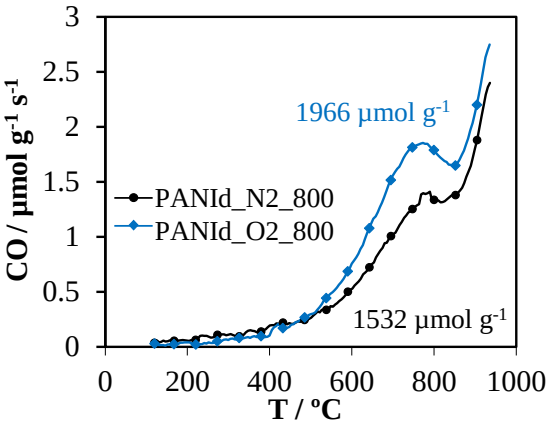

Figure 3.6: CO-TPD profiles for PANId_N2_800 and PANI_O2_800.

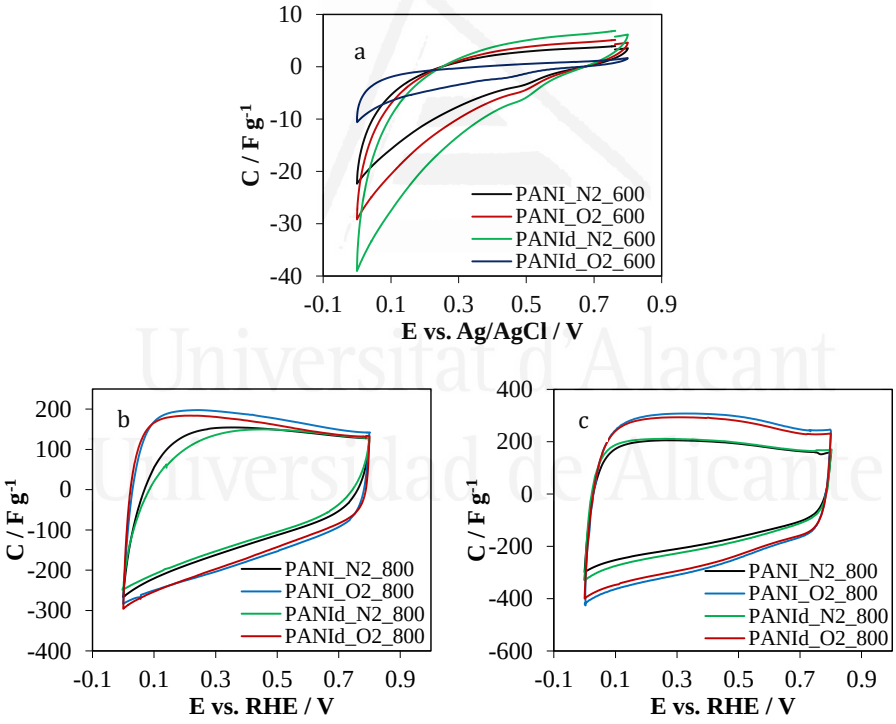

Figure 3.7: Steady state voltammograms for the different materials prepared at (a) 600 ºC in 0.1 M KOH solution and 800 °C in (b) 0.1 M KOH and (c) 0.1 M $HClO_4$. v = 2 mV s^{-1}.

3.3.3 Electrochemical characterization

The voltammograms of the samples heat-treated at 600 °C present a tilted shape (Figure 3.7), typical of materials with poor electrical conductivity. Figure 3.7 also includes the cyclic voltammograms of the samples heat treated at 800 °C in 0.1 M KOH and 0.1 M $HClO_4$, respectively. In basic medium, all samples show a trapezoidal shape with a high electrical double layer charge, being higher for the samples treated in an O_2-containing atmosphere. They have the characteristic shape observed for N-doped carbon materials in alkaline electrolytes [41]. On the other hand, voltammograms in acid medium show a quasi-rectangular shape for all materials. No significant differences are seen for the samples prepared from PANI and PANId as a precursor after applying the same heat treatment, which is expected due to their similar structures and chemical composition.

Table 3.4 includes the gravimetric capacitance values obtained from the cyclic voltammetry experiments showed in Figure 3.7 for the samples treated at 800 °C in the two electrolytes. All samples treated at 800 °C present high capacitance values up to 170 and 255 F g^{-1} in alkaline and acid electrolyte, respectively. These high values are in agreement with others reported in the literature for N-doped carbon materials, which proposed that nitrogen groups are electrochemically active or favor wettability, resulting in significantly enhanced capacitance in aqueous electrolytes [42,43]. The lower capacitance values obtained for the samples treated in N_2 can be due to the differences in surface chemistry or to slight differences in porosity that can have an important influence in electrolyte accessibility (Table 3.1).

Table 3.4 Gravimetric capacitance of the samples

Sample	Capacitance / F·g^{-1}	
	0.1 M KOH	**0.1 M $HClO_4$**
PANI_N2_800	107	180
PANId_N2_800	100	191
PANI_O2_800	170	254
PANId_O2_800	162	255

3.3.4 Electrocatalytic activity towards ORR

The electrocatalytic activities towards ORR of all materials were studied in O_2-saturated 0.1 M KOH and 0.1 M $HClO_4$ solutions. Linear sweep voltammetry analysis was performed using a RRDE at different rotation rates. The current registered in the Pt ring electrode is related to the amount of H_2O_2 formed in the disk electrode during the ORR, which is the intermediate compound found in the 2 e^- pathway. Figure 3.8 shows the LSV curves at 1600 rpm for all samples in 0.1 M KOH electrolyte. The LSV for commercial 20% Pt/Vulcan has been included for comparison purposes. Figure 3.8c shows, as an example, the LSV curves for the sample PANId_O2_800 at different rotation rates. The behaviour is similar for all tested samples. Table 3.5 presents the most relevant ORR kinetic parameters derived from the RRDE measurements.

In alkaline medium, the samples treated at 600 ºC show a poor performance (Figure 3.8a), being closer to the bare glassy carbon electrode, pointing out their low ORR activity. It can be mainly attributed to the low electrical conductivity of the materials due to the low temperature used during the treatment. On the other hand, there are no significant differences when PANI or PANId are used as precursor materials indicating that the Cl^- counter ion is removed during the heat treatment leaving no substantial changes in the final materials, and therefore in their catalytic activity.

Interestingly, significant differences are observed for samples heat-treated at 800 ºC depending on the atmosphere used during the heat treatment (Figure 3.8b). The samples treated in a slightly oxidant atmosphere show both higher onset potential values and limiting current densities, reaching in this last parameter values close to that for the commercial 20% Pt/Vulcan sample. These results could be associated with the different nitrogen and oxygen functionalities in the carbon surface. According to elemental analysis and TPD results, samples treated in inert atmosphere have lower nitrogen and oxygen contents than the samples treated in a slightly oxidant atmosphere. Additionally, the XPS showed that the use of a slightly oxidant atmosphere leads to the formation of a higher amount of N functionalities at edge sites, which have been suggested to play a role in the electrocatalytic performance to the ORR [11,14,44,45]. In addition, a larger concentration of phenol-type functional groups observed by TPD, indicates that a higher amount of both N and O functional groups at edge sites exists for the sample treated in the O_2-containing atmosphere. The results suggest that the larger amount of N-edge and O-edge sites is related to the higher

activity towards ORR observed for these samples. These heteroatoms may form N-C-O species, which can be sites with higher activity in agreement with the literature [46].

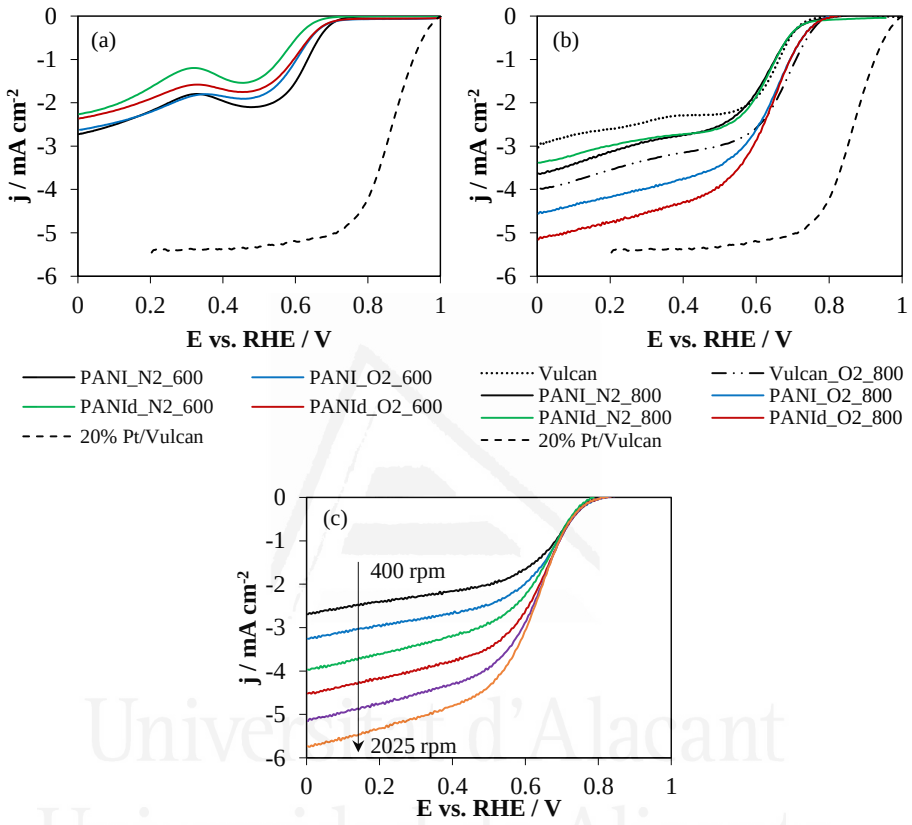

Figure 3.8: (a,b) Linear sweep voltammetry curves for the prepared materials in O_2-saturated 0.1 M KOH at 5 mV s^{-1} and 1600rpm. (c) Linear sweep voltammetry curves of PANId_O2_800 electrode in O_2-saturated 0.1 M KOH at 5 mV s^{-1} at different rotation rates.

In order to confirm the beneficial use of slightly oxidant atmosphere, Vulcan sample was also tested as electrocatalyst towards ORR. The same treatment at 800 ºC in the oxidant atmosphere was performed for this material. Figure 3.8b shows the LSV curve for this sample, and pristine Vulcan is also included for comparison purposes. It is possible to see that the heat treatment using the oxidant atmosphere improves the catalytic activity of the pristine Vulcan, with an onset potential close to the obtained for PANI_O2_800 and

PANId_O2_800 but with a lower current density. However, non-treated Vulcan has a performance similar to the PANI samples treated in N_2. This means that the surface oxygen functionalities generated during the treatment increase the ORR activity. However, the higher ORR activity found for the PANI samples treated in an O_2-containing atmosphere indicates that the carbon atom sites with neighbour nitrogen and oxygen functionalities have an enhanced ORR activity.

Table 3.5: Electrochemical parameters calculated from the RRDE experiments of the different electrocatalysts in O_2-saturated 0.1 M KOH and 0.1 M $HClO_4$ at 5 mV s^{-1} and 1600 rpm.

Sample	0.1 M KOH		0.1 M $HClO_4$	
	***E*$_{onset}$ vs. RHE / V**	***n* at 0.3 V**	***E*$_{onset}$ vs. RHE / V**	***n* at 0.1 V**
PANI_N2_600	0.68	2.2	--	--
PANId_N2_600	0.63	2.2	--	--
PANI_O2_600	0.72	2.6	--	--
PANId_O2_600	0.71	2.3	--	--
PANI_N2_800	0.66	2.6	0.33	3.4
PANId_N2_800	0.66	2.5	0.35	3.2
PANI_O2_800	0.75	2.8	0.46	3.8
PANId_O2_800	0.75	3.0	0.47	3.8
Vulcan	0.71	2.2	--	--
Vulcan_O2_800	0.75	2.5	--	--
20% Pt/Vulcan	0.94	3.9	0.93	4.0

Figure 3.9 includes the LSV curves in 0.1 M $HClO_4$ solution for the samples treated at 800 ºC since they showed the best performance towards ORR in alkaline medium. As expected, the samples treated in a slightly oxidant atmosphere display an enhanced ORR activity compared to the prepared using N_2 atmosphere. The onset potential and current density are far from the obtained

for the commercial Pt/Vulcan sample, although slightly higher current densities than the previously reported in the literature have been obtained [11,47].

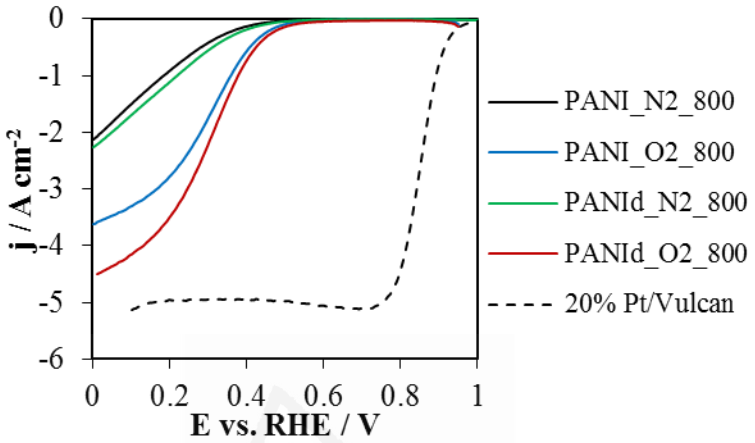

Figure 3.9: Linear sweep voltammetry curves of the prepared materials in O_2-saturated 0.1 M $HClO_4$ at 5 $mV \cdot s^{-1}$ and 1600rpm.

The electron transfer number obtained during the ORR was followed by the current registered in the Pt ring during the experiments. Table 3.5 presents the values at 0.3 V for all materials in alkaline medium. Interestingly, samples PANI_O2_800 and PANId_O2_800 show an electron transfer number close to 3 in alkaline electrolyte, which could be related to a combined mechanism of a 2 and 4 e^- pathway or a 2 + 2 e^- pathway. The former is related to the possibility of having two different active sites and the latter to a first 2 e^- reduction to hydroperoxide, and a second 2 e^- reduction of the hydroperoxide intermediate to water, which can occur during the diffusion of the molecules inside the porosity of the carbon material [48,49]. In acid medium, in spite of the much lower activity, the 4e^- mechanism is favorable for the samples treated in an O_2-containing atmosphere (Table 3.5).

3.3.5 Stability of the catalyst

The stability of PANId_O2_800 was evaluated under potentiostatic conditions since it was the catalyst that showed the best electroactivity towards ORR. Figure 3.10 shows the current versus time plots for PANId_O2_800 and 20% Pt/Vulcan catalysts. The experiments were performed in 0.1 M KOH at a potential of 0.57 V in which the limiting specific current was reached for these catalysts. The results show a 20% loss in the current for PANId_O2_800 after

15 h. An initial decrease is observed during the first 3 h and, after that, the activity of the catalyst remains constant. In contrast, the decrease in activity for the Pt-based catalyst is 38% after the same testing time, pointing out the good stability of prepared material looking forward to practical applications.

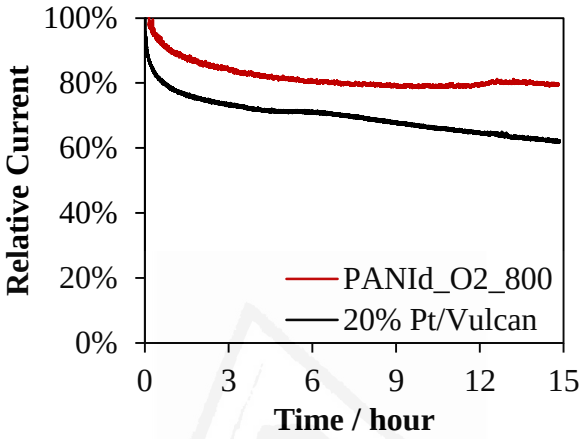

Figure 3.10: Chronoamperometric response of PANId_O2_800 and 20% Pt/Vulcan in O_2-saturated 0.1 M KOH at 0.57 V (vs. RHE) and 1600 rpm.

3.3.6 Computational study

In order to examine the possible active sites present in the catalysts, calculations of the electronic density were performed for different simple model structures. According to the experimental results, it seems that the carbon atoms in N-C-O species may constitute the active sites with the highest activity for the ORR. Figure 3.11 shows the model structure of different possible actives sites that could be present in the prepared materials. The effective charge of each atom is also plotted for the different model structures. Figure 3.11a includes a pyridone group; the calculation of the electronic density of the molecule allows us to confirm that the carbon atom between the nitrogen and oxygen atoms has the largest positive charge value, being the site where the dioxygen molecule would be adsorbed and then reduced. Figure 3.11b includes two consecutive pyridone groups in which the two carbon atoms bonded to N and O, have a charge similar to the structure with only one pyridone (Figure 3.11a). Finally, Figure 3.11c corresponds to a structure containing two pyridine functional groups. In this case, the neighbor carbon atoms have a smaller change in electronic density compared to the structures with the –OH functional groups.

This suggests that the ORR activity will be higher for the carbon atoms with nitrogen and oxygen heteroatoms in its vicinities, which is in agreement with the experimental results. The low activity of pyridine like species has already been proposed in the literature [50]. The effective charge of the adjacent C atom in an N-C-O type group (0.452) is considerable higher than in other type of species, such as C-N (-0.024), C-O (0.257) or N-C-C-O (0.281), suggesting the higher activity for N-C-O sites. All proposed structures are stable, according to the computational calculations, with close values of energy.

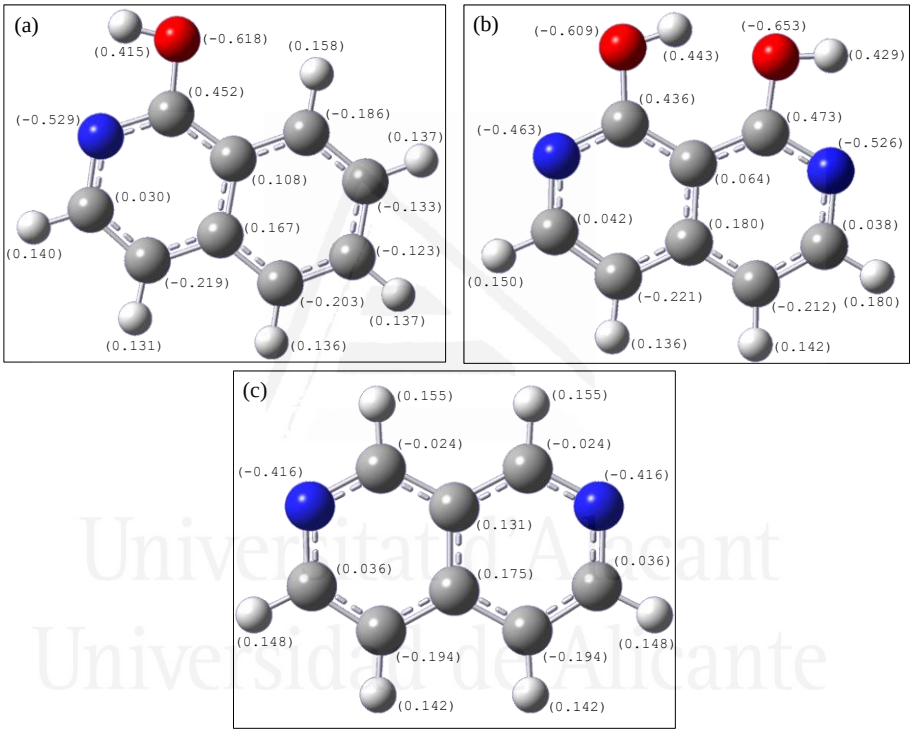

Figure 3.11: Model structures for different heteroatom-containing molecules and the calculated electronic density of all atoms: (a) one pyridone group, (b) two adjacent pyridones groups and (c) pyridine N. H is white, C is grey, N is blue, and O is red.

From the previous model structures, we propose two different possible pathways for the ORR, which are shown in Figure 3.12. The first one (Figure 3.12a) starts with the presence of one N-C-O active site (model structure shown in Figures 3.11a and b), in which the dioxygen molecule is adsorbed forming the intermediate –C–O–O*. Subsequently, the reduction of the oxygen goes

through the addition of 2 H^+ and 2 e^-, from the electrolyte and the electrode, respectively, forming -OOH that can be desorbed as H_2O_2. It has been reported that porosity plays a role in the reduction of the formed H_2O_2 in another active site, which could result in the reduction to water [48,49,51,52]. The calculated distance of the O–O atoms supports this mechanism. Initially the O=O molecule has a distance of 1.207 Å [53], when the molecule is adsorbed and reduced the distance increases to a value close to the one for the hydrogen peroxide molecule (H_2O_2: $d_{O\text{-}O}$ = 1.490 Å [53]).

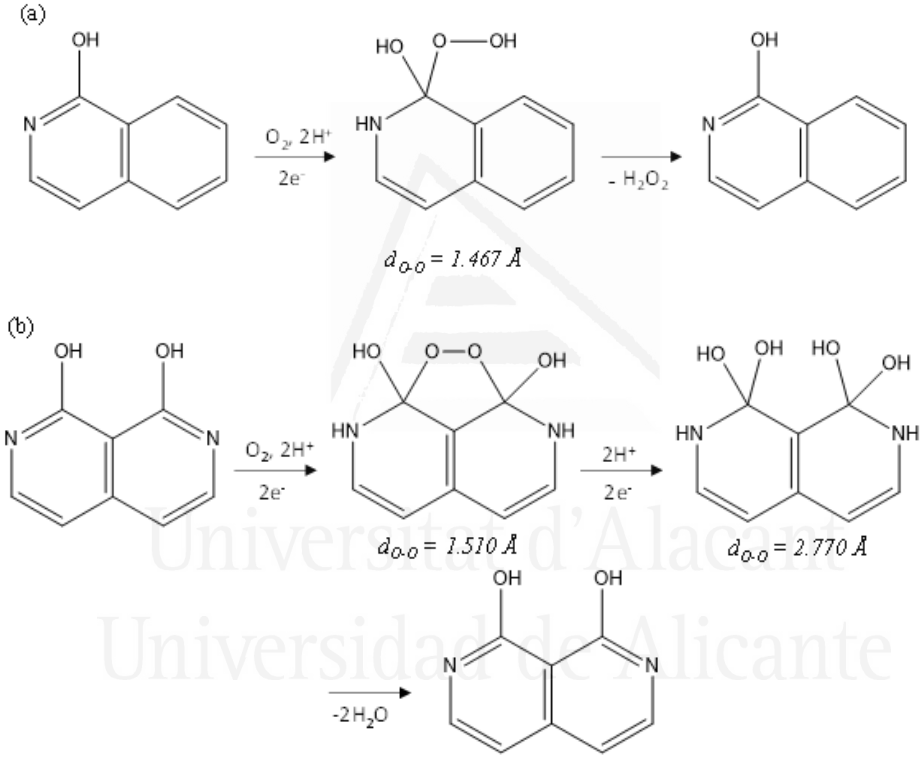

Figure 3.12: Proposed pathway for ORR with (a) one active site and, (b) two active sites.

In the second mechanism (Figure 3.12b), there are two active sites due to the presence of two adjacent N-C-O species. In this case, the adsorption of the dioxygen in the two active sites may form a bridge-like –C–O–O–C– configuration (step 2 in Figure 3.12b). The breaking of the O–O bond leads to

the formation of –OH groups and, subsequently, the formation of H_2O molecules without the formation of H_2O_2. The distance between the oxygen atoms confirms this possibility. In the bridge-like structure the O–O distance is slightly higher than in the case of the first mechanism although a value close to H_2O_2 is obtained. When the second 2 e^- step occurs and –OH are formed the calculated O–O distance is much higher (2.770 Å), which is close to the distance between the water molecules (H_2O-H_2O: $d_{O\text{-}O}$ = 2.83 Å [54]), proving the dioxygen dissociation.

Thus, the presence of these sites may produce a change in ORR selectivity, being as close as 4e^- pathway with H_2O as final product, with increasing the number of double N-C-O sites. The experimental results show that the PANI carbon materials prepared in an O_2-containing atmosphere have a higher amount of N and O edge sites and, then, a higher probability of having the above-mentioned sites, which explains the higher electron transfer number, being close to 4 in acidic conditions (Table 3.5).

3.4 Conclusions

N- and O-containing carbon materials have been prepared from PANI and evaluated as electrocatalysts for the ORR. The synthesis was performed using two different temperatures and atmospheres during the treatment, which leads to materials with different surface chemistry. Materials treated in the inert atmosphere showed lower yields than the prepared using an O_2-containing atmosphere, which points out that the use of a slightly oxidant atmosphere promotes the crosslinking reactions and further condensation reactions during the carbonization. Slight differences in porosity are observed due to the low amount of O_2 used. The heat treatment at 800 ºC in an O_2-containing atmosphere generates, compared to the treatment in N_2, a higher amount of N-functionalities at edge sites (i.e., pyridine and pyridone/pyrrole groups) as well as an increase in phenol-type groups.

The prepared materials at 800 ºC in an O_2-containing atmosphere have a high electroactivity towards ORR in basic electrolyte with limiting specific currents close to the commercial sample 20% Pt/Vulcan. A detailed study of the effect of N and O functionalities confirms that a combination of N and O-containing groups at edge sites in the carbon material produced the highest ORR

activity and higher selectivity to the $4e^-$ pathway, especially in acid electrolyte. It is suggested that the presence of N-C-O species is the responsible for the enhanced ORR activity of the carbon materials prepared from PANI in the O_2-containing atmosphere.

These results are supported by preliminary computational calculations. It was observed that the N-C-O groups produce a much higher positive charge density in the C atom than the nitrogen groups without the presence of oxygen in the vicinities, which favors dioxygen adsorption and activation. It is proposed that one N-C-O site would mainly produce hydrogen peroxide through a $2e^-$ pathway while the existence of two near sites (like two pyridones) can produce the direct reduction of dioxygen to water.

3.5 References

[1] M. Winter, R.J. Brodd, What are batteries, fuel cells, and supercapacitors?, Chem. Rev. 104 (2004) 4245–4269.

[2] A.S. Aricò, P. Bruce, B. Scrosati, J.M. Tarascon, Nanostructured materials for advanced energy conversion and storage devices, Nat. Mater. 4 (2005) 366–377.

[3] C.W.B. Bezerra, L. Zhang, H. Liu, K. Lee, A.L.B. Marques, E.P. Marques, H. Wang, J. Zhang, A review of heat-treatment effects on activity and stability of PEM fuel cell catalysts for oxygen reduction reaction, J. Power Sources. 173 (2007) 891–908.

[4] X. Zhao, S. Chen, Z. Fang, J. Ding, W. Sang, Y. Wang, J. Zhao, Z. Peng, J. Zeng, Octahedral Pd@Pt1.8Ni core-shell nanocrystals with ultrathin PtNi alloy shells as active catalysts for oxygen reduction reaction, J. Am. Chem. Soc. 137 (2015) 2804–2807.

[5] X. Yu, S. Ye, Recent advances in activity and durability enhancement of Pt/C catalytic cathode in PEMFC: Part II: Degradation mechanism and durability enhancement of carbon supported platinum catalyst, J. Power Sources. 172 (2007) 145–154.

[6] B. Xu, X. Yang, X. Wang, J. Guo, X. Liu, A novel catalyst support for DMFC: Onion-like fullerenes, J. Power Sources. 162 (2006) 160–164.

[7] F. Zaragoza-Martín, D. Sopeña-Escario, E. Morallón, C.S.-M. de Lecea, Pt/carbon nanofibers electrocatalysts for fuel cells: Effect of the support oxidizing treatment, J. Power Sources. 171 (2007) 302–309.

[8] A. Morozan, B. Jousselme, S. Palacin, Low-platinum and platinum-free catalysts for the oxygen reduction reaction at fuel cell cathodes, Energy Environ. Sci. 4 (2011) 1238.

[9] L. Zhang, J. Zhang, D.P. Wilkinson, H. Wang, Progress in preparation of non-noble electrocatalysts for PEM fuel cell reactions, J. Power Sources. 156 (2006) 171–182.

[10] F. Jaouen, E. Proietti, M. Lefèvre, R. Chenitz, J.P. Dodelet, G. Wu, H.T. Chung, C.M. Johnston, P. Zelenay, Recent advances in non-precious metal catalysis for oxygen-reduction reaction in polymer electrolyte fuel cells, Energy Environ. Sci. 4 (2011) 114–130.

[11] J. Ozaki, S. Tanifuji, A. Furuichi, K. Yabutsuka, Enhancement of oxygen reduction activity of nanoshell carbons by introducing nitrogen atoms from metal phthalocyanines, Electrochim. Acta. 55 (2010) 1864–1871.

[12] C.V. Rao, C.R. Cabrera, Y. Ishikawa, In search of the active site in nitrogen-doped carbon nanotube electrodes for the oxygen reduction reaction, J. Phys. Chem. Lett. 1 (2010) 2622–2627.

[13] W. Shen, W. Fan, Nitrogen-containing porous carbons: synthesis and application, J. Mater. Chem. A. (2013) 999–1013.

[14] V.V. Strelko, V.S. Kuts, P.A. Thrower, On the mechanism of possible influence of heteroatoms of nitrogen, boron and phosphorus in a carbon matrix on the catalytic activity of carbons in electron transfer reactions, Carbon 38 (2000) 1499–1503.

[15] V.V. Strelko, N.T. Kartel, I.N. Dukhno, V.S. Kuts, R.B. Clarkson, B.M. Odintsov, Mechanism of reductive oxygen adsorption on active carbons with various surface chemistry, Surf. Sci. 548 (2004) 281–290.

[16] S. Maldonado, K.J. Stevenson, Influence of nitrogen doping on oxygen reduction electrocatalysis at carbon nanofiber electrodes, J. Phys. Chem. B. 109 (2005) 4707–4716.

[17] K. Gong, F. Du, Z. Xia, M. Durstock, L. Dai, Nitrogen-doped carbon nanotube arrays with high electrocatalytic activity for oxygen reduction, Science 323 (2009) 760–764..

[18] J.D. Wiggins-Camacho, K.J. Stevenson, Mechanistic Discussion of the Oxygen Reduction Reaction at Nitrogen-Doped Carbon Nanotubes, J. Phys. Chem. B. 115 (2011) 20002–20010.

[19] M.J. Mostazo-López, R. Ruiz-Rosas, E. Morallón, D. Cazorla-Amorós,

Generation of nitrogen functionalities on activated carbons by amidation reactions and Hofmann rearrangement: Chemical and electrochemical characterization, Carbon 91 (2015) 252–265.

[20] E. Raymundo-Pinero, D. Cazorla-Amorós, A. Linares-Solano, S. Delpeux, E. Frackowiak, K. Szostak, F. Béguin, High surface area carbon nanotubes prepared by chemical activation, Carbon 40 (2002) 1614–1617.

[21] D. Salinas-Torres, J.M. Sieben, D. Lozano-Castello, E. Morallón, M. Burghammer, C. Riekel, D. Cazorla-Amorós, Characterization of activated carbon fiber/polyaniline materials by position-resolved microbeam small-angle X-ray scattering, Carbon 50 (2012) 1051–1056.

[22] E. Raymundo-Piñero, D. Cazorla-Amorós, Á. Linares-Solano, The role of different nitrogen functional groups on the removal of SO2 from flue gases by N-doped activated carbon powders and fibres, Carbon 41 (2003) 1925–1932.

[23] K.P. Singh, M.Y. Song, J.-S. Yu, Iodine-treated heteroatom-doped carbon: conductivity driven electrocatalytic activity, J. Mater. Chem. A. 2 (2014) 18115–18124.

[24] G. Ćirić-Marjanović, I. Pašti, N. Gavrilov, A. Janošević, S. Mentus, Carbonised polyaniline and polypyrrole: towards advanced nitrogen-containing carbon materials, Chem. Pap. 67 (2013) 781–813.

[25] D. Cazorla-Amorós, J. Alcañiz-Monge, M.A. de la Casa-Lillo, A. Linares-Solano, CO2 As an Adsorptive To Characterize Carbon Molecular Sieves and Activated Carbons, Langmuir. 7463 (1998) 4589–4596.

[26] M.D. Hanwell, D.E. Curtis, D.C. Lonie, T. Vandermeerschd, E. Zurek, G.R. Hutchison, Avogadro: An advanced semantic chemical editor, visualization, and analysis platform, J. Cheminform. 4 (2012) 17.

[27] M.J. Frisch, G.W. Trucks, H.B. Schlegel, G.E. Scuseria, M.A. Robb, J.R. Cheeseman, G. Scalmani, V. Barone, B. Mennucci, G.A. Petersson, H. Nakatsuji, M. Caricato, X. Li, H.P. Hratchian, A.F. Izmaylov, J. Bloino, G. Zheng, J.L. Sonnenberg, M. Hada, M. Ehara, K. Toyota, R. Fukuda, J. Hasegawa, M. Ishida, T. Nakajima, Y. Honda, O. Kitao, H. Nakai, T. Vreven, J.A. Montgomery, J.E. Peralta, F. Ogliaro, M. Bearpark, J.J. Heyd, E. Brothers, K.N. Kudin, V.N. Staroverov, R. Kobayashi, J. Normand, K. Raghavachari, A. Rendell, J.C. Burant, S.S. Iyengar, J. Tomasi, M. Cossi, N. Rega, J.M. Millam, M. Klene, J.E. Knox, J.B. Cross, V. Bakken, C. Adamo, J. Jaramillo, R. Gomperts, R.E. Stratmann, O. Yazyev, A.J. Austin, R. Cammi, C. Pomelli, J.W. Ochterski, R.L. Martin, K. Morokuma, V.G. Zakrzewski, G.A. Voth, P. Salvador, J.J. Dannenberg, S. Dapprich, A.D. Daniels, Farkas, J.B. Foresman, J. V Ortiz, J. Cioslowski, D.J. Fox, Gaussian 09, Revision B.01, Gaussian 09,

Revis. B.01, Gaussian, Inc., Wallingford CT. (2009).

[28] J. Alcañiz-Monge, D. Cazorla-Amorós, A. Linares-Solano, A. Oya, A. Sakamoto, K. Hoshi, Preparation of general purpose carbon fibers from coal tar pitches with low softening point, Carbon 35 (1997).

[29] S. Leyva-García, E. Morallón, D. Cazorla-Amorós, F. Béguin, D. Lozano-Castelló, New insights on electrochemical hydrogen storage in nanoporous carbons by in situ Raman spectroscopy, Carbon 69 (2014) 401–408..

[30] S. Biniak, G. Szymański, J. Siedlewski, A. Świątkowski, The characterization of activated carbons with oxygen and nitrogen surface groups, Carbon 35 (1997) 1799–1810.

[31] E. Raymundo-Piñero, D. Cazorla-Amorós, A. Linares-Solano, J. Find, U. Wild, R. Schlögl, Structural characterization of N-containing activated carbon fibers prepared from a low softening point petroleum pitch and a melamine resin, Carbon 40 (2002) 597–608..

[32] D. Salinas-Torres, S. Shiraishi, E. Morallón, D. Cazorla-Amorós, Improvement of carbon materials performance by nitrogen functional groups in electrochemical capacitors in organic electrolyte at severe conditions, Carbon 82 (2015) 205–213.

[33] S. Kuroki, Y. Hosaka, C. Yamauchi, A solid-state NMR study of the carbonization of polyaniline, Carbon 55 (2013) 160–167.

[34] Z. Rozlívková, M. Trchová, M. Exnerová, J. Stejskal, The carbonization of granular polyaniline to produce nitrogen-containing carbon, Synth. Met. 161 (2011) 1122–1129.

[35] J.. Figueiredo, M.F.. Pereira, M.M.. Freitas, J.J.. Órfão, Modification of the surface chemistry of activated carbons, Carbon 37 (1999) 1379–1389.

[36] Y. Otake, R.G. Jenkins, Characterization of oxygen-containing surface complexes created on a microporous carbon by air and nitric acid treatment, Carbon 31 (1993) 109–121.

[37] M.C.C. Román-Martínez, D. Cazorla-Amorós, A. Linares-Solano, C.S.-M. de Lecea, TPD and TPR characterization of carbonaceous supports and Pt/C catalysts, Carbon 31 (1993) 895–902.

[38] P. Burg, D. Cagniant, Characterization of Carbon Surface Chemistry. In: Radovic LR, editor. Chemistry & Physics of Carbon. Vol. 30. Taylor & Francis (CRC Press); 2008. p. 129–75.

[39] R. Berenguer, J.. Marco-Lozar, C. Quijada, D. Cazorla-Amorós, E. Morallón, Effect of electrochemical treatments on the surface chemistry of activated carbon, Carbon 7 (2008) 1018–1027.

[40] H.F. Gorgulho, J.P. Mesquita, F. Gonçalves, M.F.R. Pereira, J.L. Figueiredo, Characterization of the surface chemistry of carbon materials by potentiometric titrations and temperature-programmed desorption, Carbon 46 (2008) 1544–1555.

[41] O. Ornelas, J.M. Sieben, R. Ruiz-Rosas, E. Morallón, D. Cazorla-Amorós, J. Geng, N. Soin, E. Siores, B.F.G. Johnson, On the origin of the high capacitance of nitrogen-containing carbon nanotubes in acidic and alkaline electrolytes, Chem. Commun. 50 (2014) 11343–11346..

[42] D. Hulicova, J. Yamashita, Y. Soneda, H. Hatori, M. Kodama, Supercapacitors Prepared from Melamine-Based Carbon, Chem. Mater. 17 (2005) 1241–1247.

[43] D. Hulicova-Jurcakova, M. Kodama, S. Shiraishi, H. Hatori, Z.H. Zhu, G.Q. Lu, Nitrogen-Enriched Nonporous Carbon Electrodes with Extraordinary Supercapacitance, Adv. Funct. Mater. 19 (2009) 1800–1809.

[44] L. Zhang, Z. Xia, Mechanisms of oxygen reduction reaction on nitrogen-doped graphene for fuel cells, J. Phys. Chem. C. 115 (2011) 11170–11176.

[45] Kim H, Lee K, Woo SI, Jung Y, Sheng W, Gasteiger HA, et al. On the mechanism of enhanced oxygen reduction reaction in nitrogen-doped graphene nanoribbons. Phys Chem Chem Phys. 2011;13(39):17505

[46] R. Silva, D. Voiry, M. Chhowalla, T. Asefa, Efficient metal-free electrocatalysts for oxygen reduction: Polyaniline-derived N- and O-doped mesoporous carbons, J. Am. Chem. Soc. 135 (2013) 7823–7826.

[47] J. I. Ozaki, N. Kimura, T. Anahara, A. Oya, Preparation and oxygen reduction activity of BN-doped carbons, Carbon 45 (2007) 1847–1853.

[48] J.E. Park, Y.J. Jang, Y.J. Kim, M.S. Song, S. Yoon, D.H. Kim, S.J. Kim, Sulfur-doped graphene as a potential alternative metal-free electrocatalyst and Pt-catalyst supporting material for oxygen reduction reaction, Phys. Chem. Chem. Phys. 16 (2014) 103–109.

[49] C. Domínguez, F.J. Pérez-alonso, M. Abdel, S.A. Al-thabaiti, A.Y. Obaid, A.A. Alshehri, J.L. Gómez, D. Fuente, J.L.G. Fierro, S. Rojas, On the relationship between N content, textural properties and catalytic performance for the oxygen reduction reaction of N/CNT, Applied Catal. B, Environ. 162 (2015) 420–429.

[50] T. Ikeda, M. Boero, S.F. Huang, K. Terakura, M. Oshima, J. I. Ozaki, Carbon

alloy catalysts: Active sites for oxygen reduction reaction, J. Phys. Chem. C. 112 (2008) 14706–14709.

[51] M. Seredych, K. Singh, T.J. Bandosz, Insight into the capacitive performance of sulfur-doped nanoporous carbons modified by addition of graphene phase, Electroanalysis. 26 (2014) 109–120.

[52] W.Y. Wong, W.R.W. Daud, A.B. Mohamad, A.A.H. Kadhum, K.S. Loh, E.H. Majlan, K.L. Lim, Electrochimica Acta The Impact of Loading and Temperature on the Oxygen Reduction Reaction at Nitrogen-doped Carbon Nanotubes in Alkaline Medium, Electrochim. Acta. 129 (2014) 47–54.

[53] N.N. Greenwood, A. Earnshaw, Chemistry of Elements. 2nd ed. Elsevier Butterworth-Heinemann, 1997.

[54] E. Clementi, Determination of Liquid Water Structure In: B. Carpenter, P. Ceroni, B. Kirchner, K. Landfester, J. Leszczynski, T.Y. Luh, , in: Lecture Notes in Chemistry vol. 2. 1st ed. Berlin, Heidelberg, Springer, 1976.

CHAPTER IV

OXYGEN-REDUCTION CATALYSIS OF N-DOPED CARBONS PREPARED VIA HEAT TREATMENT OF POLYANILINE AT OVER 1100 ºC

4.1 Introduction

Hydrogen fuel cells (FCs) and direct methanol FCs arise as a substitute for current internal combustion engines due to their high energy efficiency and the lack of pollutant emissions compared to traditional car engines [1]. One important issue that makes difficult its implementation is the use of platinum (Pt) as electrocatalyst in both the hydrogen (or methanol) oxidation and oxygen reduction reactions (ORR). The high cost and low abundance of this metal [2], which corresponds to one-third of the fuel cell total cost, make necessary either to decrease the amount of Pt in the catalyst or to substitute it by another active catalyst. In addition, most of the Pt (almost 90% of total Pt in the FCs [3]) is used in the cathode due to the low rate of the ORR. Finally, deactivation due to metal nanoparticle agglomeration and poisoning by traces of carbon monoxide (present in hydrogen) or methanol, causes the decrease of the catalytic activity with life-time [2,4]. In this sense, recent research have focussed on the development of new cathode catalysts which can make a substantial advantage towards fuel cells expansion [5]. Thus, new materials that can produce similar catalytic activity as Pt towards ORR have been developed [6–12].

N-doped carbon materials are one of the candidates to replace Pt in fuel cells [5]. As they do not contain metals, a dramatic reduction of the catalyst cost may result. In some cases, the Pt activity has almost been reached, but these materials are based on expensive chemical reagents, like graphene, and complex and expensive synthetic methods which increases the final catalyst cost [8,12]. Although the effect of the N on the carbon materials has been studied extensively, there is still a strong debate about the nature of N functionalities which generates an improvement in the catalytic activity towards ORR [13].

Polyaniline (PANI) has been employed as a precursor of carbon materials for its use as support of metal nanoparticles [9–11] because of its high amount of N functional groups and its interesting properties [14]. N-doped carbon materials derived from PANI have also been studied as metal-free catalysts [15–20]. However, their catalytic activity towards

ORR is too low to be applied in a commercial fuel cell. All these works have synthesized carbon materials through the pyrolysis of PANI at temperatures lower than 1000ºC in an inert atmosphere. Some exceptions can be found in the literature where the temperature used is higher than 1000ºC [21,22]. However, the use of templates modifies the structural order and the properties of the carbon materials, which may introduce differences in the effect of the heat treatment. Moreover, in these works, the presence of metal traces (Fe [21] and Mn [22]) cannot be discarded from the preparation method used.

The present chapter studies the effect of heat treatment temperature on the catalytic activity. The key experimental parameter is the carbonization temperature and the use of metal-free PANI as N-doped carbon precursor. When the carbonization temperature is 1100 or 1200ºC, the PANI-derived carbon materials show excellent catalytic properties towards ORR in alkaline conditions and very good stability with resistance to methanol poisoning. This makes these catalysts suitable for utilization in fuel cells that work at low temperature and in alkaline conditions (hydrogen, methanol, ethanol, etc.). This route is a facile, high yield and low-cost synthesis method of N-doped carbon materials from PANI which reach an ORR activity in alkaline electrolyte similar to commercial Pt.

4.2 Experimental

4.2.1 Materials

Aniline was purchased from Sigma Aldrich and distilled by refluxing under reduced pressure prior to its use in order to remove the impurities. Ammonium persulfate ($(NH_4)_2(S_2O_8)$), ammonium hydroxide (NH_4OH), potassium hydroxide (KOH) and 20wt% Pt/Vulcan were purchased from Sigma Aldrich. Perchloric acid (60%, $HClO_4$) were purchased from VWR-Chemicals Prolabo. All the solutions were prepared using ultrapure water (18MΩ cm from an Elga Labwater Purelab system). The gases N_2 (99.999%), O_2 (99.995%), H_2 (99.999%) and synthetic air were provided by Air Liquide and were used without any further purification or treatment.

4.2.2 PANI preparation

Polyaniline was prepared by chemical polymerization from a solution of 1 M HCl containing 0.067 M of aniline and ammonium persulfate in a

stoichiometric ratio. The mixture was kept under stirring (500rpm) for 3 h at 0ºC. In order to obtain the dedoped-polyaniline, polyaniline was treated with 1M NH_4OH for 24 h. The synthesized PANI was washed several times with distilled water and dried at 80ºC overnight.

4.2.3 Heat treatment

The samples of PANI (150 mg) were heat-treated in a tubular furnace at differences temperatures between 600 and 1200ºC for 1h using a heating rate of $5ºC \cdot min^{-1}$ in a nitrogen-atmosphere. The final carbon material is named as PANI_X, being X the temperature used during the treatment.

All PANI-derived carbon materials are obtained as a powder (from the TEM images in Figure 4.1, it is possible to observe that the particles are below 1 µm and are formed by aggregation of individual nanosized particles of around 20-200 nm). The furnace was purged for 1h before the heat treatment in the corresponding atmosphere, the flow rate was maintained at 100 $ml \cdot min^{-1}$ during the treatment. The same treatment at high temperature has been carried out in the presence of argon-atmosphere in order to confirm the inert properties of the nitrogen-atmosphere at the experimental conditions used. The resulting material is named as PANI_Ar_X, where X is the temperature used during the heat treatment.

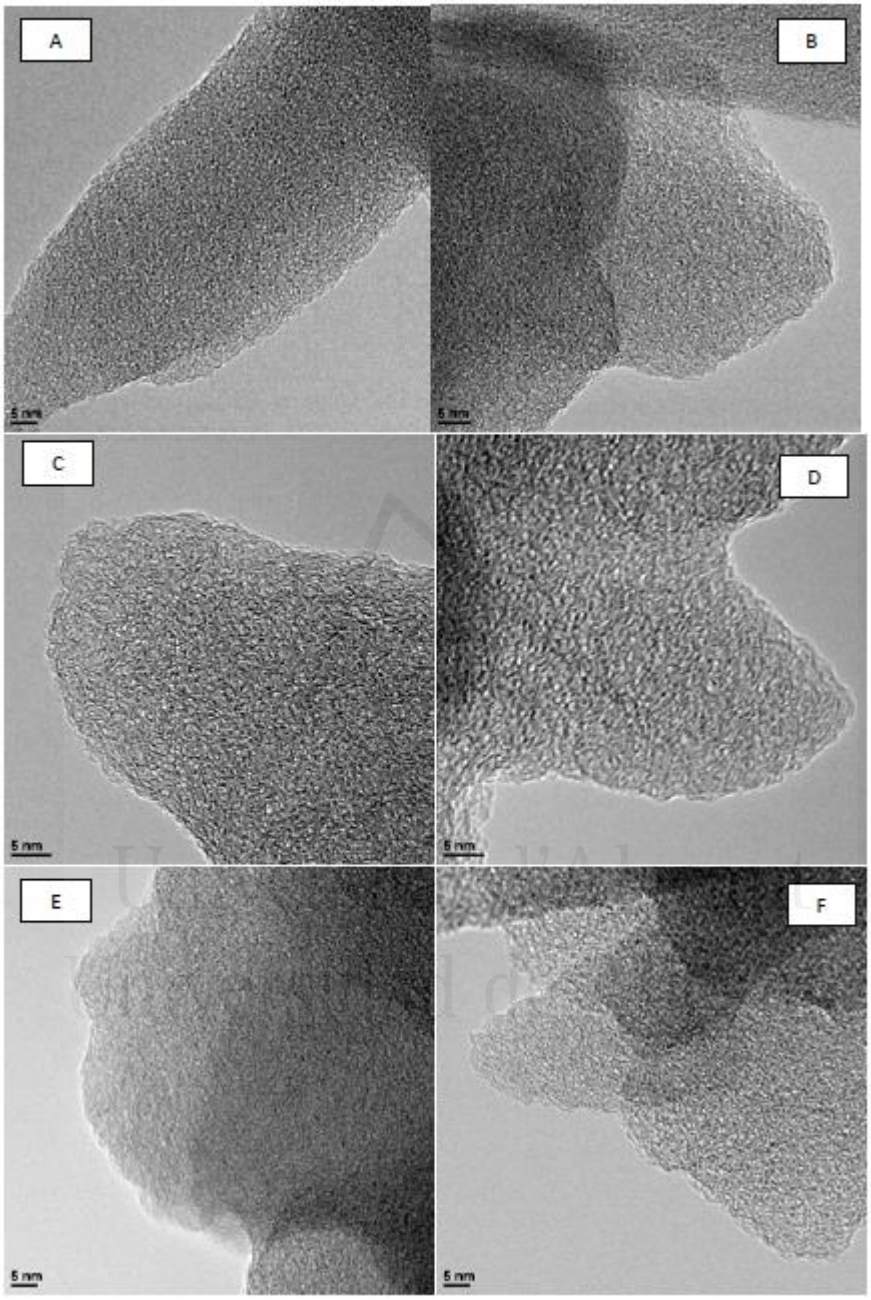

Figure 4.1: TEM images of (a) PANI_600, (b) PANI_800, (c) PANI_900, (d) PANI_1000, (e) PANI_1100 and (f) PANI_1200.

4.2.4 Characterization

The study of the electrocatalytic activity towards ORR has performed in an Autolab PGSTAT302 (Metrohm, Netherlands) potentiostat. A rotating ring-disk electrode (RRDE, Pine Research Instruments, USA) equipped with a glassy carbon disk (5.61 mm diameter) and an attached platinum ring was used as the working electrode, a platinum wire as the counter electrode and a reversible hydrogen electrode immersed in the working electrolyte as the reference electrode. The amount of catalyst on the disk electrode was optimized in order to reach the highest limiting current, being 120 µg the optimum value. Therefore, the glassy carbon disk was modified with the samples using 120 µl of a 1 $mg \cdot ml^{-1}$ dispersion of each carbon material (20% isopropanol, 0.02% Nafion ®), obtaining a catalyst loading of 0.48 $mg \cdot cm^{-2}$. The electrocatalytic activity towards ORR was studied by linear sweep voltammetry (LSV) in O_2 saturated 0.1 M KOH between 0.0 and 1.0 V (vs RHE) at different rotation rates, from 400 to 2025 rpm and at a scan rate of 5 $mV \cdot s^{-1}$. The potential of the ring was held constant at 1.5 V (vs. RHE) during all measurements. The H_2O_2 yield and the number of electrons were calculated from the hydrogen peroxide oxidation in the Pt ring electrode as follows:

$$H_2O_2(\%) = 200 \cdot \frac{I_R/N}{\left(I_R/N\right) + I_D}$$

$$n = \frac{4 \cdot I_D}{I_D + I_R/N}$$

where I_R and I_D are the current measured at the ring and the disk, respectively, and N is the collection efficiency of the ring, which was experimentally determined to be 0.37. The number of electrons and H_2O_2 generation was discussed by RRDE and not by Koutecky-Levich (KL) theory in order to reflect more faithfully the results obtained. Nevertheless, the number of electrons calculated by KL are included in the comparison with the bibliography in Table 4.1. Moreover, a rotating disk electrode (RDE, Pine Research Instruments, USA) equipped with a glassy carbon disk (5 mm diameter) and graphite as a counter electrode was used in order to discard the possibility of Pt contamination from the counter electrode and platinum ring.

Table 4.1: Comparison on the electrocatalytic activity of the recently reported ORR catalysts.

Catalyst	Mass used / $mg \cdot cm^{-2}$	ONSET Potential	Half-wave potential / V	Limiting current / $mA \cdot cm^{-2}$	Number of electrons	References
PANI_1100	0.48	0.94	0.85	5.4	3.9 (RRDE) / 4.0 (KL)	This chapter
20 wt.% Pt/Vulcan	0.41	0.98	0.84	5.4	4.0 (RRDE) / 4.0 (KL)	This chapter
PANId_O2_800	0.48	0.75	0.66	5.2	3.0 (RRDE)	Chapter 3
NA_NCNT/GC	-	0.95	-	Not showed and not achieved	3.9 (RRDE)	**[23]**
N-RG-O 1000ºC	0.5	0.85	0.66	4.2	2.25 (KL)	**[19]**
N-Graphene	0	0.82	0.68	0.8 (at 1000rpm)	3.6 (KL)	**[8]**
PDMC800	0.1	0.85	-	Not achieved	3.2 (KL)	**[15]**
N550-GD	0.4	0.84	0.68	4.0	3.7 (RRDE) / 3.7 (KL)	**[24]**
PDI-900/GC	0.1	0.82	0.75	Not achieved	3.9 (KL)	**[25]**
G-C3N4@CMK-3	0.084	0.88	-	Not achieved	4.0 (KL)	**[26]**
N-CN	0.2	0.80	0.70	4.0	3.5 (KL)	**[27]**
N-HCNSS	0.4	0.85	0.75	3.0	-	**[28]**

Thermogravimetric analysis has been performed using a thermobalance (SDT 2960 Instrument, TA). Heat treatment in air conditions (100 ml·min^{-1}) of carbon materials was characterized in air at 900ºC (heating rate of 10ºC·min^{-1}).

In order to study the stability performance and methanol poisoning test, chronoamperometric experiments were performed. The stability experiments were performed in 0.1 M KOH at a potential of 0.65 V and 1600 rpm for 2 hours. In order to study the stability of the catalysts in presence of methanol, after the 2 hours of the stability test, methanol was added into the electrolyte until achieving 1 M methanol.

The textural properties of the materials were evaluated by N_2 adsorption isotherms at -196ºC in an automatic adsorption system (Autosorb-6, Quantachrome). Prior to the measurements, the samples were degassed at 250ºC for 4h. Apparent surface areas have been determined by BET method (S_{BET}). Figure 4.2 includes the N_2 isotherms for three representative materials and Table 4.2 summarizes the BET surface areas for all the materials prepared.

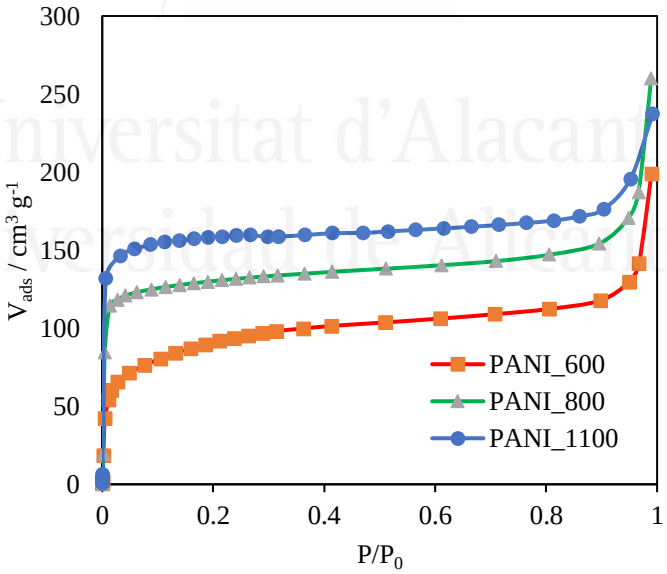

Figure 4.2: N_2-adsorption isotherms at -196ºC of the PANI-derived carbon materials prepared at 600, 800 and 1100ºC.

Table 4.2: Surface area data for all the materials prepared.

Sample	S_{BET} / $m^2 \cdot g^{-1}$
PANI_600	340
PANI_800	526
PANI_900	624
PANI_1000	728
PANI_1100	743
PANI_1200	735

The results show an increase in surface area with heat treatment temperature and that it reaches the highest values for heat treatment temperatures above 1000ºC. The development of porosity by carbonization of polymers is very much dependent on the physical and chemical properties of the precursor. In all the cases, the porosity goes through a maximum with increasing the heat treatment temperature, but the values of porosity are dependent on the precursor. For example, in the case of infusible polymers like PVDC, surface areas as high as 1200 $m^2 \cdot g^{-1}$ are obtained at heat treatment temperatures of 1300ºC, but in the case of fusible polymers like PFA, the maximum of surface area (around 450 $m^2 \cdot g^{-1}$ is obtained at 750ºC [29].

PANI is an example of conjugated polymer that can be directly carbonized with good yields due to the strong intra and inter π-π interaction [30]. And porous nanostructured carbons can be directly obtained through direct carbonization, that is, using template free strategies [30]. In addition, very different porosities are obtained depending on the preparation conditions and even using the same template [30].

The samples were characterized by Transmission Electron Microscopy (TEM) coupled to EDX with a JEOL JEM-2010 microscope operating at 200kV with a spatial resolution of 0.24 nm.

The electrical conductivity of all samples has been evaluated using electrochemical impedance spectroscopy (EIS) in an Autolab PGSTAT302.

Impedance spectra were measured at 0.5 V vs. RHE in the frequency range of 10 mHz to 100 kHz with an amplitude for the voltage signal of 10 mV in 0.1 M KOH solution.

Raman spectra were collected on a Jasco NRS-5100 spectrometer. A 3.9 mW He-Ne laser at 633 nm was used. The spectra were acquired for 120 s. The detector was a Peltier cooled charge-coupled device (CCD) (1024 x 255 pixels). Calibration of the spectrometer was performed with a Si slice (521 ± 2 cm^{-1}).

The surface composition and oxidation states of the elements of the prepared materials were studied using XPS in a VG-Microtech Multilab 3000 spectrometer with an Al Kα radiation source (1253.6 eV). The deconvolution of the N1s XPS spectra was done by least squares fitting using Gaussian-Lorentzian curves, while a Shirley line was used for the background determination.

The determination of the electronic density was performed with Gaussian 09 software using density functional theory (DFT) with B3LYP/6-31G(d) level of approximation.

Table 4.3: Yield of the heat treatment (weight %), percentage of nitrogen and percentage of each nitrogen functional group for all materials.

Sample	Yield / %	N content / %	Pyridine / %	Pyrrole or pyridone	Quaternary N / %	Oxidized N / %	Amides / %
PANI_600	61	7.7	29	49	-	-	22
PANI_800	53	7.0	40	35	25	-	-
PANI_900	49	4.3	35	34	26	5	-
PANI_1000	39	3.0	31	35	28	6	-
PANI_1100	32	1.8	24	34	32	10	-
PANI_1200	29	1.0	18	35	33	14	-

4.3 Results & Discussion

PANI was synthesized by chemical polymerization and heat-treated in a tubular furnace at temperatures between 600 and 1200ºC in a N_2 atmosphere. The yield of the carbonizations is included in Table 4.3.

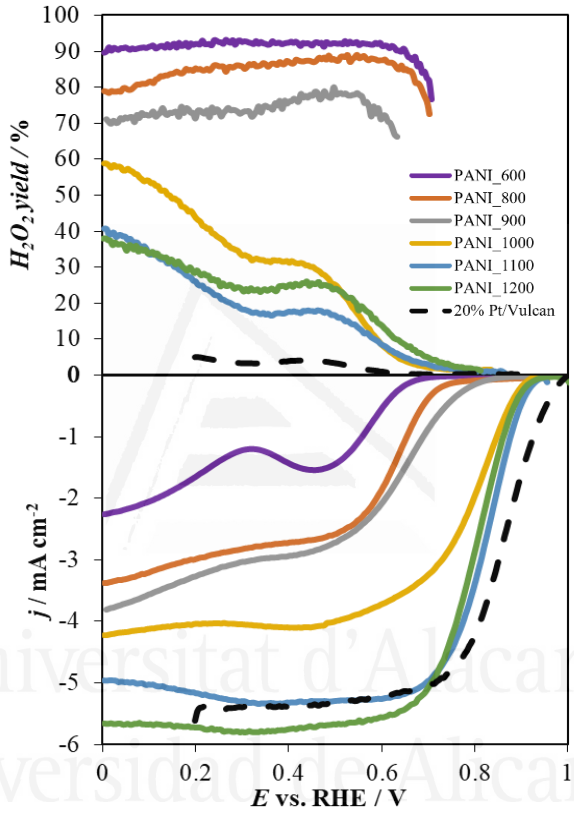

Figure 4.3: (up) H_2O_2 yield and (down) Linear Sweep Voltammetry curves for the prepared materials in O_2-saturated 0.1 M KOH at 5 mV·s^{-1} and 1600 rpm.

The H_2O_2 selectivity and ORR activity in 0.1 M KOH solution of the obtained carbon materials and a 20 wt. % Pt/C reference catalyst are shown in Figure 4.3. The sample treated at low temperature (600ºC) shows a poor activity and selectivity in the ORR, which is very far from the commercial Pt catalyst. The H_2O_2 yield is higher than 90%, which makes impossible its use as electrocatalyst in ORR; however, it could be useful in H_2O_2 formation reaction [31]. At intermediate temperatures (800-

900ºC), the materials start to acquire better ORR activities. Despite their better catalytic activity towards ORR, these samples are still not adequate compared to the commercial catalyst. In these cases, a decrease in H_2O_2 yield, with values around 70-80%, is observed. At higher temperatures (≥1000ºC) a remarkable improvement in ORR activity happens, and at T ≥ 1100ºC, materials with excellent ORR activities are obtained, which are close to 20% Pt/Vulcan. On the other hand, the H_2O_2 yield of the PANI-derived carbon materials obtained at high temperature is very low in the useful potential range of the FCs (0.6 – 1.0 V) which prevents the formation of harmful by-products during the operation of fuel cells. Similar results are obtained when using argon atmosphere (included in Figure 4.4). RDE experiments using graphite as a counter electrode (Figure 4.5) are similar to those with RRDE.

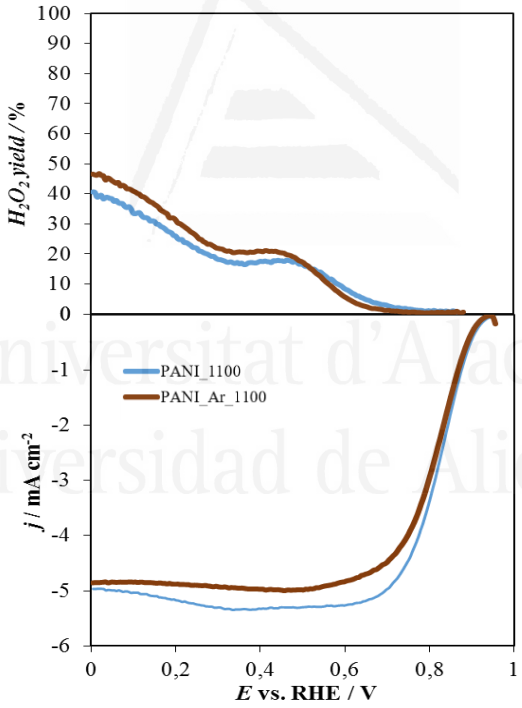

Figure 4.4: (up) H_2O_2 yield and (b) Linear sweep voltammetry curves of PANI_1100 and PANI_Ar_1100 in O_2-saturated 0.1 M KOH at 5 $mV \cdot s^{-1}$ and 1600 rpm.

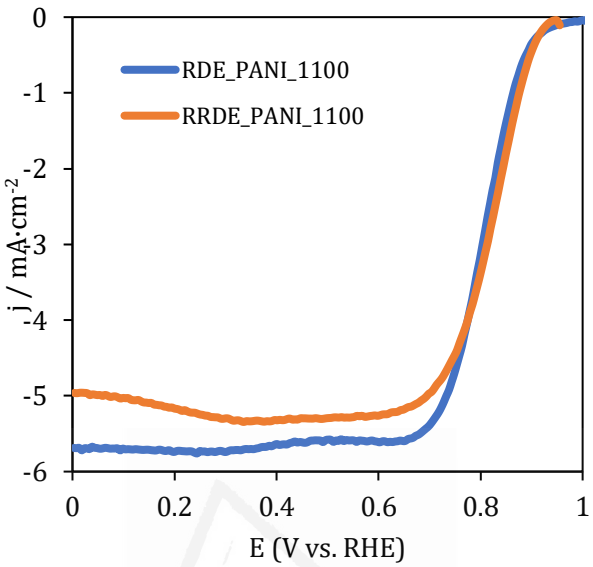

Figure 4.5: RDE study of PANI_1100 in O_2-saturated 0.1 M KOH at 5 $mV \cdot s^{-1}$ at different rotation rates. RRDE study of the same sample was added for comparison purposes.

Another major problem of the Pt-based catalysts is the stability performance and the carbon monoxide and methanol poisoning. Methanol poisoning study was done because it is the easiest way to evaluate carbon monoxide poisoning (present in traces in hydrogen gas) [32]. The stability of PANI_1100 was evaluated under potentiostatic conditions (Figure 4.6). The results are promising since the 20 wt.% Pt/Vulcan sample reaches 87% of its initial activity after 2 hours of reaction (arrow in Figure 4.6), whereas PANI_1100 material has 95% of its initial activity after this reaction time. Even after adding methanol, PANI_1100 activity is almost 90% of the initial value over 3 hours. However, the current of the 20wt% Pt/Vulcan sample drops to zero immediately after addition of methanol. The experiment supports the fact that PANI-derived carbon materials are suitable in terms of stability and resistance towards methanol and carbon monoxide. Moreover, they can be good candidates to be used in direct methanol fuel cells because of its tolerance to methanol poisoning. A detailed characterization of the materials was done to understand the reasons for their excellent catalytic activity towards ORR.

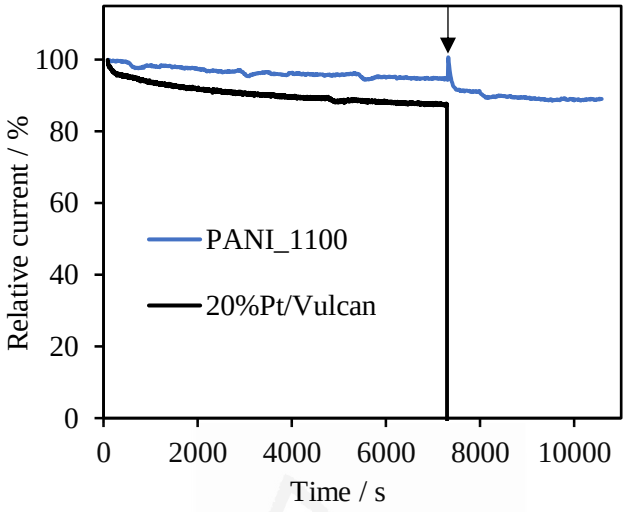

Figure 4.6: Current versus time for PANI_1100 and 20%Pt/Vulcan at 0.65 V vs RHE in O_2-saturated 0.1 M KOH solution at 1600 rpm and 25ºC.

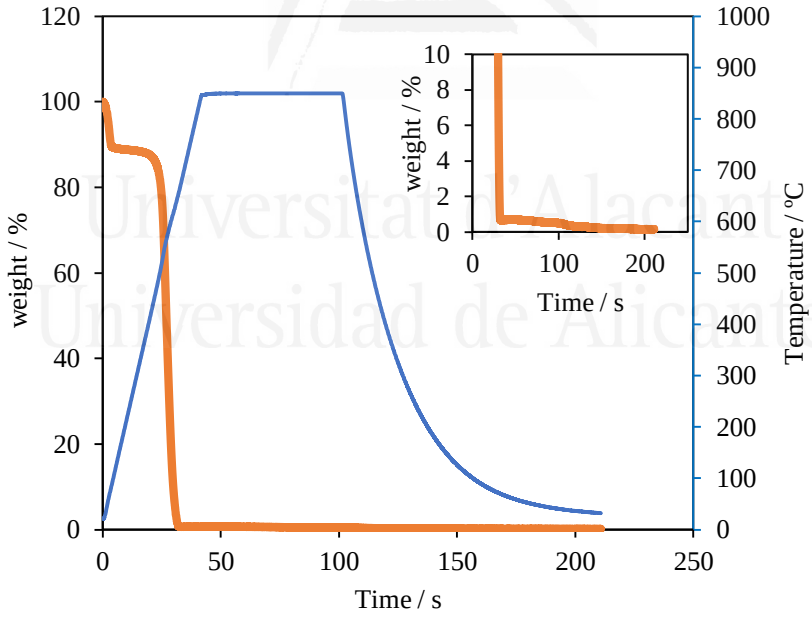

Figure 4.7: TG analysis profiles of PANI_1100 in air at 10ºC·min^{-1} until 900ºC in air atmosphere.

Figure 4.7 shows the thermogravimetric analysis of PANI_1100 in an air atmosphere. The material is completely burnt-off, showing its high purity and the lack of inorganic residues. The porosity and morphology of PANI-derived carbon materials were characterized via TEM images and N_2 adsorption isotherms, respectively. TEM images (Figure 4.1) show that the increase in heat treatment temperature does not produce a relevant increase in long-range structural order, but sheet-like structures are observed. Figure 4.2 shows that there is a good development of porosity with heat treatment temperature. The surface area data (Table 4.2) show that it reaches the highest values for heat treatment temperatures above 1000ºC. Thus, the increase in surface area is beneficial for increasing the catalytic activity [13]. However, since there is an additional improvement in catalytic activity when the heat treatment is done at 1100ºC or 1200ºC, the changes in structural order and chemical composition must play a relevant role in the catalytic activity.

Electrochemical impedance spectroscopy (Figure 4.8) gives typical results for carbon-based materials. The size of the semicircle in the medium to high frequency range is related to the resistance of charge transfer through the grain-boundaries at the rough electrode-electrolyte interface [33,34] that allows dielectric polarization of the solution. In this sense, with increasing the heat treatment temperature, the diameter of the semicircle decreases, what is indicative of the better electrical conductivity and charge propagation [35].

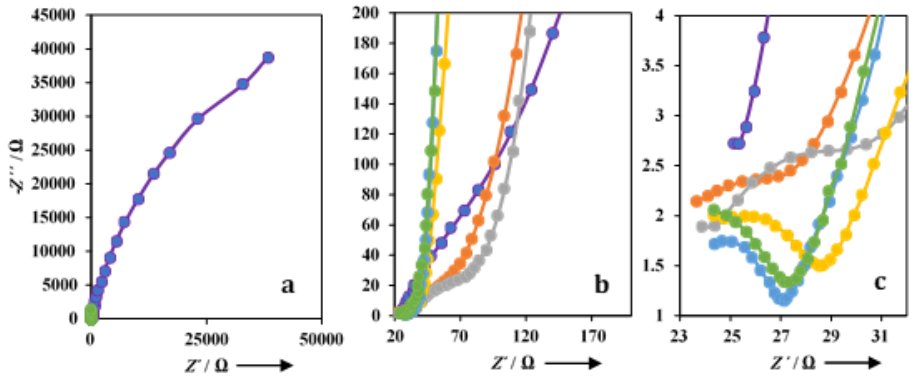

Figure 4.8: Nyquist plots corresponding to carbon materials obtained by heat treatment in N_2 atmosphere at 600ºC (violet line), 800ºC (grey line), 900ºC (red line), 1000ºC (yellow line), 1100ºC (blue line) and 1200ºC (green line) in 0.1 M KOH solution.

Raman spectra of all samples are presented in Figure 4.9. The increase in temperature results in a narrowing of the D band and a displacement of G band towards higher wavelength reaching values closer to the D_2 band. This band is associated to a lattice vibration analogous to that of the G band but involving graphene layers which are not directly sandwiched between two other graphene layers (i.e. 'boundary layer planes') [36–39]. Samples treated at 1100 and 1200 ºC have similar Raman spectra. This means that upon increasing the heat treatment temperature, the local structural order increases.

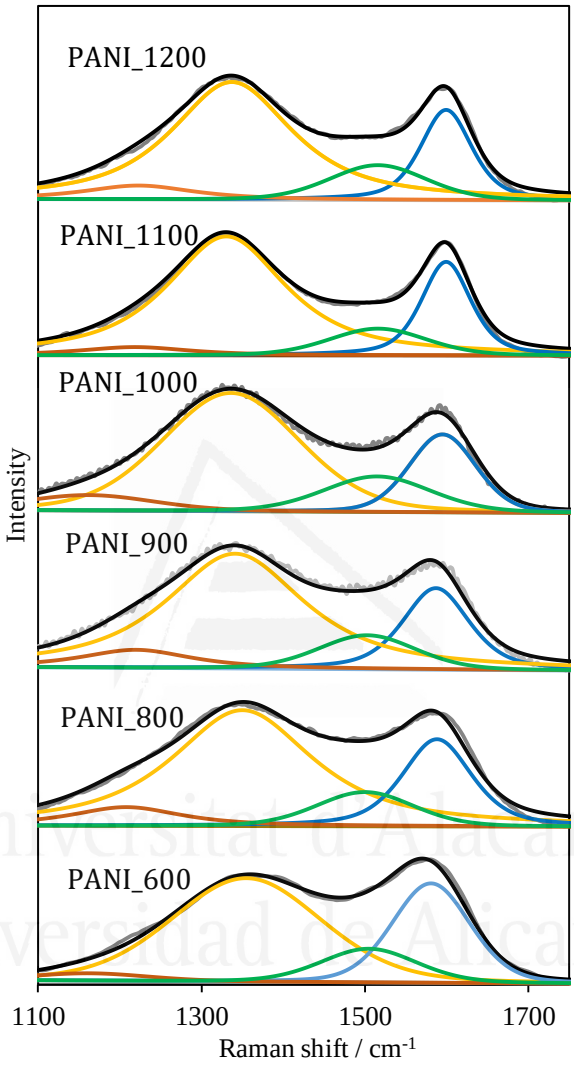

Figure 4.9: Raman spectra of all materials.

However, in order to have a good ORR electrocatalytic activity in carbon materials, a good electrical conductivity, porosity and structural order are not enough to achieve excellent properties. For instance, pristine graphene does not present high activity towards ORR [8]. Thus, in addition to a good electron transfer from the cathode electrode, it is also

necessary the presence of catalytically active sites, where the oxygen molecule is chemisorbed and reduced. In this sense, it is known that nitrogen (N) plays a fundamental role on ORR electroactivity [40] and that PANI-derived carbon materials contain a high amount of N-functionalities [14]. Thus, these functional groups can be responsible for the creation of the catalytically active sites that produce the high activity observed for the materials treated at high temperature. Then, a detailed characterization of N species has been done. Figure 4.10 shows N1s spectra of XPS for all materials prepared and Table 4.3 collects the quantification for each functionality detected. Low heat treatment temperatures produce pyridine, amines and pyrrole/pyridone species [41]. As temperature increases until 800-900ºC, a contribution of quaternary N appears and amines disappear due to their lower thermal stability [41]. Once a higher temperature (1000ºC) is reached, N-O species are observed and there is an important increase in quaternary N contribution while pyridine N species decrease and almost disappear in PANI_1200. Then, there is a conversion of pyridine to quaternary N due to condensation reactions that increase the size of the graphene layers [42].

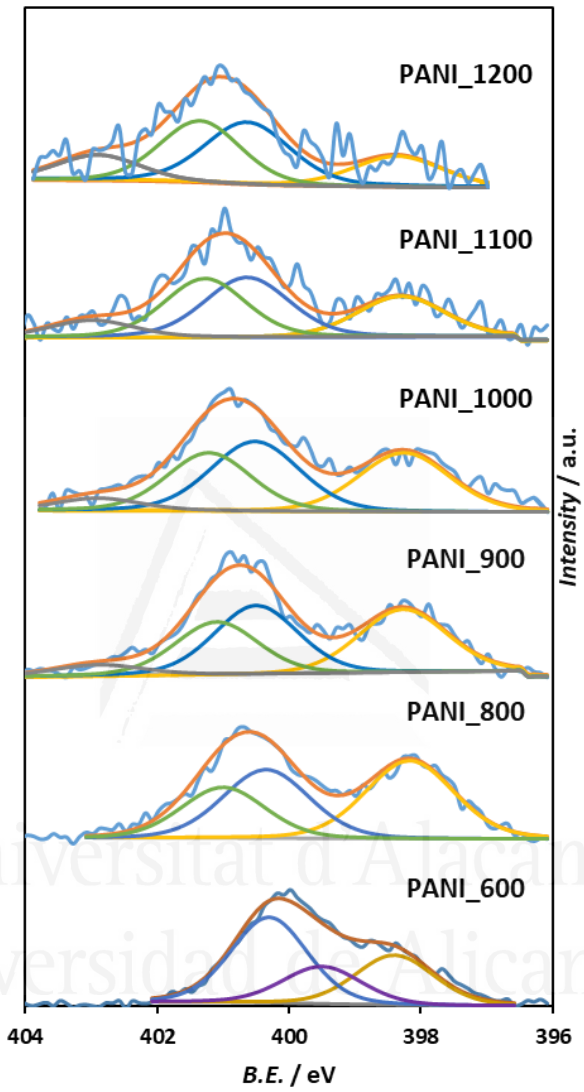

Figure 4.10: N1s spectra of all materials. Yellow represents pyridines, violet represents amines, blue represents pyrrole or pyridones, green represents quaternary nitrogen and grey represents oxidized nitrogen species.

From the H_2O_2 selectivity evolution (Figure 4.3), there is a change in H_2O_2 yield between samples treated at low-intermediate temperatures (i.e., 600-900ºC) and samples treated at high temperature (≥1000ºC). This

suggests that the chemical nature of the species, which work as active sites towards ORR, changes with the increase in temperature during the treatment. The samples treated at high temperatures make the oxygen reduction happens via $4e^-$ (0% H_2O_2 yield) until ≃0,75V because of the presence of new active sites formed by high temperature treatment (these are named as species I). Below this potential, the H_2O_2 profile for this sample changes and the contribution of oxygen reduction via $2e^-$ process increases. This suggests that less active species, which act as active sites in the samples treated at intermediate temperature (species II), that will also exist in high temperature samples, start to contribute to dioxygen reduction through the $2e^-$ mechanism producing an increase in H_2O_2 formation. Thus, there must exist a competition between the two actives sites for the O_2 reduction. In this sense, XPS analysis suggests that the modification of the nature of the active sites is due to the conversion of N pyridinic species to quaternary N and some small amount of oxidized N. Quaternary N species can activate the two contiguous carbon atoms that can constitute the neighbouring active sites that promote ORR through direct reduction to H_2O (via $4e^-$)[20].

In order to gain a better understanding of the nature of these active sites, Figures 4.11 show the model structure and the atom effective charge for the different possible functional groups that could work as active sites in the samples treated at high temperature. The arrows in these figures point out the two carbon atoms which can act as neighbouring active sites, that are connected to a N atom and that could be responsible for the $4e^-$ O_2 reduction.

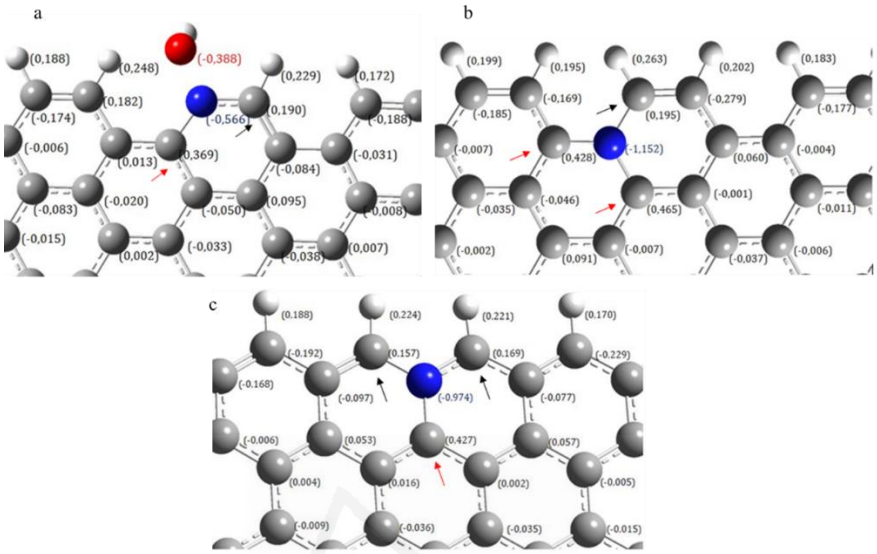

Figure 4.11: Model structure and atom effective charge of (a) oxidized nitrogen, edge-type quaternary nitrogen in (b) armchair and (c) zigzag positions. Blue represents nitrogen atom, red spheres represents oxygen atoms, grey sphere represents carbon atoms and white represents hydrogen atoms.

In the case of N-O species (Figures 4.11a), the large negative charge in N-O functionality produces an important electron withdrawal in the carbon atoms, which may result in a strong chemisorption of O_2 and further carbon atom oxidation. This suggests that these groups do not work as efficient active sites for ORR. Moreover, if ORR could occur, it would be expected that in order to reduce the charge repulsion with the N-O species, the O_2 molecule would be preferentially chemisorbed on the positively charged carbon atom in a terminal configuration through one oxygen atom (Figure 4.12a), making the ORR on these groups preferentially via $2e^-$. A similar situation may occur in quaternary N species in armchair position (Figure 4.11b). In this case, there is an asymmetric charge distribution for the neighbouring C atoms. One of these C atoms has a high positive charge, what makes probable either oxygen chemisorption followed by carbon oxidation, or the $2e^-$ oxygen reduction route. However, in the case of quaternary N in zig-zag position (Figure 4.11c), the oxygen molecule could be bonded through the edges of the graphene plane, where the repulsion between O_2 and N atom will

be reduced to the minimum and each oxygen atom would be adsorbed in a bridge configuration to the two positively charged (but weakly) carbon atoms (Figure 4.12b). This suggests that quaternary N in the zig-zag position may produce the most active sites on carbon materials treated at high temperatures.

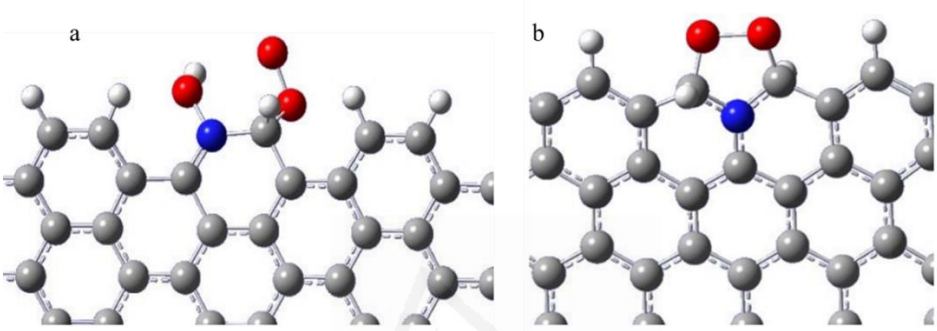

Figure 4.12: Model structure of the oxygen reduction reaction intermediate in (a) oxidized nitrogen and (b) edge-type quaternary nitrogen species.

Regarding quaternary N species, internal and edge functionalities should be differentiated. Although internal quaternary N species are considered to be non-active [40], edge-type quaternary N groups in the zig-zag position have been proposed as active sites in the literature via computational modelling [40]. This means that the conversion at high temperatures (proposed in the literature [42]) from pyridinic N species to quaternary species at edge sites seems to be the responsible for the improvement in the catalytic activity towards ORR. It should be noted that pyridinic N does not seem to have a high activity towards ORR [40].

4.4 Conclusions

In summary, the heat treatment of PANI at high temperatures in N_2 atmosphere produces excellent catalysts for ORR in an alkaline electrolyte. The activity of the materials prepared at 1100ºC is similar to that of 20wt% Pt/Vulcan and better than other N-doped carbon materials prepared via different methods or at lower temperatures (see Table 4.1). The simple synthesis method makes these materials very promising for the future low-cost FCs commercialization. Moreover, we have proved that

the porosity, electrical conductivity and structural order play a decisive role towards ORR. The pyridine functional group conversion to edge-type quaternary N species in the zig-zag position during the heat treatment seems to be responsible for the formation of the most active sites in PANI-derived carbon materials. The selection of the heat treatment temperature is crucial to achieve both an improved conductivity and a higher concentration of the most active, $4e^-$ catalytic active sites.

4.5 References

[1] B.C. Steele, A. Heinzel, Materials for fuel-cell technologies., Nature. 414 (2001) 345–352.

[2] I.E.L. Stephens, A.S. Bondarenko, U. Grønbjerg, J. Rossmeisl, I. Chorkendorff, Understanding the electrocatalysis of oxygen reduction on platinum and its alloys, Energy Environ. Sci. 5 (2012) 6744.

[3] H.A. Gasteiger, J.E. Panels, S.G. Yan, Dependence of PEM fuel cell performance on catalyst loading, J. Power Sources. 127 (2004) 162–171.

[4] N. Travitsky, L. Burstein, Y. Rosenberg, E. Peled, Effect of methanol, ethylene glycol and their oxidation by-products on the activity of Pt-based oxygen-reduction catalysts, J. Power Sources. 194 (2009) 161–167.

[5] A. Morozan, B. Jousselme, S. Palacin, Low-platinum and platinum-free catalysts for the oxygen reduction reaction at fuel cell cathodes, Energy Environ. Sci. 4 (2011) 1238.

[6] J. Zhang, M.B. Vukmirovic, Y. Xu, M. Mavrikakis, R.R. Adzic, Controlling the catalytic activity of platinum-monolayer electrocatalysts for oxygen reduction with different substrates, Angew. Chemie - Int. Ed. 44 (2005) 2132–2135.

[7] F. Jaouen, E. Proietti, M. Lefèvre, R. Chenitz, J.-P. Dodelet, G. Wu, H.T. Chung, C.M. Johnston, P. Zelenay, Recent advances in non-precious metal catalysis for oxygen-reduction reaction in polymer electrolyte fuelcells, Energy Environ. Sci. 4 (2011) 114–130.

[8] Z.-J. Lu, S.-J. Bao, Y.-T. Gou, C.-J. Cai, C.-C. Ji, M.-W. Xu, J. Song, R. Wang, Nitrogen-doped reduced-graphene oxide as an efficient metal-free electrocatalyst for oxygen reduction in fuel cells, RSC Adv. 3 (2013) 3990..

[9] N. Gavrilov, I.A. Pašti, M. Mitrić, J. Travas-Sejdić, G. Ćirić-Marjanović, S. V. Mentus, Electrocatalysis of oxygen reduction reaction on polyaniline-derived nitrogen-doped carbon nanoparticle surfaces in alkaline media, J. Power Sources. 220 (2012) 306–316.

[10] H.W. Liang, W. Wei, Z.S. Wu, X. Feng, K. Müllen, Mesoporous metal-nitrogen-doped carbon electrocatalysts for highly efficient oxygen reduction reaction, J. Am. Chem. Soc. 135 (2013) 16002–16005.

[11] G. Wu, K.L. More, C.M. Johnston, P. Zelenay, High-Performance Electrocatalysts for Oxygen Reduction Derived from Polyaniline, Iron, and Cobalt, Science 332 (2011) 443–447.

[12] D.R. Paul, W.J. Koros, R.Y.F. Liu, Y.S. Hu, E. Baer, A. Hiltner, H.D. Keith, R.Y.F. Liu, A. Hiltner, E. Baer, R.E. Cohen, A. Bellare, R.J. Albalak, W. Hu, G. Reiter, Nitrogen-Doped Carbon Nanotube, 323 (2009).

[13] K.H. Wu, D.W. Wang, D.S. Su, I.R. Gentle, A Discussion on the Activity Origin in Metal-Free Nitrogen-Doped Carbons for Oxygen Reduction Reaction and their Mechanisms, ChemSusChem. 8 (2015) 2772–2788.

[14] G. Ćirić-Marjanović, I. Pašti, N. Gavrilov, A. Janošević, S. Mentus, Carbonised polyaniline and polypyrrole: towards advanced nitrogen-containing carbon materials, Chem. Pap. 67 (2013) 781–813.

[15] R. Silva, D. Voiry, M. Chhowalla, T. Asefa, Efficient metal-free electrocatalysts for oxygen reduction: Polyaniline-derived N- and O-doped mesoporous carbons, J. Am. Chem. Soc. 135 (2013) 7823–7826.

[16] J. Zhang, Z. Zhao, Z. Xia, L. Dai, A metal-free bifunctional electrocatalyst for oxygen reduction and oxygen evolution reactions, Nat. Nanotechnol. 10 (2015) 444–452.

[17] F. Zhou, G. Wang, F. Huang, Y. Zhang, M. Pan, Polyaniline derived N- and O-enriched high surface area hierarchical porous carbons as an efficient metal-free electrocatalyst for oxygen reduction, Electrochim. Acta. 257 (2017) 73–81.

[18] A. Zhao, J. Masa, M. Muhler, W. Schuhmann, W. Xia, N-doped carbon synthesized from N-containing polymers as metal-free catalysts for the oxygen reduction under alkaline conditions, Electrochim. Acta. 98 (2013) 139–145.

[19] L. Lai, J.R. Potts, D. Zhan, L. Wang, C.K. Poh, C. Tang, H. Gong, Z. Shen, J. Lin, R.S. Ruoff, Exploration of the active center structure of nitrogen-doped graphene-based catalysts for oxygen reduction reaction, Energy Environ. Sci. 5 (2012) 7936.

[20] J. Quílez-Bermejo, C. González-Gaitán, E. Morallón, D. Cazorla-Amorós, Effect of carbonization conditions of polyaniline on its catalytic activity towards ORR. Some insights about the nature of the active sites, Carbon 119 (2017) 62–71.

[21] K. Wan, Z.-P. Yu, Z.-X. Liang, Polyaniline-Derived Ordered Mesoporous Carbon as an Efficient Electrocatalysts for Oxygen Reduction Reaction, Catalysts. 5 (2015) 1034–1045.

[22] W. Gao, D. Havas, S. Gupta, Q. Pan, N. He, H. Zhang, H.-L. Wang, G. Wu, Is reduced graphene oxide favorable for nonpreciuous metal oxygen reduction catalysts?, Carbon 102 (2016) 346–356.

[23] K. Gong, F. Du, Z. Xia, M. Durstock, L. Dai, Nitrogen-Doped Carbon Nanotube Arrays with High Electrocatalytic Activity for Oxygen Reduction, Science 323 (2009) 760–764.

[24] R. Liu, D. Wu, X. Feng, K. Müllen, Nitrogen-doped ordered mesoporous graphitic arrays with high electrocatalytic activity for oxygen reduction, Angew. Chemie - Int. Ed. 49 (2010) 2565–2569.

[25] R. Liu, D. Wu, X. Feng, K. Müllen, Nitrogen-doped ordered mesoporous graphitic arrays with high electrocatalytic activity for oxygen reduction, Angew. Chemie - Int. Ed. 49 (2010) 2565–2569.

[26] Y. Zheng, Y. Jiao, J. Chen, J. Liu, J. Liang, A. Du, W. Zhang, Z. Zhu, S.C. Smith, M. Jaroniec, G.Q. (Max) Lu, S.Z. Qiao, Nanoporous Graphitic-C_3N_4@Carbon Metal-Free Electrocatalysts for Highly Efficient Oxygen Reduction, J. Am. Chem. Soc. 133 (2011) 20116–20119.

[27] K. Qu, Y. Zheng, S. Dai, S.Z. Qiao, Graphene oxide-polydopamine derived N, S-codoped carbon nanosheets as superior bifunctional electrocatalysts for oxygen reduction and evolution, Nano Energy. 19 (2016) 373–381.

[28] T. Yang, J. Liu, R. Zhou, Z. Chen, H. Xu, S.Z. Qiao, M.J. Monteiro, N-doped mesoporous carbon spheres as the oxygen reduction reaction catalysts, J. Mater. Chem. A. 2 (2014) 18139–18146.

[29] H. Marsh, F. Rodriguez-Reinoso, Activated Carbon, 1st Edition, Elsevier, 2006, ISBN:9780080455969, Chapter 2, p.30.

[30] F. Xu, D. Wu, R. Fu, B. Wei, Design and preparation of porous carbons from conjugated polymer precursors, Mater. Today. 20 (2017) 629–656.

[31] C.M. Sa, A.J. Bard, Hydrogen Peroxide Production in the Oxygen Reduction Reaction at Different Electrocatalysts as Quantified by Scanning Electrochemical Microscopy, 81 (2009) 8094–8100.

[32] Q. Li, R. He, J.O. Jensen, N.J. Bjerrum, Approaches and Recent Development of Polymer Electrolyte Membranes for Fuel Cells Operating above 100 °C, Chem. Mater. 15 (2003) 4896–4915.

[33] D. Salinas-Torres, R. Ruiz-Rosas, M.J. Valero-Romero, J. Rodríguez-Mirasol, T. Cordero, E. Morallón, D. Cazorla-Amorós, Asymmetric capacitors using lignin-based hierarchical porous carbons, J. Power Sources. 326 (2016) 641–651.

[34] P. Kurzweil, A. Hildebrand, M. Weiß, Accelerated Life Testing of Double-Layer Capacitors: Reliability and Safety under Excess Voltage and

Temperature, ChemElectroChem. 2 (2015) 150–159.

[35] R. Kötz, M. Carlen, Principles and applications of electrochemical capacitors, Electrochim. Acta. 45 (2000) 2483–2498.

[36] S. Leyva-García, K. Nueangnoraj, D. Lozano-Castelló, H. Nishihara, T. Kyotani, E. Morallón, D. Cazorla-Amorós, Characterization of a zeolite-templated carbon by electrochemical quartz crystal microbalance and in situ Raman spectroscopy, Carbon 89 (2015) 63–73.

[37] R.J. Bowling, R.T. Packard, R.L. McCreery, Activation of Highly Ordered Pyrolytic Graphite for Heterogeneous Electron Transfer: Relationship between Electrochemical Performance and Carbon Microstructure, J. Am. Chem. Soc. 111 (1989) 1217–1223.

[38] J. Schwan, S. Ulrich, V. Batori, H. Ehrhardt, S.R.P. Silva, Raman spectroscopy on amorphous carbon films, J. Appl. Phys. 80 (1996) 440–447.

[39] A. Sadezky, H. Muckenhuber, H. Grothe, R. Niessner, U. Pöschl, Raman microspectroscopy of soot and related carbonaceous materials: Spectral analysis and structural information, Carbon 43 (2005) 1731–1742.

[40] T. Ikeda, M. Boero, S.F. Huang, K. Terakura, M. Oshima, J. Ozaki, Carbon alloy catalysts: Active sites for oxygen reduction reaction, J. Phys. Chem. C. 112 (2008) 14706–14709.

[41] S. Kuroki, Y. Hosaka, C. Yamauchi, A solid-state NMR study of the carbonization of polyaniline, Carbon 55 (2013) 160–167.

[42] J.R. Pels, F. Kapteijn, J.A. Moulijn, Q. Zhu, K.M. Thomas, Evolution of nitrogen functionalities in carbonaceous materials during pyrolysis, Carbon 33 (1995) 1641–1653.

CHAPTER V

TOWARDS UNDERSTANDING OF THE ACTIVE SITES FOR ORR IN N-DOPED CARBON MATERIALS THROUGH A FINE-TUNING OF NITROGEN FUNCTIONALITIES: AN EXPERIMENTAL AND COMPUTATIONAL APPROACH

5.1 Introduction

In an age dominated by an increasing worldwide demand for energy, the combustion of fossil fuels is still the main energy source which supports the requirements of the power system. However, the depletion of this energy system and the environmental concerns associated with its use have led to huge scientific efforts on the use of renewable energy sources. Among these efforts, fuel cells (FCs) have been developed as a promising technology for energy supply and conversion as a substitute for combustion engines in vehicles [1]. In contrast to fossil fuels, these devices are not completely optimized, and they still present some limitations. One key factor in the development and commercialization of the FC is the oxygen reduction reaction (ORR) because of its slow kinetics and high overpotential [2,3]. In order to address this concern, the use of highly efficient electrocatalysts is necessary. The main disadvantage of ORR catalysts is the use of platinum as electrocatalyst [4]. The low abundance in the Earth and the high price of this metal increase the total cost of the FC until values higher than those of current engines [2–4], which make these devices an unattractive alternative for widespread use.

One solution to overcome this problem is the design of low-cost electrocatalysts towards the ORR. The work done on this topic can be classified into two groups according to the type of catalyst analysed or under development. The aim of the first of them is to replace platinum by another more abundant metal (usually a non-precious metal, such as Co [5] or Pd [6]) and, therefore, less expensive. The limitations of this strategy rely on the use of metals and the problems associated with them; that is, they have not reduced the cost significantly [7] and also metals can agglomerate or lixiviate, resulting in the loss of catalytic activity and low durability [7]. The second and more innovative alternative is the development of metal-free catalysts based on heteroatom-doped carbon materials [8]. In this sense, nitrogen-doped carbon materials are one of the most promising materials due to their low price and high catalytic activity towards ORR. Moreover, N-doped carbon materials are free from carbon monoxide poisoning and they exhibit longer stability than platinum-based catalysts [8].

The study and development of advanced metal-free catalysts based on N-doped carbon materials have a large impact on the scientific community. The identification of the active sites towards the ORR in these materials is mandatory

for the design of advanced metal-free catalysts with platinum-like performance. However, there is a great controversy about the nature of active sites. On the basis of experimental results, some authors propose pyridinic N species [9–11] as responsible for the improvement in catalytic activity because of the conjugation effect of the nitrogen lone pair electrons and graphene π-system, which can increase the electron donating properties and facilitate reductive O_2 adsorption. Nevertheless, there are studies that propose basal-type graphitic N (also referred to as quaternary N) [12,13] as the N functionality that reduces the electron density on the adjacent C atoms and facilitates electron transfer from adjacent carbon atoms to N atoms and N back donation to adjacent C p_z orbitals. Moreover, experimental studies suggest that edge-type graphitic nitrogen [14,15] and pyrrolic nitrogen species [16,17] can also act as active sites. In recent years, N-C-O species [18,19] have also been proposed as active sites towards the ORR due to the large positive charge density of the C atom adjacent to N and O atoms. This controversy of the experimental results is mainly due to the difficulty to isolate the nitrogen species in carbon materials while maintaining the morphology, structural order and electrical conductivity of the compared samples.

On the other hand, computer modelling studies have tried to overcome these limitations since studying isolated nitrogen species is easy in simulations [20]. However, the demonstration of theoretical calculations has to be done through comparison with experimental results. Therefore, the combination of both approaches is essential to understand the nature of the active sites in N-doped carbon materials.

In this context, this work presents an experimental method that permits fine-tuning of N functionalities in N-doped carbon materials through a double stage heat treatment of polyaniline (PANI). The combination of a heat treatment in a slightly oxidizing atmosphere followed by heat treatment in an inert atmosphere results in selective etching of the carbon material which allow us to tailor the N-species present in the material while maintaining the porosity and structural order. Therefore, the selective evaluation of the contribution in the ORR from the different nitrogen species is possible. Furthermore, density functional theory (DFT) calculations have been carried out in order to support the experimental results. Pyridinic, pyrrolic, basal and edge-type graphitic, pyridonic and oxidized nitrogen functionalities have been computed towards oxygen reduction catalysis.

5.2 Experimental Section

5.2.1 Materials and reagents

Aniline was purchased from Sigma Aldrich and was distilled by refluxing under reduced pressure prior to its use in order to remove the impurities. Ammonium persulfate, ammonium hydroxide, potassium hydroxide (KOH) and Pt/Vulcan (20 wt% loading) were purchased from Sigma Aldrich. XC-72F Vulcan carbon black was supplied by Cabot Corporation. Hydrochloric acid (37% HCl) was purchased from VWR-Chemicals Prolabo. All the solutions were prepared using ultrapure water (18 MΩ cm from an Elga Labwater Purelab system). The gases N_2 (99.999%), O_2 (99.995%), H_2 (99.999%) and synthetic air were provided by Air Liquide and were used without any further purification or treatment.

5.2.2 PANI preparation

Polyaniline was prepared by chemical polymerization from a solution of 1 M HCl containing 0.067 M of aniline and ammonium persulfate in a stoichiometric ratio. The mixture was kept under stirring (500 rpm) for 3 h at 0 ºC. In order to remove the Cl^- counter ion, after the 2 h of the polymerization process, the obtained polymer was treated with 1 M NH_4OH for 24 h, producing PANI. The synthesized PANI was washed several times with distilled water and dried at 80 ºC overnight.

5.2.3 Heat treatment

150 mg of PANI was heat-treated in a tubular furnace in a two-step process. First, PANI was heat-treated under an oxygen-containing atmosphere (5000ppm O_2/N_2) at 1000 ºC for 1 h using a heating rate of 5 ºCmin^{-1} and then cooled down to room temperature at 10ºC·min^{-1}. The flow rate was maintained at 100 mL·min^{-1}. The sample obtained by this first treatment is named PANI_O2_1000. The heat treatment under 5000 ppm oxygen content in a nitrogen atmosphere at 1000ºC produces a carbon material with a higher yield and porosity than that produced by heat treatment in nitrogen, as we already reported [18]. It seems that it favours crosslinking and condensation reactions that take place during the treatment, similar to a stabilization treatment of a softening material [18].

The second step consists of heat treatment at 800, 1000 and 1200ºC for 1h using a heating rate of 5 ºC·min^{-1} under an inert (N_2) atmosphere. The flow rate was maintained at 200 mL·min^{-1}. The obtained samples are named

PANI_O2_1000_N2_X, with X being the temperature of the second treatment, under an inert (N_2) atmosphere. The furnaces were always purged for 1h before the heat treatment in the corresponding atmosphere and flow rate.

5.2.4 Physicochemical Characterization

Raman spectra were collected on a Jasco NRS-5100 spectrometer. A 3.9 mW He-Ne laser at 633 nm was used. The spectra were acquired for 120 s. The detector was a Peltier cooled charge-coupled device (CCD) (1024 x 255 pixels). Calibration of the spectrometer was performed with a Si slice (521 ± cm^{-1}). The textural properties of the materials were evaluated by N_2 adsorption isotherms at -196 °C and CO_2 adsorption at 0ºC in an automatic adsorption system (Autosorb-6, Quantachrome). Prior to the measurements, the samples were degassed at 250 °C for 4 h. Apparent surface areas have been determined by BET method [21] (S_{BET}) and the total micropore volume (pores of size < 2 nm) has been assessed by applying the Dubinin-Radushkevich (DR) equation to the N_2 adsorption isotherms [22]. Temperature programmed desorption (TPD) experiments were performed in a DSC-TGA equipment (TA Instruments, SDT 2960 Simultaneous) coupled to a mass spectrometer (Thermostar, Balzers, GSD 300 T3) which was used to follow the m/z lines related to the decomposition of surface functional groups from the surface of the carbon materials. The thermobalance was purged for 2 hours under a helium flow rate of 100 ml min^{-1} and then heated up to 950°C (heating rate 20°C min^{-1}). The surface composition and oxidation states of the elements of the prepared materials were studied using XPS in a VG-Microtech Mutilab 3000 spectrometer with an Al Kα radiation source (1253.6 eV). The deconvolution of the N1s XPS spectra was done by least squares fitting using Gaussian-Lorentzian curves, while a Shirley line was used for the background determination.

5.2.5 Electrocatalytic activity towards ORR

The study of the electrocatalytic activity towards ORR was performed on an Autolab PGSTAT302 (Metrohm, Netherlands) potentiostat. A rotating ring-disk electrode (RRDE, Pine Research Instruments, USA) equipped with a glassy carbon disk electrode (5.61 mm diameter) and an attached platinum ring was used as the working electrode, graphite was used as the counter electrode and a reversible hydrogen electrode (RHE) immersed in the working electrolyte through a Luggin capillary was used as the reference electrode. The amount of catalyst on the disk electrode was optimized in order to attain the highest limiting current intensity, with 120 µg being the optimum value. Therefore, the

glassy carbon disk was modified with the samples using 120 µl of a 1 mg ml^{-1} dispersion of each carbon material (20% isopropanol and 0.02% Nafion®), obtaining a catalyst loading of 0.48 mg cm^{-2}. XC-72F Vulcan carbon black as a non-doped carbon material and 20wt%Pt/Vulcan samples were also used for comparison purposes. The electrocatalytic activity towards ORR was studied by linear sweep voltammetry (LSV) in an O_2 saturated 0.1 M KOH solution between 1.0 and 0.0 V (vs. RHE) at different rotation rates, from 400 to 2025 rpm, and at a scan rate of 5 $mV \cdot s^{-1}$. The potential of the ring electrode was held constant at 1.5 V (vs. RHE) during all measurements. The electron transfer number was calculated from the hydrogen peroxide oxidation in the Pt ring electrode as follows:

$$n = \frac{4\, I_d}{I_d + I_r/N}$$

Where I_r and I_d are the current measured at the ring electrode and the disk electrode, respectively, and N is the collection efficiency of the ring, which was experimentally determined to be 0.37. A long-time stability test was also carried out for the most active sample in an O_2-saturated 0.1 M KOH solution by cycling between 1.00 and 0.00 V vs RHE during 10,000 seconds at a scan rate of 5 $mV \cdot s^{-1}$.

5.2.6 Computational models

Density functional theory (DFT) at the B3LYP/6-31G(d) level was used in this study through Gaussian 09 software, using restricted and unrestricted Hamiltonians for closed shell (S=0) and open-shell (S=1/2) systems, respectively. Partial atomic charges were computed with Mülliken population analysis. The change in energies for each transformation was computed as the energy differences of optimized geometries neglecting vibrational corrections and is reported in eV (1 hartree = 27.2116 eV). The model structures consist of a rectangular graphene carbon layer with 110 carbon atoms and 6x7 benzenic rings on zigzag and armchair edges, respectively. Since the properties of graphene flakes depend on size [23,24], the 6x7 rectangular flake was selected in order to represent graphene edges more accurately yet remain computationally feasible. Self-consistent reaction field (SCRF) models of solvation, with the polarized continuum model (PCM) [25] representing the water medium were used in all models to account for the environment of the electrocatalytic experiment. The energy diagrams of ORR have been calculated

based on the computational hydrogen electrode model potential, proposed by Norskov et. al [26]. The free energy change for each oxygen reduction stage is defined as $\Delta G = \Delta E' + \Delta G_{pH} + \Delta G_U$, where $\Delta E'$ is the difference of the DFT computed total energies, and ΔG_{pH} and ΔG_U are the changes in free energies associated to the pH and electrode potential, respectively. $\Delta G_{pH} = k_B \cdot \ln 10 \cdot pH$, where k_B is Boltzmann´s constant and the pH is adjusted to 13, using 0.1 M KOH solution used during catalytic experimental. $\Delta G_U = n \cdot e \cdot E$, where E is the electrode potential and n is the number of transferred electrons in each reduction step. The number of unpaired electrons has been considered in the models as follows; the pristine non-doped carbon and N-doped carbon configurations were computed as singlet, closed-shell states, for all cases. After the introduction of the electron-proton pairs, a doublet multiplicity was used in the first and third reductions and a singlet state in the second and fourth reduction stages. The oxygen molecule ground state was computed as a triplet.

5.3 Results and discussion

5.3.1 Experimental results

Table 5.1 includes the heat treatment yields of the pre-treated and double stage treated samples. Figure 5.1a shows the N_2-adsorption isotherms of PANI-derived carbon materials. All samples present type I isotherms, characteristic of microporous materials and the pore size distributions are similar in all the cases (Figure 5.1b). The BET surface areas for the materials are similar, except for the sample PANI_O2_1000_N2_800 which has a somewhat higher surface area. In this case, due to the preparation method, the oxygen groups created during the treatment (which includes cooling in the oxidative atmosphere) are removed when heating in N_2 at 800ºC resulting in some gasification and formation of porosity. However, the heat treatment at higher temperatures in N_2 (i.e., samples PANI_O2_1000_N2_1000 and PANI_O2_1000_N2_1200) result in not only oxygen groups removal but also some porosity shrinkage.

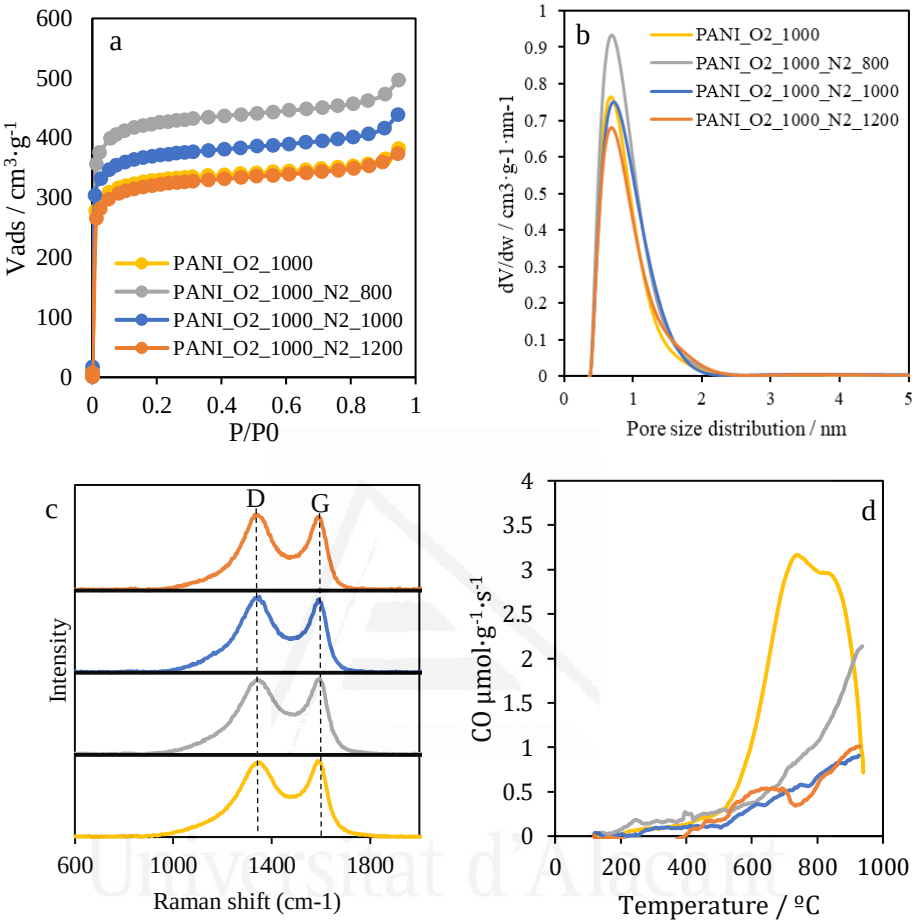

Figure 5.1: (a) N_2-adsorption isotherms, (b) pore size distribution, (c) Raman spectra and (d) CO-TPD profiles of all materials. Yellow represents PANI-O2-1000, grey represents PANI-O2-1000-N2-800, blue represents PANI-O2-1000-N2-1000 and orange represents PANI-O2-1000-N2-1200.

Table 5.1: Heat treatments yield, BET surface area, the atomic percentage of oxygen and nitrogen and atomic percentage of the nitrogen functionalities as determined from XPS.

SAMPLE	YIELD / %	BET SURFACE AREA / $m^2.g^{-1}$	O CONTENT / AT.%	N CONTENT / AT.%	PYRIDINIC CONTENT / %	PYRROLIC OR PYRIDONIC CONTENT / %	GRAPHITIC N CONTENT / %	OXIDIZED N CONTENT / %
PANI_O2_1000	36	1360	4.2	2.5	31	33	36	-
PANI_O2_1000_N2_800	33	1680	2.1	2.8	37	25	31	8
PANI_O2_1000_N2_1000	30	1440	2.7	2.3	30	18	47	5
PANI_O2_1000_N2_1200	27	1360	2.8	1.4	-	-	100	-

Regarding the structural order, Raman spectra for all samples are presented in Figure 5.1c. The second treatment under an inert atmosphere does not result in significant modification of the structural order since there is change neither in the D and G bands nor in the I_D/I_G ratio (I_D/I_G close to 1.0 in all the samples). Therefore, all PANI-derived carbon materials are similar in pore size distribution and structural order.

The surface chemistry was studied by temperature-programmed desorption (TPD). The decomposition of surface oxygen functionalities using TPD is extensively used for characterizing the surface functionalities of carbon materials. CO_2 peaks results from carboxylic acids at temperatures below 500ºC and from lactones at temperature between 500-700ºC. Carboxylic anhydrides produces both CO and CO_2 peaks, while phenols and carbonyls produce both CO peaks at around 750 and 850ºC, respectively [27–30]. For these materials, CO_2 desorption does not show relevant differences among all treatments. However, CO profiles reveal important changes. Figure 5.1d shows the CO-TPD profiles for all PANI-derived carbon materials. N-doped carbon materials obtained by the pre-treatment under an oxygen-containing atmosphere have a higher amount of oxygen groups because of the reaction between the oxygen from the atmosphere and the carbon materials [18]. This is especially remarkable in sample PANI_O2_1000 since the cooling is done in the oxygen-containing atmosphere. In this case, the CO-TPD profile exhibits a peak at around 750ºC, which is related to the presence of phenolic groups [18,29], and a second peak at around 850ºC which is associated with the presence of carbonyl/quinone groups [29]. For the rest of the samples, the higher the temperature of the second treatment in a N_2 atmosphere, the lower the CO evolution. Therefore, the second treatment under an inert atmosphere removes oxygen groups from the surface of the carbon materials. Interestingly, the sample PANI_O2_1000_N2_1200 still shows some CO desorption in its TPD-profile, which can indicate that the carbon materials react with air once the heat treatment in an inert atmosphere has finished and the sample is exposed to the environment, thereby creating oxygen groups.

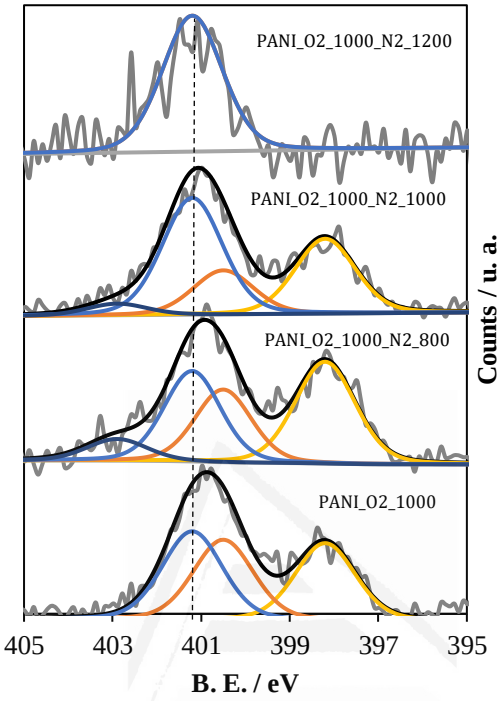

Figure 5.2: N1s spectra of all PANI-derived carbon materials.

In order to identify the N functionalities in the PANI-derived carbon materials, XPS analyses have been performed. The N1s spectra of all materials (Figure 5.2) show differences in the type of nitrogen species present in the sample depending on the temperature of both treatments. The deconvolution of the N1s spectra has been done based on the literature [31–33]. All N-doped carbon materials mainly show three peaks: (i) pyridinic nitrogen at 398.2 eV, (ii) pyridonic and pyrrolic nitrogen at 400.5 eV and (iii) graphitic -type nitrogen species at 401.2 eV. In some samples, the presence of oxidized nitrogen is also observed at 402.9 eV (always below 10 at.%). The sample treated in the oxidizing atmosphere (sample PANI_O2_1000) has a high amount of pyridonic species (33 at.% in PANI_O2_1000), in agreement with our previous work [18]. Furthermore, the presence of pyridine and graphitic-type nitrogen species is also observed. Once the second treatment is applied in N_2 atmosphere at 800ºC, the pyridonic type species slightly decrease with an increase in the pyridinic type groups, which is in agreement with the loss of oxygen (see Table 5.1) and the

CO-TPD profiles. Furthermore, if the second treatment is done at 1000ºC, a significant decrease in the pyridinic and also pyridonic species is detected which occurs with the increase in the graphitic-type nitrogen species (Table 5.1). Interestingly, only one symmetric peak is detected in PANI_O2_1000_1200 at 401.2 eV. Complete disappearance of pyridinic and pyridonic species is observed and only graphitic-type nitrogen exists in this sample. This fact is strongly related to the already proposed transformation of pyridinic nitrogen (and also pyridonic species) into edge-type graphitic nitrogen atoms in zig-zag positions [14,32] because of condensation reactions that increase the size of the graphene layers [14,15,32]. Therefore, the presented experimental procedure seems to promote the formation of edge-type graphitic nitrogen in the carbon framework, maintaining the structural order and porosity.

The electrocatalytic activities towards ORR of all materials were studied in an O_2-saturated 0.1M KOH solution. Linear Sweep Voltammetry (LSV) analysis was performed using a RRDE at different rotation rates. The current registered in the Pt ring electrode is related to the amount of H_2O_2 formed in the disk electrode during the oxygen reduction reaction, which is the intermediate compound found in the 2e- pathway. Figure 5.3 shows the LSV curves and the number of transferred electrons at 1600 rpm for all samples in the 0.1 KOH electrolyte. The LSV for commercial 20wt% Pt/Vulcan and a commercial non-doped carbon material (C) have been included for comparison purposes.

The sample obtained by the oxygen-containing pre-treatment (PANI_O2_1000) has an interesting catalytic activity compared with the non-doped commercial carbon material (Figure 5.3a). This enhancement can be mainly attributed to the pyridonic-type species formed by the reaction between the molecular oxygen and nitrogen species of the PANI-derived carbon material during the heat treatment, as it has already been proposed [18].

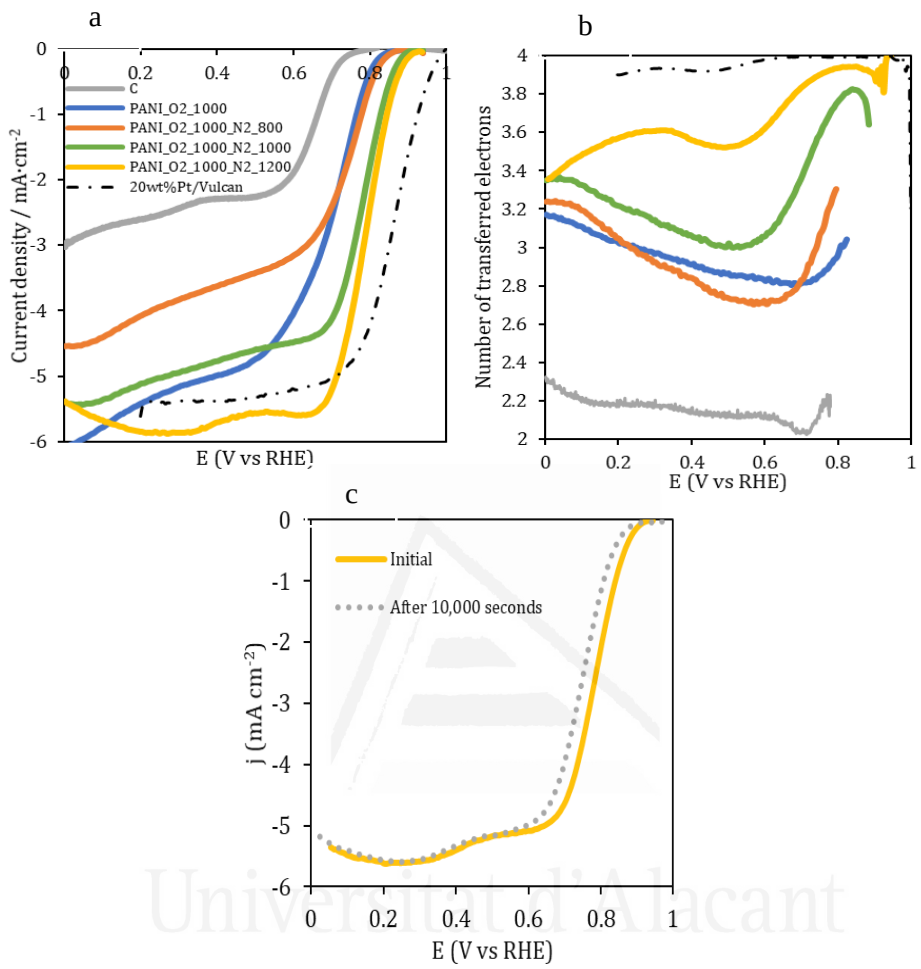

Figure 5.3: (a) LSV curves and (b) the number of transferred electrons of PANI-derived carbon materials at 1600 rpm in an oxygen-saturated 0.1 M KOH solution, using a scan rate of 5mV·s^{-1}. (c) Long-time stability test of PANI_O2_1000_N2_1200 in an oxygen-saturated 0.1 M KOH solution at a scan rate of 5mV·s^{-1}.

Interestingly, significant differences are observed for samples obtained by the double stage heat treatment. The sample heat-treated under an inert atmosphere at 800ºC shows similar performance to the material obtained by treatment in the oxygen-containing atmosphere (PANI_O2_1000 sample) although with a lower limiting current (Figure 5.3a). This seems to occur because this second treatment results in some decrease in pyridonic species with the corresponding increase in pyridines (see Table 5.1).

Interestingly, the higher the temperature used during such second treatment, the higher the catalytic activity of the carbon material. In fact, PANI-O2-1000-N2-1200 has the closest performance to the platinum catalyst mainly with respect to the current density. According to XPS and TPD analysis, this high catalytic activity seems to be associated with the presence of graphitic nitrogen, since the transformation of pyridines and pyridones into edge-type graphitic species (See Table 5.1 and Figure 5.2) results in an enhancement of the catalytic activity towards the ORR. This fact is supported in the literature since edge-type graphitic nitrogen has been proposed as enhanced active centres for this reaction [14,15]. Graphitic N at edge sites cannot be clearly differentiated from edge and internal locations with XPS. In contrast, the use of computational models allows us to explore directly both scenarios.

Figure 5.3b displays the number of transferred electrons during the oxygen reduction reaction. The carbon materials prepared by one or two-stage heat treatments with a maximum temperature of 800ºC show a number of electrons close to 3, superior to the obtained with the non-doped carbon material. This means that the mechanism of the oxygen reduction reaction catalysed by these samples leads to hydrogen peroxide and water generation in the same percentage. Significant changes are observed when the second heat treatment temperature is 1000 ºC and, especially, 1200 ºC. In these samples, the number of transferred electrons increases significantly mainly at more positive potentials. This means that edge-type graphitic nitrogen species seem to favour oxygen reduction through water generation. This behaviour was already observed in PANI-derived samples obtained by heat treatment at high temperatures [15].

A long-time stability test has also been carried out for the sample PANI_O2_1000_N2_1200 in 0.1 M KOH solution (Figure 5.3c). Interestingly, after 10,000 seconds of cycling, the LSV profile of this sample shows almost identical limiting current density compared to the initial profile. The onset potential has shifted 0.02 V to more negative potentials. This probably could be related to the H_2O_2 generated at the low potential range, which can damage the most active species. A detailed study of this issue will be the subject of further research.

5.3.2 Computational modelling

DFT models were used to explore the role of the different potential sites of N-doped carbon materials in the oxygen reduction reaction. In this sense, all nitrogen functionalities found experimentally in N- doped carbon materials have been evaluated in the context of the ORR. The effect of oxygen functional groups was not considered in the model as it was not deemed fundamental in PANI-derived carbon materials. It has been argued that the oxidation of carbon materials increases the concentration of paramagnetic centres (via aryloxyl radical formation) and a high concentration of such centres promotes the decrease of hydrogen peroxide formation during the ORR [34]. However, oxygen reduction with oxidised pyrolytic graphite starts in the potential range of 0.6-0.8 V vs RHE. Consequently, at potentials higher than 0.8 V, the oxygen reduction reaction would be mainly governed by nitrogen species and not by oxygen functional groups in PANI-derived carbon materials.

In addition, previous studies with carbon materials with different oxygen content (pristine material and heat treated) do not provide significant differences yielding similar catalytic activities [36]. In fact, the highest activity was observed when N species are introduced in the materials [36]. Experimentally, N functional groups favour the formation of sites with higher catalytic activity. Nevertheless, the combination of N and O species may be relevant if N-C-O species are formed, which are also catalytic towards the ORR [18]. Furthermore, the amount of O in PANI-derived carbon materials is low after the second heat treatment. Considering all this, oxygen groups were not considered in the models.

Figure 5.4 shows relevant parts of the model structures used for all nitrogen functionalities. The full model structure consists of a carbon layer of 6 x 7 benzene rings where different functionalities have been introduced. The non-doped carbon material has also been included for comparison purposes.

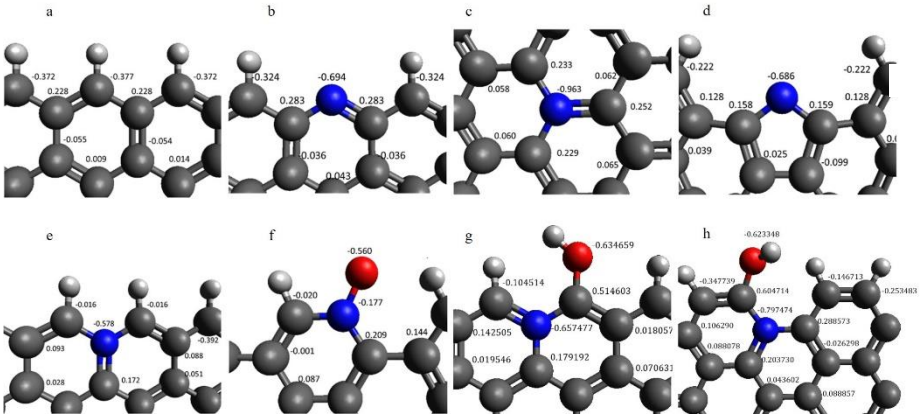

Figure 5.4: Model structures and the atomic effective charge of: (a) non-doped carbon material, (b) pyridinic nitrogen, (c) basal-type graphitic nitrogen, (d) pyrrolic nitrogen, (e) edge-type graphitic nitrogen, (f) oxidized nitrogen, (g) pyridonic nitrogen in zig-zag position and (h) pyridonic nitrogen in armchair position. Hydrogen is white, carbon is grey nitrogen is blue, and oxygen is red.

In an alkaline aqueous environment, which is the condition used in the experimental study, the ORR can be described by the following elementary steps [37]:

Four electrons pathway:

$$O_2 + \blacksquare \rightarrow O_2{}^{\blacksquare} \qquad 1.1$$

$$O_2{}^{\blacksquare} + H_2O + e^- \rightarrow OOH^{\blacksquare} + OH^- \qquad 1.2$$

$$OOH^{\blacksquare} + H_2O + e^- \rightarrow O^{\blacksquare} + OH^- + H_2O \qquad 1.3$$

$$O^{\blacksquare} + H_2O + e^- \rightarrow OH^{\blacksquare} + OH^- \qquad 1.4$$

$$OH^{\blacksquare} + H_2O + e^- \rightarrow H_2O + OH^- + \blacksquare \qquad 1.5$$

$$O_2 + 2\,H_2O + 4\,e^- \rightarrow 4\,OH^- \qquad \text{Global}$$

Two electrons pathway:

$$O_2 + \blacksquare \rightarrow O_2{}^{\blacksquare} \qquad 2.1$$

$$O_2{}^{\blacksquare} + H_2O + e^- \rightarrow OOH^{\blacksquare} + OH^- \qquad 2.2$$

$$OOH^{\blacksquare} + H_2O + e^- \rightarrow H_2O_2 + OH^- + \blacksquare \qquad 2.3$$

$$O_2 + 2\,H_2O + 2\,e^- \rightarrow H_2O_2 + 2\,OH^- \qquad \text{Global}$$

where ■ represents the catalytic active site for each N- or N- O- functional group and $X^{\blacksquare}$ represents the chemisorption of *X* species on the active site.

In order to illustrate the procedure used in the calculations, edge-type graphitic nitrogen species in a zig-zag edge position is chosen in the following discussion as an example. In all the cases, the computation has been done accordingly.

In the proposed mechanisms, the oxygen reduction reaction begins with the chemisorption of the oxygen molecule and there is some agreement on the identification of the catalytic active sites. Carbon atoms adjacent to the nitrogen suffer a change in their charge density, which can promote the oxygen chemisorption, with these being considered as the active sites for the oxygen adsorption step [9,38]. Dissociative oxygen chemisorption has been proposed to occur through two carbon atoms [15,39] or a single carbon atom [40,41]. There are previous studies in which the dissociative O_2 chemisorption is proposed to occur on a single carbon active site, which makes the presence of carbene type defects necessary. This mechanism explains the catalytic activity of graphene (i.e., pure carbon materials) [40]. This approach is in agreement with previous studies in which a correlation between the ORR catalytic activity of non-doped carbon materials and the O_2 carbon gasification reactivity was demonstrated [42]. Thus, the presence of defects is necessary to explain the catalytic activity of pure carbon materials.

Recently, the catalytic activity of N-containing graphene has also been explained considering the presence of carbene species [41]. However, dissociative chemisorption can also be interpreted considering chemisorption through two carbon atoms in a hydrogen terminated cluster [39,43]. In this study, all (both basal and edge-type) carbon atoms adjacent to nitrogen are considered as possible active sites towards oxygen molecule chemisorption and all of them have been evaluated through terminal and bridging binding modes for the oxygen molecule. Hydrogen-terminated clusters have only been considered in this theoretical study which can be useful for comparison purposes.

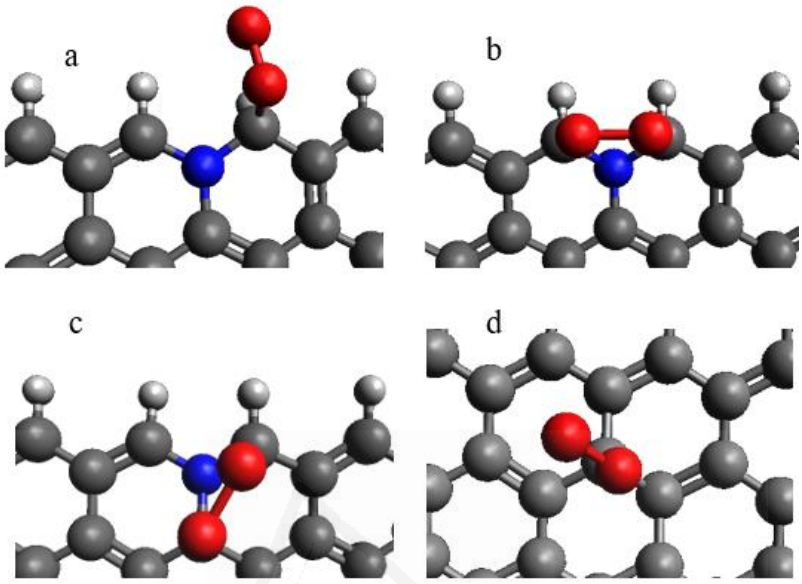

Figure 5.5: Illustrative configurations for the oxygen chemisorption into edge-type graphitic nitrogen through: (a) one edge-carbon atom in a terminal binding mode, (b) two edge-carbon atoms in a bridging binding mode, (c) one basal-carbon atom and one edge-carbon atom in a bridging binding mode and (d) a non-doped basal position in a terminal binding mode. Hydrogen is white, carbon is grey, nitrogen is blue, and oxygen is red.

In the case of using edge-type graphitic nitrogen as an example, Figure 5.5 illustrates the possible oxygen chemisorption configurations where the adjacent carbon atoms play a role. Four possible conformations have been considered: oxygen chemisorption through one active site in terminal binding mode (Figure 5.5a), two edge-carbon atoms in bridging binding mode (Figure 5.5b), both one edge and one basal carbon atoms (Figure 5.5c) in bridging binding mode and a basal carbon atom located at a distant position with respect to the N atom (Figure 5.5d). Table 5.2 includes the chemisorption energies for all these conformations.

Adsorption through a basal carbon atom located far from the N atom (Figure 5.5d) is not favoured. In fact, geometric optimization of the interaction between the chemisorption site and the oxygen molecule repels the oxygen molecule. This shows the difficulty for basal chemical adsorption on pristine graphene. In addition, adsorption through one active site (Figure 5.5a) and through one basal-carbon atom and one edge-carbon atom in bridging binding

mode (Figure 5.5c) is thermodynamically unfavored although with a low chemisorption energy. Only the adsorption configuration through two edge-carbon atoms in bridging bonding mode (Figure 5.5b) is thermodynamically favoured. This indicates that oxygen molecules react more easily with the edge carbon atoms adjacent to the nitrogen functionality, resulting in a C-O-O-C bridge binding as it was already proposed in literature [44].

Table 5.2: Chemisorption energy of the different configurations in edge-type graphitic nitrogen.

CONFORMATION (POSITION/NUMBER OF ACTIVE SITES)	CHEMISORPTION ENERGY (eV)
EDGE / ONE (FIGURE 5.5A)	0.07
EDGE-EDGE / TWO (FIGURE 5.5B)	-1.15
BASAL-EDGE / TWO (FIGURE 5.5C)	0.20
BASAL / ONE (FIGURE 5.5D)	No chemisorption occurs

Once the oxygen molecule is adsorbed in the most favourable chemisorption configuration, the next process is the first reduction or, in other words, the first electron and proton supply from the cathode and electrolyte (water in alkaline medium), respectively [26]. This is a common reaction in the 2 or 4 electron mechanisms.

In order to provide the correct intermediates, the reduction step has been managed as two consecutive processes. The reduction stage has been divided into first the electron supply and then, the proton supply. Applying this principle, interesting effects are observed in the DFT calculations. Electron addition to the chemisorbed intermediate through two active sites (C-O-O-C bonds) shows that the charge on the oxygen atoms, approximately quantified as Mülliken charges, increases as a result of the electrons collection ($\Delta\delta(-)$ = 177%). Moreover, the distance of the oxygen-oxygen bond is slightly higher than that for the chemisorbed species without electron addition (from 1.41 A when the electron is not applied to 1.44 A when the electron is supplied), which evidences weakening of the oxygen-oxygen bond. This behaviour can be taken as an early indication of the posterior rupture of the bond.

The oxygen-oxygen bond rupture of the chemisorbed species has been computed considering the addition of electrons during the reduction step. Figure 5.6 illustrates this process comparing the effect of electrons supply. For the

starting, positively charged, doped system, the cleavage of the oxygen-oxygen bond is unfavoured. Interestingly, this becomes favourable when one electron is supplied (-0.17 eV); and, if a second electron is added to the chemisorbed species, then the oxygen-oxygen bond rupture is heavily favoured (-1.13 eV). These results suggest that the electrons from the cathode are collected into the oxygen atoms, which weaken the oxygen-oxygen bond, favouring its scission. This means that the reaction occurs through a dissociative mechanism for the oxygen molecule.

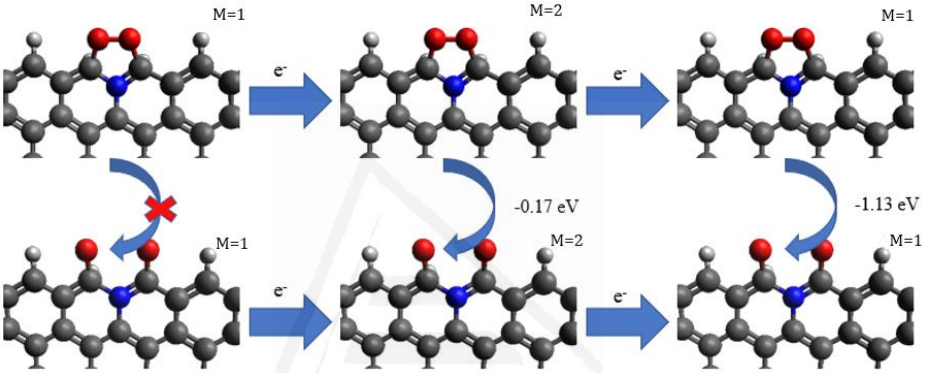

Figure 5.6: Illustrative model of the geometries, multiplicity, and energies during electron supply to the chemisorbed oxygen in a bridging binding mode through two edge-carbon atoms of the edge-type graphitic nitrogen species. Hydrogen is white, carbon is grey, nitrogen is blue, and oxygen is red.

After the electron supply, the proton must be introduced into the model structure to complete the first reduction stage. Figure 5.7a illustrates this process. The proton is attracted towards the oxygen atoms that have collected the electrons forming an intramolecular hydrogen bond.

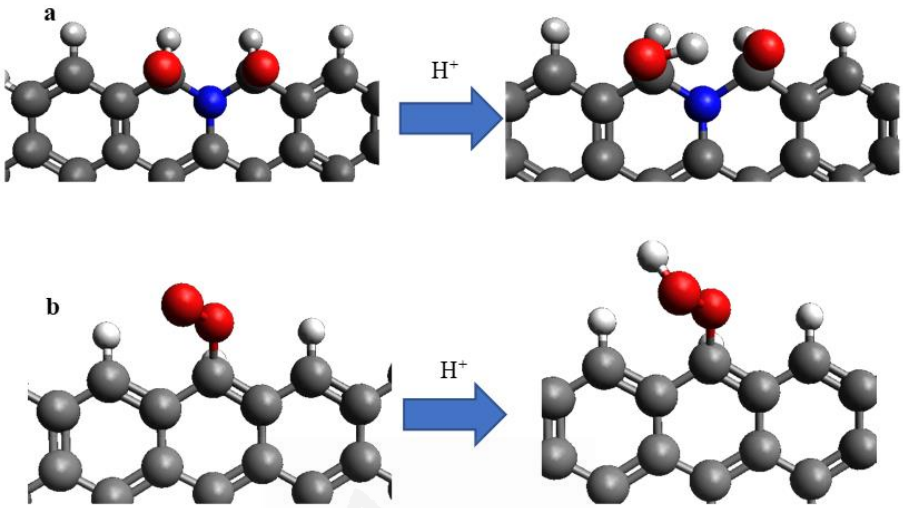

Figure 5.7: Illustrative model of the configuration of the first electron-proton supply for N-doped (a) and non-doped materials (b). Hydrogen is white, carbon is grey, nitrogen is blue, and oxygen is red. Hydrogen is white, carbon is grey nitrogen is blue and oxygen is red.

In the case where the most thermodynamically favoured chemisorption is through terminal binding mode, i.e., C-O-O bond, such as in the case of non-doped carbon materials, the first reduction stage leads to a C-O-O-H species [43] (Figure 5.7b). This means that oxygen chemisorption via two carbon active sites through bridging binding mode, leads to a dissociative mechanism where the oxygen molecule is broken, whereas chemical adsorption through one carbon active site (C-O-O) keeps the oxygen molecule bonded and the reduction occurs via an associative mechanism. However, if a carbene type defect is considered, then dissociative oxygen chemisorption may occur [40]. In N-doped carbon materials, it is commonly accepted that the oxygen reduction occurs via an associative mechanism [37], even for those studies which focus on edge-type graphitic nitrogen [45]. Nevertheless, this is not the first time that a dissociative mechanism is proposed in edge-type graphitic nitrogen [38,43,44], which reinforces our hypothesis. The observation of the dissociative mechanism in edge-type graphitic nitrogen is possible when the electron supply and proton supply are separated into two steps, which makes reasonable to propose a modification in the reaction mechanism which fits our experimental observations better. It is also possible that the presence of a carbene type defect

in a neighbour carbon atom, favours dissociative oxygen chemisorption through a single carbon atom [41].

The first oxygen reduction step for the other nitrogen functionalities has been computed following the same procedure as explained above. The next elementary steps for all the functionalities to achieve the final reduction of the oxygen molecule have also been calculated following the same methodology. This allows us to build the energy diagrams for the dioxygen reduction for all nitrogen species. Figure 5.8 displays the computed energy diagrams for all nitrogen species. In addition, the diagram for the non-doped carbon material is also presented for comparison purposes.

Basal-type graphitic nitrogen is not presented in Figure 5.8 because the oxygen molecule does not bond to the surface regardless of the starting geometrical configuration (for both one and dual-site oxygen chemisorption), which reflects the poor catalytic activity of this site. Furthermore, pyridinic, pyrrolic and, especially, oxidized nitrogen functionalities show ORR stages with higher free energies than the non-doped carbon materials. The high energetic cost of the initial chemisorption step indicates that the presence of these species in carbon materials would not result in a relevant enhancement in their catalytic activity. The oxygen reduction reaction would mainly occur as in the non-doped carbon material.

Nevertheless, some nitrogen species significantly reduce the free energy of the ORR in carbon materials. The most favourable species for ORR is edge-type graphitic nitrogen functionalities, followed by pyridonic-type functionalities. Furthermore, the chemisorption of the oxygen molecule in a bridging binding mode (i.e., C-O-O-C bridge) through two adjacent carbon atoms of the edge-type graphitic nitrogen seems to favour the oxygen molecule dissociation, resulting in a four-electron mechanism forming two molecules of water at the end of the reduction.

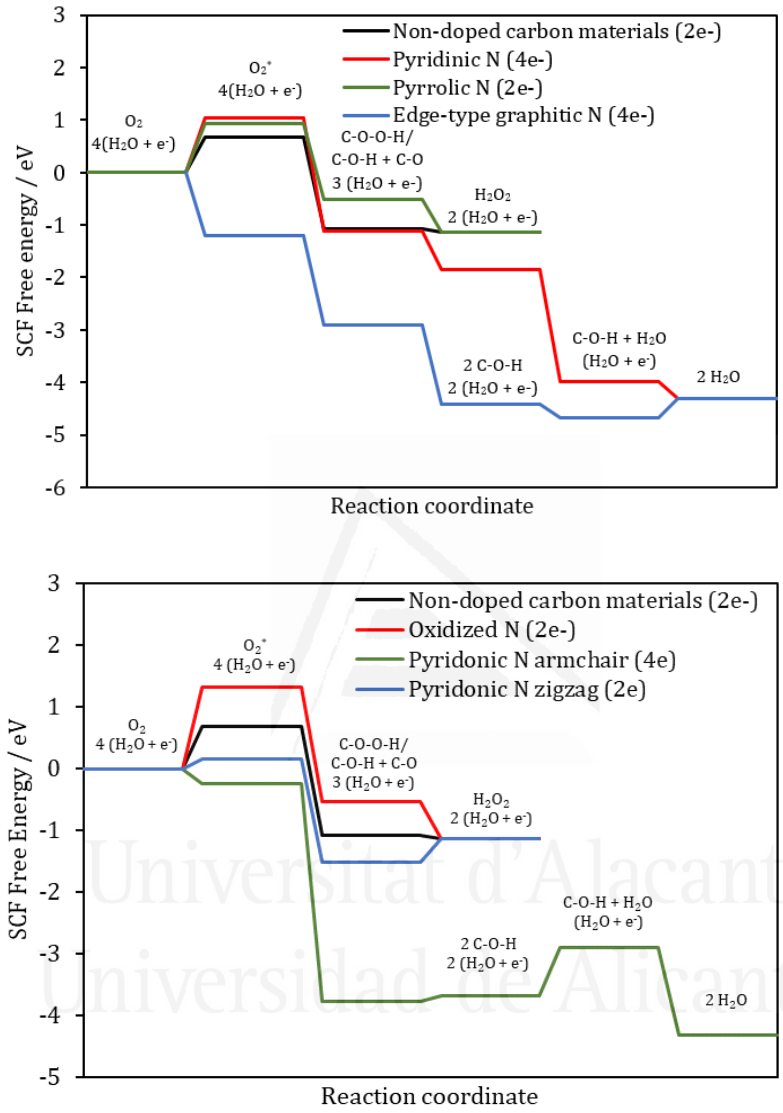

Figure 5.8: SCF energy diagram for ORR of all nitrogen functionalities at 0.00 V.

Figure 5.9 shows the SCF energy diagrams of edge-type graphitic nitrogen at different potentials. The diagram for E = 0.000 V corresponds to the reaction running by short-circuiting the cell, where all elementary steps are strongly exothermic. However, by shifting the potential to the thermodynamic potential (1.229 V), the second, third and fourth reduction processes become uphill, with

the last one being the step that shows the highest free energy (1.44 eV) and, therefore, it could be the rate-limiting step. This reinforces the need for applying an overpotential to overcome the limiting barriers and achieve an adequate reaction rate.

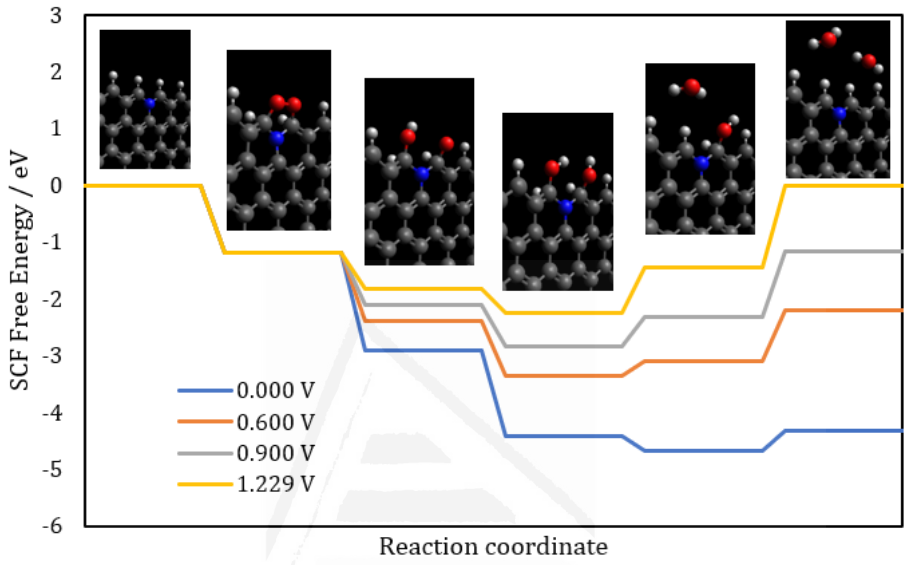

Figure 5.9: SCF energy diagram for ORR of edge-type graphitic nitrogen at 1.229 and 0.000 V. Hydrogen is white, carbon is grey, nitrogen is blue, and oxygen is red.

On the basis of the catalytic test for PANI_O2_1000_N2_1200 (Figure 5.3), other relevant potentials have been computed. At 0.900 V (approximately the onset potential measured for this sample, Figure 5.3), the second and third reduction step becomes more thermodynamically favourable and, moreover, a slight energy decrease in the fourth oxygen reduction stage is observed (1.15 eV). These results may be used to indicate the beginning of the ORR. Furthermore, at 0.600 V (where approximately the limiting current density is achieved, Figure 5.3), the free energy is much lower (0.73 eV), which could be an indicator of efficient catalysis.

The results of this computational study are fully consistent with the catalytic activities of PANI-derived carbon materials. The experimental results show that the transformation of pyridinic and pyridonic nitrogen species into edge-type graphitic nitrogen species is responsible for the highly efficient electrocatalysis with high water selectivity. The sample containing mainly graphitic N species

(i.e., sample PANI_O2_1000_N2_1200) is the one having the highest activity and selectivity towards the 4 electrons mechanism. Moreover, the chemisorption of the oxygen molecule in bridging binding mode, which leads to a dissociative mechanism, can explain why the oxygen reduction reaction for the materials containing these species occurs through four electrons pathway. Nevertheless, other active sites like defects [40,41] are possible and may contribute to the ORR in these complex systems.

The sample only treated in an oxygen-containing atmosphere (that is, without applying the second heat treatment in N_2, PANI_O2_1000) shows a better performance towards the ORR than a non-doped carbon material, although it is inferior to the double heat treatment PANI-derived carbon materials. This can be due to the presence of pyridonic-type species, as deduced from TPD and XPS analyses. The computational results are consistent with the experimental results (Figure 5.8). The N-C-O species can catalyse the ORR in an easier way than non-doped carbon materials, but their catalysis is poorer than that obtained by edge-type graphitic nitrogen species. Furthermore, DFT calculations also show differences between the armchair and zig-zag positions for pyridonic species. Whereas the armchair position seems to favour the reduction via the 4 electrons pathway, the zig-zag position leads to oxygen molecule chemisorption through one edge-carbon atom in a terminal binding mode configuration, resulting in a 2 electrons reduction process. However, both functionalities show similar limiting energy barriers which can explain why the sample prepared by treatment only in the oxygen-containing atmosphere has a number of transferred electrons close to 3, suggesting that the population of both functionalities can be similar.

5.4 Conclusions

N-doped carbon materials have been prepared through a double stage heat treatment of polyaniline, first under an oxygen-containing atmosphere at 1000ºC and, then, under an inert atmosphere in a range of temperatures between 800 and 1200ºC. PANI-derived carbon materials were characterized by Raman spectroscopy, XPS, TPD and N_2-adsorption isotherms. The detailed characterization demonstrates that the samples pre-treated only in the oxygen-containing atmosphere have a higher amount of surface oxygen groups, and the N-species are mainly pyridonic groups. Once the second treatment is applied,

the high-temperature treatment using an inert atmosphere promotes the transformation of pyridinic nitrogen into graphitic nitrogen species, resulting in a material which essentially contains only this species. All these changes in the chemical nature of the functional groups are not accompanied by important modifications in porosity and structural order. The resultant carbon materials exhibit near platinum-like performance towards the ORR with high selectivity towards water generation. DFT calculations were carried out considering all nitrogen functionalities and the results are contrasted with the experiments. The computational results are in excellent agreement with the experimental results, reinforcing the key role that edge-type graphitic nitrogen plays as the most active and selective catalytic site for ORR.

5.5 References

[1] B.C. Steele, A. Heinzel, Materials for fuel-cell technologies, Nature. 414 (2001) 345–352.

[2] Y. Nie, L. Li, Z. Wei, Recent advancements in Pt and Pt-free catalysts for oxygen reduction reaction, Chem. Soc. Rev. 44 (2015) 2168–2201.

[3] I.E.L. Stephens, A.S. Bondarenko, U. Grønbjerg, J. Rossmeisl, I. Chorkendorff, Understanding the electrocatalysis of oxygen reduction on platinum and its alloys, Energy Environ. Sci. 5 (2012) 6744-6762.

[4] Y. Jiao, Y. Zheng, M. Jaroniec, S.Z. Qiao, Design of electrocatalysts for oxygen- and hydrogen-involving energy conversion reactions, Chem. Soc. Rev. 44 (2015) 2060–2086.

[5] A. Gabe, J. García-Aguilar, Á. Berenguer-Murcia, E. Morallón, D. Cazorla-Amorós, Key factors improving oxygen reduction reaction activity in cobalt nanoparticles modified carbon nanotubes, Appl. Catal. B Environ. 217 (2017) 303–312.

[6] J. Zhang, M.B. Vukmirovic, Y. Xu, M. Mavrikakis, R.R. Adzic, Controlling the catalytic activity of platinum-monolayer electrocatalysts for oxygen reduction with different substrates, Angew. Chemie - Int. Ed. 44 (2005) 2132–2135.

[7] F. Jaouen, E. Proietti, M. Lefèvre, R. Chenitz, J.-P. Dodelet, G. Wu, H.T. Chung, C.M. Johnston, P. Zelenay, Recent advances in non-precious metal catalysis for oxygen-reduction reaction in polymer electrolyte fuelcells, Energy Environ. Sci. 4 (2011) 114–130.

[8] L. Dai, Y. Xue, L. Qu, H.-J. Choi, J.-B. Baek, Metal-Free Catalysts for Oxygen Reduction Reaction, Chem. Rev. 115 (2015) 4823–4892.

[9] D. Guo, R. Shibuya, C. Akiba, S. Saji, T. Kondo, J. Nakamura, Active sites of nitrogen-doped carbon materials for oxygen reduction reaction clarified using model catalysts, Science 351 (2016) 361–365.

[10] C.V. Rao, C.R. Cabrera, Y. Ishikawa, In search of the active site in nitrogen-doped carbon nanotube electrodes for the oxygen reduction reaction, J. Phys. Chem. Lett. 1 (2010) 2622–2627.

[11] T. Xing, Y. Zheng, L.H. Li, B.C.C. Cowie, D. Gunzelmann, S.Z. Qiao, S. Huang, Y. Chen, Observation of active sites for oxygen reduction reaction on nitrogen-doped multilayer graphene, ACS Nano. 8 (2014) 6856–6862.

[12] K. Gong, F. Du, Z. Xia, M. Durstock, L. Dai, Nitrogen-Doped Carbon Nanotube Arrays with High Electrocatalytic Activity for Oxygen Reduction, Science 323 (2009) 760–764.

[13] L. Lai, J.R. Potts, D. Zhan, L. Wang, C.K. Poh, C. Tang, H. Gong, Z. Shen, J. Lin, R.S. Ruoff, Exploration of the active center structure of nitrogen-doped graphene-based catalysts for oxygen reduction reaction, Energy Environ. Sci. 5 (2012) 7936-7942.

[14] T. Sharifi, G. Hu, X. Jia, T. Wågberg, Formation of active sites for oxygen reduction reactions by transformation of nitrogen functionalities in nitrogen-doped carbon nanotubes, ACS Nano. 6 (2012) 8904–8912.

[15] J. Quílez-Bermejo, E. Morallón, Cazorla-Amorós, Oxygen reduction catalysis of N-doped carbons prepared via heat treatment of polyaniline at over 1100ºC, Chem. Commun. 54 (2018) 4441-4444.

[16] W. Ding, Z. Wei, S. Chen, X. Qi, T. Yang, J. Hu, D. Wang, L.J. Wan, S.F. Alvi, L. Li, Space-confinement-induced synthesis of pyridinic- and pyrrolic-nitrogen-doped graphene for the catalysis of oxygen reduction, Angew. Chemie - Int. Ed. 52 (2013) 11755–11759.

[17] J. Zheng, C. Guo, C. Chen, M. Fan, J. Gong, Y. Zhang, T. Zhao, Y. Sun, X. Xu, M. Li, R. Wang, Z. Luo, C. Chen, High content of pyridinic- and pyrrolic-nitrogen-modified carbon nanotubes derived from blood biomass for the electrocatalysis of oxygen reduction reaction in alkaline medium, Electrochim. Acta. 168 (2015) 386–393.

[18] J. Quílez-Bermejo, C. González-Gaitán, E. Morallón, D. Cazorla-Amorós, Effect of carbonization conditions of polyaniline on its catalytic activity towards ORR. Some insights about the nature of the active sites, Carbon 119 (2017) 62–71.

[19] R. Silva, D. Voiry, M. Chhowalla, T. Asefa, Efficient metal-free electrocatalysts for oxygen reduction: Polyaniline-derived N- and O-doped mesoporous carbons, J. Am. Chem. Soc. 135 (2013) 7823–7826.

[20] L. Zhang, C.Y. Lin, D. Zhang, L. Gong, Y. Zhu, Z. Zhao, Q. Xu, H. Li, Z. Xia,

Guiding Principles for Designing Highly Efficient Metal-Free Carbon Catalysts, Adv. Mater. 31 (2018) 1805252.

[21] S. Brunauer, P.H. Emmett, E. Teller, Adsorption of Gases in Multimolecular Layers, J. Am. Chem. Soc. 60 (1938) 309–319.

[22] M.M. Dubinin, The potential theory of adsorption of gases and vapors for adsorbents with energetically nonuniform surfaces, Chem. Rev. 60 (1960) 235–241.

[23] K. Nakada, M. Fujita, G. Dresselhaus, M.S. Dresselhaus, Edge state in graphene ribbons: Nanometer size effect and edge shapa dependence, Phys. Rev. B 54 (1996) 17954–17961.

[24] S.E. Stein, R.L. Brown, ρ-Electron Properties of Large Condensed Polyaromatic Hydrocarbons, J. Am. Chem. Soc. 109 (1987) 3721–3729.

[25] J. Tomasi, B. Mennucci, R. Cammi, Quantum Mechanical Continuum Solvation Models, Chem. Rev. 105 (2005) 2999–3094.

[26] J.K. Nørskov, J. Rossmeisl, A. Logadottir, L. Lindqvist, J.R. Kitchin, T. Bligaard, H. Jónsson, Origin of the overpotential for oxygen reduction at a fuel-cell cathode, J. Phys. Chem. B. 108 (2004) 17886–17892.

[27] H.F. Gorgulho, J.P. Mesquita, F. Gonçalves, M.F.R. Pereira, J.L. Figueiredo, Characterization of the surface chemistry of carbon materials by potentiometric titrations and temperature-programmed desorption, Carbon 46 (2008) 1544–1555.

[28] R. Berenguer, J.P. Marco-Lozar, C. Quijada, D. Cazorla-Amorós, E. Morallón, Effect of electrochemical treatments on the surface chemistry of activated carbon, Carbon 47 (2009) 1018–1027.

[29] J.L. Figueiredo, M.F.R. Pereira, M.M.A. Freitas, J.J.M. Órfão, Modification of the surface chemistry of activated carbons, Carbon 37 (1999) 1379–1389.

[30] Y. Otake, R.G. Jenkins, Characterization of oxygen-containing surface complexes created on a microporous carbon by air and nitric acid treatment, Carbon 31 (1993) 109–121.

[31] E. Raymundo-Piñero, D. Cazorla-Amorós, Á. Linares-Solano, The role of different nitrogen functional groups on the removal of SO2 from flue gases by N-doped activated carbon powders and fibres, Carbon 41 (2003) 1925–1932.

[32] J.R. Pels, F. Kapteijn, J.A. Moulijn, Q. Zhu, K.M. Thomas, Evolution of nitrogen functionalities in carbonaceous materials during pyrolysis, Carbon 33 (1995) 1641–1653.

[33] M. Jaymand, Recent progress in chemical modification of polyaniline, Prog. Polym. Sci. 38 (2013) 1287–1306.

[34] J. Balej, K. Balogh, P. Stopka, O. Špalek, Relation between the activity of electrodes from various carbonaceous meterials for reduction of oxygen to hydrogen peroxide and concentration of their paramagnetic centers, Collect. Czechoslov. Chem. Commun. 45 (1980) 3249–3253.

[35] C. Paliteiro, A. Hamnett, J.B. Goodenough, The electroreduction of oxygen on pyrolytic graphite, J. Electroanal. Chem. 233 (1987) 147–159.

[36] M.J. Mostazo-López, D. Salinas-Torres, R. Ruiz-Rosas, E. Morallón, D. Cazorla-Amorós, Nitrogen-doped superporous activated carbons as electrocatalysts for the oxygen reduction reaction, Materials 12 (2019) 1346.

[37] K.H. Wu, D.W. Wang, D.S. Su, I.R. Gentle, A Discussion on the Activity Origin in Metal-Free Nitrogen-Doped Carbons for Oxygen Reduction Reaction and their Mechanisms, ChemSusChem. 8 (2015) 2772–2788.

[38] G.L. Chai, Z. Hou, D.J. Shu, T. Ikeda, K. Terakura, Active sites and mechanisms for oxygen reduction reaction on nitrogen-doped carbon alloy catalysts: Stone-wales defect and curvature effect, J. Am. Chem. Soc. 136 (2014) 13629–13640.

[39] T. Ikeda, M. Boero, S.F. Huang, K. Terakura, M. Oshima, J. Ozaki, Carbon alloy catalysts: Active sites for oxygen reduction reaction, J. Phys. Chem. C. 112 (2008) 14706–14709.

[40] L.R. Radovic, Active sites in graphene and the mechanism of CO2 formation in carbon oxidation, J. Am. Chem. Soc. 131 (2009) 17166–17175.

[41] L.R. Radovic, in The World Conference of Carbon, Lexington, Kentucky, 2019.

[42] A. Gabe, R. Ruiz-Rosas, E. Morallón, D. Cazorla-Amorós, Understanding of oxygen reduction reaction by examining carbon-oxygen gasification reaction and carbon active sites on metal and heteroatoms free carbon materials of different porosities and structures, Carbon 148 (2019) 430–440.

[43] T. Ikeda, Z. Hou, G.L. Chai, K. Terakura, Possible oxygen reduction reactions for graphene edges from first principles, J. Phys. Chem. C. 118 (2014) 17616–17625.

[44] X. Hou, Q. Hu, P. Zhang, J. Mi, Oxygen reduction reaction on nitrogen-doped graphene nanoribbons: A density functional theory study, Chem. Phys. Lett. 663 (2016) 123–127.

[45] Z. Shi, J. Zhang, Z.S. Liu, H. Wang, D.P. Wilkinson, Current status of ab initio quantum chemistry study for oxygen electroreduction on fuel cell catalysts, Electrochim. Acta. 51 (2006) 1905–1916.

CHAPTER VI

SILICA AND TITANIA-TEMPLATED ORDERED MESOPOROUS N-DOPED CARBON THIN FILMS. HIGHLY EFFICIENT CATALYSTS TOWARDS OXYGEN REDUCTION REACTION

6.1 Introduction

The oxygen reduction reaction (ORR), occurring in the cathode electrode of the Fuel Cells (FCs), is one of the main limitations of these devices because of the slow reaction rate and high overpotential of the reaction [1,2]. The development of new materials capable of increasing the kinetics of the ORR and being cheaper in comparison to the current commercial catalyst, based on platinum, is necessary for the industrial commercialization of these electrochemical devices [3,4]. In this regard, metal-free catalysts based on heteroatom-doped carbon materials arises as one of the most promising alternative due to its highly efficient catalysis, low-cost and long durability towards ORR [5–8].

Among the heteroatom-doped carbon materials, it should be highlighted the use of nitrogen [9–11], phosphorus [12], sulphur [13,14] and oxygen [15–17], as a doping agent. Among all these heteroatoms, nitrogen functionalization has been by far the most studied. Dai et. al. [18] demonstrated the highly efficient catalysis of N-doped carbon nanotubes with platinum-like performance in alkaline medium. Nevertheless, there are three factors that limit the catalysis of oxygen reduction reaction with N-doped carbon electrocatalysts [19]: (i) the chemical nature of the active sites, (ii) electrical conductivity and (iii) the specific surface area and porous structure. The debate about the chemical nature of the active sites is now decreasing due to the synergy between experimental [20–22] and computational results [20,23,24] of some works, which point out the edge-type quaternary nitrogen and pyridine species in armchair position as the most active sites among nitrogen functionalities [20]. Moreover, carbon materials by themselves often exhibit high electrical conductivity.

However, surface area and porous structure are also important properties because they determine the accessibility of the active sites and the transport properties of the ORR-intermediates through the pores to the active sites. Unfortunately, the most common preparation methods of N-doped carbon materials are based on the heat treatment of a mixture of nitrogen and carbon containing precursors [25] or via direct carbonization of a nitrogen precursor [26], such as a conducting polymer. The main problem of these routes of synthesis is the non-control over the porosity and surface area.

In this sense, we report a method to synthesize N-doped mesoporous carbon materials thin films with high control over the N active sites towards oxygen reduction reaction and maintaining a well-ordered porosity. To do this, a thin film of polyaniline is electropolymerized in Silica and Titania ordered mesoporous templates by aniline adsorption and subsequent chronoamperometric polymerization. Once the electropolymerization was performed, the samples were heat treated with the aim of creating highly active species in the resultant composite nitrogen-doped mesoporous carbon material/template. The electrochemical behaviour and physicochemical properties of the prepared samples were determined by XPS, TEM and, cyclic voltammetry in presence and absence of dioxygen in the alkaline electrolyte.

6.2 Experimental

6.2.1 Materials and reagents

Aniline was purchased from Sigma Aldrich and was distilled under reduced pressure prior its use, in order to remove the impurities (e.g. aniline oligomers formed by oxidation during the storage). Potassium hydroxide (KOH) was purchased from Sigma-Aldrich. Sulphuric acid (98% H_2SO_4) were purchased from VWR Chemicals. Titanium tetraisopropoxide (TTIP), tetraethyl orthosilicate (TEOS), Pluronic123 (P123) and Pluronic®F127 were purchase in Sigma Aldrich. All the solutions were prepared using ultrapure water (18 M cm from an Elga Labwater Purelab system). The N_2 (99.999%) and O_2 (99.995%) was provided by Air Liquide and were used without any further purification or treatment. The carbon support, consisting of commercial macroporous carbon sheets (thickness = 0.3 mm, mean pore size 0.7 μm) was provided by Poco Graphite.

6.2.2 Silica template

Nanostructured silica thin films were successfully synthesized onto the graphite current collector and used as the hard template. Pluronic®F127 (2.52 g) was dissolved in absolute ethanol (40 mL) by stirring during 24 h under a controlled relative humidity (50 %). TEOS (6.72 mL) was added and stirred during 1 h to a HCl solution (16.7 μL of HCl (37%) in 2.52 mL of water). Then, both solutions were mixed and stirred during 1 h under the same relative humidity. The final molar ratio of the mixed solution was 1 TEOS: $6.6 \cdot 10^{-3}$ Pluronic©F127: $6.66 \cdot 10^{-3}$ HCl: 4.62 H_2O: 22.6 EtOH (that has been previously used to synthesize a rhombohedral silica thin film [27,28]).

The commercial graphite current collector sheet of around 1 x 1 cm^2 was dip-coated in the mixed solution. The constant withdrawal rate was 60 $mm \cdot min^{-1}$ and the relative humidity was maintained at 50%. The film was aged at room temperature during 24h. Then, the synthesized thin film was heat treated at 450 ºC for 5 h in a nitrogen atmosphere in order to eliminate the surfactant. The flow rate was maintained at 100 $mL \cdot min^{-1}$ and the heating rate was 1 $ºC \cdot min^{-1}$. The final sample is named as G/Si.

6.2.3 Titania template

Mesoporous TiO_2 thin films were grown by a route found in the literature which gives rise to hexagonal thin films. In the synthetic protocol, 1.05 g of Pluronic 123 were added to 16.21 g of absolute ethanol. The solution was stirred until completely clear, and then 4.03 g of concentrated (37%) HCl were added dropwise. To the resulting mixture, 5.70 g of TTIP were added dropwise, giving the final solution the following molar composition: 1 TTIP: 0.01 P123: 17.6 EtOH: 1.9 HCl: 7.2 H_2O (that has been previously used to synthesize a hexagonal Titania thin film [29,30]). Titania films were produced by dip-coating at a withdrawal speed of 1 $mm \cdot s^{-1}$ on the commercial graphite support (1 cm x 1 cm) and using the dip-coating procedure. The relative humidity (RH) during dip-coating was set at 50%. After deposition, films were aged at RH 50% for 24 h. Calcination of the films was performed in a furnace at 550 ºC for 1 h under inert atmosphere (N_2). In all experiments, the heating rate was 1 $ºC \cdot min^{-1}$. The samples were named as G/Ti.

6.2.4 PANI electropolymerization

The electrochemical polymerization was performed in a Biologic VSP potentiostat using a standard three-electrode cell configuration, with graphite as counter electrode and Ag/AgCl/Cl^-(sat.) electrode as reference electrode. However, all potentials will be referred to the reversible hydrogen electrode (RHE).

Bare G, G/Si and G/Ti were initially immersed into a solution of 0.1 M aniline + 0.5 M H_2SO_4 during 3 minutes to produce the adsorption of aniline monomer within the Silica and Titania pores. Then, the electrode was transferred to the electrochemical polymerization cell containing 0.5 M H_2SO_4 solution (without aniline) at a controlled potential of 0.2 V vs RHE for 10 seconds. After this period, chronoamperometric polymerization was carried out at 0.85, 0.95 and 1.05 V vs RHE for 5 minutes. While the polymerization does

not take place at 0.85 V, the potential of 1.05 V is too high to reach control over the polyaniline electropolymerized. Therefore, the selected potential was 0.95 V vs RHE and different polymerization times are used (10 s, 30 s and 5 min) with the aim of achieving different quantities of resultant polyaniline. The resultant samples were referred as G/Si-PANI-X or G/Ti-PANI-X, where X is the time employed during the aniline polymerization.

6.2.5 Heat treatments

The samples were heat treated in a tubular furnace at 900 ºC for 1 h using a heating rate of 5 ºC min^{-1} in an inert atmosphere (N_2). The furnace was purged for 1 h before the heat treatment in the corresponding atmosphere, the flow rate was maintained at 100 ml·min^{-1} during the treatment. The samples were named as G/Si-PANI-X-900 and G/Ti-PANI-X-900, being X the time employed during the polymerization.

6.2.6 Physicochemical characterization

The surface composition and oxidation states of the elements in the carbon materials were studied by XPS in a VG-Microtech Mutilab 3000 spectrometer and Al Kα radiation (1253.6 eV). The deconvolution of the XPS N1s region was done by least squares fitting using Gaussian-Lorentzian curves, while a Shirley line was used for the background determination. The samples were characterized by Transmission Electron Microscopy (TEM) coupled to EDX with a JEOL JEM-2010 microscope operating at 200kV with a spatial resolution of 0.24 nm.

6.2.7 Electrochemical characterization

Electrochemical characterization of all synthesized materials was performed in a 0.1 M H_2SO_4 and/or 0.1 M KOH solutions, using the three-electrode cell configuration. The electrochemical behavior was studied by cyclic voltammetry (CV) in a nitrogen-saturated solution between 0.0 and 0.8 V vs RHE at 50 mV·s^{-1}. 1 x 1 cm^2 of the electrode was immersed into the electrolyte as the working electrode. Graphite was used as a counter electrode and Ag/AgCl (3 M KCl) as the reference electrode. All the potentials are referred to the reversible hydrogen electrode.

The electrocatalytic activity towards oxygen reduction reaction was studied by linear sweep voltammetry (LSV) in O_2-saturated 0.1 M KOH solutions between 0.0 and 1.0 V (vs RHE).

6.3 Results and discussion

6.3.1 Electrochemical polymerization and characterization of G/Si-PANI and G/Ti-PANI composites

The chronoamperograms recorded during the growth of polyaniline on G, G/Si and G/Ti electrodes are presented in Figure 6.1a. The dashed red line shows the current for the bare macroporous graphite, the dotted blue line corresponds to the polymerization on G/Si and the solid green line shows the growth of polyaniline on G/Ti surface. The current versus time curves observed are common responses for electrochemical deposition. A maximum of the current is observed for the three electrodes as consequence of the consumption of aniline during the electrochemical polymerization and then, the current decreases as corresponds to a diffusion process. The maximum current for G/Si is observed at approximately 5 s after the pulse, whereas the maximum for the polymerization over the pristine G and G/Ti needs more time (7 and 10 s, respectively). This fact reflects the different kinetics towards the aniline polymerization, being G/Si the most electroactive electrode. After 5 min of the chronoamperometric pulse, the adsorbed aniline monomers are completely polymerized regardless of the electrode used. The measured charge together with the amount of deposited polyaniline after the chronoamperometric polymerizations are shown in Table 6.1 [31,32].

G/Ti material contains the higher amount of polyaniline. This fact should be related to the pore volume of the Titania thin film. The higher the pore volume, the higher the adsorption of aniline monomer and, consequently the amount of electrodeposited polyaniline. As G is a macroporous material, the pore volume is low and, in comparison with those materials where the mesoporosity predominates (such as G/Ti and G/Si), the amount of resultant polyaniline is much lower. Figure 6.1b shows the steady voltammograms in 0.5 M H_2SO_4 solution of the electrodes prepared in Figure 6.1a after 5 min of polymerization. G/Si and G/Ti samples show the typical profile of polyaniline in sulphuric acid. Moreover, the voltammetric charge of these electrodes is higher than the equivalent electrode over G. This is due to the differences in surface area. Polyaniline grown in the Silica or Titania pores presents a higher electroactive surface than the electrode without the inorganic matrix. The peak corresponding to the leucoemeraldine-emeraldine transition appears at around 0.4 V vs RHE

[31,33] and the second peak can be associated to the redox process of quinone-type species as consequence of the overoxidation of polyaniline [31,32].

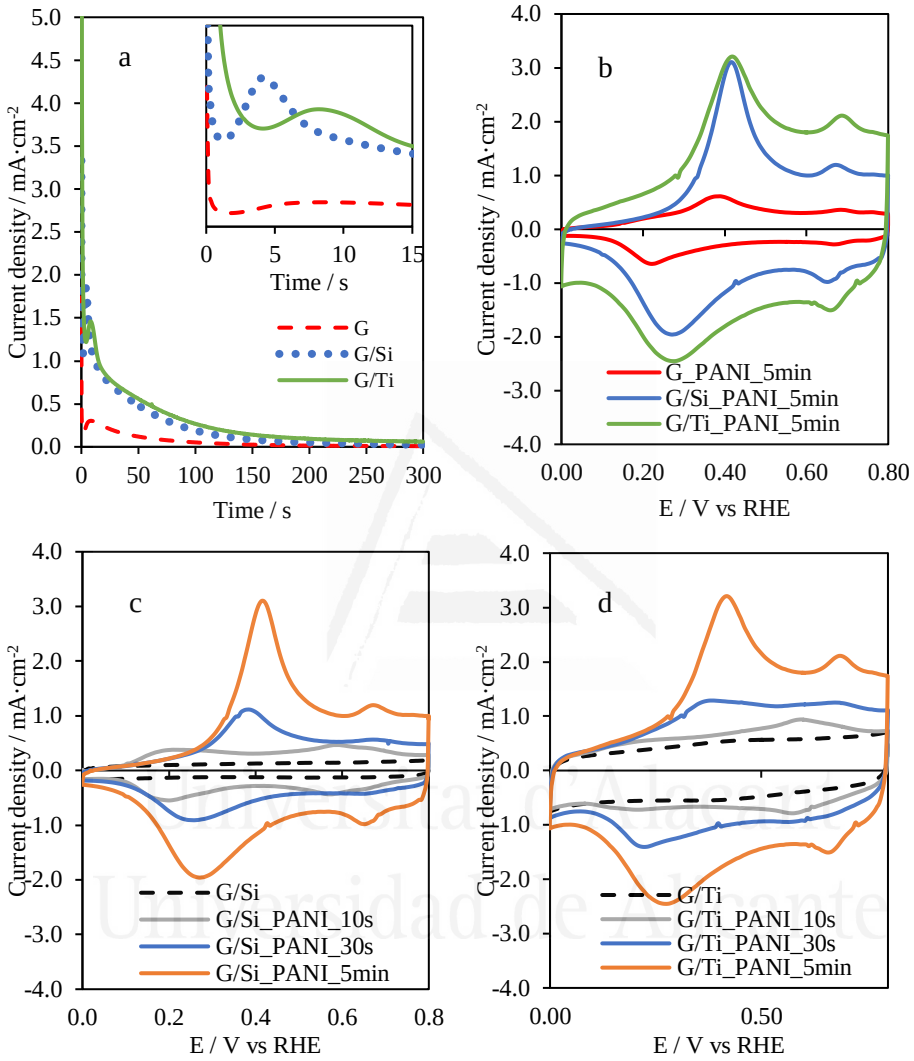

Figure 6.1: (a) Chronoamperometric profiles of aniline polymerization at 0.95 V vs RHE during 5 min on G, G/Si and G/Ti, (b) CV-profiles of the resultant samples (G, G/Si, G/Ti) after 5 min of aniline polymerization, (c,d) CV-profiles of all G/Si-PANI-X and G/Ti-PANI-X samples, respectively. Scan rate = 50 $mV \cdot s^{-1}$. 0.1 M H_2SO_4.

In order to control the length of the polymer chain maintaining the mesoporous structure, G/Si and G/Ti electrodes were also subjected to 10 and 30 seconds of the chronoamperometric pulse. After all polymerizations, the

resulting G/Si-PANI and G/Ti-PANI samples were electrochemically characterized by cyclic voltammetry in 0.5 M H_2SO_4 solution (Figure 6.1c and 6.1d). For G/Si-PANI and G/Ti-PANI electropolymerized during 10s, a pair of reversible peaks at around 0.6 V is observed. The further growth of the aniline loading results in a shift of this reversible peak to higher potentials. This peak at 0.6 V observed for the lowest polyaniline loading can be associated to the response of a major product of aniline dimerization in acid media [34–36]. Thus, the shape of the voltammograms is governed by polymer content and becomes similar to the polyaniline for the samples with higher polyaniline content. This behaviour has been previously observed for carbon/polyaniline composites [35].

Table 6.1: Charge obtained from the chronoamperometric pulse and the calculated amount of electrodeposited polyaniline on each electrode.

Electrode	Time	Q / mC	Polyaniline amount */ µg
G_PANI	10 s	2.64	2
	30 s	7.43	7
	5 min	18.25	17
G/Si_PANI	10 s	13.80	13
	30 s	30.39	29
	5 min	70.92	67
G/Ti_PANI	10 s	19.83	19
	30 s	38.31	36
	5 min	93.95	88

* Assuming a value of 1 electron per deposited aniline monomer

Then, the time employed during the chronoamperometric experiment is directly related with the electrochemical response of the final material, which means that it is possible to have some control over the thickness of the deposited polyaniline and over the polymer length. While G/Si-PANI-30s and G/Si-PANI-5min clearly show the typical redox processes, G/Si-PANI-10s exhibits an important broadening of both peaks. This confirms the presence of small oligomers because of the short period of time employed during the

polymerization, which does not enable the formation of large chains of polyaniline [35].

6.3.2 Electrochemical characterization of ordered mesoporous N- doped carbon-based composites

All previously characterized G/Si-PANI-X and G/Ti-PANI-X samples were heat treated at 900ºC with the aim of obtaining ordered-mesoporous N-doped carbon materials. All of them have also been electrochemically characterized by cyclic voltammetry in nitrogen-saturated 0.5 M H_2SO_4 and 0.1 M KOH solutions, using a scan rate of 50 $mV \cdot s^{-1}$. Figure 6.2 shows the voltammograms of all resultant carbon-based material samples. It also contains the CV for the G/Si and G/Ti samples after heat treatment at 900 ºC.

The electrochemical response of polyaniline in 0.1 M H_2SO_4 solution is lost after the carbonization at 900ºC. Polyaniline decomposes forming a carbon material in which amine and imine species from polyaniline lead to the formation of heterocyclic nitrogen functionalities, such as pyridine, pyrrole, quaternary-type nitrogen and pyridone functional groups with a very different electroactivity [26]. Figure 6.2a shows an important decrease in current density of G/Si-PANI-5min-900, in comparison with G/Si-PANI-5min (Figure 6.1b). In any case, the resultant carbon-based composites exhibit an enhancement in the electrochemical response with regard to the G/Si sample (Figure 6.2a). This should be related to the presence of a thin film formed by the N-doped carbon material on the inorganic matrix.

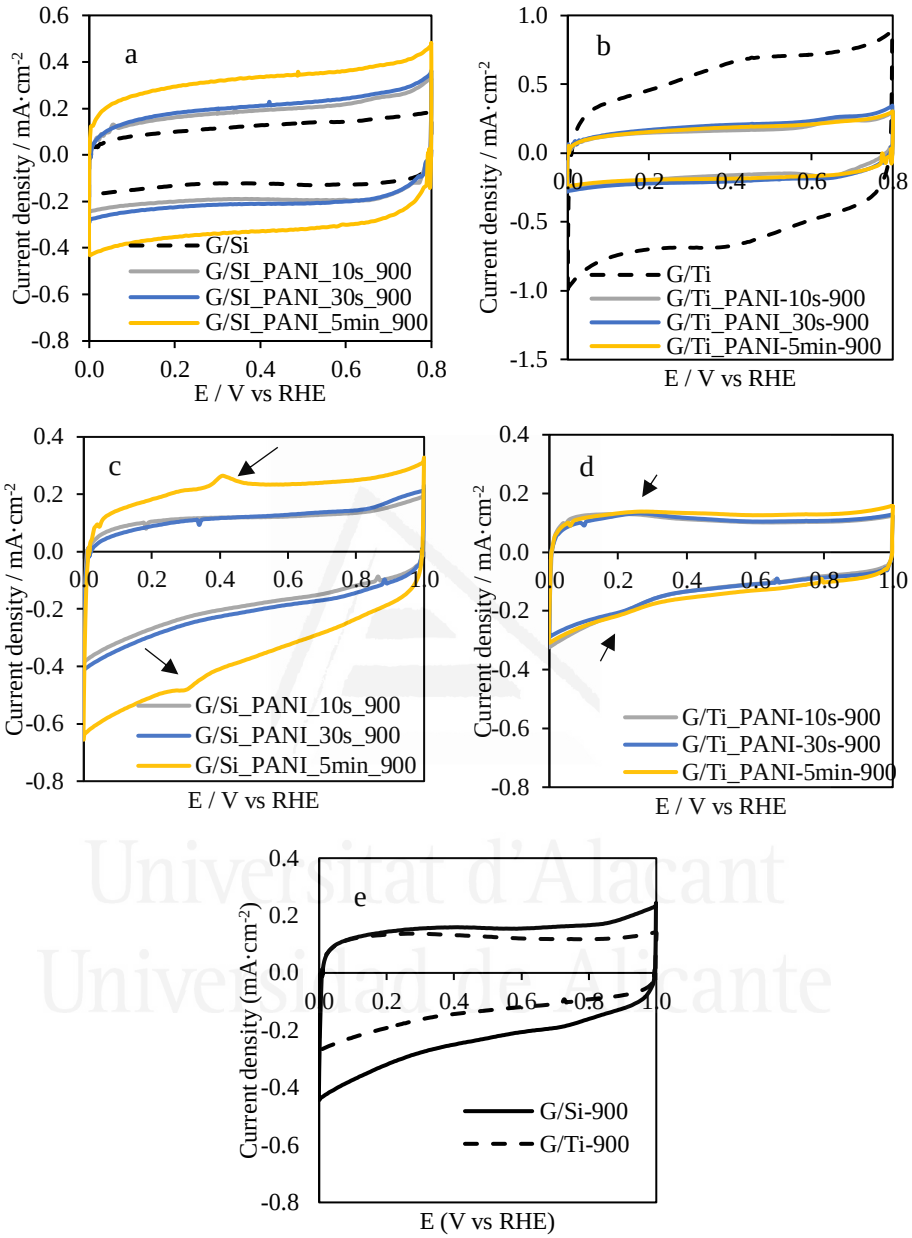

Figure 6.2: CV profiles of (a) G/Si-PANI-5min and (b) G/Ti-PANI-5min after the heat treatment in 0.1 M H_2SO_4 solution. CV profiles of the heat-treated (c) G/Si-PANI_X_900, (d) G/Ti-PANI-X-900 and (e) G/Si-900 and G/Ti-900 samples in 0.1 M KOH solution. Scan rate = 50 $mV \cdot s^{-1}$.

However, in the case of the Titania template, the electrochemical response is lower in G/Ti_PANI_5min_900 than for the pristine G/Ti (Figure 6.2b). Taking into account that the synthesized Titania thin film is mainly formed by anatase phase [30] and that the transformation of anatase into rutile takes place at around 500 ºC [37], the most likely explanation of the voltammetric behaviour is the loss of surface area through the anatase-rutile transformation during the heat treatment at 900ºC since rutile is known to have a much lower BET surface area than anatase [38]. Furthermore, the amount of polyaniline electropolymerized does not seem to have an effect in the CV profile of the heat-treated samples, which might be because of the blocking of the resultant N-doped carbon materials within the rutile-phase Titania structure.

The electrochemical characterization of G/Si-PANI-X_900 and G/Ti-PANI-X_900 samples was also performed in a nitrogen-saturated alkaline solution. Figures 6.2c and 6.2d show the cyclic voltammetry of all resultant composites under 0.1 M KOH solution at a scan rate of 50 $mV \cdot s^{-1}$. Once again, the higher the amount of polyaniline in G/Si, the higher the amount of the resultant carbon material. Interestingly, a new redox process is observed in the profile of G/Si-PANI-5min-900 that does not appear in the other samples, and that it is neither a characteristic peak for silica nor for carbon materials. This peak might be attributed to a new species derived from a reaction between polyaniline and the silica film during the carbonization treatment. Indeed, the presence of M-O-N oxynitride species has been reported as responsible for a redox peak in alkaline solution at a potential similar to the observed in this sample [39]. A redox process is also appreciable in G/Ti-PANI-X-900 samples, although it is smaller and is shifted to less positive potentials than the observed in G/Si-PANI-5 min-900 sample. The appearance of the mentioned redox processes is due to the reaction between the polyaniline and the inorganic film during the heat treatment. This was confirmed since G/Ti and G/Si heat-treated at 900ºC in the absence of PANI, do not present such redox processes (Figure 6.2e).

6.3.3 Physicochemical characterization

TEM images of all materials are shown in Figure 6.3. Figures 6.3a and 6.3b show the mesoporous ordered structures of the Silica and Titania thin films with a pore size close to 10 nm in both cases. No significant changes were observed

once the chronoamperometric polymerization was done (Figure 6.3c and 6.3d for G/Si_PANI_5min and G/Ti_PANI_5min, respectively), which suggests the presence of a thin film of polyaniline within the porous structure of Silica and Titania. Since the porous structure is still observable, the total blocking of the porosity can be discarded. This confirms the creation of a 2D-ordered thin film of polyaniline within the porosity of both templates.

Once the heat treatment is applied, the pristine ordered-mesoporosity of the Silica film is still observed (Figure 6.3e), however, the Titania template completely loses the presence of mesopores and forms small nanoparticles as a consequence of the change in Titania structure (Figure 6.3f). Indeed, a higher resolution of TEM images confirms the presence of nanoparticles with a hexagonal morphology of around 25 nm of size (Figure 6.3g).

The formation of these small nanoparticles is in agreement with the anatase-rutile phase transformation with the heat treatment that results in a loss in surface area of the Titania template.

All samples were also studied by XPS analysis. Figure 6.4 shows the N1s spectra for all materials where PANI has been electropolymerized. G/Si-PANI-X and G/Ti-PANI-X samples show two peaks associated with polyaniline [40–42]: (i) neutral amine groups at 399.5 eV and (ii) positively charged nitrogen atoms at approximately 401.7 eV. Table 6.2 shows the ratio between positively charged nitrogen atoms and neutral amine groups and the total nitrogen atomic content. In G/Si-PANI-X samples, the higher the polymerization time, the higher the contribution of positively charged N atoms. The trend is similar for G/Ti-PANI-X samples.

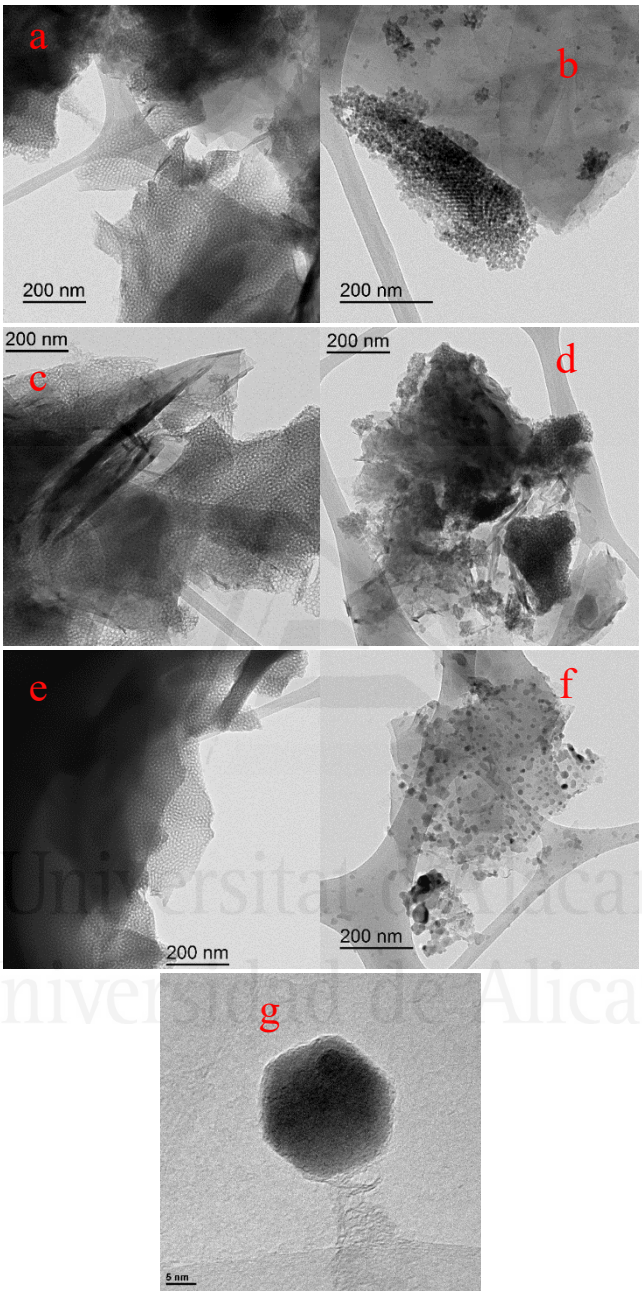

Figure 6.3: TEM images of (a) G/Si, (b) G/Ti, (c) G/Si_PANI_5min, (d) G/Ti_PANI_5min, (e) G/Si_PANI_5min_900, (f) G/Ti_PANI_5min_900 and (g) high resolution of G/Ti_PANI_5min_900.

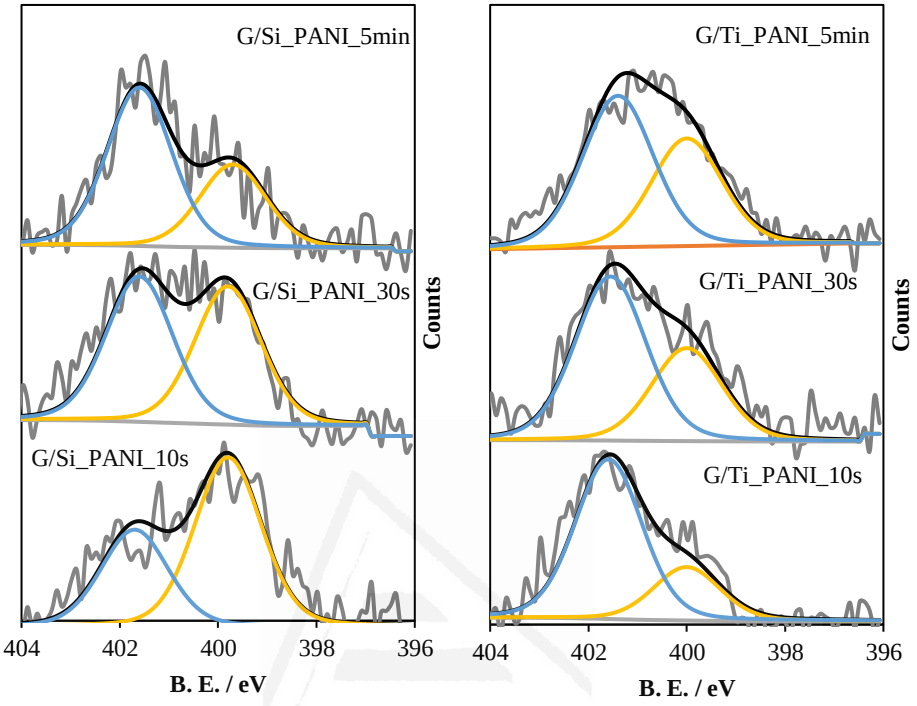

Figure 6.4: N1s spectra of all resultant G/Si-PANI-X and G/Ti-PANI-X samples. The blue line represents positively charged nitrogen, whereas the yellow line is associated with neutral amine species.

Concerning the heat-treated samples, Figure 6.5 shows the N1s spectra of all G/Si-PANI_X_900 and G/Ti-PANI_X_900 samples. All materials show two peaks, which are related to pyrrolic/pyridonic nitrogen species, at approximately 400.1 eV [43,44] and the presence of quaternary-type nitrogen species at 401.2 eV [43,44]. However, in G/Ti_PANI_X_900 samples, there is a third peak at 402 eV which can be associated with oxidised nitrogen (N-O species) [45,46].

Generally, all samples are highly enriched in quaternary-type nitrogen functional groups, but specifically, in G/Si_PANI_X_900 samples, it is observed that the higher the polymerization time, the higher the amount of quaternary-type nitrogen species after the heat treatment. In fact, G/Si_PANI_5min_900 sample mainly contains quaternary-type nitrogen species.

Table 6.2: Ratio between positively charged nitrogen species and amine groups and the atomic percentage of the nitrogen content obtained from XPS.

Sample	N^+/ N_{amine} ratio	N content/ at.%
G/Si_PANI_10s	0.54	0.3
G/Si_PANI_30s	0.95	0.6
G/Si_PANI_5min	1.74	0.7
G/Ti_PANI_10s	0.33	0.6
G/Ti_PANI_30s	0.57	0.8
G/Ti_PANI_5min	0.71	1.2
G/Si_PANI_10s_900	-	< 0.2
G/SI_PANI_30s_900	-	0.2
G/Si_PANI_5min_900	-	0.4
G/Ti_PANI_10s_900	-	< 0.2
G/Ti_PANI_30s_900	-	0.3
G/Ti_PANI_5min_900	-	0.5

Table 6.2 shows the nitrogen content of all materials obtained from XPS. In both templates, the higher the amount of polyaniline (Table 6.1), the higher the nitrogen content of the resultant N-doped carbon composite. After the heat treatment, there is an important decrease of the nitrogen content as a consequence of the carbonization of the polymeric chains. The yield of the carbonization can be determined from the nitrogen content before and after the heat treatment, being around 35%.

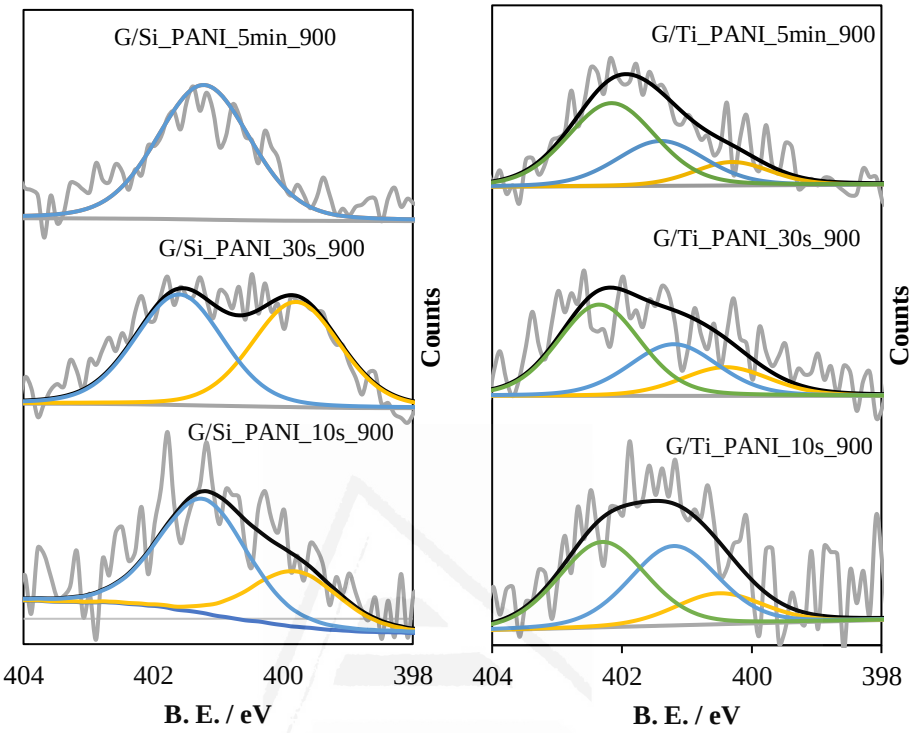

Figure 6.5: N1s spectra of all heat-treated G/Si-PANI-X-900 and G/Ti-PANI-X-900 samples.

Moreover, it should be highlighted that the shortest period of polymerization time (10 s), i.e. lower amount of polymer, leads to an amount of nitrogen after the high-temperature treatment which is within the sensitivity of the technique (less than 0.2 at.%). This seems to indicate that the dimers or oligomers of low molecular weight are volatilised during the heat treatment and do not produce carbon material.

6.3.4 Electrocatalytic activity

The electrocatalytic activity of all materials was studied in O_2-saturated 0.1 M KOH solution. The steady-state cyclic voltammogram in O_2-saturated 0.1 M KOH solution of G/Si_PANI-5min-900 and G/Ti_PANI-5min-900 are shown in Figure 6.6a and 6.6b, respectively. The large reduction current density and the tilted profile, in comparison with the N_2-saturated solution profile are characteristic features of catalytic materials towards oxygen reduction reaction.

All materials (not included in Figure 6.6 for the sake of clarity) showed similar behaviour. To get further insights, Figure 6.6c and 6.6d show the LSV curves for all samples. G/Si_900 and G/Ti_900 samples were included for comparison purposes.

Bare graphite shows the poorest catalytic activity towards oxygen reduction reaction with an onset potential close to 0.80 V vs RHE. The addition of a thin film of Silica seems to enhance the catalysis of this reaction up to 0.83 V (onset potential). Then, the heat treatment of the G/Si composite (without any polyaniline) improves the onset potential of the materials up to 0.87 V. The highly effective catalysis of silica-doped carbon has already been demonstrated from experimental and theory [47]. Si can change the charge distribution of the carbon framework and also the adsorption mode of the oxygen molecule [48].

Once the polyaniline is electropolymerized and heat treated within the porosity of SiO_2, relevant changes are observed. G/Si-PANI-10s-900 does not exhibit differences with respect to G/Si-900, probably because the amount of carbon material is very low. However, higher polymerization time and then, higher amount of polyaniline, leads to the formation of well-formed polyaniline, as electrochemical measurements and XPS analysis show. Therefore, the heat treatment leads to the formation of carbon-based composites with a nitrogen content close to 0.5 at.% (see Table 6.2). Interestingly, G/Si-PANI-30s-900 and G/Si-PANI-5min-900 samples show higher catalytic activity than G/Si- 900, achieving a E_{ONSET} close to 0.92 V.

A similar trend is also observed in G/Ti-PANI_X_900 samples. G/Ti is a highly efficient catalytic sample by itself [49] and the heat treatment does not produce a significant improvement of its electrochemical activity for ORR. Once again, the presence of small amount of oligomers does not seem to have a positive effect in the catalytic activity of G/Ti_PANI_10s_900, but a slight enhancement in catalytic activity is observed when the well-formed polyaniline is heat treated at 900ºC.

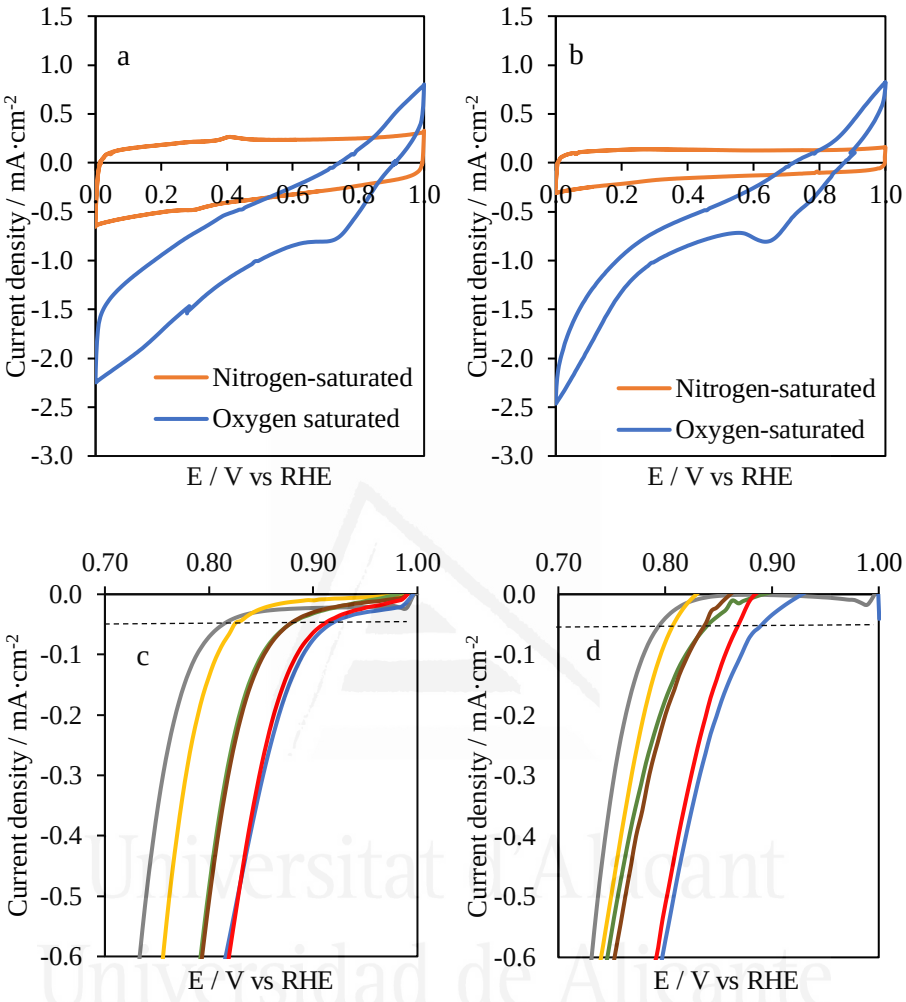

Figure 6.6: Steady voltammograms in nitrogen and oxygen-saturated 0.1 M KOH solution at 50 $mV \cdot s^{-1}$ of (a) G/Si-PANI-5min-900 and (b) G/Ti-PANI-5min-900. Linear sweep voltammetry curves in O_2-saturated 0.1 M KOH solution at 50 $mV \cdot s^{-1}$ for (c) G/Si-PANI-X-900 and (d) G/Ti-PANI-X-900 samples. In LSV curves, grey represents G, yellow represents G/X, green represents G/X_900, brown represents G/X_PANI_10s_900, blue represents G/X-PANI_30s_900 and red represents G/X_PANI_5min_900, with X being (c) Si or (d) Ti.

Table 6.3: Electrochemical parameters calculated from LSV curves of the different electrocatalysts in O_2-saturated 0.1 M KOH solution at 50 $mV \cdot s^{-1}$.

Sample	E_{ONSET} / V vs RHE ($-0.05\ mA \cdot cm^{-2}$)	Tafel slope / $mV \cdot dec^{-1}$
G	0.80	73
G/Si	0.83	65
G/Si_900	0.87	77
G/Si_PANI_10s_900	0.87	80
G/Si_PANI_30s_900	0.92	89
G/Si_PANI_5min_900	0.91	80
G/Ti	0.81	84
G/Ti_900	0.84	110
G/Ti_PANI_10s_900	0.84	131
G/Ti_PANI_30s_900	0.89	118
G/Ti_PANI_5min_900	0.87	124

Tafel slope calculated for the different materials provide also interesting information about the ORR mechanism (Table 6.3). While N-doped carbon materials/Silica composites show slopes close to 80 $mV \cdot dec^{-1}$, the N-doped carbon materials/Titania composites have higher Tafel slopes (120 $mV \cdot dec^{-1}$). The Tafel slope of 120 $mV \cdot dec^{-1}$ is characteristic of reactions whose rate determining step is the formation of superoxide species involving one electron transfer [50,51]. On the other hand, lower Tafel slopes indicate that other chemical reactions participate in the reaction mechanism [50–52]. Therefore, the ORR mechanisms in G/Si-PANI-X-900 and G/Ti-PANI-X-900 go through different pathways.

According to the physicochemical and electrochemical characterization, the enhancement in the catalytic activity of the most active samples can be associated with the presence of N-doped carbon framework within the porous structure of the Silica and Titania, which exhibits a quaternary nitrogen enriched

surface. Indeed, edge-type quaternary nitrogen species has been proposed as highly efficient catalyst towards ORR with high selectivity towards water formation due to its low kinetic barriers and bridging bonding mode for oxygen molecule chemisorption [22–24,53,54]. Furthermore, the 2D-ordered mesoporosity of these composites enables the accessibility of the oxygen molecule and the intermediates of the ORR to efficiently reach the active sites of the N-doped carbon materials.

An etching process was carried out in order to evaluate the effect of the inorganic template in the electrocatalytic activity of the resultant samples. For that purpose, the most catalytic sample, G/Si_PANI_5min_900, was immersed in a 10 M NaOH solution during 10 hours at 60ºC with the aim of removing the silica template. After that, it was washed with water several times. The resultant sample is referred as G/Si-PANI-5min-900_NaOH. Figure 6.7a shows the comparison between the catalytic activity of the samples before and after the etching. Interestingly, removal of the silica template of the composites leads to a significant decrease in the catalytic activity of the material. This fact should be associated with the modification of the most catalytic nitrogen species. In order to discern whether there is a modification of the nitrogen-functional groups due to the action of the high concentrated sodium hydroxide solution, XPS analysis after etching was performed. Figure 6.7b shows the N1s spectra of G/Si_PANI-5min-900_NaOH, where important changes are observed. The quaternary-type nitrogen species of G/Si_PANI_5min_900 sample have transformed into, mainly, pyridone species after the etching process. This transformation can only be understood if the quaternary-type nitrogen species are located at the edge of the carbon framework, since the oxidation of a basal-plane quaternary nitrogen species is thermodynamically unfavourable [55]. The results are in agreement with the higher catalytic activity of edge-type quaternary nitrogen species with respect to pyridone-type nitrogen functional groups. Even though the etching process has diminished the catalytic activity of the sample, the performance is still highly efficient, since the pyridonic-like groups have also been proposed as active sites in N-doped carbon materials [15,20].

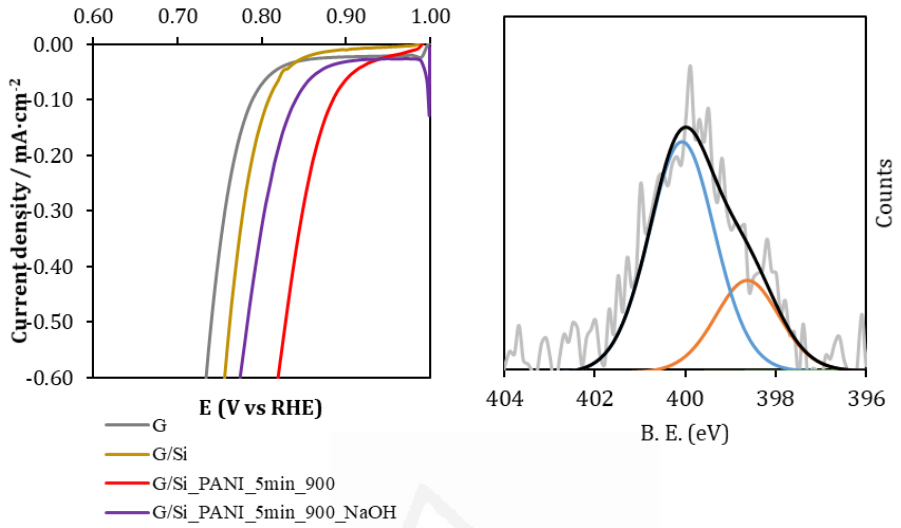

Figure 6.7: (a) Linear sweep voltammetry curves of G/Si_PANI_5min_900_NaOH in O_2-saturated 0.1 M KOH solution at 50 $mV \cdot s^{-1}$ and (b) N1s from XPS analysis of G/Si_PANI_5min_900_NaOH; blue peak represents pyridonic-like groups and orange line represents pyridine species.

6.4 Conclusions

2D-ordered polyaniline thin film was successfully prepared through the chronoamperometric polymerization of aniline within the porous structure of two ordered mesoporous templates: Silica and Titania. The polymerization time permits to control the amount of polymer electrodeposited on the surface of the templates. Moreover, XPS reveals an increase in the positively charged nitrogen species with the polymerization time and a maximum nitrogen content of 1.2 at.%, obtained in G/Ti_PANI_5min composite.

The excellent control over the polyaniline amount leads to a good control over the resultant heat-treated samples when silica is used as a template. However, the Titania phase transformation from anatase to rutile hampers the benefits of the obtained N-doped carbon materials/Titania composites. In fact, TEM images confirm the loss of surface area because of a morphological transformation of the anatase to rutile phase. On the other hand, well-ordered mesoporosity was maintained using Silica as a template. It is observed from N1s spectra that the nitrogen species are mainly quaternary-type nitrogen functional groups.

The catalytic activity of the heat-treated samples towards oxygen reduction reaction was carried out in alkaline solution. Although all samples showed an enhancement after the carbonization stage, those materials where Silica acts as template exhibited highly effective electrocatalysis, with an E_{ONSET} potential higher than 0.9 V vs RHE and lower Tafel plot. Once Silica template was removed with highly concentrated alkaline solution, the electrocatalytic activity of the samples decreases as a consequence of the transformation of edge-type quaternary nitrogen species into pyridonic nitrogen functional groups, pointing out the crucial role that quaternary nitrogen species play in ORR electrocatalysis.

6.5 References

[1] A. Kongkanand, M.F. Mathias, The Priority and Challenge of High-Power Performance of Low-Platinum Proton-Exchange Membrane Fuel Cells, J. Phys. Chem. Lett. 7 (2016) 1127–1137.

[2] J. Stacy, Y.N. Regmi, B. Leonard, M. Fan, The recent progress and future of oxygen reduction reaction catalysis: A review, Renew. Sustain. Energy Rev. 69 (2017) 401–414.

[3] S. Shahgaldi, J. Hamelin, Improved carbon nanostructures as a novel catalyst support in the cathode side of PEMFC: A critical review, Carbon 94 (2015) 705–728.

[4] H. Lv, D. Li, D. Strmcnik, A.P. Paulikas, N.M. Markovic, V.R. Stamenkovic, Recent advances in the design of tailored nanomaterials for efficient oxygen reduction reaction, Nano Energy. 29 (2016) 149–165.

[5] Z. Wu, Z. Iqbal, X. Wang, Metal-free, carbon-based catalysts for oxygen reduction reactions, Front. Chem. Sci. Eng. 9 (2015) 280–294.

[6] J. Zhang, L. Dai, Heteroatom-Doped Graphitic Carbon Catalysts for Efficient Electrocatalysis of Oxygen Reduction Reaction, ACS Catal. 5 (2015) 7244–7253.

[7] J. Zhang, Z. Xia, L. Dai, Carbon-based electrocatalysts for advanced energy conversion and storage, Sci. Adv. 1 (2015) e1500564.

[8] L. Dai, Y. Xue, L. Qu, H.J. Choi, J.B. Baek, Metal-Free Catalysts for Oxygen Reduction Reaction, Chem. Rev. 115 (2015) 4823–4892.

[9] S. Zhao, X. Lu, L. Wang, J. Gale, R. Amal, Carbon-Based Metal-Free Catalysts for Electrocatalytic Reduction of Nitrogen for Synthesis of Ammonia at Ambient Conditions, Adv. Mater. 31 (2019) 1805367.

[10] Z. Wu, M. Song, J. Wang, X. Liu, Recent Progress in Nitrogen-Doped Metal-Free Electrocatalysts for Oxygen Reduction Reaction, Catalysts. 8 (2018) 196.

[11] Z. Jiang, J. Yu, T. Huang, M. Sun, Recent Advance on Polyaniline or Polypyrrole-Derived Electrocatalysts for Oxygen Reduction Reaction, Polymers 10 (2018) 1397.

[12] C. Zhang, N. Mahmood, H. Yin, F. Liu, Y. Hou, Synthesis of phosphorus-doped graphene and its multifunctional applications for oxygen reduction reaction and lithium ion batteries, Adv. Mater. 25 (2013) 4932–4937.

[13] L. Wang, W. Jia, X. Liu, J. Li, M.M. Titirici, Sulphur-doped ordered mesoporous carbon with enhanced electrocatalytic activity for the oxygen reduction reaction, J. Energy Chem. 25 (2016) 566–570.

[14] Z. Ma, S. Dou, A. Shen, L. Tao, L. Dai, S. Wang, Sulfur-doped graphene derived from cycled lithium-sulfur batteries as a metal-free electrocatalyst for the oxygen reduction reaction, Angew. Chemie - Int. Ed. 54 (2015) 1888–1892.

[15] J. Quílez-Bermejo, C. González-Gaitán, E. Morallón, D. Cazorla-Amorós, Effect of carbonization conditions of polyaniline on its catalytic activity towards ORR. Some insights about the nature of the active sites, Carbon 119 (2017) 62–71.

[16] F. Zhou, G. Wang, F. Huang, Y. Zhang, M. Pan, Polyaniline derived N- and O-enriched high surface area hierarchical porous carbons as an efficient metal-free electrocatalyst for oxygen reduction, Electrochim. Acta. 257 (2017) 73–81.

[17] R. Silva, D. Voiry, M. Chhowalla, T. Asefa, Efficient metal-free electrocatalysts for oxygen reduction: Polyaniline-derived N- and O-doped mesoporous carbons, J. Am. Chem. Soc. 135 (2013) 7823–7826.

[18] K. Gong, F. Du, Z. Xia, M. Durstock, L. Dai, Nitrogen-Doped Carbon Nanotube Arrays with High Electrocatalytic Activity for Oxygen Reduction, Science 323 (2009) 760–764.

[19] H.W. Liang, W. Wei, Z.S. Wu, X. Feng, K. Müllen, Mesoporous metal-nitrogen-doped carbon electrocatalysts for highly efficient oxygen reduction reaction, J. Am. Chem. Soc. 135 (2013) 16002–16005.

[20] J. Quílez-Bermejo, E. Morallón, D. Cazorla-Amorós, Metal-Free Heteroatom-doped Carbon-based catalysts for ORR. A critical assessment about the role of heteroatoms, Carbon 165 (2020) 434–454.

[21] T. Sharifi, G. Hu, X. Jia, T. Wågberg, Formation of Active Sites for Oxygen Reduction Reactions by Transformation of Nitrogen Functionalities in Nitrogen-Doped Carbon Nanotubes, ACS Nano. 6 (2012) 8904–8912.

[22] J. Quílez-Bermejo, E. Morallón, D. Cazorla-Amorós, Oxygen-reduction catalysis of N-doped carbons prepared: Via heat treatment of polyaniline at over

1100 °C, Chem. Commun. 54 (2018) 4441–4444.

[23] T. Ikeda, Z. Hou, G.L. Chai, K. Terakura, Possible oxygen reduction reactions for graphene edges from first principles, J. Phys. Chem. C. 118 (2014) 17616–17625.

[24] T. Ikeda, M. Boero, S.F. Huang, K. Terakura, M. Oshima, J. Ozaki, Carbon alloy catalysts: Active sites for oxygen reduction reaction, J. Phys. Chem. C. 112 (2008) 14706–14709.

[25] M.J. Mostazo-López, R. Ruiz-Rosas, E. Morallón, D. Cazorla-Amorós, Nitrogen doped superporous carbon prepared by a mild method. Enhancement of supercapacitor performance, Int. J. Hydrogen Energy. 41 (2016) 19691–19701.

[26] G. Ćirić-Marjanović, I. Pašti, N. Gavrilov, A. Janošević, S. Mentus, Carbonised polyaniline and polypyrrole: towards advanced nitrogen-containing carbon materials, Chem. Pap. 67 (2013) 781–813.

[27] U.H. Lee, J.H. Yang, H.J. Lee, J.Y. Park, K.R. Lee, Y.U. Kwon, Facile and adaptable synthesis method of mesostructured silica thin films, J. Mater. Chem. 18 (2008) 1881–1888.

[28] S. Leyva-García, D. Lozano-Castelló, E. Morallón, D. Cazorla-Amorós, Silica-templated ordered mesoporous carbon thin films as electrodes for micro-capacitors, J. Mater. Chem. A. 4 (2016) 4570–4579.

[29] H. Oveisi, X. Jiang, Y. Nemoto, A. Beitollahi, Y. Yamauchi, Cerium-doped mesoporous TiO2 thin films: Controlled crystallization of anatase with retention of highly ordered mesostructure, Microporous Mesoporous Mater. 139 (2011) 38–44.

[30] G.F. Ortiz, Á. Berenguer-Murcia, M. Cabello, D. Cazorla-Amorós, J.L. Tirado, Ordered mesoporous titanium oxide for thin film microbatteries with enhanced lithium storage, Electrochim. Acta. 166 (2015) 293–301.

[31] M.J. Bleda-Martínez, E. Morallón, D. Cazorla-Amorós, Polyaniline/porous carbon electrodes by chemical polymerisation: Effect of carbon surface chemistry, Electrochim. Acta. 52 (2007) 4962–4968.

[32] F. Montilla, M. de los Á. Cotarelo, E. Morallón, Hybrid sol-gel-conducting polymer synthesised by electrochemical insertion: tailoring the capacitance of polyaniline, J. Mater. Chem. 19 (2009) 305.

[33] C.C. Hu, J.Y. Lin, Effects of the loading and polymerization temperature on the capacitive performance of polyaniline in NaNO3, Electrochim. Acta. 47 (2002) 4055–4067.

[34] G.A. Planes, J.L. Rodríguez, M.C. Miras, G. García, E. Pastor, C.A. Barbero, Spectroscopy evidence for intermediate species formed during aniline

polymerization and polyaniline degradation, Phys. Chem. Chem. Phys. 12 (2010) 10584–10593.

[35] A. Kuznetsov, A.B. Ayupov, P.M. Yeletsky, M. V. Lebedeva, Influence of monomer content on course of aniline polymerization in presence of high surface area carbon, J. Electroanal. Chem. 835 (2019) 73–80.

[36] L. Duic, Z. Mandic, S. Kovac, Polymer-dimer distribution in the electrochemical synthesis of polyaniline, Electrochim. Acta. 40 (1995) 1681–1688.

[37] J. Fernández-Catalá, D. Cazorla-Amorós, Berenguer-Murcia, Facile encapsulation of P25 (TiO2) in spherical silica with hierarchical porosity with enhanced photocatalytic properties for gas-phase propene oxidation, Appl. Catal. A Gen. 564 (2018) 123–132.

[38] T. Fröschl, U. Hörmann, P. Kubiak, G. Kučerová, M. Pfanzelt, C.K. Weiss, R.J. Behm, N. Hüsing, U. Kaiser, K. Landfester, M. Wohlfahrt-Mehrens, High surface area crystalline titanium dioxide: Potential and limits in electrochemical energy storage and catalysis, Chem. Soc. Rev. 41 (2012) 5313–5360.

[39] S. Wang, L. Li, Y. Shao, L. Zhang, Y. Li, Y. Wu, X. Hao, Transition-Metal Oxynitride: A Facile Strategy for Improving Electrochemical Capacitor Storage, Adv. Mater. 31 (2019) 1806088.

[40] J. Arias-Pardilla, H.J. Salavagione, C. Barbero, E. Morallón, J.L. Vázquez, Study of the chemical copolymerization of 2-aminoterephthalic acid and aniline. Synthesis and copolymer properties, Eur. Polym. J. 42 (2006) 1521–1532.

[41] P. Rannou, D. Rouchon, Y.F. Nicolau, M. Nechtschein, A. Ermolieff, Chemical degradation of aged CSA-protonated PANI films analyzed by XPS, Synth. Met. 101 (1999) 823–824.

[42] J. Quílez-Bermejo, A. Ghisolfi, D. Grau-Marín, E. San-Fabián, E. Morallón, D. Cazorla-Amorós, Post-synthetic efficient functionalization of polyaniline with phosphorus-containing groups. Effect of phosphorus on electrochemical properties, Eur. Polym. J. 119 (2019) 272–280.

[43] D.W. Wang, F. Li, L.C. Yin, X. Lu, Z.G. Chen, I.R. Gentle, G.Q. Lu, H.M. Cheng, Nitrogen-doped carbon monolith for alkaline supercapacitors and understanding nitrogen-induced redox transitions, Chem. - A Eur. J. 18 (2012) 5345–5351.

[44] C. Falco, M. Sevilla, R.J. White, R. Rothe, M.M. Titirici, Renewable nitrogen-doped hydrothermal carbons derived from microalgae, ChemSusChem. 5 (2012) 1834–1840.

[45] P. Streubel, R. Hesse, J. Friebel, H. Schmiers, R. Köpsel, Change of chemical bonding of nitrogen of polymeric N-heterocyclic compounds during pyrolysis, Carbon 37 (2002) 1965–1978.

[46] J. Lahaye, G. Nansé, A. Bagreev, V. Strelko, Porous structure and surface chemistry of nitrogen containing carbons from polymers, Carbon 37 (1999) 585–590.

[47] Z. Liu, X. Fu, M. Li, F. Wang, Q. Wang, G. Kang, F. Peng, Novel silicon-doped, silicon and nitrogen-codoped carbon nanomaterials with high activity for the oxygen reduction reaction in alkaline medium, J. Mater. Chem. A. 3 (2015) 3289–3293.

[48] Y. Chen, X.C. Yang, Y.J. Liu, J.X. Zhao, Q.H. Cai, X.Z. Wang, Can Si-doped graphene activate or dissociate O2 molecule?, J. Mol. Graph. Model. 39 (2013) 126–132.

[49] J.H. Kim, A. Ishihara, S. Mitsushima, N. Kamiya, K.I. Ota, Catalytic activity of titanium oxide for oxygen reduction reaction as a non-platinum catalyst for PEFC, Electrochim. Acta. 52 (2007) 2492–2497.

[50] E. Yeager, Electrocatalysts for O2 reduction, Electrochim. Acta. 29 (1984) 1527–1537.

[51] T. Shinagawa, Á.T. Garcia-Esparza, K. Takanabe, Insight on Tafel slopes from a microkinetic analysis of aqueous electrocatalysis for energy conversion, Sci. Rep. 5 (2015) 13801.

[52] Q. Zhang, T. Zhang, J. Ge, Y. Yin, Permeable silica shell through surface-protected etching, Nano Lett. 8 (2008) 2867–2871.

[53] T. Sharifi, G. Hu, X. Jia, T. Wågberg, Formation of active sites for oxygen reduction reactions by transformation of nitrogen functionalities in nitrogen-doped carbon nanotubes, ACS Nano. 6 (2012) 8904–8912.

[54] J. Quílez-Bermejo, M. Melle-Franco, E. San-Fabián, E. Morallón, D. Cazorla-Amorós, Towards understanding the active sites for the ORR in N-doped carbon materials through fine-tuning of nitrogen functionalities: an experimental and computational approach, J. Mater. Chem. A. 7 (2019) 24239–24250.

[55] L.R. Radovic, C. V. Mora-Vilches, A.J.A. Salgado-Casanova, A. Buljan, Graphene functionalization: Mechanism of carboxyl group formation, Carbon 130 (2018) 340–349.

CHAPTER VII

ON THE ORIGIN OF THE EFFECT OF PH IN ORR FOR NON-DOPED AND EDGE-TYPE QUATERNARY N-DOPED METAL-FREE CARBON-BASED CATALYSTS

7.1 Introduction

The oxygen reduction reaction is one of the determining limiting factors in polymer electrolyte membrane fuel cells (FC) because of the high overpotential and low reaction rate [1,2]. Platinum is nowadays the most catalytic material towards ORR; however, it has important disadvantages, such as high cost, low durability or low resistance towards methanol and CO poisoning [3]. These limitations make highly desirable the replacement of this precious metal by other materials. In this sense, carbon materials, specifically N-doped carbon materials, have been proved as a promising alternative towards platinum replacement because of their high catalytic activity along with more suitable characteristics [4]. However, this high catalytic activity has only been demonstrated in an alkaline electrolyte, whereas in an acidic electrolyte, the performance of metal-free carbon-based catalysts suffers an important decrease in terms of activity [5,6].

This is relevant since heretofore the most developed, and commercially available, polymer electrolyte membranes for the FC are proton exchange membranes [7–9]. This means that the cathode electrode, in these conditions, is surrounded by an acidic environment. Thus, the catalytic activity of those carbon-based materials in the alkaline electrolyte is inefficient for the current polymer electrolyte membrane FC. Therefore, efforts should be applied to the improvement of carbon-based catalysts for their application in an acidic environment. However, there is still a consistent lack of knowledge regarding the performance and reaction mechanisms of those catalysts in a protonic electrolyte. The fundamental reasons why carbon materials (doped or not) show poor catalytic activities towards oxygen reduction reaction in acidic environments are still unknown. Nevertheless, some works have tried to explain the reasons of this pH dependence. In a previous work, Noffke et al. addressed the reasons for this the pH-dependent behaviour from computational calculations [10]. These authors suggested the 2 electrons pathway as the preferred route in acidic environment and 4 electrons pathway as the preferred route in alkaline solutions, however, most of the experimental works available show the opposite behaviour [5,11–14]. This fact is pointed out in the work of Behan et al. [15]. They evaluated the performance of different N-doped carbon materials towards ORR as a function of the pH, where a clear decrease of the catalytic activity was observed for all carbon-based materials in acidic media

and higher selectivity towards water production. Moreover, the authors suggested that this pH effect was augmented if the ORR takes place in active sites generated by quaternary nitrogen species. Other previous experimental work [16] corroborated this aspect; the performance of carbon-based catalysts in alkaline environment is higher than in acidic media. However, to the best of our knowledge, the reasons of this pH dependence are still contradictories and unclear.

In this work, we aim to understand the effect of pH on the catalytic activity of non-doped and N-doped carbon materials through a combined experimental and computational study. To this end, a non-doped carbon material and a selectively N-doped carbon material have been tested as electrocatalysts in both environments. Then, computational modelling, based on Density Functional Theory (DFT) has been performed providing interpretation for the different behaviour for non-doped and N-doped carbon materials in ORR catalytic activity in different electrolytes.

7.2 Experiments and Methods

7.2.1 Materials and reagents

Aniline was purchased from Sigma Aldrich and, then, was distilled via refluxing under reduced pressures prior to its use. Ammonium persulfate, ammonium hydroxide and potassium hydroxide were purchased from Sigma Aldrich. Hydrochloric acid (37% HCl) was purchased from VWR-Chemicals Prolabo. All the solutions were prepared using ultrapure water (18 MΩ cm from an Elga Labwater Purelab system). XC-72F Vulcan Carbon black was supplied by Cabot Corporation. The gases N_2 (99.999%), O_2 (99.995%) and H_2 (99.999%) were provided by Air Liquide.

7.2.2 PANI preparation

Polyaniline was chemically synthesized according to our previous works [17,18]. 0.067 M of aniline was mixed in stoichiometric ratio with ammonium persulfate in 1.5 L of 1 M HCl solution. The mixture was kept under stirring (500 rpm) during 3 hours at 0ºC. The final polymer was filtered, washed with water and dried. Then, in order to obtain the undoped polyaniline, the resultant polymer was treated with 1 M ammonium hydroxide for 24 hours. The final polyaniline (PANI) was washed several times with distilled water and dried at 80 ºC for 12 hours.

7.2.3 Heat treatment

150 mg of PANI was heat-treated in a tubular furnace via double-stage process. First, PANI was heat-treated under an oxygen-containing atmosphere (5000 ppm O_2/N_2) at 1000 ºC for 1 h using a heating rate of 5 ºC min^{-1} and, then, cooled down at room temperature at 10 ºC min^{-1}. The flow rate was maintained at 100 $mLmin^{-1}$. This treatment was followed by a second heat treatment at 1200 ºC at 5 ºC min^{-1} for 1 hour under an inert (N_2) atmosphere. The flow rate was maintained at 200 $mL \cdot min^{-1}$. The furnace was purged for 1 hour prior to both heat treatments under the corresponding atmosphere and flow rate.

This specific double stage heat treatment enables the synthesis of a N-doped carbon material with only one nitrogen species [18]; edge-type graphitic nitrogen functional group. More details about the treatment can be found in Chapter V.

7.2.4 Characterization

The samples were characterized by Transmission Electron Microscopy (TEM) coupled to EDX with a JEOL JEM-2010 microscope operating at 200 kV with a spatial resolution of 0.24 nm. The textural properties of the materials have been evaluated by N_2-adsorption isotherms at -196ºC in an automatic adsorption system (Autosorb-6, Quantachrome). Prior to the measurements, the samples were degassed at 250 ºC for 4 h. Apparent surface area has been determined by BET method and total micropore volume has been assessed by applying Dubinin-Radushkevich equation to the N_2-adsorption isotherms. The surface composition and oxidation states of the elements of the prepared materials were studied using XPS in a VG-Microtech Multilab 3000 spectrometer with an Al Kα radiation source (1253.6 eV). The deconvolution of the N1s XPS spectra was done by least squares fitting using Gaussian-Lorentzian curves, while a Shirley line was used for the background determination.

The analysis of the electrocatalytic activity of the materials towards ORR was performed in an Autolab PGSTAT302 (Metrohm, Netherlands) bipotentiostat. A rotating ring-disk electrode (RRDE, Pine Research Instruments, USA) equipped with a glassy carbon disk electrode (5.61 mm diameter) was used as the working electrode and the current of the attached platinum ring electrode was registered, graphite was used as the counter electrode and a reversible hydrogen electrode (RHE) immersed in the working

electrolyte through a Luggin as the reference electrode, and all the potentials are referred to this electrode. The glassy carbon disk electrode was modified with the samples using 120 µl of a 1 mg·ml^{-1} dispersion of each carbon material (20% isopropanol, 0.02% Nafion®), obtaining a catalyst loading of 0.48 mg cm^{-2}.

The electrocatalytic activity towards ORR was studied by linear sweep voltammetry (LSV) in O_2 saturated 0.1 M KOH and 0.1 M H_2SO_4 solutions between 1.0 and 0.0 V at different rotation rates, from 400 to 2025 rpm and at a scan rate of 5 mV s^{-1}. The potential of the platinum ring electrode was held constant at 1.5 V during all measurements. The electron transfer number was calculated from the hydrogen peroxide oxidation in the Pt ring electrode as follows:

$$n = \frac{4I_d}{I_d + I_r/N}$$

Where I_r and I_d are the current measured at the ring electrode and the disk electrode, respectively, and N is the collection efficiency of the ring, which was experimentally determined to be 0.37.

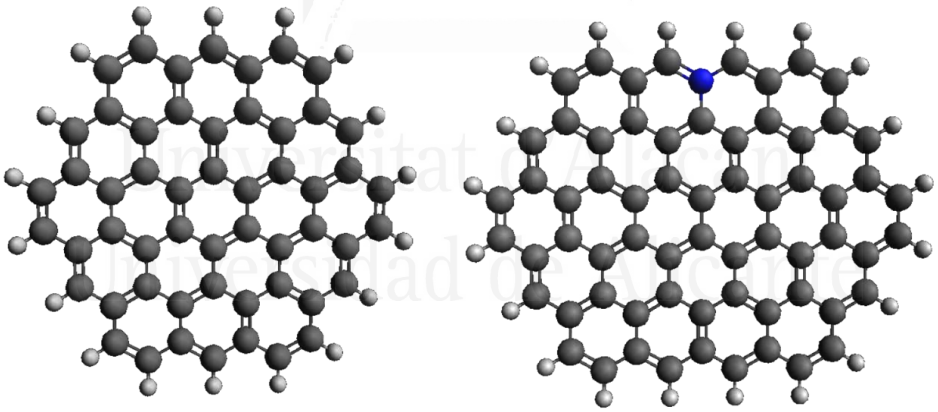

Figure 7.1. Model structure of non-doped (left) and N-doped (right) carbon flakes. White represents hydrogen, grey represents carbon and blue represents nitrogen, respectively.

7.2.5 Computational Modelling

Density functional theory (DFT) at the M06-2X/6-31G(d) level was used in this study through Gaussian 09 software, using restricted and unrestricted

Hamiltonians for closed-shell (S=0) and open-shell (S=1/2) systems, respectively. The change in energies for each transformation was computed as the Free energy differences of optimized geometries and are reported in eV for electrochemical reactions (1 Hartree = 27.2116 eV).

The energy diagrams of ORR have been calculated based on the computational hydrogen electrode model potential, proposed by Norskov et al. [19]. The free energy change for each oxygen reduction stage is defined as $\Delta G = \Delta E' - T \cdot \Delta S + \Delta G_U$, where $\Delta E'$ is the reaction energy, ΔS is the variation in entropy and ΔG_U is the change in free energy associated to the electrode potential. T represents the temperature, which was fixed at 298 K. $\Delta G_U = n \cdot e \cdot U$, where U is the electrode potential and n is the number of electrons transferred in each reduction step. The model structures used consist of finite graphene carbon monolayers (or flakes) with 72 and 86 atoms for the non-doped carbon flake and N-doped carbon flake, respectively. Figure 7.1 displays the model structures. The number of unpaired electrons has been considered in the models as follows; the non-doped carbon and N-doped carbon configurations were computed as a singlet, closed-shell states for all cases. After the introduction of the electron-proton pairs, a doublet multiplicity was used in the first and third reductions and a singlet state in the second and fourth reduction stages. The oxygen molecule ground state was computed as a triplet.

7.3 Results and Discussion

The non-doped carbon material was a commercial carbon black while the N-doped carbon material was prepared from double-stage heat treatment of polyaniline which enables the selective formation of quaternary nitrogen species [18]. The double heat treatment of polyaniline was performed, first, under oxygen-containing atmosphere to developed porosity in the resultant carbon material and, secondly, under inert atmosphere at 1200ºC to tailor the nitrogen functionalities. The resultant N-doped carbon material was characterized in detail via TEM, N_2-adsorption isotherms at -196ºC, Raman spectroscopy and XPS.

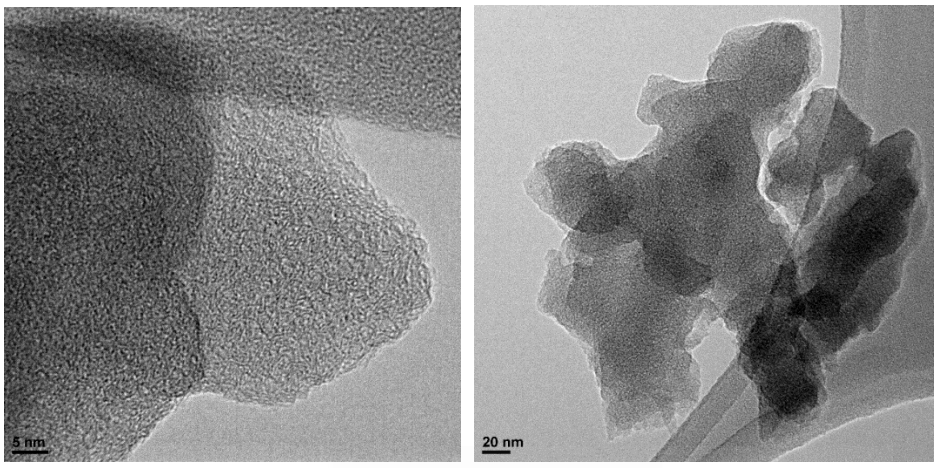

Figure 7.2: TEM images of N-doped carbon material obtained from double heat treatment of PANI.

TEM images (Figure 7.2) displays the laminar morphology of N-doped carbon material, typical of PANI-derived carbon materials [13]. The N_2-adsorption isotherm (Figure 7.3) shows that the material has both high surface area of 1400 $m^2 \cdot g^{-1}$ and a micropore volume of 0.51 $cm^3 \cdot g^{-1}$. This N_2-adsorption profile is characteristic of carbon materials with highly developed microporosity [20]. Raman spectra (Figure 7.4) contains the characteristic D (at around 1350 cm^{-1}) and G (at around 1600 cm^{-1}) bands of sp^2 based carbon materials and shows that the material contains an important contribution of defects. The ratio between I_D and I_G bands was found to be close to 1.0.

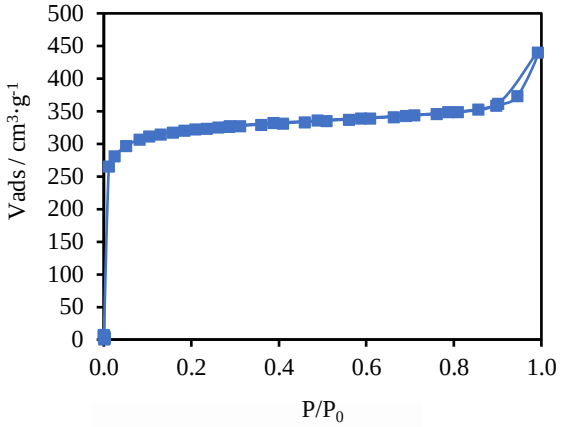

Figure 7.3: N_2-adsorption isotherm of N-doped carbon material obtained from double stage heat treatment of PANI.

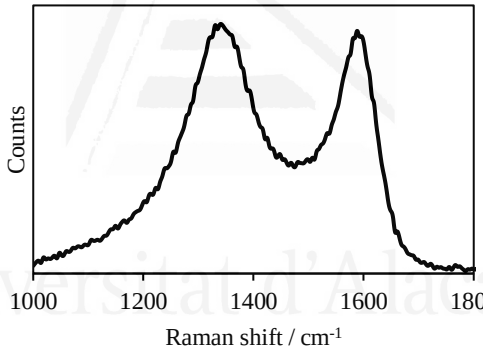

Figure 7.4: Raman spectra of N-doped carbon material obtained from double stage heat treatment of PANI.

Furthermore, Figure 7.5 shows the N1s spectra of the N-doped carbon material, in which only the presence of quaternary-type nitrogen species is appreciable. This quaternary functionalities are obtained from a transformation of pyridines and pyridone species into edge-type quaternary nitrogen due to the high temperature used during the second heat treatment [18,21]. More details of the extended characterization of this N-doped carbon material can be found in Chapter V. This N1s spectra is relevant since edge-type quaternary nitrogen species have been connected to the high catalytic performance of many carbon-based catalysts in alkaline electrolyte [18,22–24]. The obtention of only one

nitrogen species in the carbon matrix allows us to evaluate the effect of one nitrogen functional group from experimental and computational modelling points of view.

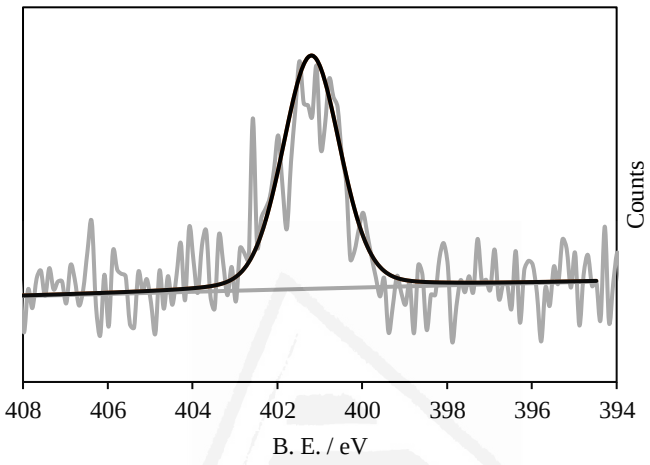

Figure 7.5: N1s spectra of N-doped carbon material obtained from double stage heat treatment of PANI. Only one peak is observed: quaternary-type nitrogen species at 401.2 eV.

According to this, non-doped commercial carbon material and the selectively N-doped carbon material, obtained from double heat treatment, were tested as electrocatalysts towards oxygen reduction reaction. The electrochemical experiments were run in two conditions: a 0.1 M KOH solution and 0.1 M H_2SO_4 solution. Figures 7.6-7.9 display the LSV curves at rotation rates from 400 to 2025 rpm for both materials in alkaline and acidic electrolyte.

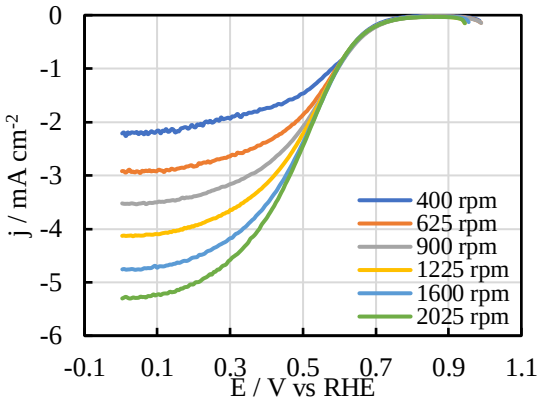

Figure 7.6: LSV curves of N-doped carbon material obtained from double stage heat treatment of PANI in 0.1M H_2SO_4 solution at different rotation rates (from 400 to 2025 rpm). Scan rate: 5 $mV \cdot s^{-1}$.

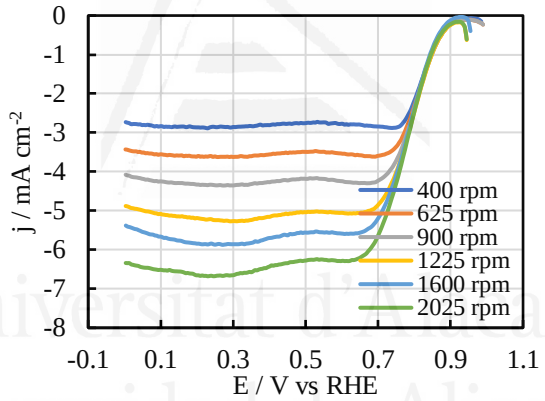

Figure 7.7: LSV curves of N-doped carbon material obtained from double stage heat treatment of PANI in 0.1 M KOH solution at different rotation rates (from 400 to 2025 rpm). Scan rate: 5 $mV \cdot s^{-1}$.

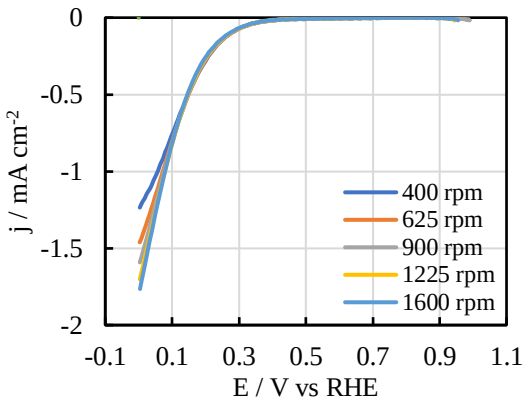

Figure 7.8: LSV curves of non-doped carbon material, Vulcan XC-72F, in 0.1 M H_2SO_4 solution at different rotation rates: from 400 to 2025 rpm. Scan rate: 5 $mV \cdot s^{-1}$.

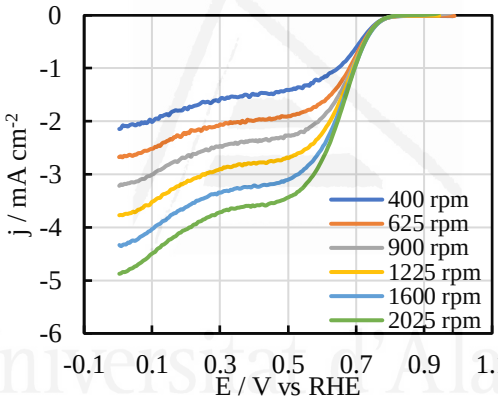

Figure 7.9: LSV curves of non-doped carbon material, XC-72F Vulcan, in 0.1 M KOH solution at different rotation rates (from 400 to 2025 rpm). Scan rate: 5 $mV \cdot s^{-1}$.

As a summary Figure 7.10 includes the LSV curves for all materials in acidic and alkaline medium at a rotation rate of 1600 rpm for comparison purposes. Concerning the non-doped carbon material, the catalytic activity of this material shows an onset potential (E_{ONSET}) of 0.80 V vs RHE and high selectivity towards H_2O_2 formation (number of transferred electrons close to 2) in alkaline solution. On the other hand, the same material in acidic solution shows a significant decrease in the catalytic activity, with an E_{ONSET} close to 0.3 V vs RHE. Regarding the selectivity in acidic medium, 4 electrons pathway seems to be the preferred route. Therefore, the non-doped carbon material seems to reduce oxygen more easily in an alkaline solution with high selectivity

towards hydrogen peroxide formation. However, water production predominates under acidic conditions although with higher overpotential.

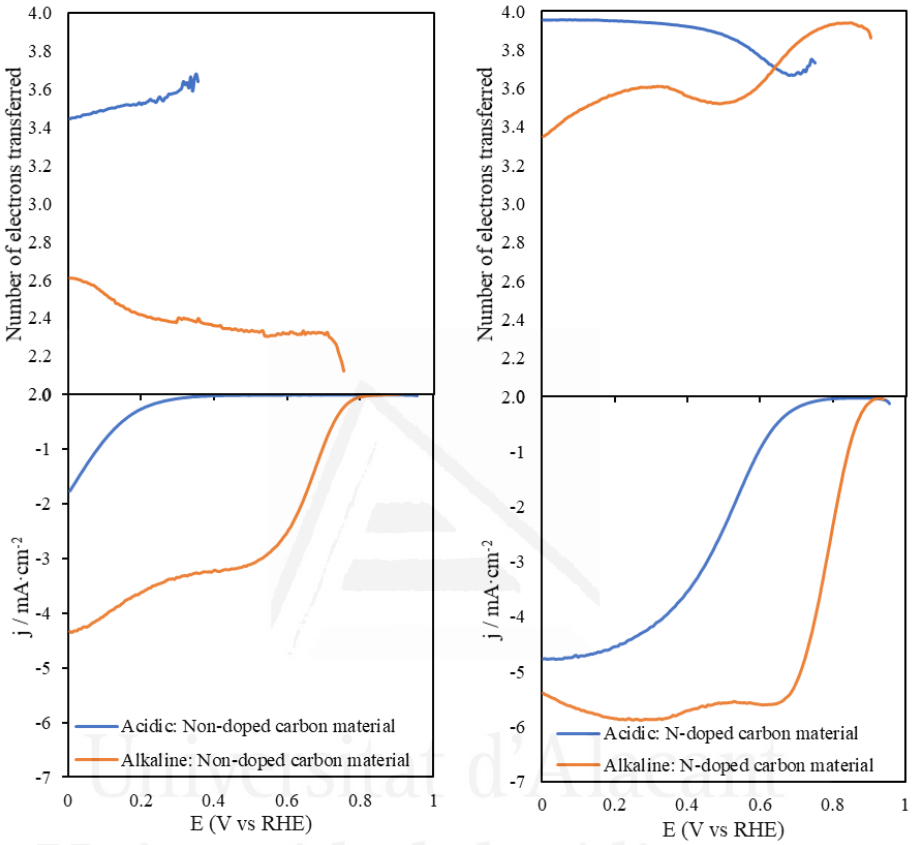

Figure 7.10: Number of electrons transferred and LSV curves for the non-doped carbon material and the N-doped carbon material in O_2-saturated 0.1 M H_2SO_4 and 0.1 M KOH solutions at 5 $mV \cdot s^{-1}$ and 1600 rpm.

Figure 7.10 also includes the LSV curves of the selectively N-doped carbon material in the same conditions. In alkaline conditions, N-doped carbon material shows high catalytic activity with higher E_{ONSET} potential, approaching platinum-like performance. Moreover, one of the most interesting properties of the N-doped catalyst is its high selectivity towards water formation. However, both limiting current density and onset potential suffer an important decrease in an acidic solution. Unfortunately, this decrease is too high, making these materials unsuitable to replace commercial platinum catalysts in acidic

conditions. Regarding the selectivity, in contrast to the non-doped material, the N-doped carbon material shows a similar number of electrons transferred regardless of the electrolyte used during the electrochemical reaction.

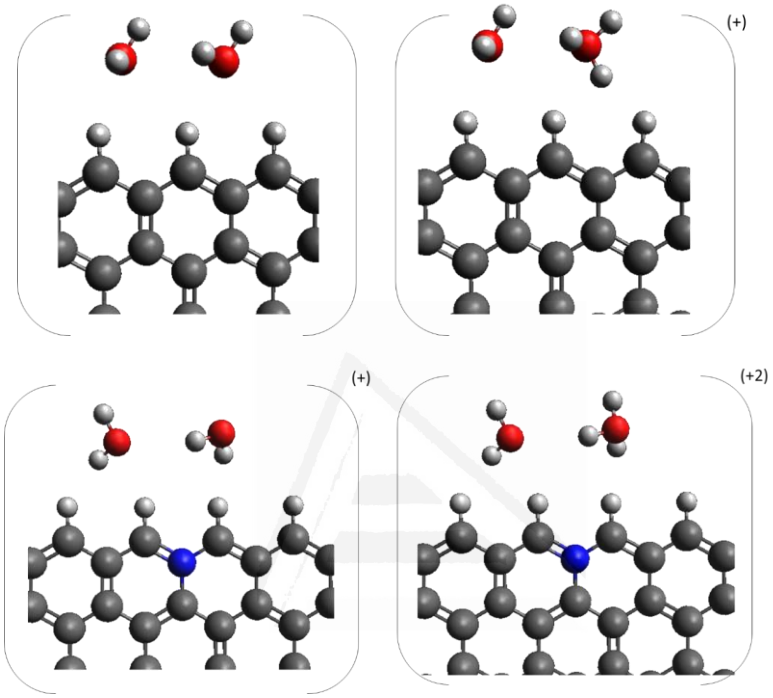

Figure 7.11: Illustration and net charges of the non-doped (up) and N-doped (down) carbon flakes in alkaline (left) and acidic (right) conditions. White represents hydrogen, grey represents carbon, blue represents nitrogen and red represents oxygen.

In order to get further insights about the different behaviour of non-doped and N-doped carbon materials, computational modelling, based on DFT, was performed. A non-doped graphene flake was selected as a model to analyse the behaviour of non-doped carbon materials as electrocatalysts for ORR. On the other hand, one nitrogen atom was introduced into the graphene flake in edge-type graphitic position representing the same edge-type graphitic nitrogen experimentally obtained in the selectively N-doped carbon material (see Figure 7.1). Therefore, the comparison between experimental ORR performance and computational modelling is possible The position of the N atom was based on the results of Chapter V. Computations were performed with the M06-2X functional with the 6-31g(d) basis set embedded in a water continuum with a

continuous polarization model as the inclusion of the environment is fundamental for the quantitative simulation of ORR. This model was augmented by two explicit water molecules which can form explicit hydrogen bonds, as recent studies demonstrate the necessity of including explicit water molecules to provide satisfactory energies in carbon-based catalysts for ORR [23,24]. The acidic environment and the role of protons in ORR carbon-based catalysts was studied by substituting one water molecule by a hydronium (H_3O^+) cation (Figure 7.11).

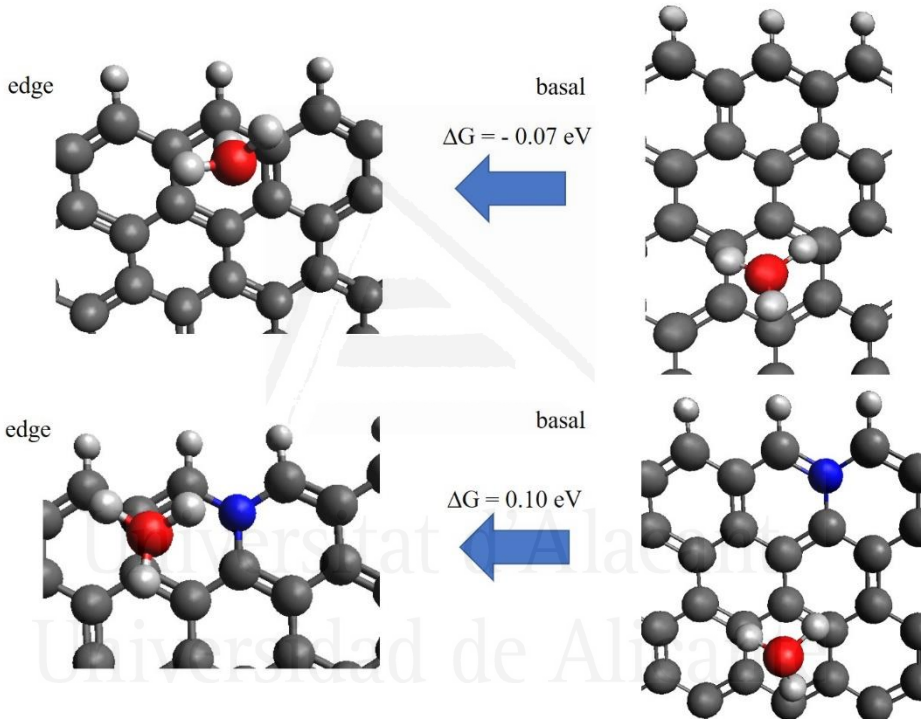

Figure 7.12: Free Energy differences and rendering of the H_3O^+ position in the non-doped (up) and N-doped (down) carbon flakes. White represents hydrogen, grey represents carbon, blue represents nitrogen and red represents oxygen.

The geometric optimization of the non-doped carbon material with H_3O^+ reveals that the cation binds to the carbon flake (Figure 7.12), probably because of the accumulation of the negative partial charges in the edges of the carbon material [25], which can attract protons to their neighbourhoods. This means that active sites are surrounded by a protonic environment. Interestingly, this effect is minimized if the simulation is applied over the N-doped carbon flake.

The heteroatom is charged positively and, consequently, a lower local concentration of protons in the vicinity of this nitrogen functionality is expected. In fact, in our calculations, H_3O^+ molecules are moved away from the active sites up to a minimum distance of 3.68 Å (Figure 7.13). These observations indicate that the acidic pH should have a lower effect in the catalysis of a carbon material doped with this nitrogen functional group.

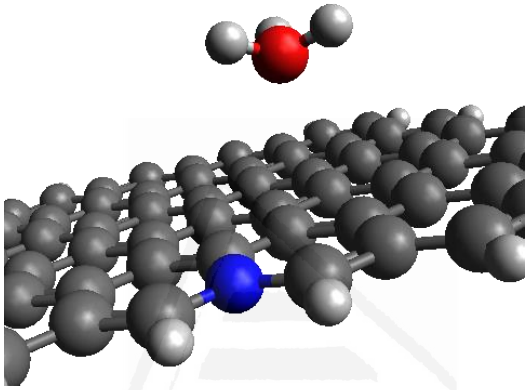

Figure 7.13: Optimized geometry of the H_3O^+ ion at a non-contact distance of 3.68 Å of the nitrogen heteroatom as a result of the repulsion charges. White represents hydrogen, grey represents carbon, blue represents nitrogen and red represents oxygen.

Figure 7.14 shows the self-consistent field (SCF) free energies of the most stable configuration for all ORR stages: reactants, oxygen chemisorption, oxygen reduction stages and products formation for both electrolytes and carbon materials.

Oxygen chemisorption is the first stage of this reaction that can occur through different configurations; terminal or bridging binding modes [26]. In the non-doped carbon flake, oxygen molecules are chemisorbed on terminal positions in both environments. However, the acidic conditions strongly favour the formation of C-O-O due to the protonation of the terminal oxygen atom from the reaction with H_3O^+, resulting in a C-O-O-H^+ configuration (Figure 7.15). Then, regardless of the electrolyte, the first reduction stage in the non-doped carbon flake leads to the C-O-O-H intermediate.

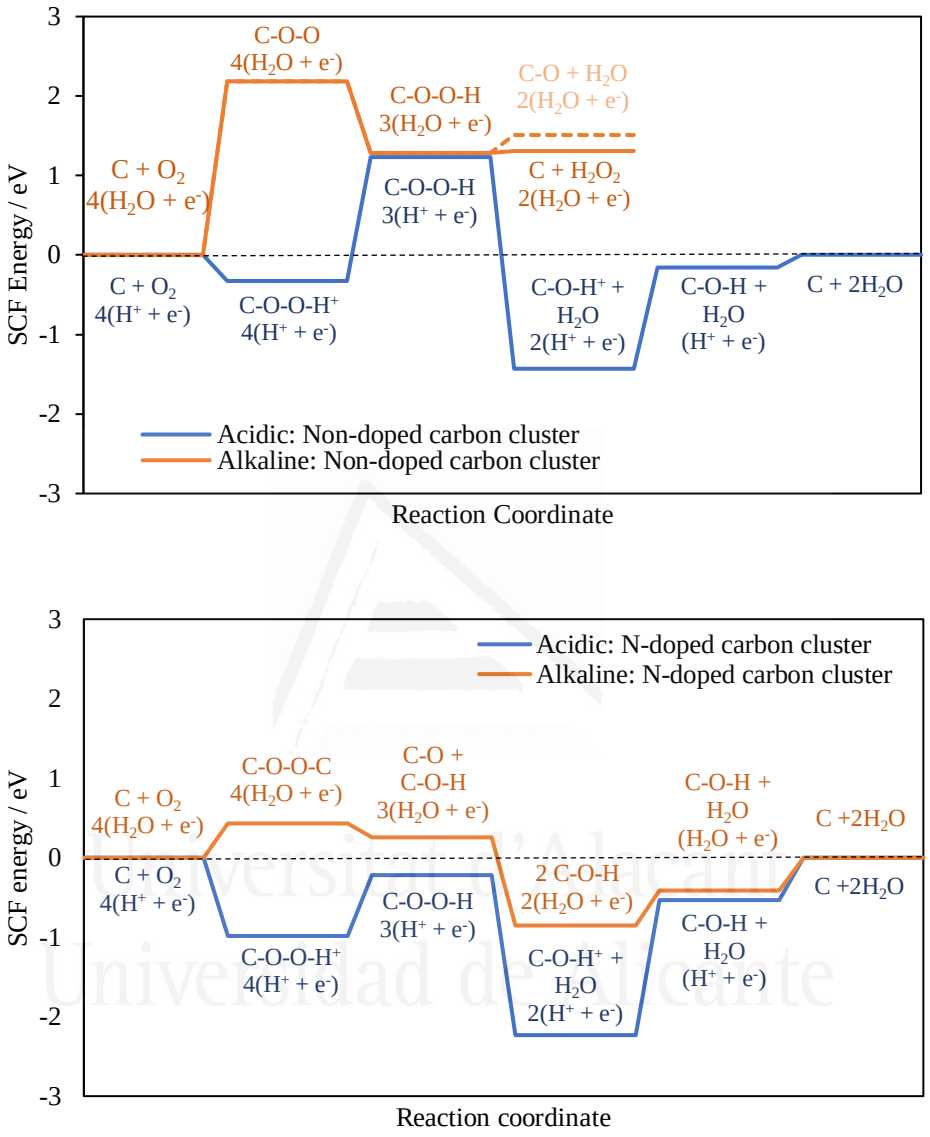

Figure 7.14: SCF Free energy diagram for the ORR of non-doped (up) and N-doped (down) carbon flakes in alkaline (orange) and acidic (blue) environments, calculated for 1.23 V NHE.

The key stage is the second reduction step, which can lead to the cleavage of the bond between both oxygen atoms (resulting in the formation of one water

molecule and a C-O intermediate) or the cleavage of the carbon and oxygen bond (which results in the formation of hydrogen peroxide). In acidic electrolyte, the most stable configuration is the formation of one water molecule and the C-O intermediate (Figure 7.16). This occurs because, in acidic conditions, the presence of protons (H_3O^+) strongly stabilize the C-O intermediate via protonation (C-O-$H^+\cdots OH_2$). In contrast, the lack of protons in alkaline environment makes the formation of a C-O intermediate more unfavourable since such stabilization is lower with water molecules. Nevertheless, both mechanisms (formation of C-O intermediate or hydrogen peroxide) are similar in thermodynamic terms for alkaline environments (see dotted line in Figure 7.14).

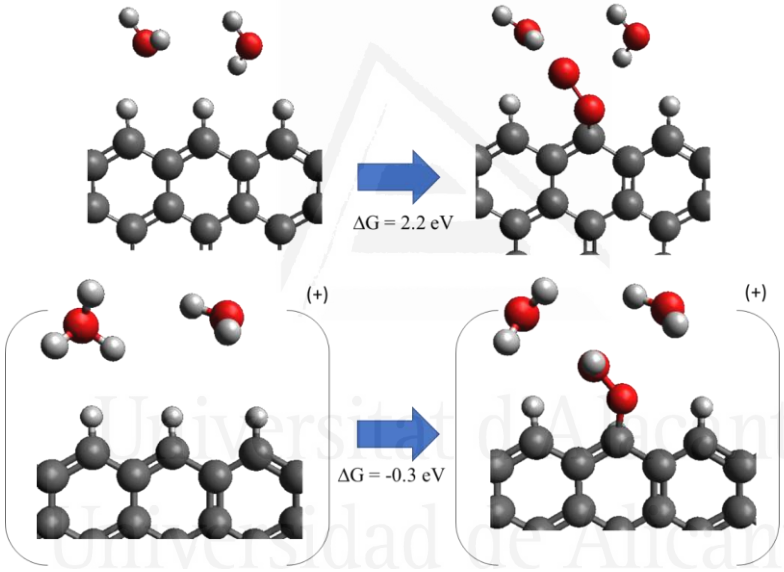

Figure 7.15: Illustration and Free Energies of the oxygen chemisorption stage by using non-doped carbon flakes as electrocatalyst under alkaline (up) and acidic (down) environment. White represents hydrogen, grey represents carbon, blue represents nitrogen and red represents oxygen.

Therefore, in order to deepen into this process, Potential Energy Surface (PES) scans were carried out during the desorption of both products (OOH^- and OH^-) in alkaline medium. For this study (Figure 7.17), the non-doped carbon flake was negatively charged with the aim of simulating the electron supply. Taking this into account, the desorption of OOH^- was found to be energetically more favoured than the desorption of OH^- anions and, consequently, the 2

electrons pathway seems to be the preferred pathway for non-doped carbon materials in alkaline medium, which is consistent with the experimental results. ORR mechanisms in acidic and alkaline medium for non-doped carbon materials are summarized and schematized in Figures 7.18 and 7.19, respectively.

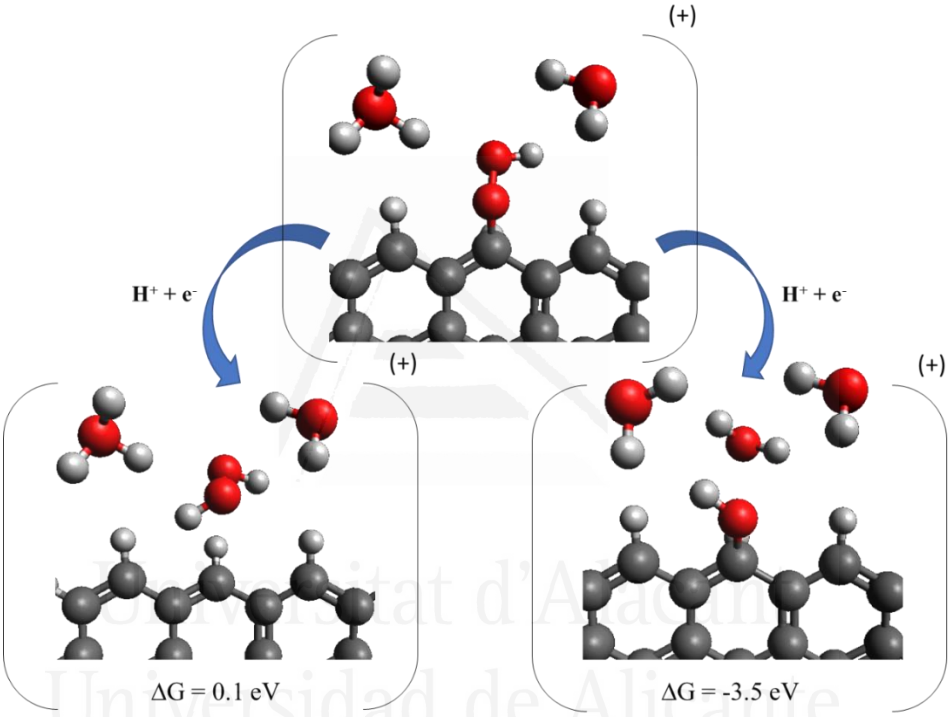

Figure 7.16: Illustration and SCF Free energies of the two possible pathways in the second reduction stage by using the carbon flake as electrocatalysts in acidic environment. Carbon in grey, oxygen in red and hydrogen in white.

The protonic environment does not only have a direct impact in the selectivity, but also plays a fundamental role in the catalytic activity. The protonation of some ORR intermediates under acidic conditions leads to a very strong stabilization, which provokes that the required energy to continue with the reaction is considerably higher in a protonic environment than in alkaline conditions.

The same computational modelling was performed for the N-doped carbon flake containing one edge-type quaternary nitrogen. In this case, the oxygen chemisorption mode is strongly dependent on pH. In an acidic environment, the terminal binding mode is the only stable configuration in thermodynamic terms. This is again due to the strong interaction between the terminal oxygen from the C-O-O and the H_3O^+ ion of the solution, in agreement with what was observed in the non-doped carbon catalysts. The following steps of the reaction are similar to those for the non-doped carbon materials in acidic conditions, where the protonic stabilization of the second ORR intermediate (C-O-H^+) leads to a 4 electrons pathway and the consequent water formation.

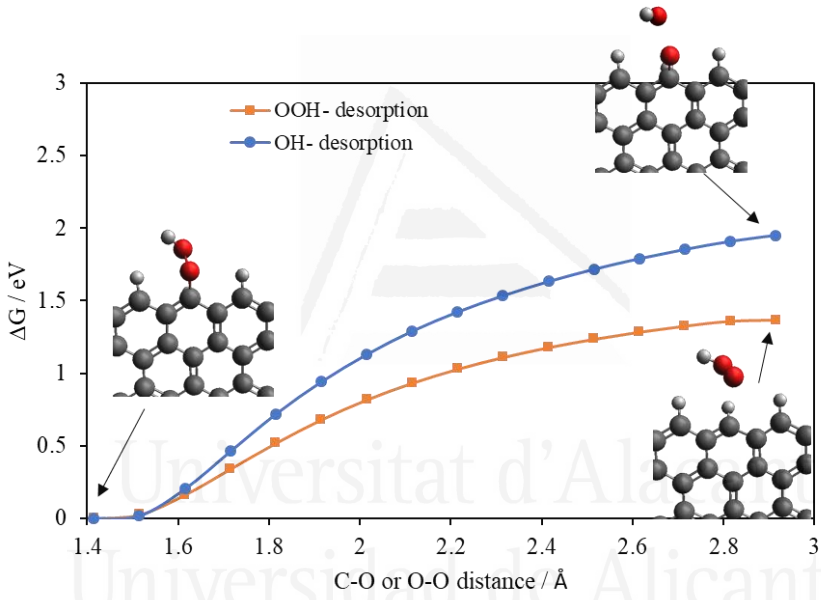

Figure 7.17: Potential Energy Surface (PES) scan of the desorption of OOH^- (orange) and OH^- (blue) of the second oxygen reduction stage in which the OOH^- desorption involves the future H_2O_2 formation and OH^- desorption leads to the formation of one water molecule and C-O as a reaction intermediate.

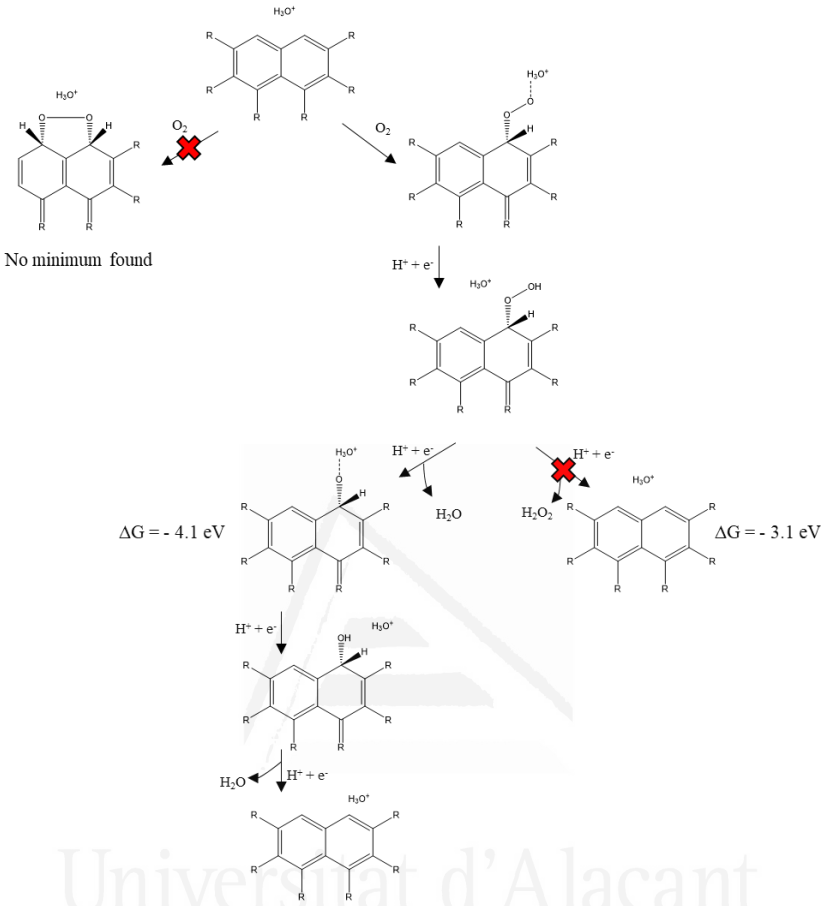

Figure 7.18: Schematic representation of the most stable ORR mechanism for a carbon flake in an acidic environment in which the least thermodynamic routes have been discarded.

ORR mechanism for edge-type graphitic nitrogen in alkaline conditions has been extensively studied in the literature [18,20,22,27–29]. Interestingly, this nitrogen functionality chemisorbs oxygen molecules in a bridging binding mode (C-O-O-C) in the absence of protons. The preference for this species in the oxygen molecule chemisorption modifies the ORR mechanism compared to the non-doped carbon material in alkaline conditions. Thus, the subsequent reduction stage leads to the cleavage of the O-O bond and, finally, to the formation of two water molecules. Figures 7.20 and 7.21 display the ORR mechanism for N-doped carbon materials in both electrolytes.

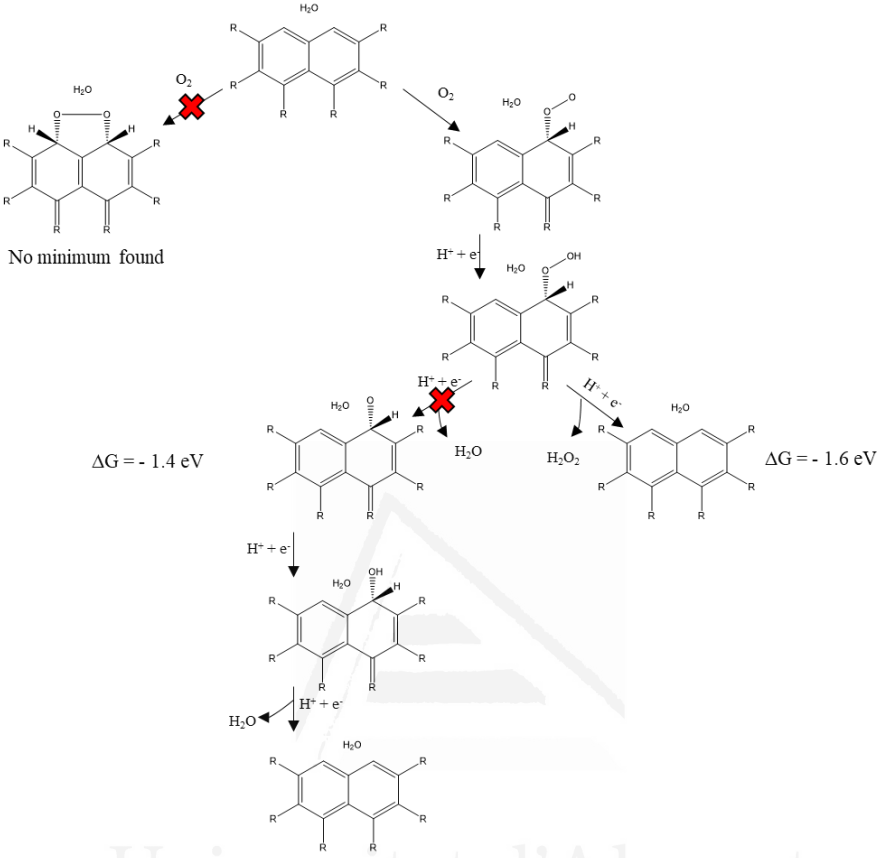

Figure 7.19: Schematic representation of the most stable ORR mechanism for a graphene flake in an alkaline environment in which the least thermodynamic routes have been discarded

Thus, regardless of the electrolyte for N-doped carbon flakes, the mechanism is always governed by a 4 electrons pathway, which is in excellent agreement with the experimental results. However, similar to non-doped carbon material, the differences in activity are related to the high stabilization that H_3O^+ ions produce over the intermediate species in acidic medium.

Sabatier´s principle [30] provides the idea that the best catalysts should not bind atoms or molecules too weakly in order to be able to activate them, but neither should bind them too strongly, to allow the reaction to proceed until the desorption of the products. Interestingly, this principle can be extrapolated to the oxygen reduction reaction in these metal-free carbon-based catalysts. In

acidic environments, the protonic stabilization in some steps of the ORR induces a too strong binding of the intermediates to the catalytic site, which hampers the completion of the reaction, whereas the lack of protons in alkaline conditions enables an easier termination of the reaction.

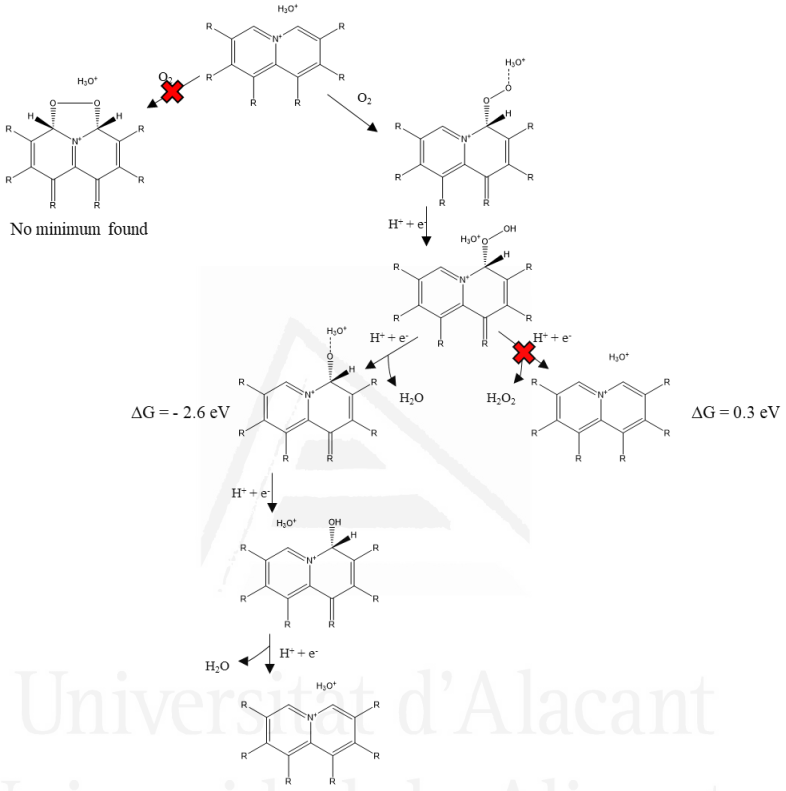

Figure 7.20: Schematic representation of the most stable ORR mechanism for a N-doped carbon flake in an acidic environment in which the least thermodynamic routes have been discarded.

7.4 Conclusions

In summary, experimental and computational approaches agree on the fact that under the presence of a protonic environment, metal-free carbon-based catalysts suffer an impoverishment in their activity because of the strong stabilization of some ORR intermediates. Due to such stabilization, the following ORR steps require high energy to occur. Furthermore, the protonic environment does not only modify the catalytic activity of these materials but

also changes the mechanism by which ORR takes place. On the one hand, in acidic solution, 4 electrons pathway is the preferred route regardless of whether carbon material is doped with nitrogen or not. On the other hand, in alkaline conditions, ORR for non-doped carbon materials occurs through a 2 electrons pathway, whereas for N-doped carbon materials the preferred reaction mechanism is the 4 electrons pathway. The understanding of the reasons why metal-free carbon-based catalysts show poorer catalytic activity in a protonic environment should be the guiding principle for the future design of advanced carbon materials with highly efficient catalysis in acidic conditions.

Figure 7.21: Schematic representation of the most stable ORR mechanism for a N-doped carbon flake in an alkaline environment in which the least thermodynamic routes have been discarded.

7.5 References

[1] Y. Nie, L. Li, Z. Wei, Recent advancements in Pt and Pt-free catalysts for oxygen reduction reaction, Chem. Soc. Rev. 44 (2015) 2168–2201.

[2] I.E.L. Stephens, A.S. Bondarenko, U. Grønbjerg, J. Rossmeisl, I. Chorkendorff, Understanding the electrocatalysis of oxygen reduction on platinum and its alloys, Energy Environ. Sci. 5 (2012) 6744–6762.

[3] Y. Jiao, Y. Zheng, M. Jaroniec, S.Z. Qiao, Design of electrocatalysts for oxygen- and hydrogen-involving energy conversion reactions, Chem. Soc. Rev. 44 (2015) 2060–2086.

[4] L. Dai, Y. Xue, L. Qu, H.-J. Choi, J.-B. Baek, Metal-Free Catalysts for Oxygen Reduction Reaction, Chem. Rev. 115 (2015) 4823–4892.

[5] M. Klingele, C. Van Pham, A. Fischer, S. Thiele, A Review on Metal-Free Doped Carbon Materials Used as Oxygen Reduction Catalysts in Solid Electrolyte Proton Exchange Fuel Cells, Fuel Cells. 16 (2016) 522–529.

[6] J. Quílez-Bermejo, E. Morallón, D. Cazorla-Amorós, Metal-Free Heteroatom-doped Carbon-based catalysts for ORR. A critical assessment about the role of heteroatoms, Carbon 165 (2020) 434–454.

[7] N. Ramaswamy, S. Mukerjee, Alkaline Anion-Exchange Membrane Fuel Cells: Challenges in Electrocatalysis and Interfacial Charge Transfer, Chem. Rev. 119 (2019) 11945–11979.

[8] Z.F. Pan, L. An, T.S. Zhao, Z.K. Tang, Advances and challenges in alkaline anion exchange membrane fuel cells, Prog. Energy Combust. Sci. 66 (2018) 141–175.

[9] Z. Sun, B. Lin, F. Yan, Anion-Exchange Membranes for Alkaline Fuel-Cell Applications: The Effects of Cations, ChemSusChem. 11 (2018) 58–70.

[10] B.W. Noffke, Q. Li, K. Raghavachari, L. Li, A Model for the pH-Dependent Selectivity of the Oxygen Reduction Reaction Electrocatalyzed by N-Doped Graphitic Carbon, J. Am. Chem. Soc. 138 (2016) 13923–13929.

[11] X. Zhang, D. Yu, Y. Zhang, W. Guo, X. Ma, X. He, Nitrogen- and sulfur-doped carbon nanoplatelets via thermal annealing of alkaline lignin with urea as efficient electrocatalysts for oxygen reduction reaction, RSC Adv. 6 (2016) 104183–104192.

[12] J. Nong, M. Zhu, K. He, A. Zhu, P. Xie, M. Rong, M. Zhang, N/S co-doped 3D carbon framework prepared by a facile morphology-controlled solid-state pyrolysis method for oxygen reduction reaction in both acidic and alkaline media, J. Energy Chem. 34 (2019) 220–226.

[13] J. Quílez-Bermejo, C. González-Gaitán, E. Morallón, D. Cazorla-Amorós, Effect of carbonization conditions of polyaniline on its catalytic activity towards ORR. Some insights about the nature of the active sites, Carbon 119 (2017) 62–71.

[14] K. Wan, Z.P. Yu, X.H. Li, M.Y. Liu, G. Yang, J.H. Piao, Z.X. Liang, pH Effect on Electrochemistry of Nitrogen-Doped Carbon Catalyst for Oxygen Reduction Reaction, ACS Catal. 5 (2015) 4325–4332.

[15] J.A. Behan, A. Iannaci, C. Domínguez, S.N. Stamatin, K. Hoque, J.M. Vasconcelos, T.S. Perova, P.E. Colavita, Electrocatalysis of N-doped carbons in the oxygen reduction reaction as a function of pH: N-sites and scaffold effects, Carbon 148 (2019) 224–230.

[16] K. Wan, Z.-P. Yu, X.-H. Li, M.-Y. Liu, G. Yang, J.H. Piao, Z.X. Liang, pH Effect on Electrochemistry of Nitrogen-Doped Carbon Catalysts for Oxygen Reduction Reaction, ACS Catal. 5 (2015) 4325–4332.

[17] J. Quílez-Bermejo, A. Ghisolfi, D. Grau-Marín, E. San-Fabián, E. Morallón, D. Cazorla-Amorós, Post-synthetic efficient functionalization of polyaniline with phosphorus-containing groups. Effect of phosphorus on electrochemical properties, Eur. Polym. J. 119 (2019) 272–280.

[18] J. Quílez-Bermejo, M. Melle-Franco, E. San-Fabián, E. Morallón, D. Cazorla-Amorós, Towards understanding the active sites for the ORR in N-doped carbon materials through fine-tuning of nitrogen functionalities: an experimental and computational approach, J. Mater. Chem. A. 7 (2019) 24239–24250.

[19] J.K. Nørskov, J. Rossmeisl, A. Logadottir, L. Lindqvist, J.R. Kitchin, T. Bligaard, H. Jónsson, Origin of the overpotential for oxygen reduction at a fuel-cell cathode, J. Phys. Chem. B. 108 (2004) 17886–17892.

[20] M. Thommes, K. Kaneko, A. V Neimark, J.P. Olivier, F. Rodriguez-reinoso, J. Rouquerol, K.S.W. Sing, Physisorption of gases , with special reference to the evaluation of surface area and pore size distribution (IUPAC Technical Report), Pure Appl. Chem. 7 (2015) 1051-1069.

[21] T. Sharifi, G. Hu, X. Jia, T. Wågberg, Formation of active sites for oxygen reduction reactions by transformation of nitrogen functionalities in nitrogen-doped carbon nanotubes, ACS Nano. 6 (2012) 8904–8912.

[22] J. Quílez-Bermejo, E. Morallón, D. Cazorla-Amorós, Oxygen-reduction catalysis of N-doped carbons prepared: Via heat treatment of polyaniline at over 1100°C, Chem. Commun. 54 (2018) 4441–4444.

[23] T. Sharifi, G. Hu, X. Jia, T. Wågberg, Formation of Active Sites for Oxygen Reduction Reactions by Transformation of Nitrogen Functionalities in Nitrogen-Doped Carbon Nanotubes, ACS Nano. 6 (2012) 8904–8912.

[24] T. Ikeda, M. Boero, S.F. Huang, K. Terakura, M. Oshima, J. Ozaki, Carbon

alloy catalysts: Active sites for oxygen reduction reaction, J. Phys. Chem. C. 112 (2008) 14706–14709.

[25] M. Reda, H.A. Hansen, T. Vegge, DFT study of stabilization effects on N-doped graphene for ORR catalysis, Catal. Today. 312 (2018) 118–125.

[26] L. Yu, X. Pan, X. Cao, P. Hu, X. Bao, Oxygen reduction reaction mechanism on nitrogen-doped graphene: A density functional theory study, J. Catal. 282 (2011) 183–190.

[27] E. Louis, E. San-Fabián, G. Chiappe, J.A. Verges, Electron enrichment of zigzag edges of armchair-oriented graphene nano-ribbons increases their stability and induces pinning of Fermi level, Carbon 154 (2019) 211–218.

[28] K.H. Wu, D.W. Wang, D.S. Su, I.R. Gentle, A Discussion on the Activity Origin in Metal-Free Nitrogen-Doped Carbons for Oxygen Reduction Reaction and their Mechanisms, ChemSusChem. 8 (2015) 2772–2788.

[29] X. Hou, Q. Hu, P. Zhang, J. Mi, Oxygen reduction reaction on nitrogen-doped graphene nanoribbons: A density functional theory study, Chem. Phys. Lett. 663 (2016) 123–127.

[30] X. Bao, X. Nie, D. Von Deak, E.J. Biddinger, W. Luo, A. Asthagiri, U.S. Ozkan, C.M. Hadad, A first-principles study of the role of quaternary-N doping on the oxygen reduction reaction activity and selectivity of graphene edge sites, Top. Catal. 56 (2013) 1623–1633.

[31] G.L. Chai, Z. Hou, D.J. Shu, T. Ikeda, K. Terakura, Active sites and mechanisms for oxygen reduction reaction on nitrogen-doped carbon alloy catalysts: Stone-wales defect and curvature effect, J. Am. Chem. Soc. 136 (2014) 13629–13640.

[32] M. Che, Nobel Prize in chemistry 1912 to Sabatier : Organic chemistry or catalysis? Catal. Today. 218–219 (2013) 162–171.

CHAPTER VIII

POST-SYNTHETIC EFFICIENT FUNCTIONALIZATION OF POLYANILINE WITH PHOSPHORUS-CONTAINING GROUPS. EFFECT OF PHOSPHORUS ON ELECTROCHEMICAL PROPERTIES

8.1 Introduction

Over the past decades, the synthesis of new nanostructured functional materials with useful properties has garnered great attention in the scientific community. In particular, conducting polymers (CPs) have generated great interest from a fundamental and applied research points of view because of their promising electrical, electrochemical, optical and biocompatibility properties [1,2]. Polyaniline (PANI) was discovered in 1977 and, among CP, it is one of the most studied due to its high electrical conductivity, environmental and thermal stability and low-cost synthesis [1–3] that makes PANI a useful material in many different applications like biological sensing [4,5], corrosion protection [6,7], charge storage [8], catalysis [9–12], organic light emitting diodes [12] and as a precursor of N-doped carbon materials [13–15], among others.

One of the most investigated applications of PANI is as catalyst of different reactions, such as synthesis of 2-substituted benzothiazoles [9], 2-substituted benzimidazoles [10,11] and bio-esters transesterification and esterification reactions [12]. Indeed, polyaniline was also used in electrocatalytic reactions such as hexavalent chromium reduction [16] or CO_2 reduction [17].

An interesting feature of most CPs is that their properties can be tailored by derivatization of the pristine polymer or of the parent monomer. In particular, in the case of PANI, the possible modifications may be listed into three groups [1]: (i) homopolymerization of substituted anilines [18,19], (ii) copolymerization of aniline with substituted anilines [20–24] and (iii) functionalization of the final polymer (PANI post-modification) [25,26].

Interestingly, the rational post-modification of PANI is actually one of the most challenging targets of the scientific community and consists in improving the material performance by modifying, through specific chemical reactions, the nature of the pristine polymer and thus its properties [2]. This approach implies a controlled modification of the polymer backbone via chemical reactions on the post-synthesized polymer [2]. In this sense, the most common post-modification of the PANI is the de-doping process of the amine group, aimed to eliminate or replace the counterion resulting from the PANI synthesis, thus triggering different properties [27,28]. It has also been shown that there is a wide range of modifications of polyaniline by nucleophilic or electrophilic reactions through acid-base chemistry, chemical modification by charge transfer groups,

electrochemical modification, photo modification or, even, modification by charge injection [29–32]. All these post-modification of PANI have led to a wide range of applications, for instance; reversible capture of Hg [33] or Li-ion batteries [34].

Another type of post-modifications of polyaniline is the derivatization with different functional groups, such as thiols, amines, boranes, halogens and cyanides [1]. Moreover, some preliminary P-modification polyaniline studies have been carried out. Plesu et al. [7] evaluated the influence of different organic phosphorus acids during the synthesis of PANI in order to improve its solubility in organic solvents. Furthermore, Eftekhari et. al. [35] used phosphoric acid as an electrolyte in the PANI polymerization. Although the polymerization was not successful, they demonstrated that the phosphoric acid promotes the formation of various phosphorus-containing functional groups on the aniline rings. However, to the best of our knowledge, no selective and efficient phosphorus-based chemical post-modification of PANI has been reported yet.

In this context, the objective of this chapter is to propose a novel and efficient route for the post-modification of PANI with phosphorus-containing groups, by selective chemical reactions between polyaniline and different phosphorus precursors, under mild conditions. The resulting functionalized materials have been characterized by X-ray photoelectronic spectroscopy (XPS), transmission electronic microscopy (TEM), cyclic voltammetry (CV), electrochemical impedance spectroscopy (EIS) and evaluated as electrocatalysts towards oxygen reduction reaction (ORR) by rotating ring-disk electrode (RRDE). For this purpose, phosphorus trichloride (PCl_3) and chlorodiphenylphosphine (PPh_2Cl) were used as derivatizing agents. Theoretical calculations based on Density Functional Theory (DFT) were also performed with the aim of understanding the functionalization reactions. The combination of experimental and computational results led to a better understanding of the reactivity of PANI, and of the effects of the introduction of phosphorus-based functional groups on its electrochemical properties.

8.2 Experimental

8.2.1 Materials and reagents

Aniline was purchased from Sigma Aldrich and was distilled under reduced pressure prior to its use, in order to remove the impurities (e.g. aniline oligomers formed by oxidation during the storage). Phosphorus trichloride and chlorodiphenylphosphine were purchased from Sigma Aldrich. Triethylamine (Net_3) was purchased from Fluka. Dichloromethane (CH_2Cl_2) was purchased from Panreac. Ammonium persulfate ($(NH_4)_2(S_2O_8)$), ammonium hydroxide (NH_4OH) and potassium hydroxide (KOH) were purchased from Sigma-Aldrich. Sulfuric acid (98%) was purchased from VWR-Chemicals Prolabo. All the solutions were prepared using ultrapure water (18 MΩ.cm from an Elga Labwater Purelab system). The N_2 (99.999%) and O_2 (99.995%) were provided by Air Liquide and were used without any further purification or treatment.

8.2.2 PANI synthesis

Polyaniline was prepared by chemical polymerization from a solution of 1 M HCl containing 0.067 M of aniline and ammonium persulfate in a stoichiometric ratio. The mixture was kept under stirring (500 rpm) during 3 h at 0 ºC. After 3 h of polymerization, doped polyaniline was treated with 1 M of NH_4OH for 24 h with the aim of obtaining the de-doped polyaniline. The synthesized PANI was washed several times with distilled water and dried at 120 ºC overnight.

8.2.3 PANI modification

Three different post-modification routes have been used. The mildest synthesis of P-modified PANI consisted in the reaction between 1 g of PANI, 1.2 g of PPh_2Cl as derivatizing agent and 5 mL of NEt_3, in 25 mL of CH_2Cl_2, at 25 ºC, during 24 h in an inert atmosphere.

The second route consisted in the use of the same phosphorus precursor, atmosphere and duration but in stronger conditions: without a base, at 120 ºC and solvent free.

Lastly, in order to study the influence of the phosphorus precursor, the last route of PANI post-modification consisted of the use of an excess of PCl_3 that worked as both reactant and solvent at 60 ºC during 24 h in an inert atmosphere.

After each functionalization, the materials were washed with isopropanol several times and dried in an oven at 100 ºC. In the case of PCl_3, the development of some gaseous HCl was observed during the washing step. This was due to the reaction of the P-Cl species with the alcohol that produces the corresponding, most stable, P-OC_3H_7 groups (XPS analysis evidences, see discussion below and Scheme 8.1) with simultaneous formation of HCl.

All post-modifications were carried out three times in order to check the reproducibility of the resultant materials.

Table 8.1 summarizes the different PANI post-modification routes and their nomenclature.

Table 8.1: Nomenclature and conditions of each phosphorus postmodification.

Precursor	Temperature (ºC)	Solvent	Nomenclature
PPh_2Cl	25	CH_2Cl_2	PANI_PPh2Cl_25
PPh_2Cl	120	No	PANI_PPh2Cl_120
PCl_3	60	No	PANI_PCl3

8.2.4 Physicochemical characterization

The samples were characterized by Transmission Electron Microscopy (TEM) coupled to EDX with JEOL JEM-2010 microscope operating at 200 kV with a spatial resolution of 0.24 nm. PANI and PANI samples after post-modification were subjected to thermogravimetric analysis in air atmosphere conditions using a thermobalance (SDT 2960 instrument, TA) in order to check the influence of the phosphorus functional groups in the gasification of the polyaniline, that is, in the reactivity towards oxygen.

The surface composition and oxidation states of the elements of the prepared materials were studied using XPS in a VG-Microtech Multilab 3000 spectrometer with an Al Kα radiation source (1253.6 eV). The deconvolution of the N1s XPS spectra was done by least squares fitting using Gaussian-Lorentzian curves, the full-width at half-maximum (FWHM) was maintained between 1.4 and 1.8 eV, while for P 2p XPS spectra analysis was performed using Gaussian functions with Lorentzian component, considering the two

doublet peaks (P 2p1/2 and P 2p3/2) separated by 0.84 eV, an area ratio of 0.5 and the same FWHM, in all cases, below 1.9 eV. In all cases, a Shirley line was used for the background determination.

8.2.5 Electrochemical measurements

The electrochemical characterization of the materials was performed in an Autolab PGSTAT302 (Metrohm, Netherlands) potentiostat. A rotating ring-disk electrode (RRDE, Pine Research Instruments, USA) equipped with a glassy carbon disk (5.61 mm diameter) and an attached platinum ring was used as the working electrode. The carbon disk was modified with the samples using 120 µL of a 1 $mg \cdot mL^{-1}$ dispersion (0.02% Nafion ® in ethanol) of each polymer, obtaining a catalyst loading of 0.5 $mg \cdot cm^{-2}$. A catalyst loading of 0.1 mg/cm^2 was also used for comparison purposes. The electrochemical behaviour was studied by cyclic voltammetry (CV) in 0.1 M H_2SO_4 between 0.0 and 1.0 V vs RHE. These measurements were performed using graphite as a counter electrode and Ag/AgCl electrode as a reference. Despite it, all potentials are referred to the reversible hydrogen electrode (RHE) in order to make easy the comparison with ORR tests. The samples were also characterized by electrochemical impedance spectroscopy (EIS). Impedance spectra were measured at 0.5 V vs RHE in the frequency range of 10 mHz to 100 kHz with an amplitude for the voltage signal of 10 mV in 0.1 M H_2SO_4 and 0.1 M KOH solutions using Ag/AgCl electrode as a reference. In the same way, all potentials are referred to the reversible hydrogen electrode (RHE).

The study of the electrocatalytic activity towards ORR was also performed in the rotating ring-disk electrode. A graphite rod was used as a counter electrode, while a reversible hydrogen electrode immersed in the working electrolyte was used as a reference. The electrocatalytic activity towards ORR was studied by linear sweep voltammetry (LSV) in an O_2 saturated 0.1 M KOH and 0.1 M H_2SO_4 aqueous solutions, in a potential range comprised between 0.0 and 1.0 V (vs RHE), at different rotation rates, from 400 to 2025 rpm and at a scan rate of 5 $mV \cdot s^{-1}$. The potential of the ring was held constant at 1.5 V (vs. RHE) during all measurements. The number of transferred electrons implied in the reaction was calculated from the hydrogen peroxide oxidation at the Pt ring electrode as follows:

$$n = \frac{4I_D}{I_D + {I_R}/{N}}$$

where I_R and I_D are the current measured at the ring and the disk, respectively, and N is the collection efficiency of the ring, which was experimentally determined to be 0.37.

8.2.6 Computational calculations

Density functional theory (DFT), applying the B3LYP/6-31G(d) method [36–39], through Gaussian 09 software [40] was used in this study. The self-consistent-field (SCF) energies were determined and are reported in kcal/mol (1 Hartree = 627.5095 kcal/mol).

The reaction energies have been calculated using the differences between the energies of the optimized structures of products and reagents.

$$Energy\ reaction = \sum_{n} E(Products) - \sum_{m} E(Reagents)$$

being *n* and *m* the number of products and reactants, respectively, and *E* is related to the SCF energy of the compounds. The results show the free energies.

8.3 Results and discussion

8.3.1 Physicochemical characterization

The post-modification of polyaniline with phosphorus groups was successfully carried out by three different methodologies. Table 8.2 shows the final weight obtained by the different routes. This final/initial weight ratio is always higher than 100% because of the introduction of new functional groups in the pristine material. Comparing the same precursor (i.e., PPh_2Cl), when stronger reaction conditions were applied, the obtained sample presented higher weight, what is consistent with a higher functionalization degree.

Table 8.2: Final weight of sample (%) and atomic percentage obtained by XPS of carbon, nitrogen, oxygen, phosphorus and chlorine.

Sample	Final weight / %	C / %	N / %	O / %	P / %	CL / %
PANI	-	83.1	11.7	3.5	-	1.7
PANI_PPh2Cl_25	105	85.4	9.6	2.9	1.1	1.0
PANI_PPh2Cl_120	131	84.6	6.6	4.0	3.7	1.1
PANI_PCl3	124	67.1	7.7	15.2	4.8	5.1

The morphology of the prepared materials was characterized by transmission electron microscopy (TEM). Figure 8.1 shows the TEM images for each modified-PANI and the pristine PANI. In general, polymer nanostructure is determined by the ratio between the intra- and interchain interactions, what can result in globular, laminar or fibre structures [41,42]. In our case, both PANI and post-modified PANI present laminar arrangement.

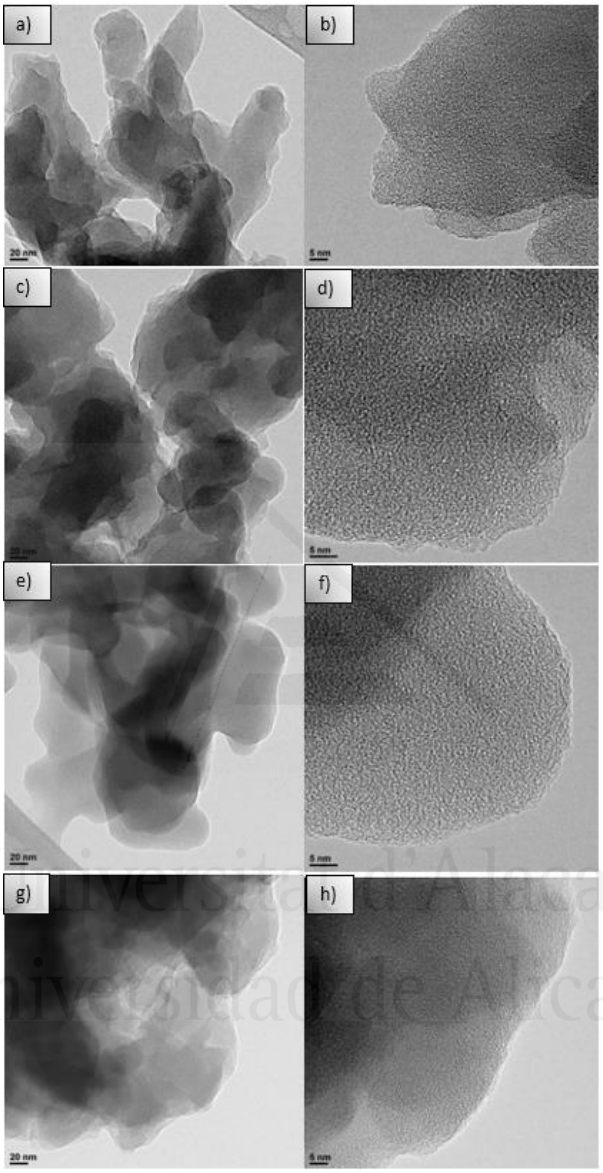

Figure 8.1: TEM images of (a-b) pristine PANI, (c-d) PANI_PPh2Cl_25, (e-f) PANI_PPh2Cl_120 and (g-h) PANI_PCl3 at different magnifications.

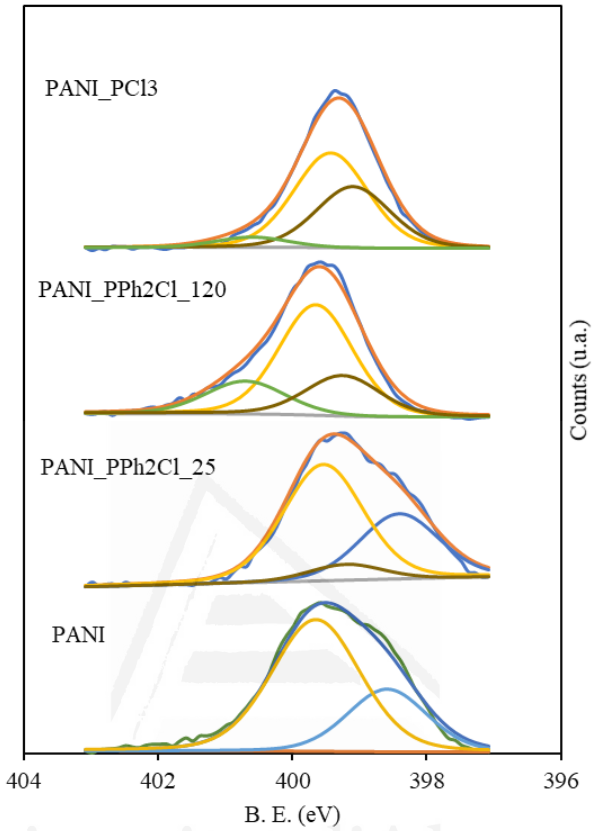

Figure 8.2: N1s spectra of pristine PANI, PANI_PPh2Cl_25, PANI_PPh2Cl_120 and PANI_PCl3.

In order to get a better understanding of the nature of the phosphorus-modified PANI and the mechanism through which the modification process occurs, XPS analysis has been performed. Table 8.2 shows the atomic percentage obtained by XPS and the N1s and P2p spectra of all materials are shown in Figures 8.2 and 8.3.

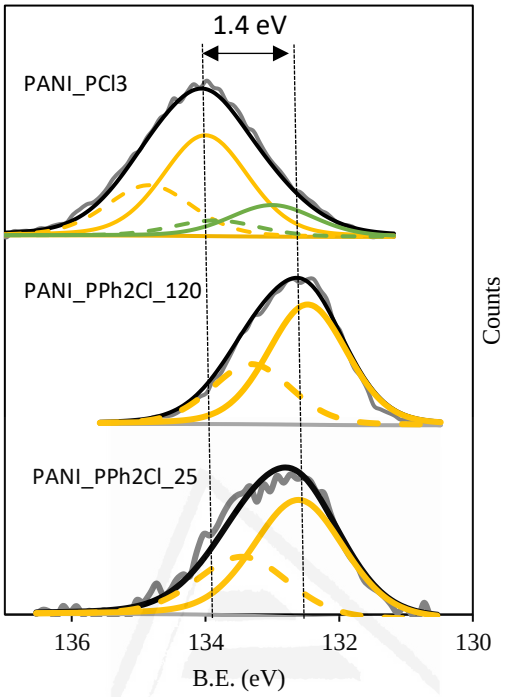

Figure 8.3: P2p spectra of all phosphorus doped PANI samples.

PANI and post-modified PANI present important differences in their elemental composition. The main difference, when PCl_3 is used as a phosphorus precursor, is the lower amount of carbon, what is indicative of a higher functionalization (Table 8.2). Moreover, the oxygen content increases from 3% in pristine PANI to 15% in PANI_PCl3. This can be explained by the substitution of some chloride atoms in the P-Cl bonds, by isopropanol during the washing, which would lead to the formation of P-OC_3H_7 groups, together with HCl formation (Scheme 8.1). This is supported by the gas observed during the washing step. It is also important to highlight the modification level; the higher the temperature used during the functionalization, the higher the phosphorus content obtained using PPh_2Cl as a reagent (Table 8.2). On the other hand, the maximum phosphorus content is obtained by the modification with PCl_3, even though the temperature used is lower than in PANI_PPh2Cl_120, what points out the relevance of the modification agent.

Figure 8.2 highlights some differences in the nature of nitrogen species present in the samples, depending on the phosphorus precursor and temperature used during the functionalization. Pristine PANI was also studied for comparison purposes. In this sense, PANI shows two peaks at 398.5 and 399.5 eV, associated with the presence of imines and amines, respectively [43–45]. The N1s spectra of PANI_PPh_2Cl_25 is similar to that of the pristine PANI, probably because of the low amount of phosphorus (1.1%, see Table 8.2), which did not produce significant changes in the N species of the polyaniline. Only a small peak appears at 399.1 eV, which could be related to N-P species [46,47], and a slight reduction of the imines contribution is produced (from 41 to 33%). On the other hand, when stronger experimental conditions where applied (sample PANI_PPh_2Cl_120), important chemical changes are observed in the N1s spectrum. Indeed, the peak associated with the amines (399.5 eV) is still present in the spectrum; however, the imines peak has completely disappeared, and the new signal associated with N-P is clearly observed in the N1s spectrum at 399.1 eV. This suggests the selective interaction of the imine species with the phosphorus precursor through the formation of N-P bonds. This selectivity towards the imine groups also explains the no need of a base during the functionalization reaction. Furthermore, a new peak appears at higher binding energies (400.6 eV), which could be related with the presence of positively-charged N produced as a consequence of the high temperature used in the modification procedure [48]. Then, the chloride anion, which has been eliminated by the nucleophilic attack between the nitrogen and the phosphorus atom, interacts with these positively charged N groups. Scheme 8.2 illustrates this proposed route and Table 8.2 supports the presence of chlorine atoms in the polymer chain.

In the case of PANI_PCl3 sample, the peak associated with the imine groups also disappears and the creation of the N-P species is observed at similar binding energies as well. In this case, the N-Cl peak is smaller than using PPh_2Cl as a precursor.

Figure 8.3 shows the P2p spectra from the XPS analysis of all materials. The first important difference among samples is that the reaction with PCl_3 produces a shift of the P2p spectrum of 1.4 eV to higher binding energies. Considering that both precursors produce X_2P-N type groups (where X = Ph, OC_3H_7), this shift in the binding energy can be ascribed to the different nature of the phosphorus substituents (X in Scheme 8.3a).

The P2p spectra of PANI_PPh2Cl_25 and PANI_PPh2Cl_120 contain one peak at 132.5 eV, which can be related to Ph_2P-N species [49]. There are no qualitative differences between the two P2p profiles when different temperatures were applied for the modification with this precursor. In fact, the higher temperature of the functionalization with PPh_2Cl only increases the phosphorus loading (see Table 8.2). PPh_2Cl contains one chloride atom; then, only one nucleophilic substitution may occur, what explains the appearance of a unique peak in the P2p spectra for the materials obtained with this phosphorus precursor.

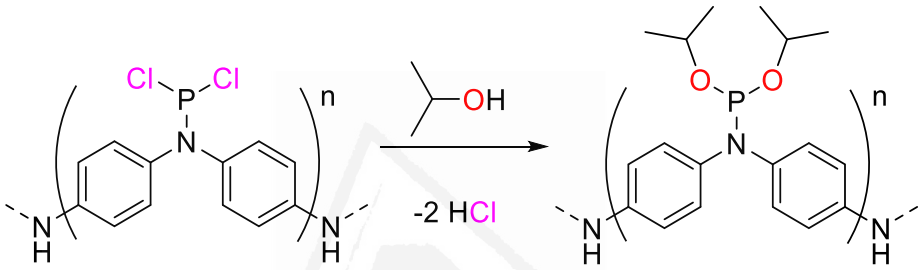

Scheme 8.1: Reaction of PANI_PCl3 with 2-propanol during the washing step.

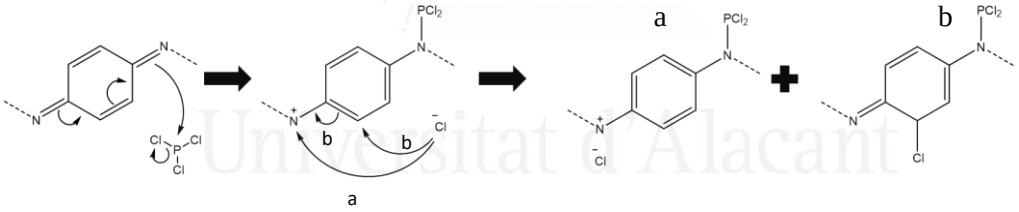

Scheme 8.2: Proposed reaction between the phosphorus precursor (PCl_3) and pristine PANI.

In the case of PANI_PCl3, two peaks are observed in the P2p spectrum. The peak at 134.0 eV lies in the typical range of binding energies for P-O compounds [50,51] and can be associated with $(C_3H_7O)_2P$-N species. A smaller peak at 132.9 eV is also observed. This lower binding energy is characteristic of phosphorus atoms surrounded by a more electropositive environment. This suggests the presence of some inter and/or intrachain cross-linking, in which the phosphorus atom acts as a bridge between two imines moieties through the formation of N-$P(OC_3H_7)$-N bonds (Scheme 8.3b).

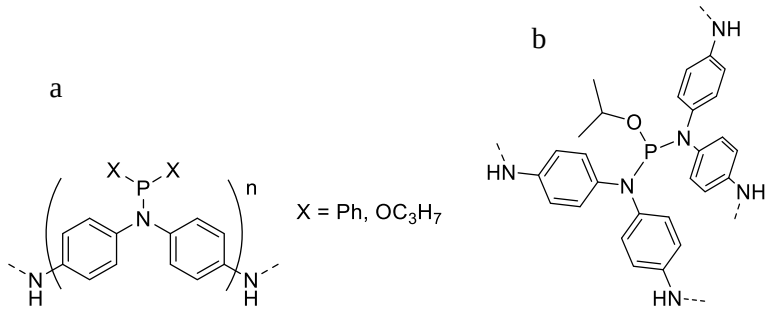

Scheme 8.3: (a) Chemical structure of the two possible X2-P-N groups in modified PANI and (b) scheme of the cross-linking in PANI_PCl3.

XPS for Cl2p has also been analysed and some differences are observed between the different polymers. Firstly, the presence of two peaks (doublets) at around 197.4 and 200.2 eV for PANI suggests the presence of chloride species and covalently bonded chlorine [52], respectively. These peaks are also observed in the P-modified polyaniline (PANI_PCl3 and PANI_PPh2Cl_120); however, in these modified polymers, the peak associated with covalently bonded chlorine increases in comparison with PANI. These features are in agreement with the scheme of reaction proposed in Scheme 8.2, where this increase might be related with a Michael addition to a carbon atom [53,54]. Interestingly, the peak associated with chloride (red peak in Figure 8.4) has different binding energies depending on the sample. This points out and supports that the chlorine atoms are in a different chemical environment.

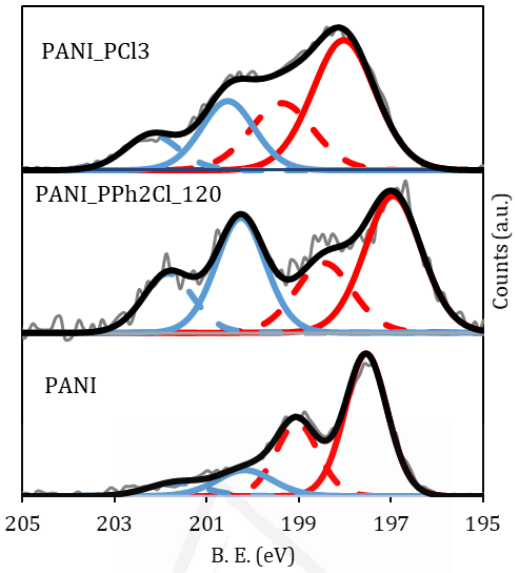

Figure 8.4. Cl2p spectra of all phosphorus-doped PANI samples.

8.3.2 Computational calculations

In order to better understand the reaction products obtained and to discern whether the previously proposed routes are reasonable, Density Functional Theory (DFT) simulations have been carried out. The energy involved in all reactions previously proposed has been evaluated. For that purpose, B3LYP/6-31G(d) energies of the pristine PANI, phosphorus precursors and possible final products have been calculated, optimizing their structures and testing that all frequencies have positive values. Table 8.3 shows the free energies of each proposed reaction between the PANI and the phosphorus precursors.

By using PCl_3 as a precursor, the reaction could proceed through two different routes (generating Cl_2-P-N groups, or N-P(Cl)-N bridging bonds, see above). The free energy of the reaction where the phosphorus is bonded through a nitrogen atom has the lowest value, suggesting that the formation of the Cl_2-P-N species is the most probable mechanism. This justifies the higher amount of $(C_3H_7O)_2$P-N than N-P(OC_3H_7)-N species in the post-modified polyaniline.

Furthermore, during the discussion of the XPS analysis, it was highlighted the importance of the washing of the final material. In this regard, the energy

evaluation of the reaction between the isopropanol with the modified PANI was also studied and confirmed a decrease in the total energy after the washing.

Therefore, the DFT calculations support the interpretation of the P2p XPS for PANI_PCl3, where the main peak is associated with the $(C_3H_7O)_2$-P-N bond, and the minor peak in the same spectrum (132.9 eV) is related to the N-P(OC_3H_7)-N species.

Table 8.3: B3LYP/6-31G(d) free energies of the possible reactions between polyaniline and PCl_3 or PPh_2Cl.

Phosphorus precursor	Reaction product	ΔGº reaction / Kcal·mol^{-1}	ΔGº Washing/ Kcal·mol^{-1}	ΔGº Total / Kcal·mol^{-1}
PCl_3	N-P-Cl_2	23.51	-0.90	22.61
	N_2-P-Cl	57.55	-2.17	55.38
PPh_2Cl	N-P-Ph_2	46.79	-	46.79

It is important to highlight the differences in the DFT energies using both phosphorus precursors. The reaction between PANI and PPh_2Cl always has higher energy than with PCl_3 and, therefore, the reaction to form PANI_PCl3 is most favourable from a thermodynamic point of view. This is coherent with the higher phosphorus content obtained by PANI_PCl3 and the need of using higher temperatures and high concentration of PPh_2Cl to achieve a significant degree of reaction.

8.3.3 Thermogravimetric analysis

Thermogravimetric analyses (TGA) were also performed with the aim of evaluating the reactivity of the polymers towards the gasification in air atmosphere. In this sense, all polymers were subjected to a heat treatment of 5ºC·min^{-1} until 900ºC in air (100 mL·min^{-1}).

Figure 8.5 displays the TGA profiles, where it can be observed that the P-containing samples exhibit lower reactivity and, consequently, higher resistance towards gasification in air. This hindrance towards the oxidation by phosphorus groups has already been studied extensively in P-doped carbon materials and it has been related to the presence of C-O-P and C-P-O species[50,55,56].

However, Figure 8.5 also shows differences depending on the kind of phosphorus precursor used in such modifications. In fact, PANI_PCl3 is the material with the lowest reactivity and does not achieve the complete burn-off until temperatures near 700 ºC, whereas PANI_PPh2Cl_120 and PANI_PPh2Cl_25 are completely gasified at 650 ºC.

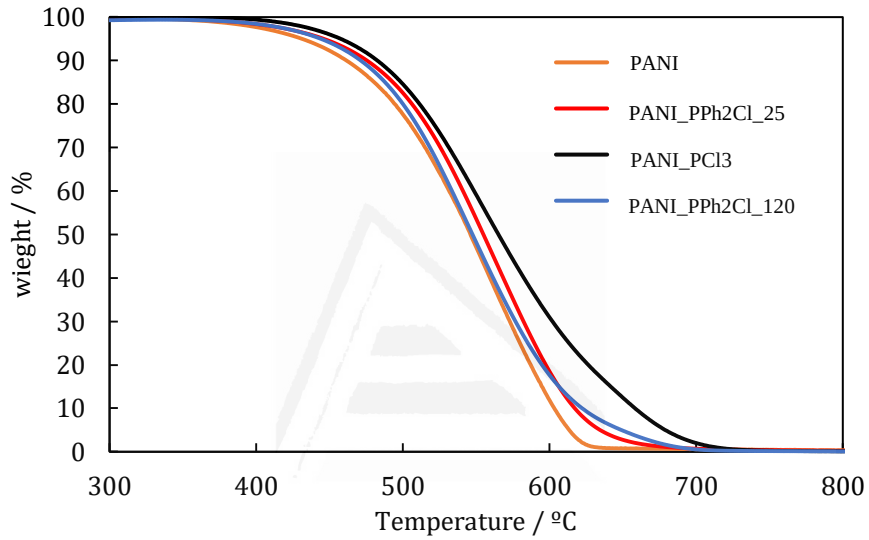

Figure 8.5. Thermogravimetric analysis profile of all polymers.

Not only the amount of phosphorus, but also the nature of the phosphorus precursor seems to have an effect on the reactivity of the materials.

8.3.4 Electrochemical results

Figure 8.6 shows the cyclic voltammograms of the post-modified PANI samples in 0.1 M H_2SO_4 aqueous solution for two loadings (i.e., 0.1 and 0.5 $mg \cdot cm^{-2}$). There are important differences in the electrochemical behaviour of the samples. Pristine PANI presents different peaks, which are indicative of the redox process associated with its changes in the oxidation state. The peak corresponding to the leucoemeraldine-emeraldine transition appears at around 0.30 V vs Ag/AgCl [57,58]. On the other hand, the second peak, which is associated with the emeraldine-pernigraniline, is not well defined (0.7 vs Ag/AgCl [59]). This is probably due to the used synthetic process. The peaks

are observed for both mass loadings (Figure 8.6a and 8.6b) although they are broader for the highest loading used due to the increased thickness of the layer.

When the mass loading is 0.1 mg/cm^2, that is for a thin layer of sample, PANI_PCl3 and PANI_PPh2Cl_25 show voltammograms similar to that of pristine PANI but with lower current, whereas PANI_PPh2Cl_120 displays a voltammogram without any significant peaks. This observation could be due to different reasons. The phenyl groups may produce an important steric hindrance, which would prevent the accessibility of the ions, making the redox reaction less probable. Furthermore, the phenyl groups increase the hydrophobicity of the polymer surface, thus, the interaction between the polymer and the electrolyte is less efficient as well. In fact, steric hindrance [60–62] and the hydrophobic character [63] are known to be responsible for poor electrochemical properties. These differences are much more important when a thicker sample layer is used, which emphasizes that the mass transfer within the polymer layer is very much affected by the functionalization.

Although a larger amount of phosphorus has been introduced in PANI_PCl3 (P ≈ 5 at.%), the sample PANI_PPh2Cl_120 (with P ≈ 4 at.%) shows the most important differences with the electrochemical behaviour of the pristine PANI. In this case, the main difference is that hydrophilic and less steric hindrance species (i.e., $(C_3H_7O)_2$P-N) are present in PANI_PCl3 sample, what permits a more efficient electrochemical response in the aqueous electrolyte. Therefore, both the amount of phosphorus and the nature of the precursor play an important role in the electrochemical properties of the P-postmodified polyaniline.

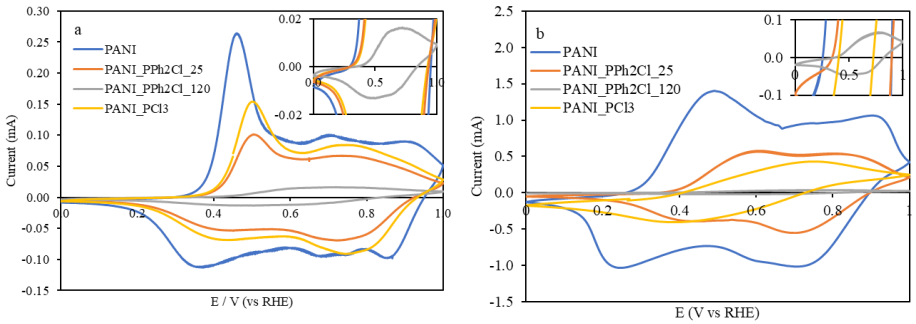

Figure 8.6. Steady-state voltammograms for the different materials obtained by the post-modification of polyaniline with a loading of (a) 0.1 mg·cm^{-2} and (b) 0.5 mg·cm^{-2}. V= 5 mV·s^{-1}, 0.1 M H_2SO_4.

Figure 8.7 shows the Nyquist plot of the three post-modified PANI and the pristine PANI at 0.5 V vs RHE in 0.1 M KOH and 0.1 M H_2SO_4 solutions, measured for the highest loading of polymer (i.e., 0.5 mg·cm^{-2}). In alkaline conditions, the plots are very similar for all the samples. All of them exhibit a similar intercept at high frequencies, which is determined by the electrolyte resistance. The slope in the medium-lower frequency region, that determines the Equivalent Distributed Resistance (EDR), are similar. The slope of the low-frequency region is not vertical because of a distribution in macroscopic path lengths, for example, due to a lack of uniformity in the active layer thickness [64]. Since at these conditions PANI and the modified polymers are not electroactive, the contribution from the charge transfer resistance is not observed.

In the Nyquist plots obtained in acidic electrolyte, the differences among samples are remarkable and reflect the differences observed in electroactivity that were described from the CV (see Figure 8.6 and discussion). There are important differences in the semicircles/arcs observed for the different materials. In the case of PANI, the smallest semicircle is observed, what reflects the faster charge transfer occurring for this material, whereas the largest is found for sample PANI_PPh2Cl_25 in which the effect from the hydrophobic and large phenyl groups is evident. Interestingly, the sample PANI_PPh2Cl_120 with the highest content of phenyl groups do not show any evidence for charge transfer and its profile is similar to that obtained in alkaline conditions.

8.3.5 Electrocatalytic activity towards oxygen reduction reaction

The electrocatalytic activity towards oxygen reduction reaction (ORR) of all materials was studied in O_2-saturated 0.1 M KOH and 0.1 M H_2SO_4 solutions. Linear sweep voltammetry analysis was performed using RRDE at different rotation rates. The ORR can take place with a 2 electrons path to produce H_2O_2, through a 4 electrons route to produce H_2O or through 2+2 electrons multi-steps path that results in the production of H_2O. The next equations summarize the reactions through which the ORR may occur.

$$O_2 + 2H_2O + 4e^- \rightarrow 4OH^- \quad (1)$$

$$O_2 + H_2O + 2e^- \rightarrow HO_2^- + OH^- \quad (2a)$$

$$HO_2^- + H_2O + 2e^- \rightarrow 3OH^- \quad (2b)$$

All materials do not show electrocatalytic activity towards oxygen reduction reaction in 0.1 M H_2SO_4 (not included) between 0.0 and 1.0 V vs RHE; however, they have in alkaline medium. In this sense, Figure 8.8 compares the electrocatalytic behaviour in 0.1 M KOH solution of PANI and all materials obtained from the post-modification of the polymer. The behaviour of glassy carbon electrode has been added for comparison purposes. LSV curves of PANI_PCl3 and PANI_PPh2Cl_25 show an improvement in the catalytic activity towards oxygen reduction reaction in comparison with pristine PANI; however, PANI_PPh2Cl_120 has similar behaviour to the original polymer with a performance close to the glassy carbon electrode. The reason that can explain the lower catalytic activity of PANI_PPh2Cl_120 could be strongly related to the already mentioned steric hindrance or hydrophobic character of the phenyl groups that impede the redox process. So, the new active sites created by the phosphorus functionalization are probably physically blocked by the high amount of -PPh_2 groups and only when the amount of phosphorus loading is lower (e.g. PANI_PPh2Cl_25) or the phosphorus precursor does not contain such substituents (e.g. PANI_PCl3) the P- active sites are accessible to the oxygen molecule.

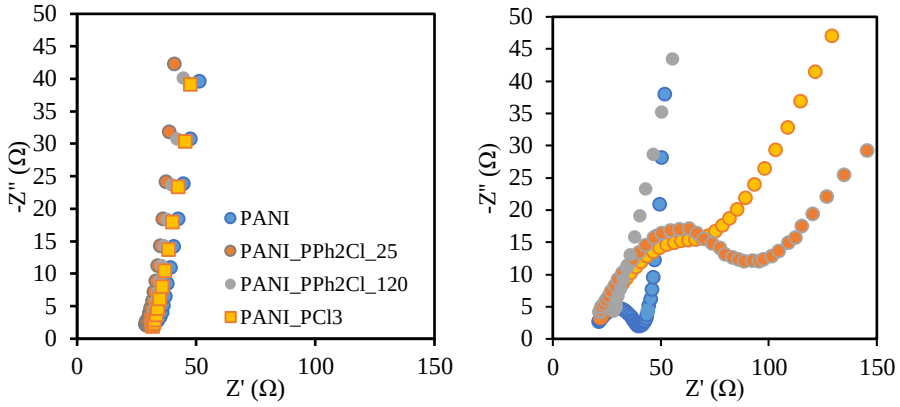

Figure 8.7. Nyquist plot of all post-modified polyanilines and pristine polyaniline in 0.1 M KOH (left) and 0.1M H_2SO_4 (right).

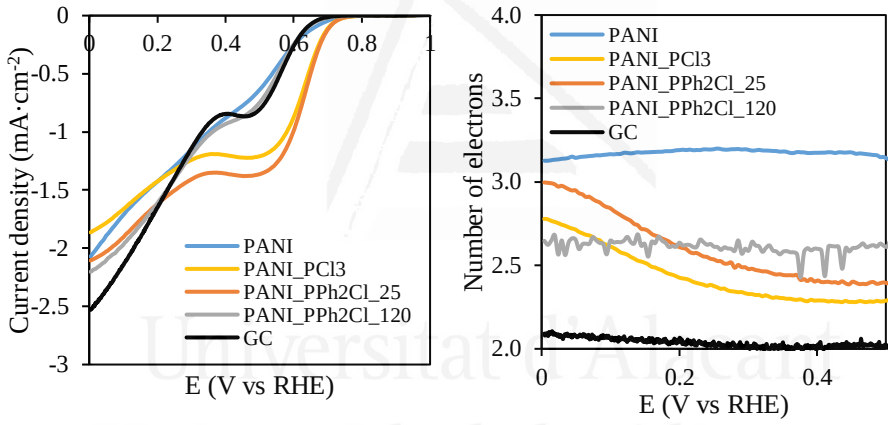

Figure 8.8. Linear sweep voltammetry curves and number of transferred electrons for the prepared materials in O_2 saturated 0.1 M KOH at 5 $mV \cdot s^{-1}$ and 1600 rpm.

These results suggest that the post-modifications, which maintain the redox properties of the pristine PANI, result in the highest activities towards ORR due to the higher catalytic activity promoted by the N-P species, which have been proposed as efficient active sites towards oxygen reduction reaction in other materials [59].

Figure 8.8 also includes the number of transferred electrons during the oxygen reduction reaction. Pristine PANI shows a number of electrons close to

3, which means a yield of 50% towards hydrogen peroxide formation and 50 % towards water generation. However, PCl_3 based post-modified polyaniline produces new catalytic species, which favour the reaction through 2 electrons pathway. Despite a different phosphorus precursor is used, PANI_PPh2Cl_25 also shows high selectivity towards hydrogen peroxide.

Regarding PANI_PPh2Cl_120, although it exhibits the same catalytic activity and number of transferred electrons-profile as pristine PANI, the number of electrons is also lower than PANI. This reflects that the activity of the active sites does not depend on the type of phosphorus precursor used during the functionalization, but it depends on the nature of the new generated N-P species.

All post-modifications of polyaniline with phosphorus groups make the catalysis of oxygen reduction favoured towards hydrogen peroxide generation. The hydrogen peroxide is a very useful product in the chemical industry. It is an environmentally friendly oxidizing agent that does not generate hazardous residues and, then, its production is also very important [65]. In this sense, the phosphorus post-synthetic modification of polyaniline makes this polymer more active and selective towards hydrogen peroxide formation.

8.4 Conclusions

Phosphorus functionalized PANI has been prepared by post-synthetic modification strategies involving the direct reaction of PANI and two phosphorus precursors, PCl_3 and PPh_2Cl in different experimental conditions. In this functionalization process, the imine groups in the PANI react selectively with PPh_2Cl precursor to form N- PPh_2 species and with PCl_3 to form terminal moieties N-$P(OC_3H_7)_2$ and cross-linked, bridging N-$P(OC_3H_7)$-N groups.

Electrochemical characterization allows us to conclude that the phenyl groups of PPh_2- species prevent electrolyte mobility because of their steric hindrance and their hydrophobic character. However, this does not occur when PCl_3 is used since the reaction with isopropanol during the washing step forms N-$P(OC_3H_7)$ species.

Such steric hindrance and hydrophobicity provided by phenyl groups also affect negatively the oxygen reduction reaction. Therefore, materials which present a high content of -PPh_2 moieties (4 at.%) displayed poor catalytic

activity, almost comparable to pristine PANI and bare glassy carbon. However, if the -PPh_2 concentration is lower (1 at.%) or the phosphorus precursor does not have phenyl groups (such as $P(OC_3H_7)_2$) the resulting catalytic activity is higher than the pristine PANI due to the presence of N-P species.

Furthermore, irrespective of the phosphorus precursor, the oxygen reduction reaction occurs through a 2 electrons pathway, where hydrogen peroxide is the main product, thus indicating that they are good candidates as catalysts for hydrogen peroxide production, in contrast with pristine polyaniline, which displays a lower activity and selectivity. Furthermore, these materials are presented as very attractive precursors of N and P-doped carbon materials.

8.5 References

[1] M. Jaymand, Recent progress in chemical modification of polyaniline, Prog. Polym. Sci. 38 (2013) 1287–1306.

[2] C. Barbero, H.J. Salavagione, D.F. Acevedo, D.E. Grumelli, F. Garay, G.A. Planes, G.M. Morales, M.C. Miras, Novel synthetic methods to produce functionalized conducting polymers I. Polyanilines, Electrochim. Acta. 49 (2004) 3671–3686.

[3] A.A. Syed, M.K. Dinesan, Review: Polyaniline-A novel polymeric material, Talanta. 38 (1991) 815–837.

[4] P. Lin, F. Yan, Organic thin-film transistors for chemical and biological sensing, Adv. Mater. 24 (2012) 34–51.

[5] T. Ahuja, I.A. Mir, D. Kumar, Rajesh, Biomolecular immobilization on conducting polymers for biosensing applications, Biomaterials. 28 (2007) 791–805.

[6] W.K. Lu, R.L. Elsenbaumer, B. Wessling, Corrosion Protection of Mild-Steel by Coatings Containing Polyaniline, Synth. Met. 71 (1995) 2163–2166.

[7] N. Plesu, G. Ilia, A. Pascariu, G. Vlase, Preparation, degradation of polyaniline doped with organic phosphorus acids and corrosion essays of polyaniline-acrylic blends, Synth. Met. 156 (2006) 230–238.

[8] A. Gabe, M.J. Mostazo-López, D. Salinas-Torres, E. Morallón, D. Cazorla-Amorós, Synthesis of conducting polymer/carbon material composites and their application in electrical energy storage, 2017.

[9] M. Abdollahi-Alibeik, S. Poorirani, Perchloric Acid – Doped Polyaniline as an Efficient and Reusable Catalyst for the Synthesis of 2-Substituted Benzothiazoles, Phosphorus, Sulfur, Silicon Relat. Elem. 184 (2009) 3182-

3190.

[10] M. Abdollahi-Alibeik, M. Moosavifard, $FeCl_3$-doped polyaniline nanoparticles as reusable heterogeneous catalyst for the synthesis of 2-substituted benzimidazoles, Synth. Commun. 40 (2010) 2686–2695.

[11] M. Abdollahi-Alibeik, M. Moosavifard, S. Poorirani, Synthesis of 2-substituted benzimidazoles in the presence of polyaniline nanoparticles doped with 12-tungstophosphoric acid as reusable heterogeneous catalyst, Synth. React. Inorganic, Met. Nano-Metal Chem. 43 (2013) 1365–1371.

[12] A. Drelinkiewicz, Z. Kalemba-Jaje, E. Lalik, R. Kosydar, Organo-sulfonic acids doped polyaniline - Based solid acid catalysts for the formation of bio-esters in transesterification and esterification reactions, Fuel. 116 (2014) 760–771.

[13] G. Ćirić-Marjanović, I. Pašti, N. Gavrilov, A. Janošević, S. Mentus, Carbonised polyaniline and polypyrrole: towards advanced nitrogen-containing carbon materials, Chem. Pap. 67 (2013) 781–813.

[14] J. Quílez-Bermejo, E. Morallón, D. Cazorla-Amorós, Oxygen-reduction catalysis of N-doped carbons prepared: Via heat treatment of polyaniline at over 1100°C, Chem. Commun. 54 (2018) 4441–4444.

[15] J. Quílez-Bermejo, C. González-Gaitán, E. Morallón, D. Cazorla-Amorós, Effect of carbonization conditions of polyaniline on its catalytic activity towards ORR. Some insights about the nature of the active sites, Carbon 119 (2017) 62–71.

[16] Y. Yang, M.H. Diao, M.M. Gao, X.F. Sun, X.W. Liu, G.H. Zhang, Z. Qi, S.G. Wang, Facile preparation of graphene/polyaniline composite and its application for electrocatalysis hexavalent chromium reduction, Electrochim. Acta. 132 (2014) 496–503.

[17] F. Köleli, T. Röpke, C.H. Hamann, The reduction of CO_2 on polyaniline electrode in a membrane cell, Synth. Met. 140 (2004) 65–68.

[18] H.J. Salavagione, J. Arias, P. Garcés, E. Morallón, C. Barbero, J.L. Vázquez, Spectroelectrochemical study of the oxidation of aminophenols on platinum electrode in acid medium, J. Electroanal. Chem. 565 (2004) 375–383.

[19] M. Abidi, S. López-Bernabeu, F. Huerta, F. Montilla, S. Besbes-Hentati, E. Morallón, The chemical and electrochemical oxidative polymerization of 2-amino-4-tert-butylphenol, Electrochim. Acta. 212 (2016) 958–965.

[20] S. Dkhili, S. López-Bernabeu, C. Kedir, F. Huerta, F. Montilla, S. Besbes-Hentati, E. Morallon, An Electrochemical Study on the Copolymer Formed from Piperazine and Aniline Monomers, Materials 11 (2018) 1012.

[21] S. Dkhili, S. López-Bernabeu, F. Huerta, F. Montilla, S. Besbes-Hentati, E. Morallón, A self-doped polyaniline derivative obtained by electrochemical

copolymerization of aminoterephthalic acid and aniline, Synth. Met. 245 (2018) 61–66.

[22] J. Arias-Pardilla, H.J. Salavagione, C. Barbero, E. Morallón, J.L. Vázquez, Study of the chemical copolymerization of 2-aminoterephthalic acid and aniline. Synthesis and copolymer properties, Eur. Polym. J. 42 (2006) 1521–1532.

[23] C. Sanchís, H.J. Salavagione, J. Arias-Pardilla, E. Morallón, Tuning the electroactivity of conductive polymer at physiological pH, Electrochim. Acta. 52 (2007) 2978–2986.

[24] M. Abidi, S. López-Bernabeu, F. Huerta, F. Montilla, S. Besbes-Hentati, E. Morallón, Spectroelectrochemical study on the copolymerization of o-aminophenol and aminoterephthalic acid, Eur. Polym. J. 91 (2017) 386–395.

[25] D. Yoo, J.J. Lee, C. Park, H.H. Choi, J.H. Kim, N-type organic thermoelectric materials based on polyaniline doped with the aprotic ionic liquid 1-ethyl-3-methylimidazolium ethyl sulfate, RSC Adv. 6 (2016) 37130–37135.

[26] Y. Wang, J. Zhang, D. Sheng, C. Sun, Preparation and applications of perfluorinated ion doped polyaniline based solid-phase microextraction fiber, J. Chromatogr. A. 1217 (2010) 4523–4528.

[27] B.H. Kim, D.H. Park, J. Joo, S.G. Yu, S.H. Lee, Synthesis, characteristics, and field emission of doped and de-doped polypyrrole, polyaniline, poly(3,4-ethylenedioxythiophene) nanotubes and nanowires, Synth. Met. 150 (2005) 279–284.

[28] C. Bian, A. Yu, De-doped polyaniline nanofibres with micropores for high-rate aqueous electrochemical capacitor, Synth. Met. 160 (2010) 1579–1583.

[29] A. Malinauskas, Self-doped polyanilines, J. Power Sources. 126 (2004) 214–220.

[30] G. Venugopal, X. Quan, G.E. Johnson, F.M. Houlihan, E. Chin, O. Nalamasu, Photoinduced Doping and Photolithography of Methyl-Substituted Polyaniline, Chem. Mater. 7 (1995) 271–276.

[31] Y. Qin, Alginate fibers: an overwiew of the production processes and applications in wound management, Polym. Int. 57 (2008) 171–180.

[32] P. Kovacic, J.W. Timberlake, Doping of Polyaniline: Mechanism, Captodative Effect, Biochemical Relationships, and Chronology, Polym. J. 20 (1988) 819–822.

[33] Y. Kim, Z. Lin, I. Jeon, T. Van Voorhis, T.M. Swager, Polyaniline Nanofiber Electrodes for Reversible Capture and Release of Mercury(II) from Water, J. Am. Chem. Soc. 140 (2018) 14413–14420.

[34] D. Wang, X. Wang, X. Yang, R. Yu, L. Ge, H. Shu, Polyaniline modification

and performance enhancement of lithium-rich cathode material based on layered-spinel hybrid structure, J. Power Sources. 293 (2015) 89–94.

[35] S. Matsumura, A.R. Hlil, C. Lepiller, J. Gaudet, D. Guay, Z. Shi, S. Holdcroft, A.S. Hay, Ionomers for proton exchange membrane fuel cells with sulfonic acid groups on the end-groups: Novel branched poly(ether-ketone)s, Macromolecules 49 (2008) 511–512.

[36] C. Lee, W. Yang, R.G. Parr, Development of the Colle-Salvetti correlation-energy formula into a functional of the electron density, Phys. Rev. B. 162 (1989) 165–169.

[37] A.D. Becke, Density-functional exchange approximation with correct asymptotic behaviour, Phys. Rev. A. 38 (1988) 3098–3100.

[38] M.M. Franci, W.J. Pietro, W.J. Hehre, Self-consistent molecular orbital methods. XXIII. A polarization-type basis set for second-row elements, J. Chemi. 77 (1982) 3654.

[39] P.C. Hariharan, J.A. Pople, The influence of polarization functions on molecular orbital hydrogenation energies, Theor. Chim. Acta. 28 (1973) 213–222.

[40] M.J. Frisch, G.W. Trucks, H.B. Schlegel, G.E. Scuseria, M.A. Robb, et. al. Cheeseman, J. R., Gaussian 09, Revision D. 01; Gaussian, Inc., Wallingford CT, (2016).

[41] T. V. Freitas, E.A. Sousa, G.C. Fuzari, E.P.S. Arlindo, Different morphologies of polyaniline nanostructures synthesized by interfacial polymerization, Mater. Lett. 224 (2018) 42–45.

[42] M. Oyharçabal, T. Olinga, M.P. Foulc, S. Lacomme, E. Gontier, V. Vigneras, Influence of the morphology of polyaniline on the microwave absorption properties of epoxy polyaniline composites, Compos. Sci. Technol. 74 (2013) 107–112.

[43] E. Raymundo-Piñero, D. Cazorla-Amorós, A. Linares-Solano, J. Find, U. Wild, R. Schlögl, Structural characterization of N-containing activated carbon fibers prepared from a low softening point petroleum pitch and a melamine resin, Carbon 40 (2002) 597–608.

[44] S. Biniak, G. Szymański, J. Siedlewski, A. Świątkowski, The characterization of activated carbons with oxygen and nitrogen surface groups, Carbon 35 (1997) 1799–1810.

[45] D. Salinas-Torres, S. Shiraishi, E. Morallón, D. Cazorla-Amorós, Improvement of carbon materials performance by nitrogen functional groups in electrochemical capacitors in organic electrolyte at severe conditions, Carbon 82 (2015) 205–213.

[46] C. Wang, Y. Zhou, L. Sun, P. Wan, X. Zhang, J. Qiu, Sustainable synthesis of

phosphorus- and nitrogen-co-doped porous carbons with tunable surface properties for supercapacitors, J. Power Sources. 239 (2013) 81–88.

[47] V.G. Bairi, U.B. Nasini, S. Kumar Ramasahayam, S.E. Bourdo, T. Viswanathan, Electrocatalytic and supercapacitor performance of Phosphorous and Nitrogen co-doped Porous Carbons synthesized from Aminated Tannins, Electrochim. Acta. 182 (2015) 987–994.

[48] M.S. Ram, S. Palaniappan, A process for the preparation of polyaniline salt doped with acid and surfactant groups using benzoyl peroxide, J. Mater. Sci. 39 (2004) 3069–3077.

[49] J.P. Paraknowitsch, Y. Zhang, B. Wienert, A. Thomas, Nitrogen- and phosphorus-co-doped carbons with tunable enhanced surface areas promoted by the doping additives, Chem. Commun. 49 (2013) 1208–1210.

[50] X. Wu, L.R. Radovic, Inhibition of catalytic oxidation of carbon/carbon composites by phosphorus, Carbon 44 (2006) 141–151.

[51] F. Quesada-Plata, R. Ruiz-Rosas, E. Morallón, D. Cazorla-Amorós, Activated Carbons Prepared through H3PO4-Assisted Hydrothermal Carbonisation from Biomass Wastes: Porous Texture and Electrochemical Performance, Chempluschem. 81 (2016) 1349–1359.

[52] H.S.O. Chan, S.C. Ng, W.S. Sim, K.L. Tan, B.T.G. Tan, Preparation and Characterization of Electrically Conducting Copolymers of Aniline and Anthranilic Acid: Evidence for Self-Doping by X-ray Photoelectron Spectroscopy, Macromolecules. 25 (1992) 6029–6034.

[53] B.D. Mather, K. Viswanathan, K.M. Miller, T.E. Long, Michael addition reactions in macromolecular design for emerging technologies, 31 (2006) 487–531.

[54] M. Aldissi, S.P. Armes, X-ray Photoelectron Spectroscopy Study of Bulk and Colloidal Polyaniline, Macromolecules. 25 (1992) 2963–2968.

[55] J.M. Rosas, R. Ruiz-Rosas, J. Rodríguez-Mirasol, T. Cordero, Kinetic study of the oxidation resistance of phosphorus-containing activated carbons, Carbon 50 (2012) 1523–1537.

[56] Y.J. Lee, L.R. Radovic, Oxidation inhibition effects of phosphorus and boron in different carbon fabrics, Carbon 41 (2003) 1987–1997.

[57] C.C. Hu, J.Y. Lin, Effects of the loading and polymerization temperature on the capacitive performance of polyaniline in NaNO3, Electrochim. Acta. 47 (2002) 4055–4067.

[58] M.J. Bleda-Martínez, E. Morallón, D. Cazorla-Amorós, Polyaniline/porous carbon electrodes by chemical polymerisation: Effect of carbon surface chemistry, Electrochim. Acta. 52 (2007) 4962–4968.

[59] D. Salinas-Torres, F. Montilla, F. Huerta, E. Morallón, All electrochemical synthesis of polyaniline/silica sol-gel materials, Electrochim. Acta. 56 (2011) 3620–3625.

[60] W. Li, A. Yu, D.C. Higgins, B.G. Llanos, Z. Chen, Biologically Inspired Highly Durable Iron Phthalocyanine Catalysts for Oxygen Reduction Reaction in Polymer Electrolyte Membrane Fuel Cells, J. Am. Chem. Soc. 132 (2010) 17056–17058.

[61] R. Baker, D.P. Wilkinson, J. Zhang, Comparison of two new substitutes iron Phthalocyanines as electrocatalysts for the oxygen reduction and hydrazing oxidation reaction, ECS Trans. 16 (2009) 43–61.

[62] S.I. Yamazaki, M. Yao, N. Fujiwara, Z. Siroma, T. Ioroi, K. Yasuda, CO electro-oxidation by carbon-supported Rh tetraphenylporphyrins that have o-methyl groups on meso-phenyl substituents, J. Electroanal. Chem. 668 (2012) 60–65.

[63] G.E. Yalovega, V.A. Shmatko, A.O. Funik, M.M. Brzhezinskaya, In: Advanced Materials, 2016.

[64] R. Kötz, M. Carlen, Principles and applications of electrochemical capacitors, Electrochim. Acta. 45 (2000) 2483–2498.

[65] A. Asghar, A.A. Abdul Raman, W.M.A.W. Daud, Recent advances, challenges and prospects of *in situ* production of hydrogen peroxide for textile wastewater treatment in microbial fuel cells, J. Chem. Technol. Biotechnol. 89 (2014) 1466–1480.

CHAPTER IX

GENERAL CONCLUSIONS

This PhD thesis has focused on the development, characterization, and computational modelling of metal-free nitrogen-doped carbon-based materials for their use as electrocatalysts towards the oxygen reduction reaction. In this sense, experimental and computational approaches were employed to unravel the origin of the catalytic activity of these materials. The results obtained from this study led to the following general conclusions:

Effect of the carbonization conditions of polyaniline and its catalytic activity towards oxygen reduction reaction. Some insights about the nature of the active sites

N- and N- O- doped carbon materials were prepared from the heat treatment of polyaniline at two different temperatures (600 and 800ºC) and two (oxidant and inert) atmospheres. The materials obtained from the heat treatment in an inert atmosphere showed lower yields during the heat treatment than those obtained from the treatment in an oxidizing atmosphere, which pointed out that the use of the oxidant atmosphere promotes crosslinking and condensation reactions during the carbonization.

The heat treatment at 800ºC in an O_2-containing atmosphere resulted in a higher amount of nitrogen functionalities located at edge sites (i.e., pyridine and pyridone/pyrrole groups) in comparison with those samples obtained under an inert atmosphere. In addition, TPD analysis confirmed the higher number of phenol-type groups in the samples obtained from the oxidizing treatment.

The prepared materials at 800ºC in an oxygen-containing atmosphere displayed high electroactivity towards the ORR in a basic electrolyte with limiting current density close to the commercial platinum catalysts. An extensive chemical and electrochemical characterization revealed that a combination of N- and O-containing groups at edge sites in carbon materials produced high catalytic activity towards the oxygen reduction reaction with high selectivity to 4 electrons path. Indeed, it was proposed the presence of N-C-O species as responsible for the enhanced ORR activity of the PANI-derived carbon materials obtained from the heat treatment in an O_2-containing atmosphere.

Moreover, the experimental results were supported by computational calculations. Optimized geometries and atomic partial charges suggested that N-C-O groups produce high positive charge density in the carbon atom located

between both heteroatoms, which might favour dioxygen adsorption and activation. It was proposed that one N-C-O site would produce hydrogen peroxide through a 2 electrons pathway, while the existence of two near N-C-O sites can produce the direct reduction of dioxygen to water.

Oxygen reduction catalysis of N-doped carbons prepared via heat treatment of polyaniline at over 1100ºC

Highly efficient ORR electrocatalysts were obtained through the heat treatment of PANI at high temperatures in an inert atmosphere. The activity of the materials prepared at temperatures above 1100ºC is similar to that of platinum-based commercial catalyst and better than other metal-free N-doped carbon materials prepared by different methods or lower temperatures. Parameters, such as porosity, electrical conductivity, and structural order, were determined as decisive towards the ORR catalysis. However, the nitrogen functional groups demonstrated to be of pivotal importance in the enhanced catalysis. It was proved that high temperatures treatment promotes the conversion of pyridine functional groups into edge-type quaternary nitrogen species located in zig-zag position, which were proposed as responsible for the high activity of PANI-derived carbon materials. The selection of the temperature of the heat treatment seemed to be crucial for achieving an improved conductivity and a higher concentration of the most active sites.

Towards understanding of the active sites for ORR in N-doped carbon materials through a fine-tuning of nitrogen functionalities: An experimental and computational approach

N-doped carbon materials were prepared through a double stage heat treatment of polyaniline. First, a heat treatment at 1000ºC was performed in an oxygen-containing atmosphere and, then, a second heat treatment was carried out in an inert atmosphere at different temperatures. The extensive characterization demonstrated that the oxygen-containing atmosphere of the first heat treatment led to a high concentration of oxygen groups, and moreover, the nitrogen functionalities were found to be mainly N-C-O groups. If the second treatment, in an inert atmosphere, is applied at high temperatures, the transformation of pyridines and pyridones groups into quaternary-type nitrogen species were observed, resulting in a material which contains essentially this nitrogen functionality. Indeed, if the second heat treatment was applied at

1200ºC, the obtained PANI-derived carbon materials exhibited only the presence of quaternary nitrogens. All these changes in the nitrogen groups were not accompanied by significant modifications in structural order or porosity. The resultant samples, obtained at high temperatures, showed platinum-like performance towards the ORR along with high selectivity towards 4 electrons pathway.

Furthermore, all nitrogen functionalities were evaluated by DFT calculations as electrocatalysts towards the oxygen reduction reaction. The computational modelling was in excellent agreement with the experimental results, which reinforces the highly efficient catalysis of edge-type graphitic nitrogen.

Silica and Titania-templated ordered mesoporous N-doped carbon thin films. A highly efficient catalyst towards oxygen reduction reaction

Polyaniline was electrodeposited within the pore structure of two ordered mesoporous templates (Silica and Titania) through chronoamperometric polymerization of aniline. The time employed during the polymerization enabled the control over the amount of deposited polymer on the surface of the templates. The higher time used during the polymerization led to 1.2 at.% of nitrogen in the final composite.

The control over the polyaniline amount also allowed us to control the properties of the resultant heat-treated samples, if Silica was used as a template. In the case of Titania, this template suffers a transformation from anatase phase to rutile phase, which hampers the benefits of the resultant N-doped carbon material/composite. TEM images confirmed the loss of surface area through the formation of Titania nanoparticles with hexagonal shape. On the other hand, well-ordered mesoporosity was maintained when using Silica as template. Furthermore, the N-doped carbon materials showed mainly quaternary-type nitrogen functional groups.

The catalytic activity of the heat-treated samples towards the oxygen reduction reaction was evaluated in alkaline solution. The materials obtained by using Silica as template exhibited highly efficient electrocatalysis towards the oxygen reduction reaction after the carbonization treatment, leading to an E_{ONSET} potential higher than 0.9 V vs RHE and with a low Tafel slope. If the Silica template is removed from the composite, there exists a decrease in the catalytic

activity because of the transformation of edge-type quaternary nitrogen functionalities into pyridone-like species because of the effect of the high concentrated NaOH solution used in the etching process.

On the origin of the effect of pH in ORR for non-doped and edge-type quaternary N-doped metal-free carbon-based catalysts

Selective N-doped carbon material was prepared on the basis of chapter V of the Thesis, with the aim of using it as a model to understand the origin of the effect of the pH in metal-free carbon-based catalysts. Furthermore, a non-doped commercial carbon material was employed to illustrate the behaviour of non-doped carbon materials in the ORR.

The experimental section consisted in the evaluation and characterization of the N-doped carbon material and non-doped carbon material in ORR in different electrolytes, in which a dependence with pH was clearly observed. N-doped carbon materials suffered an impoverishment of the catalytic activity once it is introduced into an acidic electrolyte, whereas in an alkaline environment the catalytic activity is similar to that obtained for the commercial platinum-based catalysts. Although non-doped catalyst was not as active as N-doped carbon material, the catalytic activity also decreased in an acidic medium.

Computational modelling, based on DFT, with explicit solvation model, demonstrated that this high pH dependence is associated with strong stabilization of some ORR intermediates in an acidic electrolyte because of the presence of protons in the solution. Due to such stabilization, the following ORR stages require high energy to occur. Moreover, the protonic environment does not only modify the catalytic activity of the materials but also changes the mechanisms by which ORR takes place. 4 electrons path was determined as the preferred route for both non-doped and N-doped carbon materials in a protonic medium; however, non-doped carbon materials show a preference to reduce oxygen molecules to hydrogen peroxide in an alkaline environment, while N-doped carbon material still showed higher selectivity towards water production.

Post-synthetic efficient functionalization of polyaniline with phosphorus-containing groups. Effect of phosphorus on electrochemical properties

Phosphorus functionalized polyaniline was successfully prepared through post-synthetic modification strategies involving the direct reaction of

polyaniline and different phosphorus precursors, PCl_3 and PPh_2Cl, at different experimental conditions.

In the functionalization process, the imine groups of PANI selectively react with phosphorus precursor to form N-PPh_2 and N-$P(OC_3H_7)_2$ species. Furthermore, by using PCl_3, cross-linked, bridging N-$O(OC_3H_7)$-N moieties were also formed.

The detailed characterization demonstrated that the -PPh_2- species prevent the mobility of the electrolyte because of the high steric hindrance and hydrophobic character of the phenyl groups. However, this does not occur if PCl_3 is employed as a phosphorus precursor since the reaction with isopropanol during the washing stage forms N-$P(OC_3H_7)_2$ moieties. The steric hindrance and hydrophobicity of the phenyl groups also affect negatively to the oxygen reduction reaction. Thus, materials with a high content of -PPh_2 groups exhibited poor catalytic behaviour towards the ORR, comparable with those obtained from pristine polyaniline and bare glassy carbon. However, if the -PPh_2 content is lower, or the phosphorus precursor does not contain phenyl groups, the resulting catalytic activity is higher than pristine PANI because of the highly efficient N-P species. Moreover, the oxygen reduction reaction takes place through 2 electrons pathway regardless of the phosphorus precursor, which indicates that these materials are attractive electrocatalysts towards hydrogen peroxide production. Furthermore, these materials are very attractive precursors of N and P-codoped carbon materials.